EFFICIENT AND ACCURATE ASSESSMENT OF FIRE SPREAD OVER EXTERNAL CLADDINGS IN HIGH-RISE BUILDINGS

A THESIS SUBMITTED TO THE UNIVERSITY OF MANCHESTER FOR
THE DEGREE OF DOCTOR OF PHILOSOPHY
IN THE FACULTY OF SCIENCE AND ENGINEERING

2023

CONGCONG LI
Department of Mechanical, Aerospace & Civil Engineering

Table of Contents

Total word count: 36595

List of Figures

List of Tables

Nomenclature

Symbol	Definition
A	Pre-exponential factor [s^{-1}]
E	Activation Energy [kJ/mol]
B	Spalding mass-transfer number
c	Specific heat [J/(kg k)]
D	Characteristic dimension of burner [m]
h	Heat transfer coefficient [W/(m^2 K)]
H_c	Heat of combustion [kJ/kg]
H_v	Heat of vaporization [kJ/kg]
k	Thermal conductivity [W/(m K)]
$\dot{m}''$	Mass-loss rate
q''	Heat flux [kW/m^2]
S	Stoichiometric oxygen/fuel mass ratio
T	Temperature [K]
x_A	Combustion efficiency
x_R	Fraction of energy lost to radiation
V_p	Flame spread velocity [m/s]
y_0	Mass fraction of oxygen in the air
W	Width [m]

Greek Symbol

ρ	Density [kg/m^3]
u	Velocity [m/s]
ε	Emissivity
α	Absorption coefficient
$\emptyset$	Porosity

Abbreviations	Definition
ACPs	Aluminium composite panels
AD B	Approved document B
SBI	Single Burning Item
EPS	Expanded polystyrene
TTI	Time to ignition
RHR	Rate of heat release
EHC	Effective heat of combustion
MLR	Mass loss rate
PCS	Gross calorific
FIGRA	Fire Growth Index
FDS	Fire Dynamics Simulator
THR_{600s}	Total heat release over first 600s
PF	Plain facade
VF	Ventilated facade

Abstract

The general aim of this thesis is to develop an efficient and accurate model to simulate upward flame spread in unventilated and ventilated cladding systems. The validated model is then used to assess the current Euroclass system of selecting external materials and proposes guidelines on how to improve external material selection while still within the simplistic framework of regulations.

The model consists of the following main sub-models: a one-dimensional combined heat and mass transfer model to compute gaseous fuel production due to decomposition, and a simplified model to calculate surface heat flux and transient flame growth. To demonstrate the capability of the new model, vertical burning and upward flame spread on 2.4m high panels of wood and 5.0 m high panels of PMMA are carried out and compared with experimental results and FDS simulations. The new model calculation results, including propagation of the pyrolysis front, total heat flux, and heat release rate are in good agreement with experimental and FDS's results. However, the new model requires a fraction (a few minutes of CPU time) of that for carrying out the corresponding FDS simulation (CPU time of 2 days).

The validated fire spread model was used to quantify the realistic ranges of combustible materials represented by the same SBI classification. The material properties were obtained by inverse analysis so that their combinations would exactly achieve the relevant thresholds for Class B and Class C materials according to SBI test.

This thesis assessed fire spread behaviour of these materials in Full-scale test (BS 8414) when used as cladding, either on its own, or in combination with another material, both with and without cavity ventilation. The majority, but not all Class B materials would be able to pass the BS 8414 full-scale fire test criterion for flame height. The Class B materials that do not pass the acceptance criterion are combinations of high density (>120kg/m^3) and high heat of combustion (>16 MJ/kg). Many Class C materials could still pass the BS 8414 full-scale fire test criterion for flame height. Such materials are characterized by low density (<60kg/m^3) and low heat of combustion (<16 MJ/kg).

The SBI-based material specification for multi-layered façade is severely restrictive if the insulation material is encapsulated by a non-combustible external surface. Instead of achieving Class A2, even Class C insulation materials can be used provided the thickness of the external layer is not lower than a critical thickness. This critical thickness is no more than a few mms and can be easily achieved in practice.

Declaration

No portion of the work referred to in the thesis has been submitted in support of an application for another degree or qualification of this or any other university or other institute of learning.

Copyright Statement

i. The author of this thesis (including any appendices and/or schedules to this thesis) owns certain copyright or related rights in it (the "Copyright") and s/he has given The University of Manchester certain rights to use such Copyright, including for administrative purposes.

ii. Copies of this thesis, either in full or in extracts and whether in hard or electronic copy, may be made only in accordance with the Copyright, Designs and Patents Act 1988 (as amended) and regulations issued under it or, where appropriate, in accordance with licensing agreements which the University has from time to time. This page must form part of any such copies made.

iii. The ownership of certain Copyright, patents, designs, trade marks and other intellectual property (the "Intellectual Property") and any reproductions of copyright works in the thesis, for example graphs and tables ("Reproductions"), which may be described in this thesis, may not be owned by the author and may be owned by third parties. Such Intellectual Property and Reproductions cannot and must not be made available for use without the prior written permission of the owner(s) of the relevant Intellectual Property and/or Reproductions.

iv. Further information on the conditions under which disclosure, publication and commercialisation of this thesis, the Copyright and any Intellectual Property and/or Reproductions described in it may take place is available in the University IP Policy (see http://documents.manchester.ac.uk/DocuInfo.aspx?DocID=487), in any relevant Thesis restriction declarations deposited in the University Library, The University Library's reg- ulations (see http://www.manchester.ac.uk/library/aboutus/regulations) and in The University's Policy on Presentation of Theses.

Acknowledgement

I would like to thank my supervisors, Professor Yong Wang, for his academic and professional support throughout my PhD study. The engineering and critical thinking skills I learned from him will serve me well throughout my career.

I was fortunate to meet extraordinary people from all over the world during my Ph.D. study. Thank Prof. Delichatsios (University of Ulster, UK) for sharing his experience without any reserve about flame spread modelling. Thank Assoc Prof. Jinhui Wang (SMU, CN) for the discussion on the modelling of cavity fire. Thank Dr. Long Shi (RMIT University, AU) for his selfless assistance in solving PDEs and programming of pyrolysis model.

Thanks to all my friends for their help and support during my university stay.

I would like to thank my family for making a lot of sacrifices to make me feel loved. I am especially grateful for the wonderful support I receive from my wife. It was my wife and son that kept me positive throughout the COVID-19 pandemic. The source of my motivation was them.

Lastly, I would like to thank all those who have challenged me to improve.

Chapter 1 Introduction

1.1 Research Background

In the past decades, advanced materials, including polymers and fibre-reinforced composites, were developed as lightweight and inexpensive external cladding materials for buildings that can be rapidly installed. These systems have been constructed to be cost-effective solutions for insulation production, weather protection and aesthetic finish.

However, concerns raised by a few major fire incidents involving the burning of cladding systems, especially the Grenfell Tower Fire in London in 2017 (see section 1.2 for more details), heightened awareness of the public in potential dangers of including polymer materials within cladding, which has propelled the UK government to change regulations on external lining materials by banning combustible materials in residential buildings over 18 metres high. However, this retrospective change of regulation is causing immense societal upheaval: tens of billions of pounds are needed to replace existing cladding systems perceived to be unsafe, widespread anxiety among flat owners who are unbale to sell their flats.

Whilst there is no doubt that the combustible cladding on the Grenfell tower played an important part in the observed rapid flame spread, many other aspects of the fire strategy, not least the stay-in-place evacuation plan, have contributed to the large tragic loss of life. Even with the cladding system, the observed rapid-fire spread may have been substantially contributed by chimney effects of the unstopped internal cavity. Therefore, the simple regulatory measure of banning combustible materials in external cladding cannot be considered proportionate to addressing the risk of fire spread over external cladding. It is crucial to understand how different materials and their configuration affect the fire behaviours of external cladding systems.

Currently, there are a number of methods that may be used to assess the fire performance of external cladding system and construction for fire safety, including the following:

- bench-scale test methods, like the cone calorimeter[1] and the combustibility test. They provide information of heat of combustion and ignitability of material;

- medium-scale test methods, such as the Single Burning Item (SBI)[2]. The SBI test results of a material are used to decide its material classification (A1, A2/B, C, D, E, F), which forms the basis of regulatory control of specifying external lining materials [3];
- full-scale methods, such as BS 8414 external cladding systems fire testing (Figure 1.1), are directly used to assess whether the cladding system fulfils the performance requirement of the regulation.

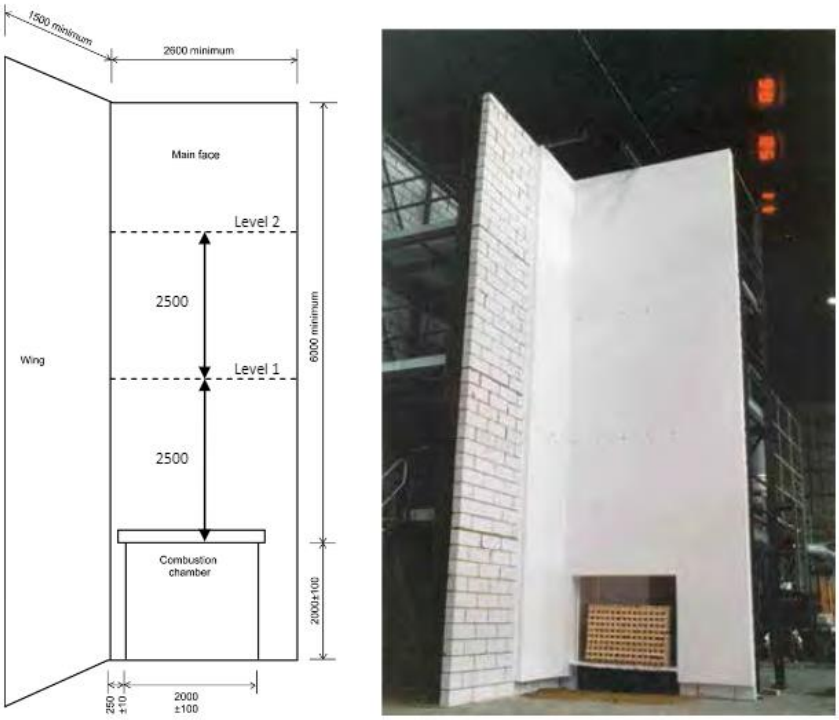

Figure 1.1 BS8414 full-scale cladding fire test rig[4]

However, whilst these standardized test methods play an important role in the establishment of fundamental data for assessing fire-related material properties, combustion characteristics, and cladding system performance in fire, there are significant shortcomings in relying on these tests to control material selection and cladding system design for fire safety. The bench scale and medium scale tests cannot represent real use situations. Due to the huge variety of building materials and their combinations and configurations in external cladding systems, it is not feasible to use the full-scale BS8414 cladding fire test to examine every material and cladding system. While BS 9414[5] helps to extend the scope of applications of large-scale cladding fire tests, due to complex behaviour of fire, it is not possible for BS 8414 to provide detailed quantitative information in many cases. Thus, should there be any variations in construction that cannot be dealt with by BS8414, even though they may be relatively minor, they may not

be allowed if they have not been certified by testing. This inflexibility is detrimental to innovation but may perversely lead to unsafe practice when unscrupulous suppliers try to cut corners.

Therefore, it is crucial that material selection and system design to achieve fire safe cladding in buildings is informed by a thorough understanding of the performance of cladding systems in fire. However, due to complexity of fire behaviour of cladding systems, numerical modelling is the only approach that is capable of developing the necessary understanding. At present, only sophisticated CFD (computational fluid dynamics) models have the necessary capabilities to simulate different aspects of fire behaviour of cladding systems with possibly infinite varieties of materials, their combinations and configurations under various fire scenarios. In order to improve fire safety design of cladding systems, a more efficient simulation model is needed.

1.2 Fire case study, Grenfell Tower, UK, 2017

Fire at Grenfell Tower [6]in London on 14 June 2017 demonstrated the importance of building fire safety and brought to light the role façades play in fire propagation. There were 72 fatalities in the Grenfell Tower fire, one of the biggest fires of the last few decades. In 2016, the Grenfell tower was refurbished with a rainscreen cladding system consisting of an inner layer of combustible polyisocyanurate (PIR) foam insulation, a cavity and an outer layer of aluminium composite panels (ACPs), made of a highly combustible polymer core material. According to reports, the fire began in a fridge-freezer on the fourth floor, then broke through the window to ignite the external cladding system, after which there was a rapid spread of flame around the building's exterior surface. The cause of Grenfell Tower's severity of fire spread can be attributed to (a) the rapid flame spread vertically and (b) the flames being able to penetrate into the cavity.

Despite a variety of factors that contributed to the large loss of life in the Grenfell Tower fire, popular images of the entire tower in inferno have made controlling cladding materials dominate decision-making. The UK government regulations have now banned using combustible materials in residential buildings over 18m high. And this regulation is retrospective, thus combustible cladding panels in existing buildings have to be replaced. This is causing immense societal upheaval. The estimated cost of replacing existing cladding panels is 50 billion pounds. Residents in such buildings feel trapped because of the prohibitive cost of replacing cladding panels without which their flats would be worthless. Perversely, this

obsessive popular focus on cladding materials may lead to compromised fire safety as limited resources are diverted away from other more effective measures of improving fire safety.

Figure 1.2 Image of the Grenfell Tower Fire.

1.3 Aim and objectives

The Grenfell Tower fire tragedy has rightly raised public awareness of the importance of fire safety, but this tragedy must be used to guide developments to improve fire safety in an effective way so that limited resources are utilised proportionately to achieve the optimal level of fire safety, through thorough understanding of combustion behaviour of external cladding in fire. This is the main driver guiding the research of this thesis.

As discussed in section 1.1, existing methods of quantifying cladding behaviour in fire and specifying external lining materials have a number of shortcomings. The aim of this research is to develop a more efficient, flexible and accurate approach to assess fire safety of external cladding systems.

To meet the aim of this research, this research will need to achieve the following objectives:

- Developing an efficient method of modelling fire spread over cladding construction, with and without cavity insulation. The new method of modelling must be able to achieve similar accuracy as sophisticated CFD models, but at a fraction of the simulation time. Because upward fire spread is dominated by fire behaviour in one direction, development of a more efficient method of modelling is possible.
- Comprehensive validation of the new simulation model.
- Assessment of applicability and limitations of existing regulatory methods of specifying external lining materials.
- Methods of improving specification of external lining materials.

1.4 Outline of the thesis

The content of this thesis is outlined below.

Chapter 2 presents a comprehensive review of research areas related to the current study. Wherever appropriate, detailed information will be provided in relevant chapters. However, chapter 2 will summarise relevant research and explain how the detailed information in various chapters will be used in this research. The topics in literature review include flame spread mechanisms of solids, existing analytical models for vertical flame spread, types of facades, standard test methods and current building regulations.

Chapter 3 presents the development and validation of an efficient and accurate model for predicting transient upward flame spread on combustible vertical surface without cavity ventilation. This model incorporates a number of simplifications including heat flux to the wall surface, heat and mass transfer and decomposition, and application of steady state flame spread models to transient behaviour. This chapter will present details of the various sub-models and detailed validations of all the assumptions. Validation of the model is completed by using the model to predict two full-scale upward fire spread tests on wood and PMMA walls, and comparison of the model's calculation results against Delichatsios' and FMRC's experiments.

Chapter 4 extends the model in Chapter 3 to cladding with air cavity.

Chapter 5 assesses the Single Burning Item classification for specifying materials on the external surface of buildings. Current regulatory specification of external lining materials throughout the world is based on controlling classification according to the so-called Single Burning Item (SBI) test. However, the same SBI classification can represent a wide range of

combustible materials. After first quantifying possible wide ranges of realistic materials that may be considered to have the same under SBI classifications, chapter uses the model developed in Chapter 3 to investigate performance of cladding materials at the borderline of allowed/not allowed materials based on current regulatory specifications in BS 8414 testing condition and proposes conditions under which current regulatory controls of external lining materials based on SBI classification should not be used.

Chapter 6 is similar in purpose as Chapter 5 but extends the work in Chapter 5 on single external cladding material without cavity to more realistic situations of composite cladding construction with and without cavity. The main foci are what combinations of the external and insulation materials in multi-layered façade can achieve the overall objectives of façade safety.

Chapter 7 concludes this research and suggests topics for further research.

Chapter 2 Literature review

Based on the aim and objectives stated in Section 1.3, this research covers the following topics: type of façade system, standard fire tests for materials, regulatory control of external lining materials, and methods of assessing fire safety of cladding systems, mechanisms of flame spread over vertical surfaces and its modelling, and flame height correlations.

2.1 Type of cladding system

Many different materials can be used to construct the external wall (cladding) of a building. In general, they form a non-ventilated system (Figure 2.1a) or a ventilated cavity system (Figure 2.1b).

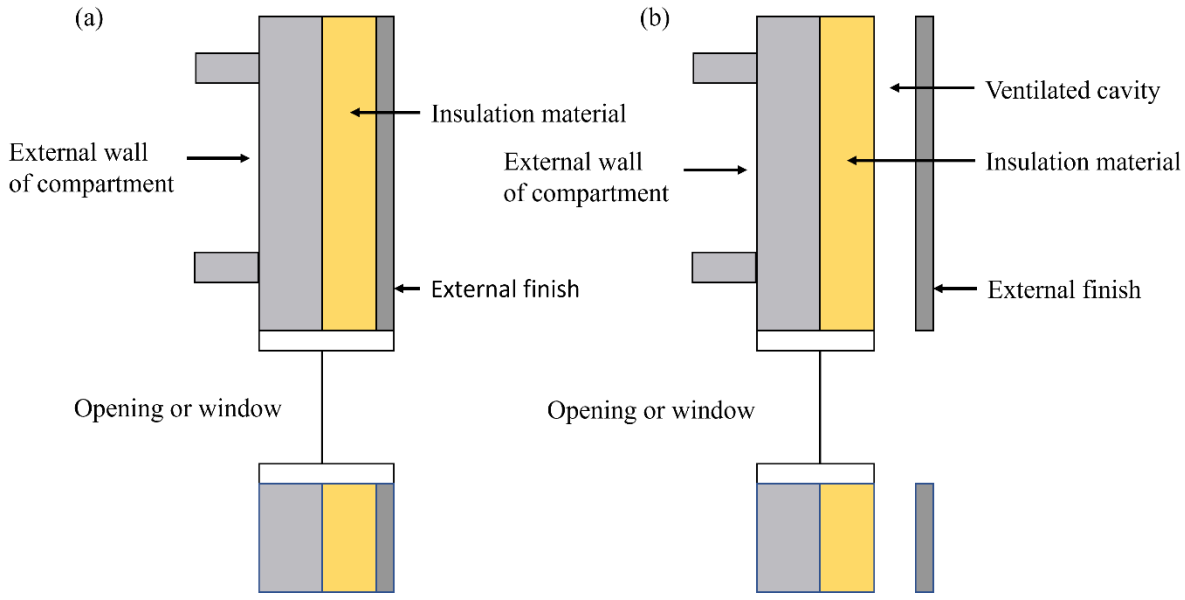

Figure 2.1 (a) non-ventilated cladding system, (b) ventilated cavity system[7]

2.1.1 Non-ventilated system

As shown in Figure 2.2, these systems are typically used for refurbishing masonry substrates with continuous background structures. Typically, two elements make up the system.

- To ensure the required level of thermal efficiency, insulation material is typically fixed to masonry backgrounds;
- A weather-resistant finish coat is generally applied to the insulation layer's external surfaces.

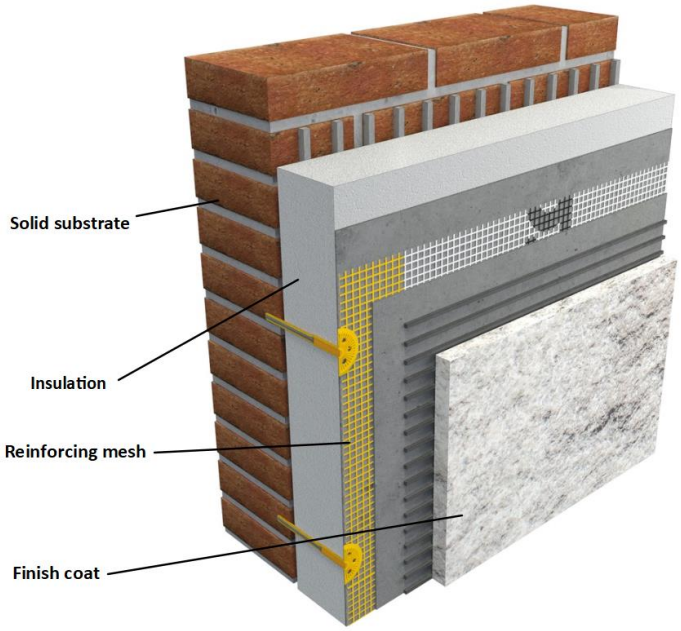

Figure 2.2 An example of non-ventilated system: exterior insulation finish system[7]

2.1.2 Ventilated cavity system

An example of a ventilated cavity system can be seen in Figure 2.3. These systems typically contain an inner insulation material and an outer cladding for weather protection.

- Insulation products fixed to the external wall substrate – Typically, the wall is insulated using polymer insulation, such as polyisocyanurate (PIR), polyurethane (PU), expanded polystyrene (EPS).
- Cavity between the insulation and external cladding
- Cladding panel – Typically, a variety of material can be used for the external panel, including metal composite cladding and sheeting.

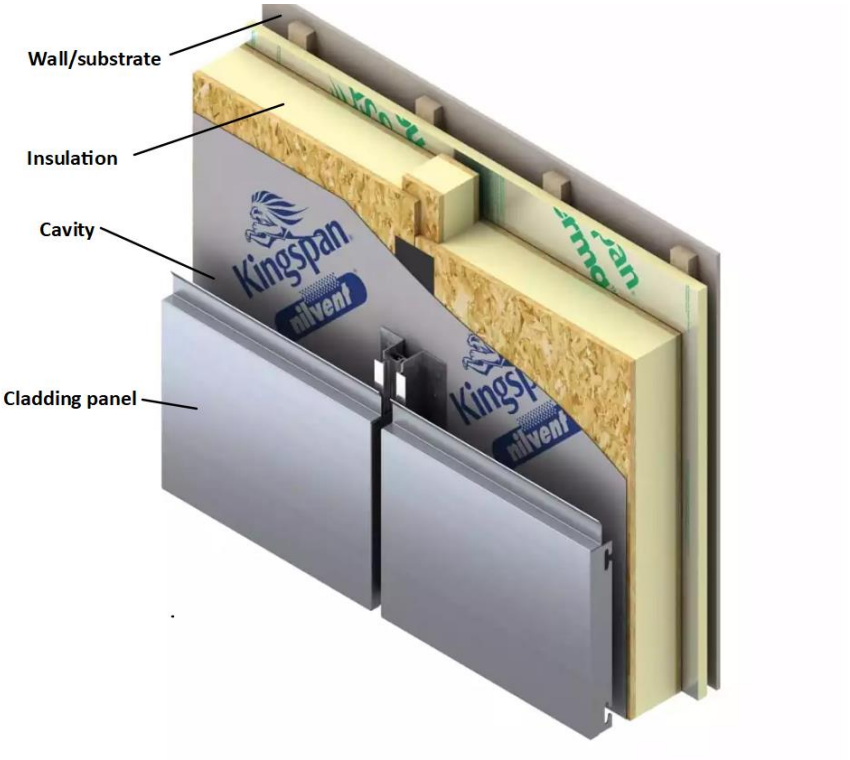

Figure 2.3 An example of ventilated cavity system: rain screen cladding system[7]

As will be shown in the next section, the regulatory requirements for the different materials in cladding system are different. Therefore, this can cause confusion in interpretation. Furthermore, the regulatory based tests are on single materials, whilst a cladding can consist of a number of materials. Therefore, there is a large uncertainty that the single material-based regulation approach is suitable for controlling the fire performance of complex cladding systems. A very important objective of this research is to examine applicability and limitations of regulatory approaches.

2.2 Standard fire tests for cladding materials and systems

In order to understand how cladding materials and systems behave when exposed to fire, several standard fire tests have been developed. This section will summarise these standard fire tests and outline how their results can be used in regulatory specification of cladding materials and systems.

2.2.1 Small-scale tests

Materials' basic properties relating to fire (ignitibility, flame spread, mass loss, and smoke production) can be quantified on a small scale. Tests of this type measure a material's fire-related properties. They are summarised in Table 2.2 and briefly described below.

Combustibility test

Combustibility test determines whether a material is combustible or non-combustible. Different versions of this test are available all over the world, such as ISO 1182[8], BS 476-4[9], ASTM E136[10], AS 1530[11], NFPA 268[12]. Typically, a small material sample is exposed to temperatures of 750 or 835ºC. The criteria of the combustibility test are: (a) sustained flame must not exceed five seconds; (b) A maximum temperature rise of 50°C; (c) Limited mass loss (less than 50%). Otherwise, the material is deemed combustible. Depending on SBI test results (2.2.2), different combustible material classifications are obtained, which are used in regulatory control of materials for fire safety.

Cone Calorimeter

Figure 2.4 Cone calorimeter [1]

The cone calorimeter test [1] is a small-scale device that measures oxygen consumption. A sample of material, 100 mm by 100 mm, is supported on a load box and exposed to radiant heat. With a cone calorimeter, one can measure the flammability of materials, such as their Time to Ignition (TTI), their Heat Release Rate (RHR), their Effective Heat of Combustion (EHC), and how much heat and smoke they release. This test cannot be directly used in regulatory specification of materials for fire safety, but its results are useful for understanding the qualitative performance of materials and for providing test data for validation of modelling.

Oxygen Bomb Calorimeter test

In the Oxygen Bomb Calorimeter test [13], a specified quantity of material is burnt inside an enclosed combustion chamber with high oxygen concentrations. The heat of combustion (gross calorific, PCS) is calculated by taking into account temperature rises in the combustion chamber. As shown in Table 2.1, classifications A1 and A2 are determined by gross calorific value. According to EN 13501-1[3], the criteria for a classification A1 is $PCS \leq 2.0\ MJ/kg$, while that for a classification A2 is $PCS \leq 3.0\ MJ/kg$.

Table 2.1 Small-scale test methods for materials

Test method	Test scenario	Criteria	Test standards	Ref.
Combustibility	Sample size:45*55mm^2 Exposed temperature 750 or 835^{o}C	No sustained flaming (typically >5s) Temperature rises ≤ 50 ^{o}C	BS 476 Part 4,ISO 1182, NFPA 268, ASTM E136, AS 1530.	[8-11]
Cone calorimeter	Heat flux: 0-100kW/m^2 Sample size:10*10cm^2		ISO 5660, ASTM E 1354 and AS/ NZS 3837	[14]
Oxygen Bomb Calorimeter test	-	A1 :$PCS \leq 2.0\ MJ/kg$ A2 :$PCS \leq 3.0\ MJ/kg$	EN ISO 1716, NFPA 259	[13]

2.2.2 Intermediate-scale fire test (BS 476 and SBI test)

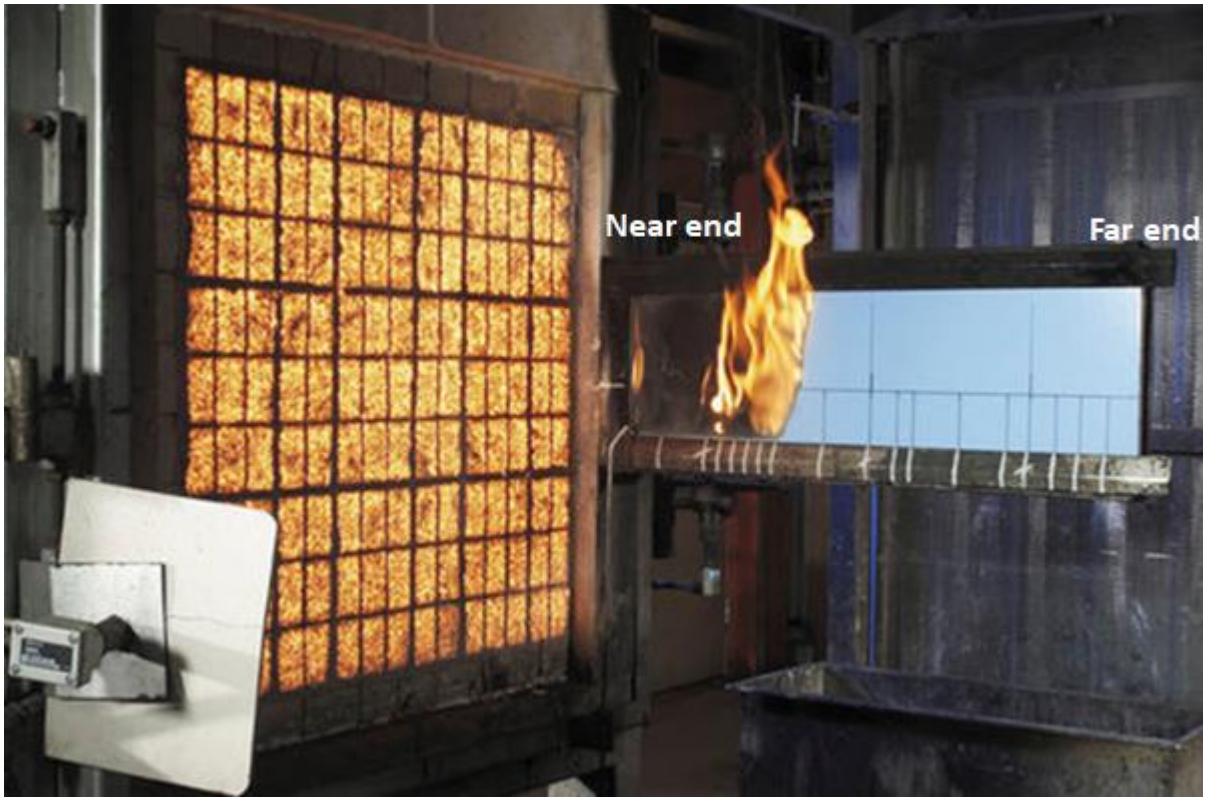

Figure 2.5 BS 476 test rig[15]

The tendency of a material to support lateral flame spread is determined by the spread of flame test (BS 476 test rig[15]). In this test, a square radiant panel is perpendicularly mounted to a large test sample. From 30 kW/m^2 along the sample at the near end to 5 kW/m^2 at the far end, radiant heat flux decreases. The product is classified into Class 1, 2, 3, or 4 based on the extent of the lateral flame spread. However, for material specification, this test has been superseded by the SBI test.

Table 2.2 classification of BS 476[15]

Classification	Spread of flame at 1.5 min, (mm)	Final Spread (mm)
Class 1	165 $\pm$ 25	165 $\pm$ 25
Class 2	215 $\pm$ 25	455 $\pm$ 25
Class 3	265 $\pm$ 25	710 $\pm$ 25
Class 4	Beyond the class 3 restrictions	

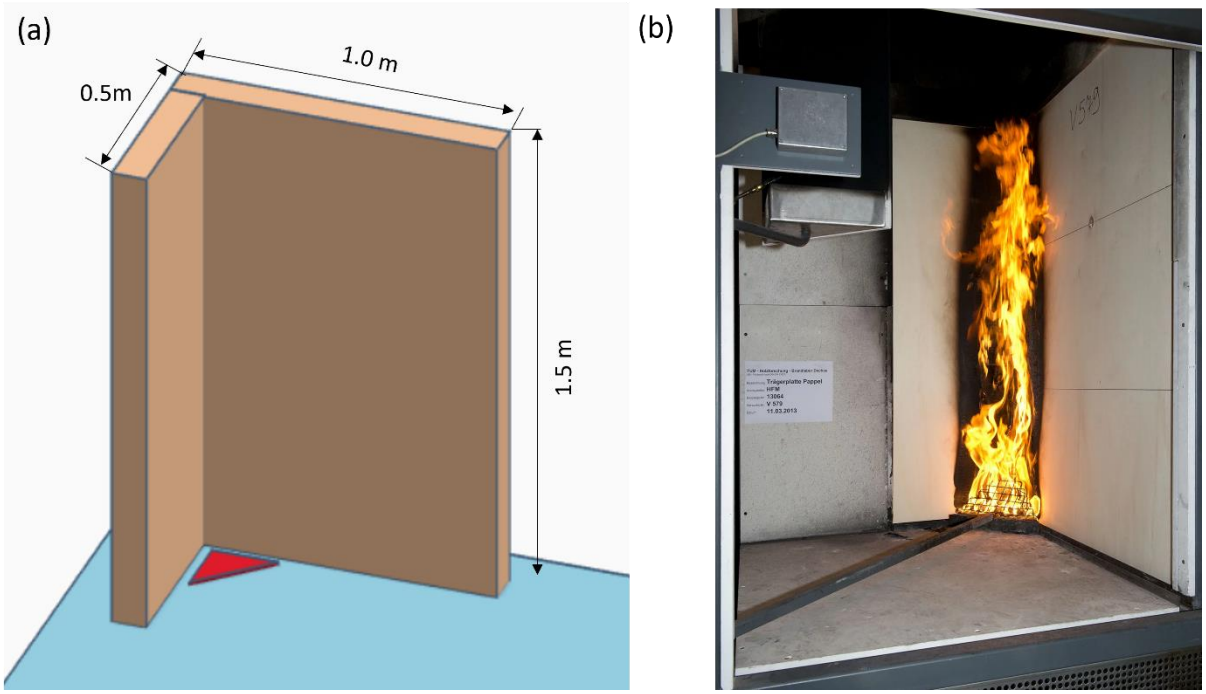

Figure 2.6 Single burning item (SBI) test[2]

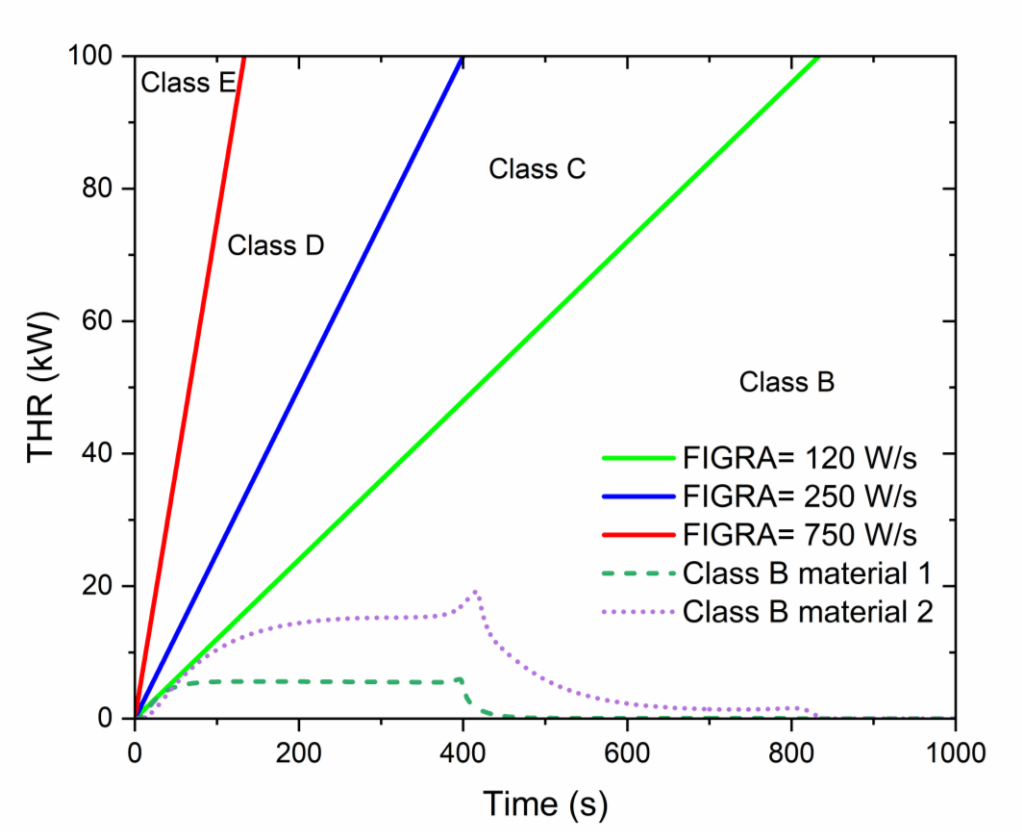

Figure 2.7 Lines representing constant FIGRA values and Examples of RHR curves

Regulatory specification of materials for fire safety is mainly dependent on the so-called single burning item (SBI) test[2]. As shown in Figure 2.6 an L shaped material sample is exposed to

a 30kW gas burner in the corner at the bottom. Dependent on the total recorded heat release rate, a value of Fire Growth Index (FIGRA) is defined as the maximum rate of heat growth rate during the test, as illustrated in Figure 2.7. It is this value if FIGRA that is used to classify the material and Table 2.3 lists their values for material classes A-E. However, as clearly shown in Figure 2.7, FIGRA is a single value that may represent different rate of heat release curves (e.g. dotted lines), whilst it is the slope of heat release curve that determines how the material would behave in fire. So it is understandable that regulatory specifications have to be based on very simple measures, it is crucial to understand their limitations. This is the subject matter of chapter 5.

Table 2.3 SBI classification criteria [2]

	A2	B	C	D	E
FIGRA, W/s	<120	120	<250	<750	other
$THR_{600s,}$ MJ	<7.5	<7.5	<15	-	-
Additional test needed	EN ISO 1182				

2.3.3 Full-scale fire tests for cladding

While small and intermediate scale tests provide useful information on some aspects of the behaviour of materials in fire, they cannot fully capture the realistic behaviour of complex cladding systems. For assessing realistic fire performance of external cladding systems, full-scale fire tests, such as that shown in Figure 2.15, can be used. Table 2.4 lists the most commonly used seven test standards, which are ISO 13785[16], BS 8414-1, UK[4]; DIN4102-20, Germany[17]; NFPA 285, USA[18]; SP FIRE 105, Sweden[19]; CAN//ULC S134, Canada[20]; and AS5113-2016, Australia[21] and summarises their test parameters, including fire source, test's dimensions and acceptance criteria. In such a full-scale test, measurements are made for surface temperature, height of flame and RHR. A number of research studies have pointed out the acceptance criteria used different full-scale test methods [22, 23] vary, mainly due to the different fuel type of the burner in chamber (wood or gas burner), different configuration of wall (plain or L shape wall), and difference in dimensions. Therefore, even a full-scale fire test cannot exactly reproduce end-use situations. However, assessing the full-scale fire test methods is beyond the scope of this research. Instead, this research will use the UK method to assess whether regulatory specifications for materials in cladding systems are consistent.

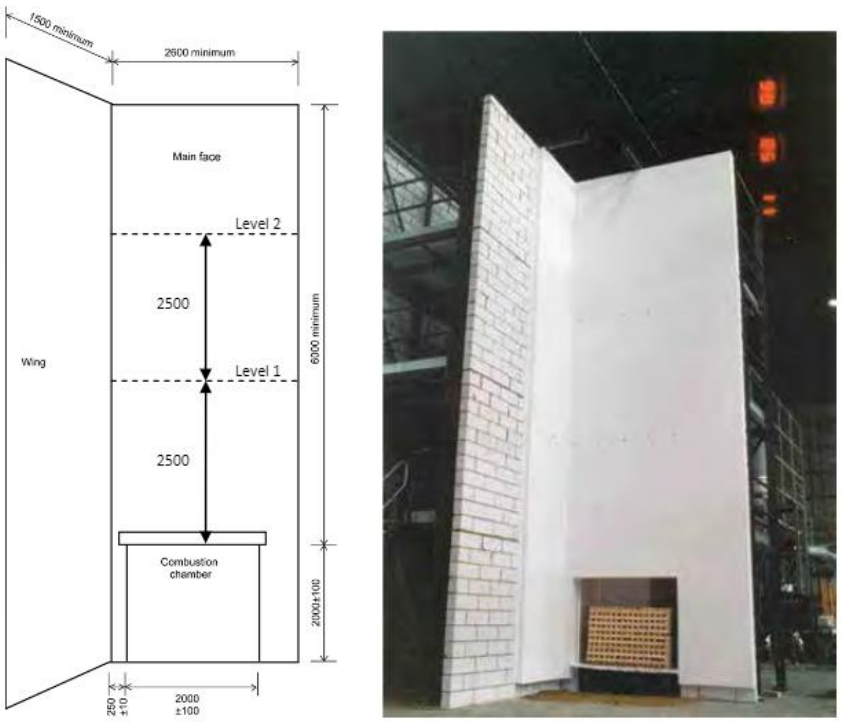

Figure 2.8 BS8414 test rig[4]

Table 2.4 Full -scale test methods for external wall system

Test method	Test dimension	Fire source	Criteria
ISO 13785-part 2	H:≥5.7m W1: ≥ 3.0m W2: ≥1.2m	Gas Burner 5.5MW	a) Temperature at 4.0m≤600ºC b) Cavity or mid depth temperature at 4.0 m ≤250 ºC Result: Pass
BS 8414 part 1 /AS 5113-2016	H: ≥8m B1: ≥2.5m B2: ≥1.5m	Timber crib 3±0.5 MW	a) Temperature>600 ºC at height of 5 m b) Flame reaches the top of the test specimen Result: Fail
DIN 4102-20	H: ≥5.5 W1: ≥2.0 W2: ≥1.4	Gas burner 320 kW	a) No damage≥3.5m b) Temperature ≤500 ºC at height ≥3.5m c) No flame spread beyond the test specimen Result: Pass
NFPA 285	H: ≥5.33 W1: ≥4.1 W2: N/A	Gas burner 690-900kW	a) External surface temperature ≤538 ºC at 3.05m b) External flame height Height≤3.05 m; width≤1.52 m Result: Pass

SP FIRE 105	H: $\geq 6.71m$ W1: ≥ 4.0 W2; N/A	Gas fuel 2.5MW	a) No flame reaches the second floor' window b) Eaves temperature $\leq$450 ^{o}C c) Radiation <80kW/m^2 Result: Pass
CAN/ULC S134	H: $\geq$10m W1: $\geq$5.0m W2: N/A	Gas Burner 5.5MW	a) Spread of flame$\leq$5m b) Heat flux at height 3.5 m $\leq$ 35kW/m^2 Result: Pass

*H is the height of the wall; W1 is the width of the main wall; W2 is the width of the side wall

2.3 Current regulations for fire safety of materials in cladding systems

Whilst manufacturers have the option to conduct full-scale fire tests on cladding systems following the methods in the previous section, regulatory specifications of materials in cladding systems can be determined by the small and intermediate scale tests as described below in this section.

UK and Europe

Most European countries, including the United Kingdom, France, and Germany, use the Euroclass system to design external cladding systems. Acceptance criteria vary from Euroclass A2 to B. Before the Grenfell fire, the Building Regulations of England and Approved Document B[24] requires the external surface of cladding materials to be at least of limited combustibility, based on "B" or better according to SBI classification[3]. There is no additional requirement for the insulation material. As a reaction to the Grenfell tower fire[6], the insulation material should be Class A2 or better.

USA

In the USA, without full-scale testing, the International Building Code (IBC)[25] specifies the following requirements for combustible plastic foam on the external surface:

- Flame spread index of insulation, external covering, and coat $\leq$ 25 (ASTM 3 84 or UL 723);
- The thickness of Insulation $\leq$ 102 mm;
- Insulation is covered by $\geq$ 0.41 mm steel or 0.81 mm aluminium.

China

The current building fire protection regulation for tall buildings in China is GB 50045 Code [26]. For external walls, they specify the fire resistance ratings and combustibility but do not include the requirements for the external insulation and claddings. It is regulated by the Provisional Fire Protection Regulation for Exterior Insulation and Finish Cladding System of Civilian Buildings[27]. For exterior insulation, the Regulation prohibits the use of B3 materials, but permits B2 and B1 materials. The classification of B1 is equivalent to B and C, and a B2 is equivalent to a D and an E in European classification.

Table 2.5 Requirements in the code for residential buildings in China

Type	Height (H, m)	Combustibility
Residential	H>100m	A
	27m<H≤100m	A, or B1
	H≤27m	A, B1, or B2

2.4 General Mechanisms of Flame Spread and Specific Features of Flame Spread over Vertical Surfaces

A positive feedback relationship between the processes of solid decomposition and gas phase burning is known to govern flame spread. Figure 2.9 depicts a hypothetical situation in which a flame propagates on the surface of an exterior wall. In a diffusion flame, when gaseous reactive species react with the ambient oxygen, a proportion of the heat created in this reaction is transmitted back to the solid surface, leading to additional decomposition and the formation of combustible gases.

As shown in Figure 2.9, the upward flame spread on the solid is composed of three basic zones. The pyrolysis zone is where burning material releases flammable volatiles, which contributes to the growth of flame. Above the pyrolysis zone but below the flame height, is referred to as the pre-heating region. In this zone, flame combustion preheats unburnt solids beyond the pyrolysis front. Beyond the flame tip is the plume zone, the heat flux decreases with the distance.

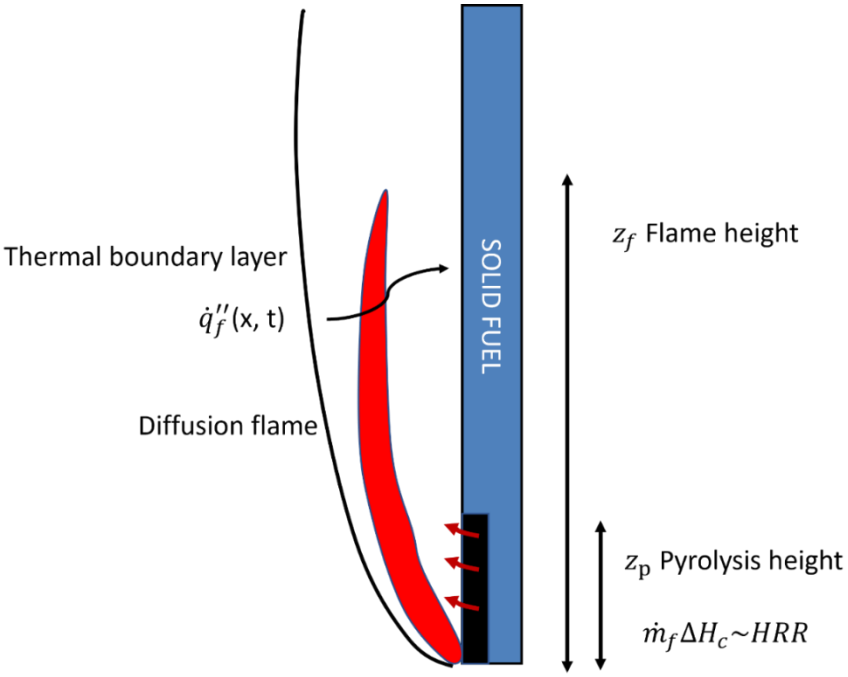

Figure 2.9 Schematic process of flame spread

Thorough understanding of both the solid phase and the gas phase of the combustion process in Figure 2.9 is necessary in order to make reasonable assumptions for the development of an efficient model.

2.5 Approaches to solid reaction modelling

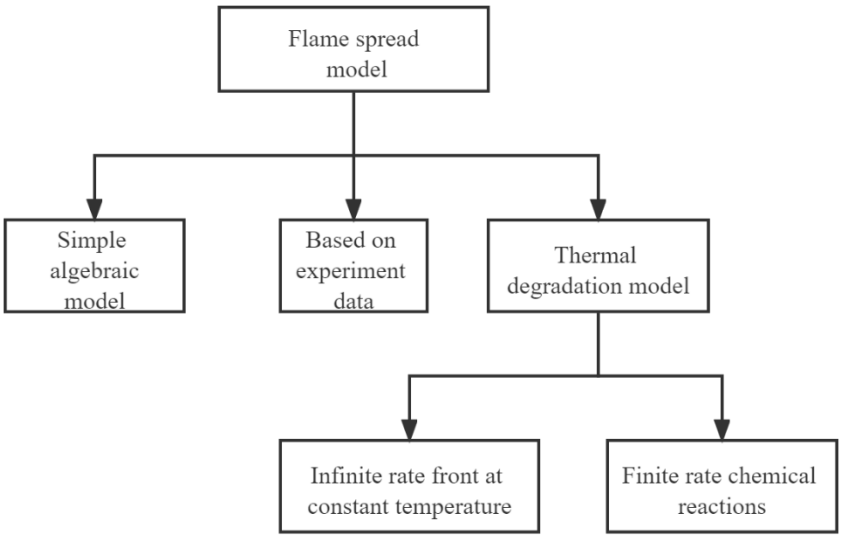

Figure 2.10 Solid reaction models with varying complexity

Based on the two essential processes during flame spread - decomposition of the solid material and heat feedback from gas phase combustion to the solid material, a variety of combustion models have been developed. They are summarised in Figure 2.10 and 2.12. Dependent on the model's purpose and resources, the appropriate solid phase and gas phase model should be chosen. Therefore, the review in this section on flame spread modelling focuses on the following two parts:

- Whether an independent solid reaction model is needed and how complex it should be.
- How is heat feedback modelled.

2.5.1 Simple algebraic model

In the simple algebraic model of Figure 2.10, it uses simple algebraic equations or even assumes a constant value for decomposition of gases and heat production[28, 29]. These models' main objective is to calculate the rate of flames spread.

For example, in the works by Williams [30], Orloff[31], and Ahmad[32], based on quasi-steady assumptions and energy balance considerations, the fundamental equation for the flame spread is as follows:

$$V_f = q''/(\rho \Delta h) \tag{2.1}$$

Where V_f is the flame spread velocity, q'' is the net heat flux, ρ is the density, $\Delta h = c(T_{ig} - T_0)$ is the enthalpy change and c is the specific heat of the solid.

Such a simple model is clearly not adequate to describe the complex behaviour of solid reaction at high temperatures (e.g. no calculation of the amount of volatiles released). It formed the foundation for several further attempts at modelling upward flame spread.

2.5.2 Direct results based on experiments

In this model, the mass loss rate or the release of decomposition gases is measured from experiments, e.g. Cone calorimeter tests. In Cone calorimeter test, a sample is exposed to a radiance heat flux that is approximately equivalent to the heat flux levels in upward flames scenarios. Among these models, such as Karlsson[33], Grand and Drydale[34] and Tsai[35], heat release rate (RHR) and ignition time (TTI) from cone calorimeter measurements were used to predict the upward spread velocity. The main assumptions in their models are:

- The material starts losing mass only when its critical ignition temperature is reached;
- Surface parameters, for example, incident heat flux should be similar between scales. The only parameter that varies are geometric.

Models of this type have the disadvantage that they can only be applied to conditions that are similar to those measured in experiments (such as thickness, incident heat flux, ambient conditions, gas velocity, orientation, etc.). In real fire conditions, the heat flux level may vary with the growth of flame. However, the heat flux level in Cone calorimeter is constant.

2.5.2 Thermal degradation with infinite rate

With the overall concept of thermal degradation modelling, there are different levels of complicity to model heat transfer to and within the solid. In infinite rate thermal models by Quintiere[36],Chen[37, 38] ,Moghtaderi[39], Spearpoint[40] , Weng[41], the following are the most common assumptions:

- The pyrolysis process of solid is assumed to start when the surface temperature reaches a critical value;
- 1D heat transfer, and temperature inside the solid is prescribed (e.g. quadratic);
- The temperature of surface remains constant during the whole process;
- Chemical kinetics are ignored;
- Combustible gases are released from an infinitely thin surface area. This was the front surface for non-charring materials and the thin pyrolysis front between char and virgin layers for charring solids (Figure 2.11).

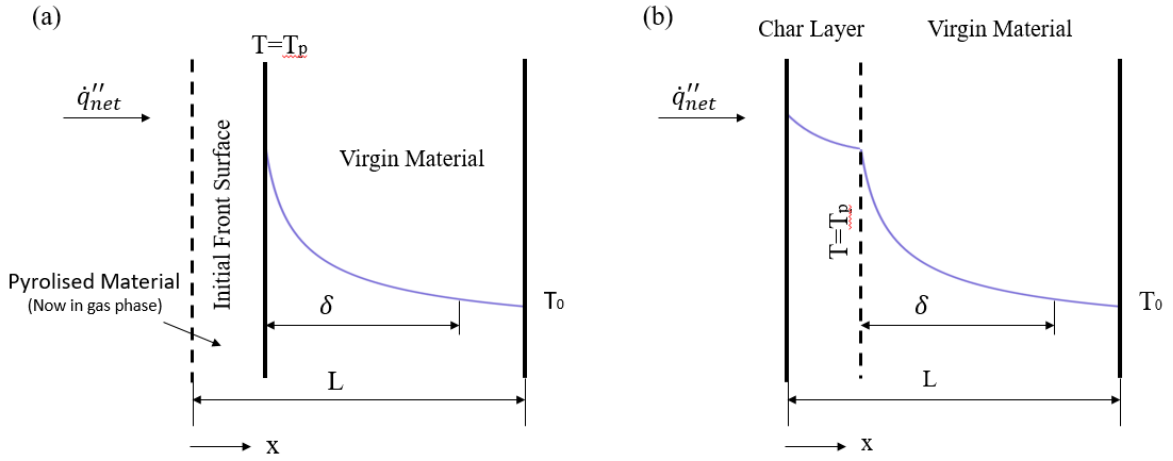

Figure 2.11 Assumption of combustible volatiles in Infinite rate models of thermal degradation

It has been found that when the boundary conditions are constant, these models function quite well. However, Moghtaderi[39] has found that when sudden increases in the external heat flux occurs, the temperature of the whole solid rose instantly and unreasonably. Such model is therefore not suitable for modelling realistic flame spread situation. Besides, since the temperature distribution in the solid is predefined (e.g., quadratic or exponential), the "infinite rate model" can at most only be applied to for the types of heating which results in the corresponding temperature profile. In realistic situations of flame spread, the external heat flux can vary with time due to the growth of flame, combustion conditions and other factors. A heating of this scenario can produce temperature profiles that differ from what was expected.

2.5.3 Pyrolysis models with finite rate

This type of models includes chemical kinetics to describe chemical reaction paths and intermediate species.[42-45]. Compared to infinite rate models, they attempt to reproduce more closely realistic behaviour of degradation in solids.

A solid's temperature rises when it is exposed to external heat flux. The material degrades as a result of the temperature increase; this process starts at the surface and moves deeper into the solid, releasing volatiles. When the temperature reaches a crucial level during the decomposition, virgin material is converted into char, or removes the material complete in the case of non-charring material after decomposing.

Usually, the process of the decomposition of material is described by one-step models [46, 47] :

$$virgin \xrightarrow{\Delta} char + pyrolysis\ gases \tag{2.2}$$

Most models use the assumption that the gases that are created inside the solid flow out instantly and without any obstacle out of the solid.

The pyrolysis processes happen at various temperatures, and an Arrhenius reaction of first order is often used to simulate them:

$$k = Ae^{-E/RT} \tag{2.3}$$

where k is the mass loss rate, A is the pre-exponential factor (s^{-1}), E is active energy (J/mol), T is the absolute temperature in K , and R is the molar gas constant (8.314 J/mol.K).

Applications of the above model include Di Blasi[48], Benkoussas[49], Nathasak Boonmee[50] and Lautenberger[51].

The overwhelming conclusion of these applications is that even the simple first order Arrhenius reaction is adequate for describing the decomposition of solid fuels in fire under variable boundary conditions. This model will be adopted in this research, but careful must be taken to assign the various constants in Eq. 2.3.

2.6 Approach for gas phase modelling

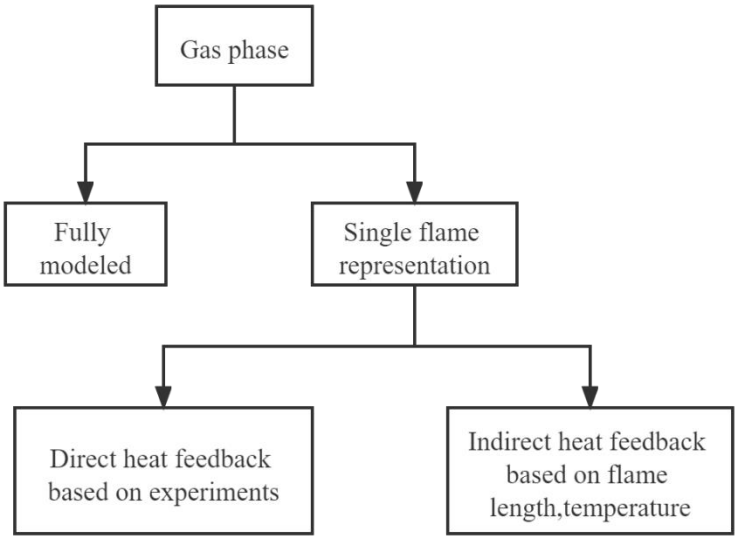

Figure 2.12 Classification of fire spread models for gas phase

Figure 2.12 summarises methods of modelling the gas phase in upward flame spread. Modelling every aspect (e.g., heat feedback, soot concentration, all modes of heat transfer) of the gas phase (fully model) has the potential to be most accurate, but this can usually only be done using time-consuming and complex computational fluid dynamics codes This is not within the scope of research of this research of developing a simplified model. Suffice to say that there are a number of very well established fire and flame spread models such as for the NIST Fire Dynamics Simulator (FDS)[52] and FireFOAM[53]. In such models, the computational cost associated with the necessity of resolving turbulent gas flow and radiation remains extremely high.

A flame representation can be used to represent the gas phase when it is not fully modelled, as in this research. The heat feedback from the gas phase to the solid was derived from experimental measurement or calculated by a simple flame model. In this case, the total heat release, flame shape, height, and temperature are utilised to calculate the flame feedback.

2.6.1 Direct heat feedback

Flames and gaseous phases aren't really necessary in this case. The solid's heat feedback is the only factor to be considered. The feedback of flames has been predicted based on experimental data or empirical correlations. In the zone under the flame, flame heat flux is frequently reported as constant[54, 55]. For the zone above the flame top, some assume an exponentially or power law decaying heat flux [56-60].

Azhakesan[54] conducted a rigorous analysis of the upper limits of heat flux level for typical combustible materials. The heat flux above the pyrolysis front is around $25\ \mathrm{kW}/m^2$. A constant value (30 kW/m^2) for heat flux is used by Delichatsios [55]. Heat flux beyond the flaming zone is assumed to be zero.

Quintiere[61] measured the heat flux from flame to wall surface. It was found that the total heat flux is approximately constant in the pyrolysis region, and falls as a power law. For a line fire, curve fits have been found as follows

$$\dot{q}_e'' = \begin{cases} 5.39\left(\frac{z}{z_f}\right)^{-2.41} & \frac{z}{z_f} \geq 0.53 \\ 23\,\frac{kw}{m^2} & \frac{z}{z_f} < 0.53 \end{cases} \tag{2.4}$$

Where z is the position in the wall, z_f is the flame height.

Back[60]conducted comprehensive experimental research to evaluate the heat flux from flame to the wall. Figure 2.13 depicts the heat flux data measured along the centreline of the wall. Peak heat fluxes were reported at the bottom of the flame ($0.4 \cdot z_f$). Heat fluxes over this location were shown to decrease with height from floor. The correlation of the data is found to be:

$$q'' = \begin{cases} q''_{peak} & z/z_f \leq 0.4 \\ q''_{peak} - \frac{5}{3}(z/z_f - \frac{2}{5})(\,q''_{peak} - 20) & 0.4 < z/z_f \leq 1.0 \\ 20(\,z/z_f)^{-5/3} & z/z_f > 1.0 \end{cases} \tag{2.5}$$

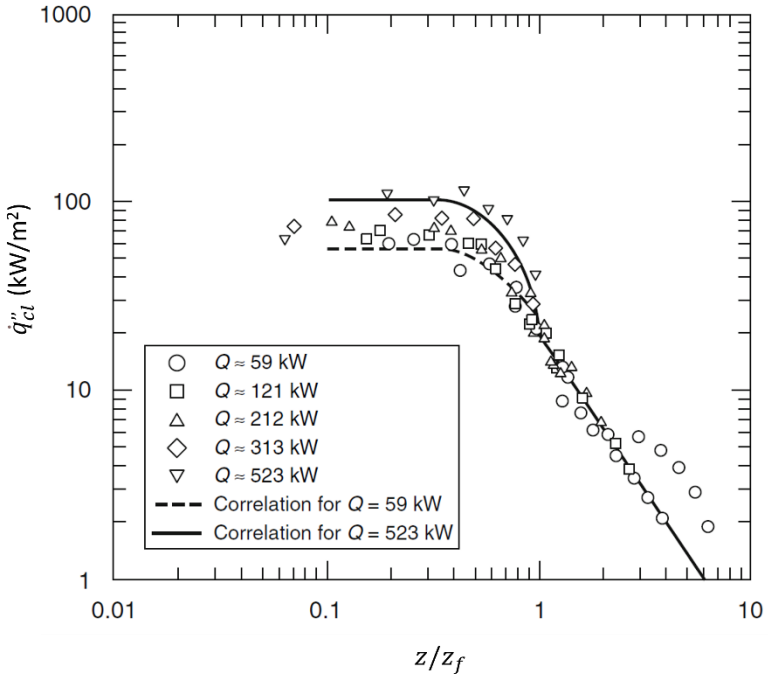

Figure 2.13 Vertical heat flux distribution alone the centreline[60]

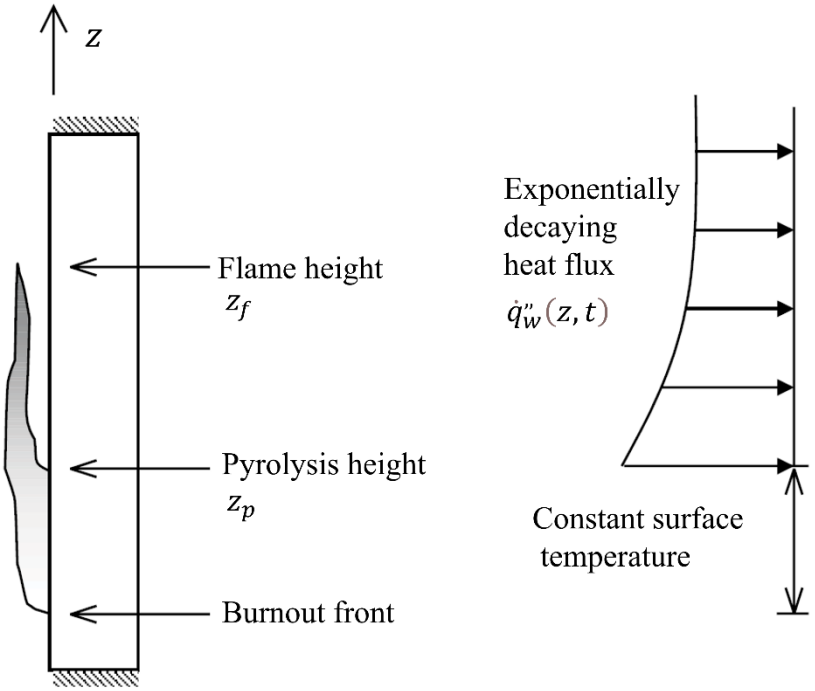

Figure 2.14 Boundary conditions for solid material[58]

Incorporating an exponential decaying function, Kulkarni[58] describe the total heat flux to the solid boundary as a function of height (see Figure 2.14 for definition of coordinates) as follows:

$$\dot{q}''_w(z,t) = \dot{q}''_{w0} exp\left(C_0 \frac{z-z_p}{z_f-z_p}\right) + \dot{q}''_{ext} - \dot{q}''_{rerad} \qquad (2.6)$$

where $\dot{q}''_{w0}$ is a material dependent constant. Eq. 2.6 is usually used for the heat boundary above the pyrolysis front. For the pyrolysis zone, the heat flux is assumed to be zero. The decay factor C_0 is -1.37.

The significant shortcoming to this experiment-based model is that the correlation depends on the material and initial heat flux. An improved, and more general model should be developed. This model is adapted from the indirect heat feedback system presented in the sub-section 2.6.2.

2.6.2 Indirect heat feedback

These types of models calculate the heat feedback from the gas phase to the solid boundary with a simplified flame representation. As an example, Van Hees' model [62] assumed a uniform temperature for flame, as shown in Figure 2.15. Chemical reactions are not considered. The sum of numerous heat fluxes gives the net incident heat flux.

$$\dot{q}''_{net} = \dot{q}''_{f,i} + \dot{q}''_{ext,i} + \dot{q}''_{conv,i} - \dot{q}''_{r,i} \tag{2.7}$$

where $\dot{q}''_{net}$ is the total net incident heat flux, $\dot{q}''_{f,i}$ is the radiation heat flux of the flame, $\dot{q}''_{ext,i}$ is the external heat flux, $\dot{q}''_{conv,i}$ is the convective heat flux, $\dot{q}''_{r,i}$ is the radiation heat losses

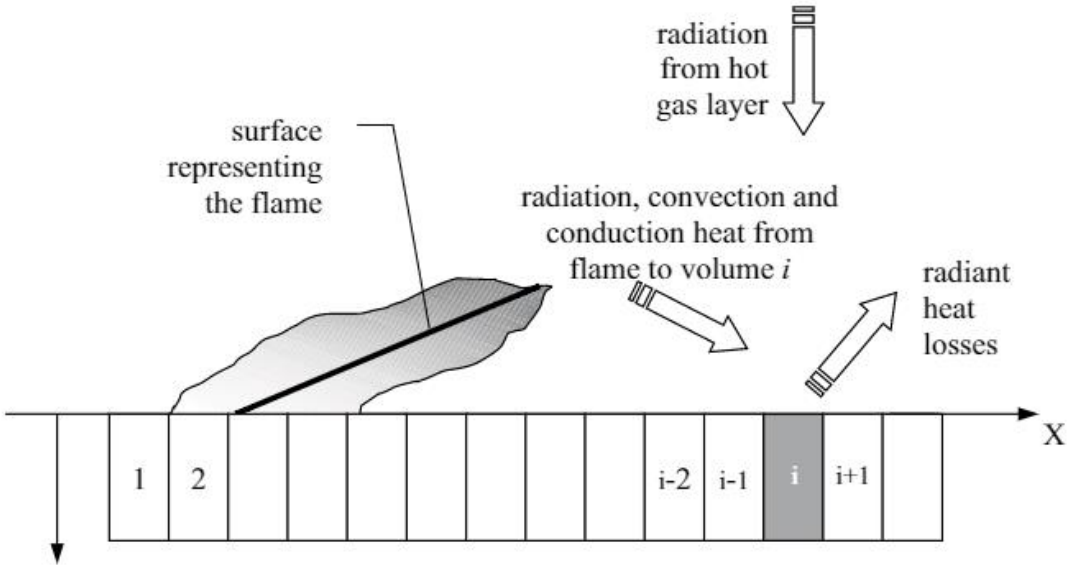

Figure 2.15 Heat fluxes for a solid volume

Chapter 3 will describe how this general method is implemented in this research.

2.7 Flame height correlation

In order to develop a simplified upward flame spread model, detailed gas phase behaviour is not modelled. This is feasible because upward flame spread is driven by heat flux in the vertical direction with little effect of diffusion in other directions. Therefore, this research will adopt an existing flame height correlation model. It is important that the flame height correlation model reflects the representation of flame (transient) and provides correct information for quantifying heat feedback to the boundary of the exposed cladding surface.

The following two subsections present an overview of flame correlation models on the external surface of cladding and within the cavity of cladding, as sketched in Figure 2.1.

2.7.1 Flame correlation models for external surface

Numerous experimental and analytical studies, investigating flame behaviour under both solid fuels and wall fire, have thus been performed to determine the height of external flames. In these research studies, rate of heat release is controlled by the gas burner and burning is steady state.

In general [63, 64], the flame height is correlated to the heat release rate of the fire through a power function as follows:

$$z_f = k\dot{Q}_l^{*n} \tag{2.8}$$

Where k is the constant, $\dot{Q}^* = \frac{\dot{Q}}{c\rho_0 T_0 g^{1/2} D^{5/2}}$ is the Froude number, D is diameter of the burner, and $\dot{Q}$ is the heat release rate.

The power "n" is different for different fire scenarios. The correlation of flame height for pool fire, presented by Heskestad[65], is expressed with n=2/5 as

$$z_f = 0.083\dot{Q}^{2/5}\text{-}1.02\ \text{D} \tag{2.9}$$

For the line wall fire, correlation for the flame height and dimensionless parameters have been developed by Delichatsios[66] and Hasemi[67]. They obtained

$$z_f = k\dot{Q}^{*n} \tag{2.10}$$

where z_f is the flame height, $\dot{Q}^* = \frac{\dot{Q}'}{c\rho_0 T_0 g^{1/2}}$ is the Froude number and k is a constant. They obtained a value of n=2/3. However, the empirical constant k has a value 6.0 in the model of Hasemi[67], while that was 5.6 in Delichatsios[66].

Tu and Quintiere[68] studied burning of PMMA samples and found that the flame height correlation also obeys the 2/3 power of Eq. 2.10 as for Delichatsios'[66], but a higher value of k=7.0 should be used.

All of the flame height correlation for wall fire follows the expression with n=2/3 as

$$z_f = \gamma\,(\dot{Q}')^{2/3} \tag{2.11}$$

The empirical constant γ varies from 0.052 by Delichatsios[66] to 0.066 by Tu and Quintiere[68]. This research will use the Eq. 2.11 with power "n" to be 2/3 but will check (1) which value of "γ" is more accurate, and (2) whether the equation based on steady state burning can be extended to transient burning which will happen when combustible materials are involved.

2.7.2 Burning in cavity

In ventilated cladding, if the flame gets inside the ventilation cavity, the flame height will be very large due to limited oxygen supply, as illustrated in Figures 2.1 and 2.3. This may have been the major cause of rapid flame spread in the Grenfell tower fire in 2017.

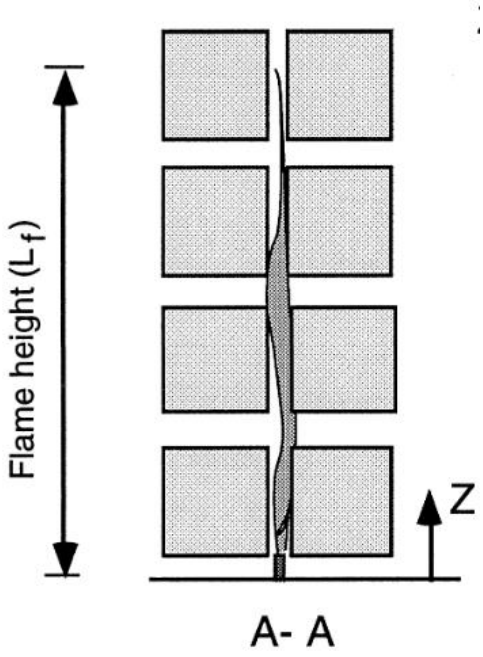

Figure 2.16 A 2-D rack storage with non-combustible material[69].

However, there is little systematic research has been carried out on effect of cavity on fire height. The scenario of rack storage fire is similar to that of cavity fire. Karlsson [70], Ingason

[69, 71], and Ingason and Ris [72] conducted experimental studies on rack storage mock-ups. They investigated the influence of burner release rate and distance between storage racks on flame height. They have found that the correlation is approximately linear, as expressed below after regression analysis:

$$z_f = 0.307 + 0.00095 \times (\frac{\dot{Q}'}{W}) \quad (2.12)$$

Where $\dot{Q}'$ is the rate of heat release per unit width and W is the width of the cavity.

In a more recent study, Livkiss [73] investigated the influence of cavity between two parallel facing walls on flame heights. The association between the flame height and cavity width was found to follow the linear correlation in Eq 2.12, as proposed by Ingason[69].

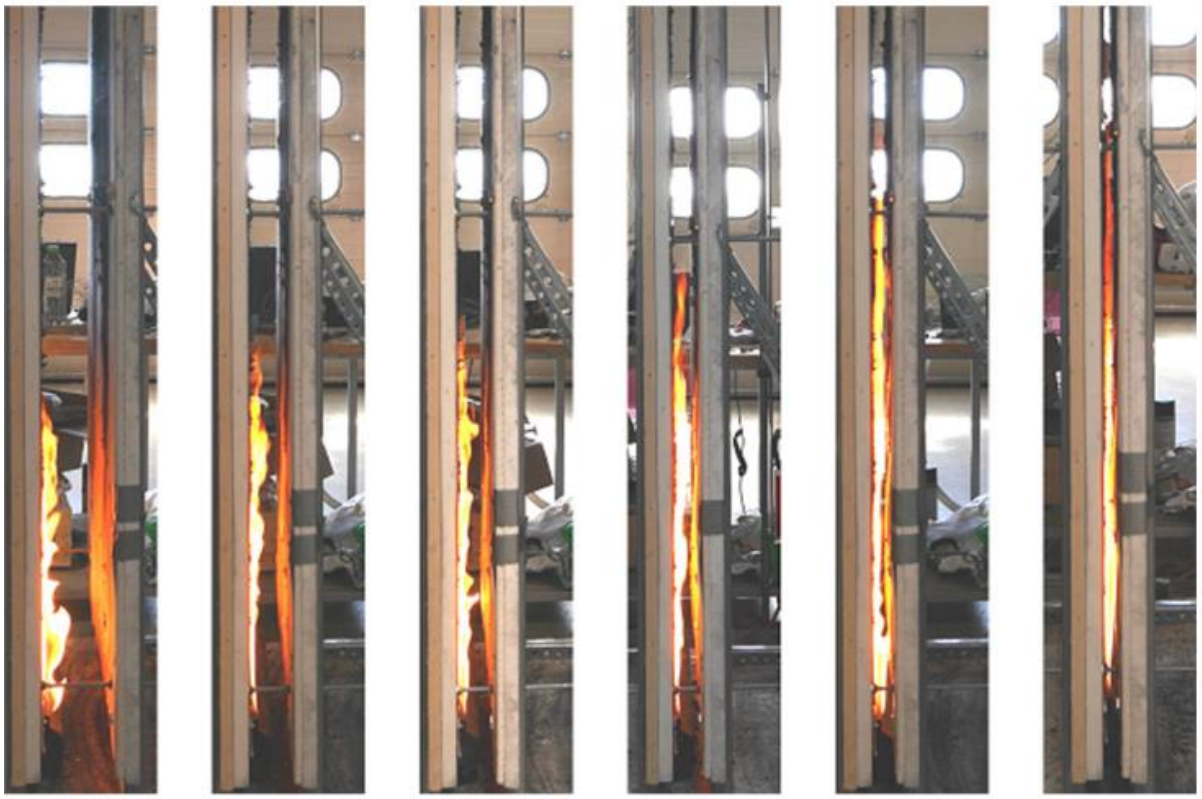

Figure 2.17 Flame height in two inert parallel facing plates[73]

2.8 Conclusion

This chapter presented a comprehensive review of the existing cladding systems, standard test methods, regulatory specifications for materials in cladding systems, and developments in modelling the solid and gas phases of combustion that are involved in upward flame spread.

Based on this review, it is possible to consider the following major components for the development of a simplified and efficient method for modelling upward flame spread over cladding:

- Arrhenius kinetic based pyrolysis model that computes solid phase reactions
- Indirect feedback model that predicts heat flux boundary as a function of the mass loss rate of the solid phase and flame height
- Two types of cladding system were identified: non-ventilated system and ventilated system

This review has also revealed a number of major issues in current regulatory specification of materials in cladding systems. These issues will be investigated in detail in Chapters 5 and 6 and include:

- *Limitations of the SBI Euroclass system*
  Currently, the small or mediate scale fire test (SBI) is used for classification material. The SBI test's reference scenario is a fire in a room. It is therefore not possible to evaluate the behaviour of the material product on its behaviour in the real external wall fire. However, The SBI based classification is rarely examined in full scale test, and its appropriateness is rarely questioned. Besides, since the SBI classification is based on one snapshot of material combustion behaviour, the same SBI classification may represent a variety of materials with different potentials of fire.
- *Appropriation of the new amended Building Regulation for England*
  Following the Grenfell fire, the latest edition of Approved Document B bans the use of combustible insulation. However, the requirement for the external surface remains unchanged as Class B. And there is no clear specification of the definition of the external surface. Furthermore, the USA and other countries allow composite insulation by using a flame spread index result and requiring a thickness for aluminium and steel coverings. The guidance in Approved Document B might prove too restrictive.

Chapter 3 Modelling of transient upward flame spread on combustible element

3.1. Introduction

There is an alarmingly high frequency of flame spread over the external cladding of residential buildings (e.g. Figure 3.1), and it has been attributed as the leading cause of fire growth over the height of the tower block in the tragic accident of the Grenfell fire in London on 14 June 2017 that claimed 72 lives[6]. This incident is having immense societal impacts in the UK. As a direct reaction and consequence to this event, no combustible materials are now allowed on the external cladding of residential buildings over 18m in height. Whilst this will no doubt make buildings safer from fire, this exclusion of any combustible materials in cladding is at an enormous cost to everyone in the UK: the astronomical cost of removing cladding containing combustible materials from existing buildings, misery to tenants and home owners who face financial ruin due to huge increases in home insurance cost and being unable to find a buyer for their properties to move on, and compromise on insulation performance of external walls. A more sensible approach should be employed so that the fire performance of cladding can be effectively assessed to ensure that fire safety is achieved even when combustible materials are contained in the cladding without excessive cost to society.

The current method of assessing the fire performance of cladding is through full-scale tests such as BS8414[4]. Full-scale fire tests are time consuming and very expensive. Also, since only a very small number of tests can be done, they cannot be made to cover the large range of cladding systems with an almost infinite choice of arrangement of construction details that may be used. While BS 9414[5] helps to extend the scope of applications of large-scale cladding fire tests, due to complexity of fire behaviour, it is not possible for BS 9414 to provide detailed quantitative information in many cases. Thus, should there be any variations in construction that cannot be dealt with by BS9414, even though they may be relatively minor, they may not be allowed if they have not been certified by testing. This inflexibility is detrimental to innovation, but may perversely lead to unsafe practice when unscrupulous suppliers try to cut

corners. Bench scale tests, e.g. cone calorimeter, can also be utilised as part of the toolkit to help assessing flame spread over cladding materials, but they typically can only provide qualitative response of material under constant heat flux level, such as ignition time and rate of heat release (RHR)[74]. They do not provide direct information for the assessment of fire risk of complex and full-scale cladding systems. Furthermore, without specialist knowledge and expertise, conflicting results may arise when extrapolating the results of bench scale tests to different fire scenarios.

Figure 3.1 Grenfell tower fire 2017[23]

As with other aspects of performance-based fire safety design, calculation methods may be used to complement fire test for the assessment of cladding/façade fire performance. However, existing calculation methods (e.g. Saito[75] or Sibulkin and Kim[63]) either can only offer very quick qualitative solutions due to their inherent limitations (such as constant heat flux boundary and flame height, and infinite-rate reaction kinetics) in applicability or rely on sophisticated CFD,. e.g. the NIST Fire Dynamics Simulator (FDS)[52], Gpyro[51], Nilsson, et al[76] and Anderson, et al[77]). CFD modelling is time-consuming, mainly due to the need for detailed evaluation of radiation.

An alternative calculation method that combines the flexibility and accuracy of CFD simulation tools with the simplicity and ease of use of analytical methods is desirable. This is the motivation of the research reported in this chapter. Fortunately, it is possible to develop such an efficient and accurate method to model upward flame spread on cladding as explained below.

As shown in Figure 3.1, upward fire spread is dominated by flow in the vertical direction with near uniform width and thickness in the other two directions. This enables drastically simplifying assumptions to be made thereby eliminating the need for complex CFD modelling of the gas phase and radiation. Instead of dividing the gas phase into numerous volumes and modelling each of them in details, this research will adapt analytical models of others for overall flame spread. Such analytical equations rely on input data of heat release rate, which can be dealt with by a sub-model of decomposition.

Therefore, by combining analytical solutions for the gas phase with simplified numerical modelling of pyrolysis of the solid element, it is possible to develop a simplified, efficient semi-analytical/semi-numerical model to accurately predict upward flame behaviour. This is the aim of this chapter. However, developing such a simplified and efficient upward flame spread model requires some assumptions and adaptation of existing analytical solutions beyond their original intended ranges of applicability. Therefore, an important part of this development is to ensure that the assumptions and the adaptations are acceptable. The following section describes the assumptions and adaptations that will be thoroughly checked in the main part of this chapter.

3.2. Main components and assumptions

Figure 3.2 shows a sketch of the upward flame spread scenario. Whilst the flame is assumed to have uniform properties, the solid materials of the wall will have non-uniform properties along the height and in the thickness direction. However, across the width of the wall, it is assumed that the properties are uniform. Therefore, along the height of the wall (z-direction in Figure2), the surface is divided into four regions and each of which into a large number of nodes (Figure 3.2.), each having different thermal boundary conditions. In theory, due to non-uniform temperature distribution along the height of the wall (z-direction), heat and mass transfer occurs in this direction, as well as in the thickness direction of the wall. However, it is assumed heat and mass transfer in the vertical direction is weak within each region. At the transition positions from one region to another, mass and heat transfer can be high, but these positions have a very

small amount of space. Therefore, in the model, it is assumed that heat and mass transfer occur only in the thickness (x) direction. This allows considerable simplification to be made in the model, but this simplifying assumption will be checked.

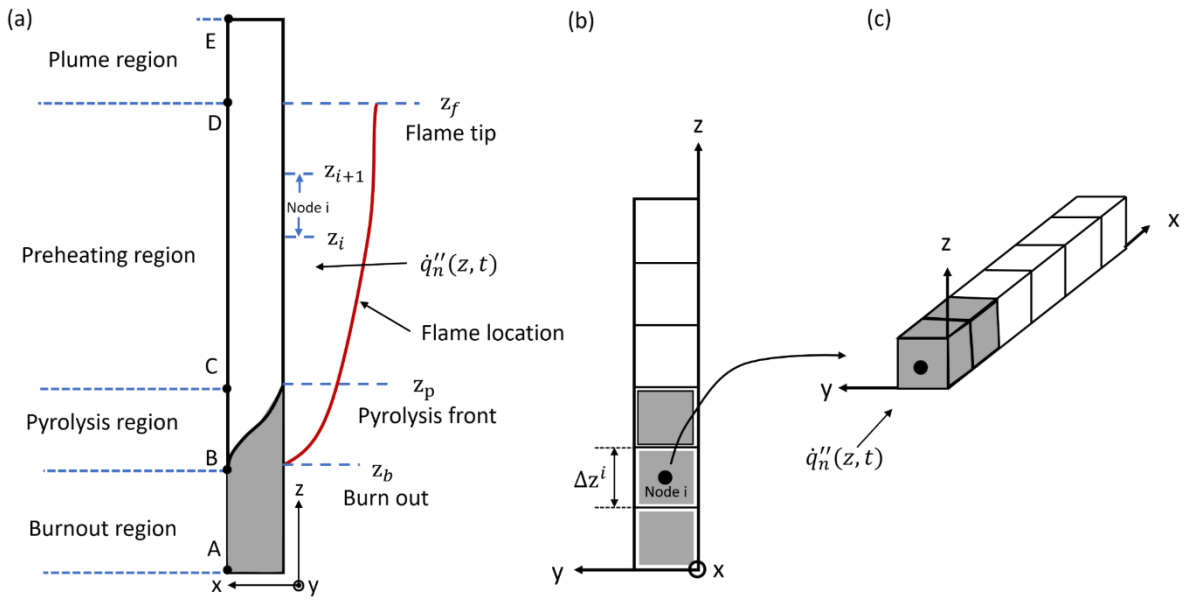

Figure 3.2 Schematic view of the model (a) Seen in the x-z (thickness-height) plane, (b) Seen in the y-z (width-height plane), (c) An arbitrary section in the thickness direction.

As previously mentioned, analytical solutions of flame spread will be used in this model to calculate the overall properties (dimensions, temperature) of the flame. These models provide steady state solutions of flame properties. They will be applied to generate transient flame properties and this extrapolation will be checked later. The analytical solutions of flame spread require input data of the heat release rate of fire. This data will be computed based on the aforementioned 1D heat and mass transfer model which will calculate the production of gaseous volatiles from the different nodes of the surface. The gaseous volatiles are then instantaneously combusted to generate heat. The following section will provide details of how these assumptions are implemented.

3.3. Details of the simplified model and implementation

3.3.1 Scope of simplified model

Modelling combustion in fire is complex, therefore, different assumptions are made by different modellers depending on the scope of their research. In general, modelling gas/gas and gas/solid reactions is the most difficult and time-consuming aspect of modelling fire dynamics. Thus, for example, Lautenberger et al.'s model (Gpyro)[51] is general and includes heterogeneous gas/solid reactions and homogeneous gas/gas reactions. In contrast, the aim of this research is to develop a simplified method to model the specific situation of vertical fire spread on vertical element. Fortunately, many fundamental research studies have been carried out on the subject of vertical fire spread which have resulted in analytical solutions to obtain flame size and temperature under steady state condition. The fundamental work by Delichatsios[66] demonstrated that flame height was independent of stoichiometry and was a power function of heat release rate as expressed by $Z_f/D = k(\dot{Q}_l'^*)^n$. More recent observations from experiments on gaseous wall line burners[78] and vertical samples of solid PMMA[79, 80] further confirm this relationship. The recent theoretical work of Ren et al. [81] gives a value of 2/3 for power "n" in the above expression. However there is some uncertainty about the value of constant "k" in the above expression, which has been found to vary from 0.052[66] to 0.066[68]. In this research, efforts are made to identify the best analytical model (sections 3.3.2-3.3.4) for quantifying flame size and heat flux, rather than explicitly modelling gas and gas/solid phase combustion behaviour.

3.3.2 Instantaneous Flame Heights

Numerous research studies[31, 66], based on experimental work, have been performed to develop analytical solutions of steady state flame height – heat release rate relation. The flame heights under steady-state burning have been shown to depend only on the heat release rate per unit wall width, $\dot{Q}_l'$. For a line fire that describes the fire source of this research, Eq.(3.1) is used:

$$Z_f = k\dot{Q}_l'^{2/3} \tag{3.1}$$

where Z_f is the flame height, k is a constant and $\dot{Q}_l'$ is the rate of heat release (RHR) per unit width of the fire. The experiments conducted by Delichatsios[55] for gaseous line/wall-fire burners suggest a value of k=0.052. For vertical combustible wall fires, Tu and Quintiere[68] give a value $k = 0.066$.

In order to verify which of the above values is to be used in this research, a series of numerical simulations have been conducted by using the widely used Fire Dynamics Simulator (FDS) to

simulate flame spread on a non-combustible wall exposed to a gaseous burner of different constant heat release rates. Figure 3.3 shows the simulation model, based on the wall fire experiment of Coutin [82]. The computational domain is set at 1m×1.2m×2.9m in the x, y, z dimensions (z is the vertical dimension). A mesh resolution $D^*/\Delta x$ =10 is considered adequate [83]. Therefore, based on the expected RHR, a mesh grid size of 1cm is used. Open boundary conditions were applied at all domain boundaries, except for the wall that had adiabatic boundary. A 0.5m height and 0.4 m wide methane gas burner was located at the bottom centre of the wall as shown in Figure 3.3. The methane fuel is defined by chemical formula C_1H_4 with CO yield of $y_{co} = 0.01$ [84]. The recorded heat release rate of the burner was directly used as input so as to avoid any uncertainty about combustion.

In FDS, flame height is defined according to the percentage of fuel consumption. McGrattan[85] examined the effects of using 99% and 95% and found that flame heights based on the 95% value would give flame heights shorter by 15-25%. Therefore, in this research, the flame height is defined as the distance above the pan at which 99% of the fuel has been consumed.

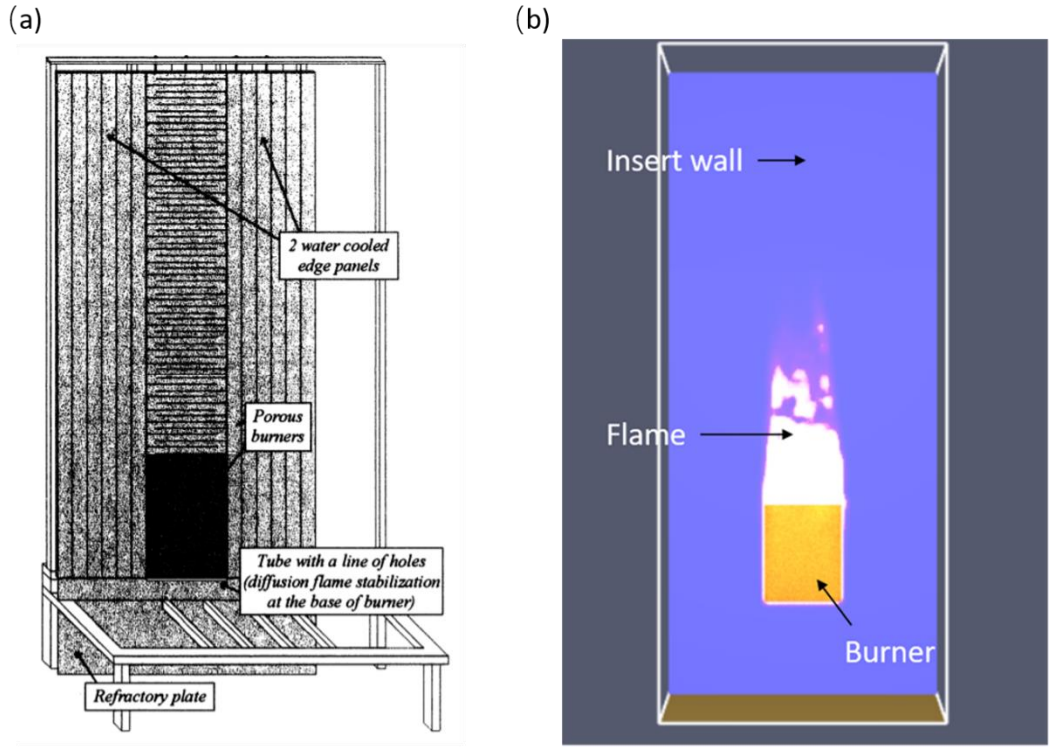

Figure 3.3 (a) Experimental setup, and (b) Computational domain in FDS for simulation of a wall fire

Figure 3.4 compares results of steady state flame height-heat release rate relations, between FDS simulation, and analytical solutions using Delichatsios[66] and Tu and Quintiere[68]

correlations. The results show that the Tu and Quintiere's correlation gives more accurate predictions than then Delichatsios correlation. The Tu and Quinteire correlation will be adopted in this research.

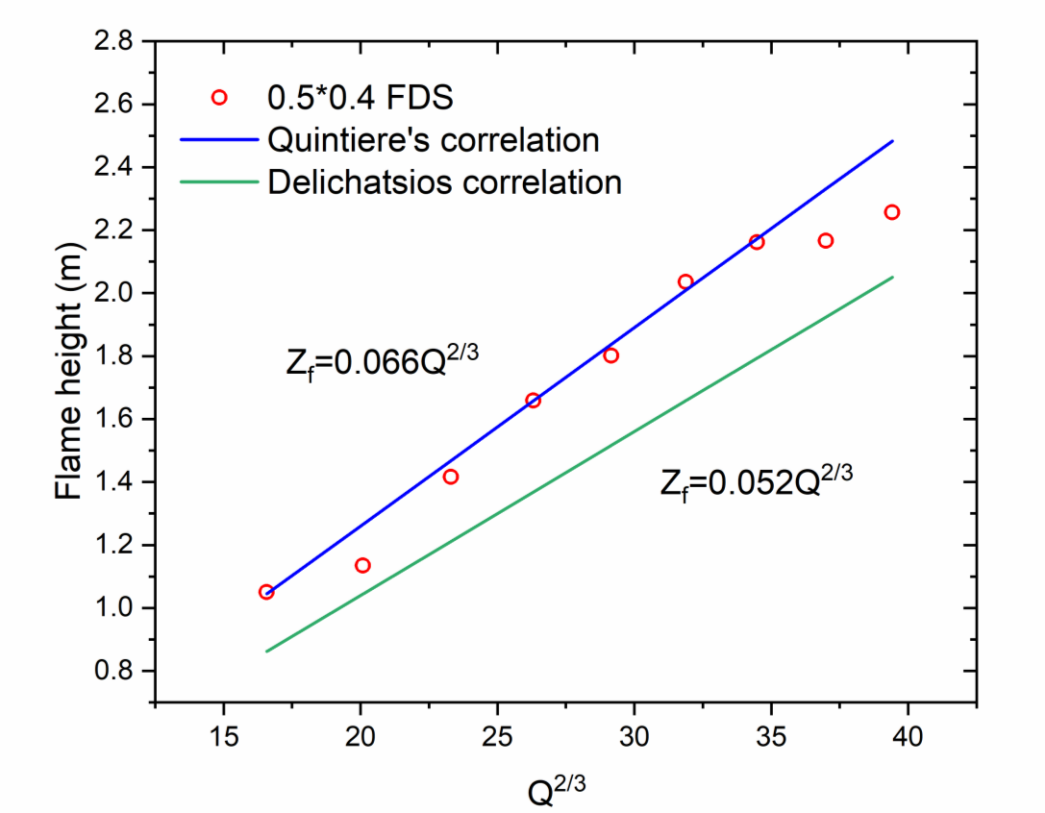

Figure 3.4 Comparison of two steady state flame height – heat release rate correlations with FDS simulations

In upward flame spread over combustible element, the process is transient with variable rate of heat release (RHR). In this research, the above steady state flame height-RHR relationship is extrapolated to the transient situation using the RHR-time history as input. The time dependent RHR is then directly used in the steady state flame height-RHR equation of Tu and Quintiere [68], which implies that the steady state condition is reached instantaneously. For validation, this assumption is checked by comparison against the following transient state FDS simulation results.

The FDS simulations are for variable flame heights under a number of T-squared fires ($\dot{Q} = \alpha t^2$). The T-squared fires have ultra-fast, fast and medium growth fire growth rates until a maximum RHR of 50 kW. Figure 3.3 shows the simulation model, based on the wall fire experiment of Coutin [82]. Figure 3.5 compares for the transient flame height-time

relationships between FDS simulation results and extrapolating the Tu and Quintiere [68] analytical solution. The results confirm near instantaneous change in flame height with changing RHR so that the steady state flame height-RHR equation of Tu and Quintiere [68] can be directly applied to quantify transient flame height-variable RHR relation.

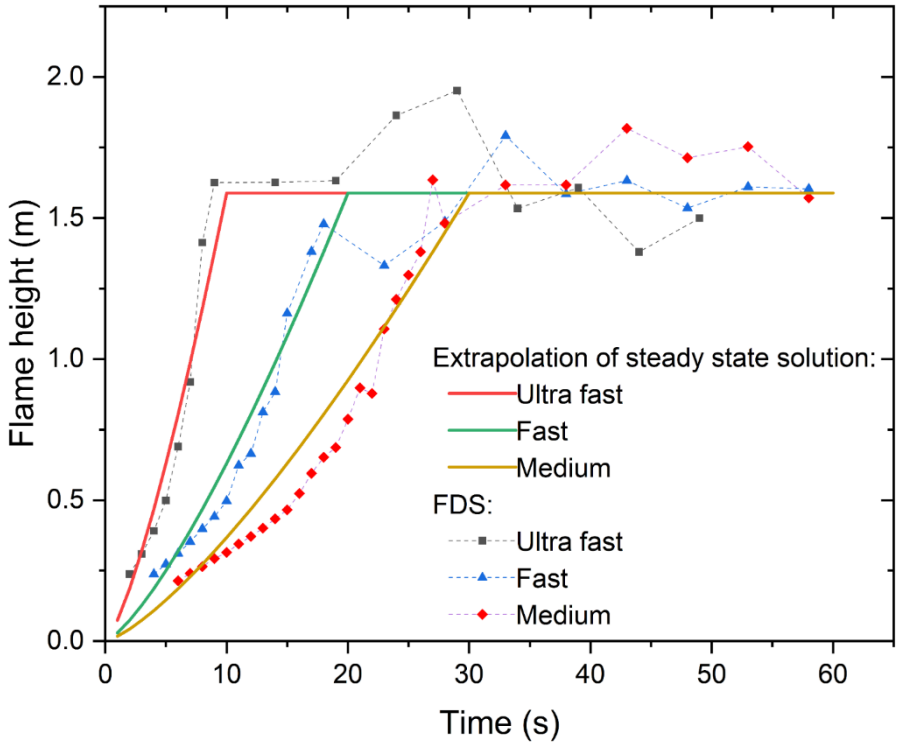

Figure 3.5 Comparison of transient flame height between FDS simulation and extrapolation of the steady state analytical solution of Tu and Quintiere [68]

3.3.3 Flame Heat Feedback

In order to determine boundary of the vertical element surface to compute decomposition of the material and hence the transient heat release rate, it is necessary to know the heat flux from flame to the vertical wall.

The simplest assumption is that the heat flux is constant between the burnout front and the flame tip (position B in Figure 3.2, and position D in Figure 3.2), and zero above[34, 75]. However, this crude assumption may lead to grossly inaccurate results. A more refined, yet simple, method is necessary.

The heat flux from the flame/plume to the vertical element is the sum of convective fluxes $\dot{q}''_{conv,i}$ and radiative fluxes $\dot{q}''_{f,i}$. Methods of their calculations are presented as follows.

3.3.1 Convective flux

3.3.1.1 Pyrolysis region

During pyrolysis of the solid, mass transfer of the surface generates a blowing velocity that alters the thermal and momentum boundary layers, thus affecting the heat and mass transfer coefficients. Therefore, in the pyrolysis region (between positions B and C in Figure 3.2), to account for the effects of mass flow on convective heat transfer, and due to the difficulty of reliably calculating the flame temperature, the convective flux is calculated as follows [86].

$$\dot{q}''_{conv,i} = \frac{\dot{m}''_i B^{'} H_v}{\exp(\dot{m}''_i C_p/h)-1} \tag{3.2}$$

where h is the heat transfer coefficient in W/(m^2•K), C_p the specific heat of gas in J/(kg·K), H_v is the heat of vaporization in kJ/kg, $B^{'}$ is the dimensionless Spalding mass transfer potential and $\dot{m}''_i$ is the mass pyrolysis rate per unit area in kg/m^2.

In CFD modelling, e.g. FDS, the heat transfer coefficient is determined by the maximum value of three correlations as functions of surface temperature, fluid velocity in the gas phase and gas phase cell size [87]. This is a complex process. In this research, since the focus of is vertical plate in natural convection condition, it is possible to use the following much simpler correlation [88]:

$$h = 76.0 \cdot T_f^{-0.66} \cdot \left|T_{s,i} - T_g\right|^{1/3} \tag{3.3}$$

where T_f is the average of the surface and ambient temperature in K, $T_{s,i}$ the surface temperature and T_g is the air temperature.

The equation for the Spalding mass transfer number[86, 89] is

$$B = [SH_c - C_p(T_{s,i} - T_g)]/H_v \tag{3.4}$$

where, S is mass stoichiometric fuel to air ratio, H_c is the heat of combustion of the fuel in kJ/kg, T_g is the ambient gas temperature and $T_{s,i}$ is the temperature of the surface. The first term is the increase in internal energy of a unit weight of the air/fuel mixture in combustion. If combustion is incomplete, and there is energy loss from the combustion zone via radiation as well, then the H_c should be replaced by the following equivalent value of H_c'

$$H_c' = (x_A - x_R)H_c \tag{3.5}$$

where x_A is the combustion efficiency coefficient and x_R is the fraction of the fire's heat release rate lost due to thermal radiation. The values of x_A and x_R for various pure fuels are based on measurements by Beyler[90] and Tewarson[91].

3.3.1.2 Preheating region

In the preheating and plume region (above position C in Figure 3.2), there is no mass movement, therefore, the convective heat flux to the wall is

$$\dot{q}''_{conv,i} = h \cdot (T_{p,i} - T_{s,i}) \tag{3.6}$$

where $T_{p,i}$ is the plume temperature, $T_{s,i}$ the wall surface temperature and the h is the convective heat transfer coefficient given by Eq. (3.3).

According to Ahmad and Faeth[32], the plume temperature $T_{g,i}$ (in K) can be approximately calculated according to the following equation:

$$T_{g,i} = 298 + 1113\exp\left[-0.636\left(z/z_f\right)^2\right] \tag{3.7}$$

where z_f represents flame height.

3.3.2 Radiative Flux

The flame temperature cannot be reliably calculated in large-scale fires. Because radiative flux is T^4 dependent, an alternative method of accurate calculation of radiative flux is needed[85]. A practical alternative is to specify explicitly the proportion of the total heat that is released in the form of radiation and the distribution of radiative flux along the height. Studies by Hasemi[67] for line burner fires with RHR ranging from 16.7 to 218.2 kW/m against wall and Quintiere's [92] for steady burning of vertical walls made of a variety of materials have concluded (i) the radiative flux for flat wall fires is a function of the normalized height (ratio of wall height to flame height) ; (ii) radiative flux distributions are nearly the same regardless of materials. The large-scale fire tests of Orloff 's [31, 93] indicate that the flux peak lies at the pyrolysis front. Kulkarni[58] and Brehob[57] found an exponential fall-off for the tail of the distribution. Therefore, the radiative flux increases monotonically up to a maximum at z_u and then stays constant thereafter up to the pyrolysis front (z_p) (position B in Figure 3.2). The exponential fall-off can be obtained from the correlation according to [57, 58]. Thus, the radiative flux model can be formulated as

$$\dot{q}''_{f,i} = \begin{cases} \lambda x\,, & 0 \le z < z_u \\ \phi_p\,, & z_u \le z < z_p \\ \phi_p \exp\left[-v\left(z - z_p\right)\right], & z_p \le z \end{cases} \tag{3.8}$$

where $\lambda = 164\chi_R$ kW/m^3 and χ_R is the fraction of energy lost by radiation.

The maximum flux ϕ_p and the value of z_u are needed to find $\dot{q}''_{f,i}$. This is done as follows.

Noting that the radiation flux at the flame tip (the 50% intermittence point) is about 25% of what it is at the peak[94], the value of v in Eq. (3.8) can be obtained as:

$$v = \ln 4 / \left(z_f - z_p\right) \tag{3.9}$$

Whatever distribution is chosen for the radiation flux, it must satisfy a simple symmetry condition: half of the flame flux moves away from the wall and half towards the wall [55]. Therefore, the instantaneous total radiant heat release to the wall is:

$$\int_0^\infty \dot{q}''_{f,i}(z)\,dz = \chi_R \dot{Q}'/2 \tag{3.10}$$

where $\dot{Q}'$ is the total heat release rate.

Finally, the value of z_u is given by substituting Eq. (3.8) in Eq. (3.9)

$$z_u = 0.5\left[D - \sqrt{D^2 - 4\chi_R \dot{Q}'/\lambda}\right] \tag{3.11}$$

where $D = 2(z_p + \left(z_f - z_p\right)/\ln 4)$.

The first expression in Eq. (3.8) must be ϕ_p, at $z = z_u$. Hence, ϕ_p is given by

$$\phi_p = \lambda z_u \tag{3.12}$$

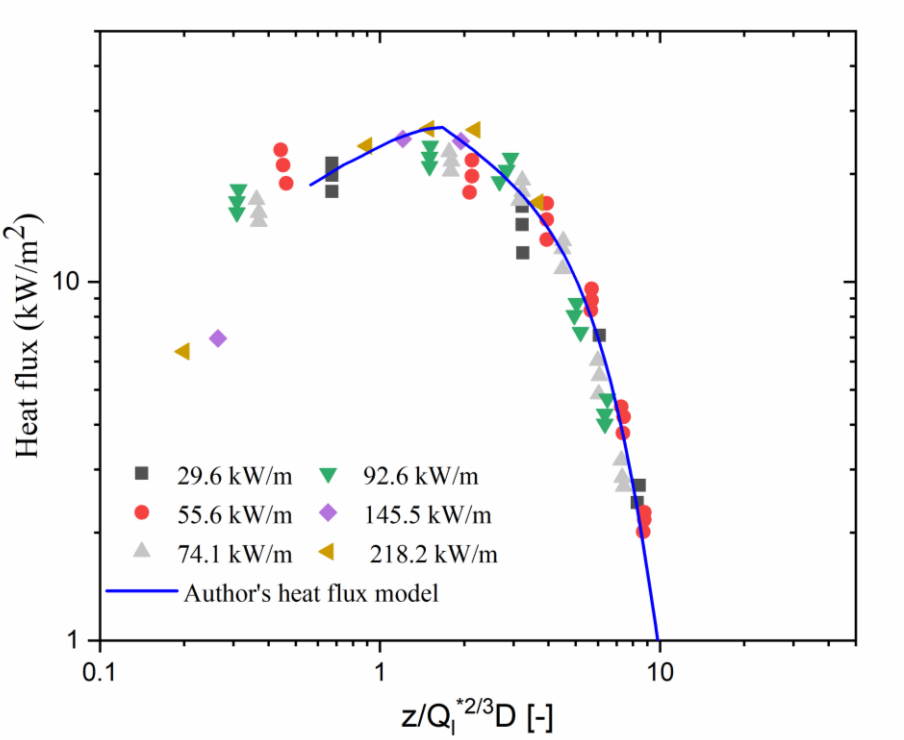

Figure 3.6 Heat flux to wall plotted against the dimensionless height[67]

To demonstrate validity of this analytical method, calculation results using this method are compared with measured radiative heat flux reported by Hasemi [67]. In their experiments, the rate of heat release per unit width of the line burner varied between 16.7 and 218.2 kW/m. Their recorded heat flux distributions along the dimensionless height from the line burner against the flat wall are shown in Figure 3.6 and are compared with the above analytical method proposed by the authors. The agreement between the calculation and measured results is very good for all RHR values.

3.3.4 Solid pyrolysis submodel

Due to high heat flux of flame on the surface of façade, heat transfer in the solid may be assumed to be one dimensional in the thickness direction. This assumption will be validated in this section.

During pyrolysis, reactants are continuously transformed from the virgin material into various solid species and gaseous products, according to the following general equation:

$$Solid1 \xrightarrow{k_j} \theta Solid2 + (1-\theta)Gas1 \tag{3.13}$$

The stoichiometry of reactions is expressed on a mass basis. The thermal decomposition scheme follows 1st order Arrhenius reaction:

$$\Theta_i = \sum_j \theta_j k_j \rho_j^{n_j}, \; k_j = A_j exp\left(-\frac{E_j}{RT}\right) \tag{3.14}$$

in which where k is the mass loss rate, A is the pre-exponential factor (s^{-1}), E is active energy (kJ/mol), T is the absolute temperature in K ,and R is the molar gas constant

As explained in section 3.1, gas/gas phase reactions and gas/solid phase reactions are not explicitly modelled in this research. Therefore, the energy conservation equation for pyrolysis of the material is described as[51]:

$$\sum_{i=1}^{N_s+N_g} \frac{\partial \rho_i \emptyset_j C_{p,i} T}{\partial t} + \sum_{j=1}^{N_g} \frac{\partial \rho_j \emptyset_j C_{p,i} T u_j}{\partial x} = \frac{\partial}{\partial x}\left(\lambda \frac{\partial T}{\partial x}\right) + Q_{reac} + Q_{rad} \tag{3.15}$$

And Eq. (3.16) and Eq. (3.17) are mass conservations for solid and gas species, respectively.

$$\frac{\partial \rho_i}{\partial t} = \Theta_i \tag{3.16}$$

$$\frac{\partial \rho_g \phi}{\partial t} + \frac{\partial \rho_g \phi u}{\partial x} = -\Theta_i \tag{3.17}$$

The first term on the left-hand side of Eq. (3.15) is the absorbed heat for heating up the material ($Q = mC_p dT$), which can either be solid (s) and gas (g) ,the second term is the heat taken away by gas species. The first term on the right-hand side of Eq. (3.15) is the heat into the material by conduction; the second term is the reaction heat Q_{reac}, which is given by Eq. (3.19), and the last term is the in-depth radiation heat (radiative heat flux that penetrates through the surface of the material) Q_{rad} , to be defined by Eq. (3.20). The symbols in Eq. (3.15) are defined as follows: ρ: density (kg m^{-3}); $\emptyset$: porosity; C_p : specific heat capacity (J kg^{-1} k^{-1}); T:temperature (K); t: time (s); u : velocity (m s^{-1}); x Cartesian coordinate (m); N_s and N_g are the numbers of solid and gas species.; and λ: thermal conductivity, (W m^{-1} K^{-1}).

The transfer of volatile is supposed to follow Darcy's Law [95] as

$$m = -\frac{\gamma_g}{\mu_g}\frac{\partial P}{\partial x} \tag{3.18}$$

where γ_g is the gas permeability in m^2, μ_g is the dynamic viscosity in Pa.s, and pressure P can be calculated by the ideal gas law($P = \frac{\rho_g RT}{M}$).

The heat produced or absorbed by pyrolysis processes is referred to as

$$Q_{\text{reac}} = \sum_{i=1}^{N_R} (\Delta h_i) k_i \tag{3.19}$$

where Δh_i is the heat of reaction, N_R is the number of reactions.

Due to opaqueness, it is not necessary to consider the influence of in-depth absorption of radiation on burning of charring materials. However, in-depth absorption of radiation has been reported to have considerable effects on the burning behavior of non-charring materials such PMMA[96, 97]. As combustion of PMMA is used for validation of author's model, in-depth absorption of radiation is included in this research. For wood, the absorption coefficient can be specified as ∞.

Absorption of radiation inside the solid can be expressed by the Beer-Lambert law as follows:

$$\dot{q}''_{rad} = f \exp(-\kappa x) \tag{3.20}$$

where f is the radiative heat flux that penetrates the surface of the material in kW m^{-2}; and κ is the absorption coefficient in m^{-1}.

The densities of the solid were supposed to remain constant at various temperature. The breadth of the control volume was considered to be proportional to the volume of the virgin material and its products:

$$\Delta x = \Delta x_0 \sum_{i=1}^{N_s} \frac{\rho_i}{\rho_{i,0}} \tag{3.21}$$

The sum of control volume widths was used to compute the transient thickness of the solid:

$$L = \sum_{i=1}^{M} \Delta x_i \tag{3.22}$$

3.4.1 Validation of 1D heat transfer assumption

To validate the 1D heat transfer assumption, results of 1D heat transfer using the authors' simplified model were compared with 2D simulation results for a solid element subjected to 2D heat flux boundary condition as depicted in Figure 3.7. The solid element has a thickness of $l = 100\ mm$ and the height is $h = 1.0\ m$. The comparison is carried out for two materials at the two-opposing spectrum of heat transfer, steel (non-combustible and fast heat transfer) and PMMA (slow heat transfer and combustible). The 2D simulation of heat transfer in steel and PMMA is performed by commercial software ANSYS and FDS (HT3D), respectively.

Figure 3.7 shows the 2D heat transfer model in ANSYS simulation. The height and thickness of the element are 1000mm and 100 mm respectively. Quadrilateral elements of mesh size 2mm×2mm were used. An exponentially decaying heat flux along the height ($\dot{q}''_{net} = 30 * e^{-1.733 \cdot z}$ kW/m^2) was applied to the front edge of the element and the other edges of the element were assumed to be insulated. The initial temperature was 293.15k.

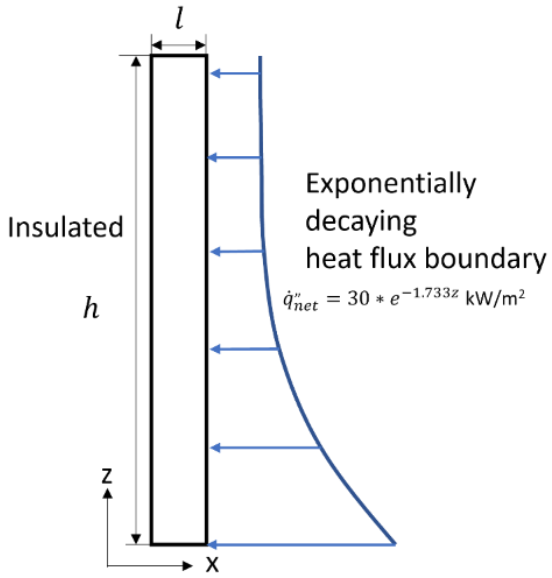

Figure 3.7 Boundary conditions for heat transfer inside a solid material

In the authors' FDS model, the mesh size of the computational domain was 0.2mx0.1mx1m, which was divided into 1x1x1 cm numerical grid cells. Inside the solid, the grid size was automatically chosen according to the FDS user guide[52] . The material's surface was exposed to a specified heat flux while its back side was assumed to be insulated. Since only solid heat transfer was considered in this section, the gas phase computation was turned off to speed up simulation.

Tables 3.1-4 list the various material properties used in the simulations and their sources. For steel, there is no combustion and Table 3.1 lists the solid phase properties. For PMMA, three condensed phase species were considered in the simulations: PMMA, bPMMA (melted PMMA) and char. Tables 3.2 and 3.3 list the relevant properties of the condensed species and gaseous species respectively. A two-step reaction mechanism, as shown in Eqs. 3.23 and 3.24, is assumed with the associated kinetic values in Table 3.4.

$$PMMA \rightarrow bPMMA \tag{3.23}$$

$$bPMMA \rightarrow 0.015Char + 0.975Pyrolysis\ gases \tag{3.24}$$

Table 3.1 Condensed phase parameters for steel

Material	Density Kg/m^3	Cond. W/(m k)	Spec. Heat kJ/(kg k)	Emissivity	Absorption coefficient
STEEL, plain	7854[98]	60.5[98]	434[98]	0.85[98]	∞ [98]

Table 3.2 Condensed phase parameters for PMMA

Property	Density (kg/m³)	Cond. (W/(m·K))	Spec. Heat (kJ/(kg·K))	Emissivity	Absorption coefficient	Gas permeability (m^2/(s Pa))
PMMA	1100[99]	0.16[99]	1.5[99]	0.95[96]	960[96]	5.80×10^{-18}[100]
bPMMA	1000[99]	0.21[99]	2.2[99]	0.95[96]	960[96]	5.80×10^{-16}[100]
Char	1100[99]	0.21[99]	2.2[99]	0.95[96]	0.1[96]	5.80×10^{-16}[100]

Table 3.3 Gas phase parameters for simulation

Name	Cond. (W/(m·K))	Spec. Heat (kJ/(kg·K))	Dynamic viscosity (Pa·s)
Gas	0.03[101]	1.0[102]	0.96[103]

Table 3.4 Reaction parameters for PMMA

From	To	Pre-Exp. Factor (1/s)	Act. Energy (kJ/kmol)	Heat of Reac. (kJ/kg)	Residue Frac.
PMMA	bPMMA	2.8×10^{47}[104]	366.2[104]	0[105]	1[85]
bPMMA	Char	8.6×10^{12}[99]	188.0[99]	846[105]	0.015[85]

PMMA is a non-charring material that burn cleanly. To avoid empty grid when the material is completely burnt off, it is assumed there is a very small amount of char left. The density of char in modelling was taken as the same as that of PMMA.

Since it is the pyrolysis gases release during the pyrolysis reaction that drive the combustion process, when validating the assumption of 1D heat and mass transfer, both temperature-time history and total rate of mass loss evolution should be compared with results of 2D heat and mass transfer simulation. The comparisons are presented in Figure 3.8 and Figure 3.9 respectively.

The results in Figure 3.8 indicate that the 2D and 1D simulations give almost identical results, even though the surface heat flux distribution (Figure 3.7) along the height has a substantial

gradient. Figure 3.9 confirms that the 1D and 2D results of mass loss are very close with a maximum difference of 1.1%. The above comparisons confirm that any vertical heat conduction in the solid is negligibly small, and it is acceptable to treat the solid phase heat and mass transfer in the vertical wall problem as one-dimensional.

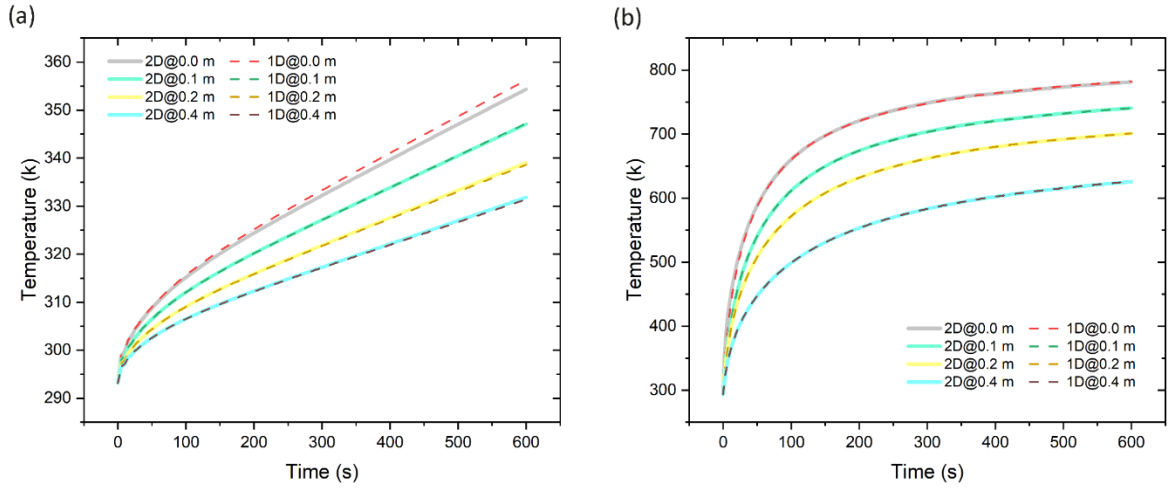

Figure 3.8 Comparison of surface temperatures between 1D and 2D simulation results for (a) Steel and (b) PMMA

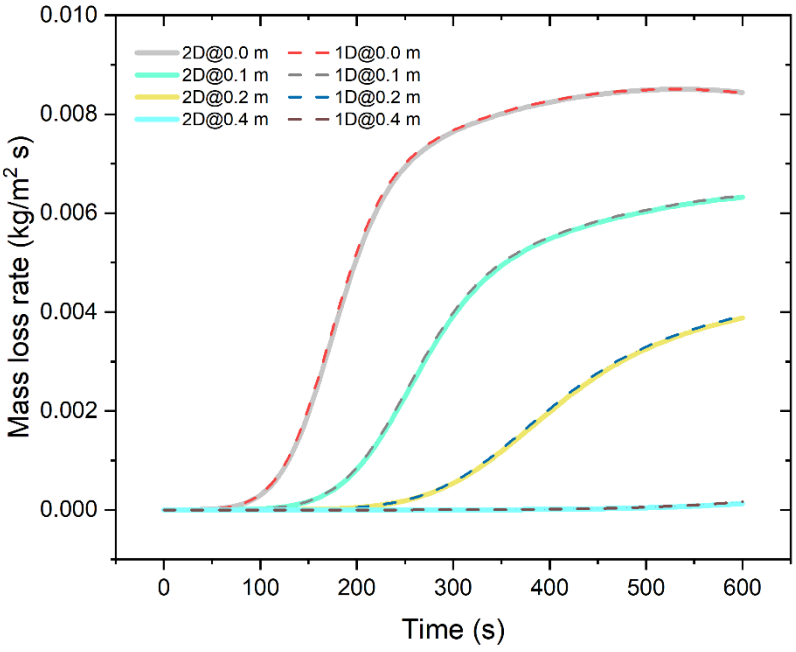

Figure 3.9 Comparison of the 1D and 2D mass loss rate calculations

3.3.5 Implementation procedure

Figure 3.10 shows a general flowchart of the simulation model. At each time step, the flame size is updated. This results in a new set of thermal boundary conditions on the surface, which then leads to updated mass decomposition (if combustible materials are used) and temperatures inside the solid materials. The combined 1-dimensional heat and mass transfer requires numerical solution of a set of nonlinear partial differential equations for which a fully implicit finite difference method is employed.

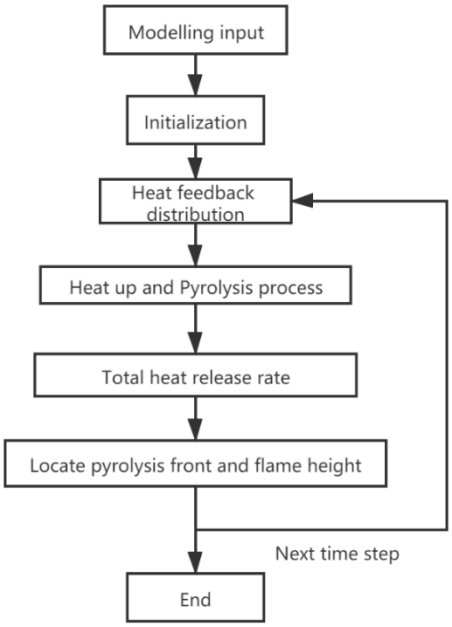

Figure 3.10 Flow chart: solution procedure for upward flame spread

3.4 Validation and application examples

To demonstrate and validate different features of the proposed method, a number of application examples are provided. Solutions of the proposed method are compared with the authors' cone calorimeter tests or other experimental results wherever available and FDS simulation results. These application examples include the following:

- Gasification of charring wood and non-charring PMMA: to check the pyrolysis submodel,
- Upward flame spread over combustible vertical surface: to check the combined flame feedback submodel and pyrolysis submodel.

3.4.1 Sensitivity study: time step and gas permeability in PMMA

Simulating burning behaviour requires a large number of input parameters, some of which, such as time step and the exact permeability value of PMMA, cannot be found in existing literature. A sensitivity study has been performed to minimise uncertainty of the simulation results. The sensitivity study case is a 10mm thick PMMA element exposed to external 50kW/m^2 heat flux.

In FDS modelling, the time step is set automatically. Therefore, there is no need to specify a value for the time step in FDS. The variable time step is usually very small (0.01s)[52]. However, since the authors' model does not perform detailed computations of the gas phase, a large time step can be used to speed up calculations. The results of this sensitivity study, shown in Figure 3.11(a), indicate that a time step of 0.1s can be used.

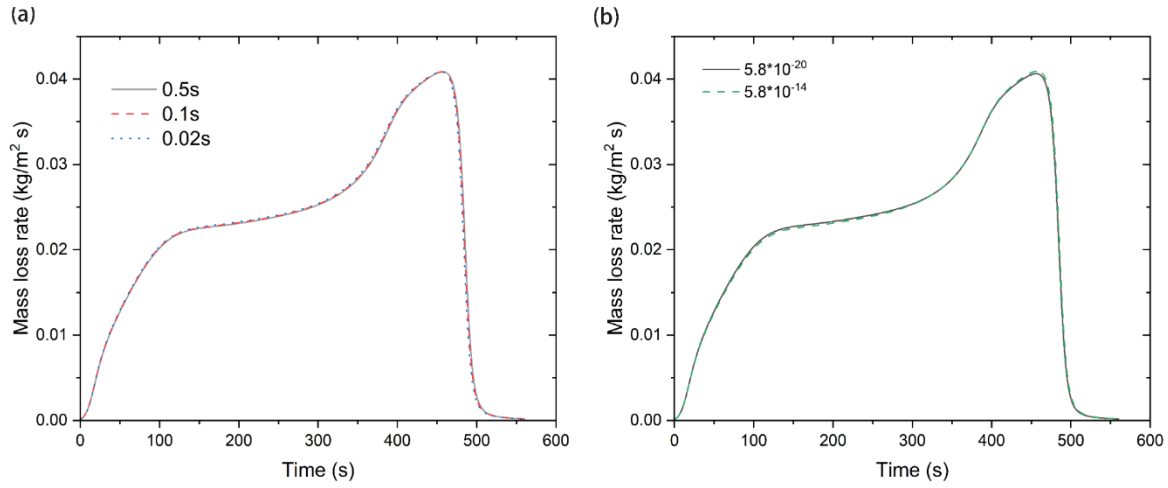

Figure 3.11 Sensitivity of mass loss rate to (a) time step, and (b) gas permeability in PMMA

No precise value can be found for permeability of gaseous species through PMMA. A permeability value of 5.8*10^{-18} for PMMA membranes may be used [100]. However, the results of the authors' sensitivity study, as shown in Figure 3.11(b), indicate that when the permeability value of PMMA changes within a very large range of 5.8*10^{-14}-5.8*10^{-20}, the error in the calculated mass loss rate is negligibly small at 0.165%.

3.4.2 Calculation of gasification of charring Wood and non-charing PMMA

Two typical materials, wood (charring material) and PMMA (non-charring), are considered.

To validate the pyrolysis submodel, the authors carried out two independent cone calorimeter tests, one for wood and one for PMMA, as sketched in Figure 3.12.

In cone calorimeter tests, an external heat flux value below 20 kw/m^2 is usually applied to examine ignition and flammability and a higher external heat flux of 25-50 kw/m^2 is applied to study flame spread and to measure combustion properties [106]. Using an external heat flux of 50 kw/m^2 gives better reproducibility of measurement results and has been commonly used in cone calorimeter tests [107]. In the authors' cone calorimeter tests, heat flux levels of 30kW/m^2 and of 50kW/m^2 were used and their results have been compared with the authors' calculation results using the authors' simplified model. The back side of the sample was assumed to be insulated because it was in contact with a 13mm thick ceramic fiber blanket of low thermal conductivity.

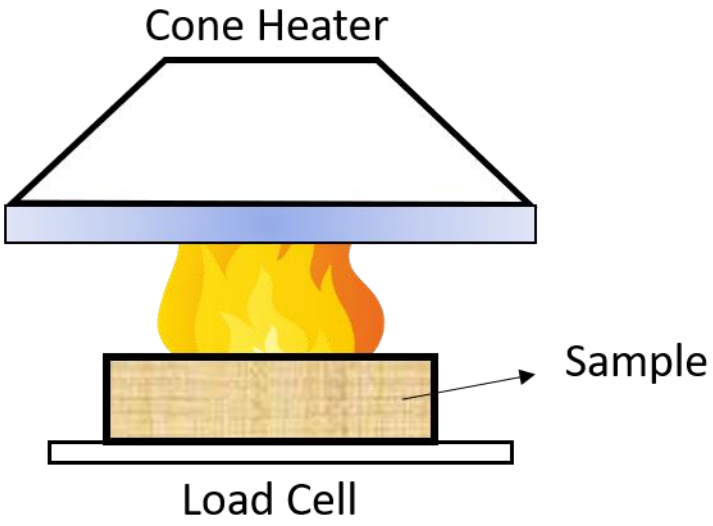

Figure 3.12 Schematic view of cone calorimeter

4.2.1 Charring gasification-wood

The simulations consider three condensed phase species:(1) wood, (2) char, and (3) ash. A two-step reaction mechanism (from wood to char, and from char to ash, as shown in equation 3.25 and 3.26) is assumed. Tables 3.5 and 3.6 list the relevant properties of wood and relevant two-step reaction kinetics values, respectively. The thickness of wood is 10 mm. Wood is assumed to be opaque, therefore the absorption coefficient is set as ∞.

$$Virgin\ wood \rightarrow 0.26Char + 0.74Pyrolysis\ gases \quad (3.25)$$

$$Char \rightarrow 0.2Ash + 0.8Pyrolysis\ gases \quad (3.26)$$

Table 3.5 Condensed phase parameters for wood

Name	Density (kg/m³)	Cond. (W/(m·K))	Spec. Heat (kJ/(kg·K))	Emissivity	Absorption coefficient	Gas permeability (m^2/(s Pa))
Wood	600[108]	0.2[108]	3.0[108]	0.76[109]	∞ [109]	3×10^{-13} [110]
Char	350[111, 112]	0.17[108]	1.0[108]	0.96[109]	∞ [109]	8×10^{-11}[110]
Ash	48.6[111]	0.17[108]	1.0[108]	0.96[109]	∞ [109]	8×10^{-11}[110]

Table 3.6 Reaction parameters for wood

From	To	Pre-Exp. Factor (1/s)	Act. Energy (kJ/kmol)	Heat of Reac. (kJ/kg)	Residue Frac.
Wood	Char	2.49×10^{6}[113]	106.5[113]	418[113]	0.26[114]
Char	Ash	9.79×10^{13}[109]	192.4[109]	75[113]	0.20[114]

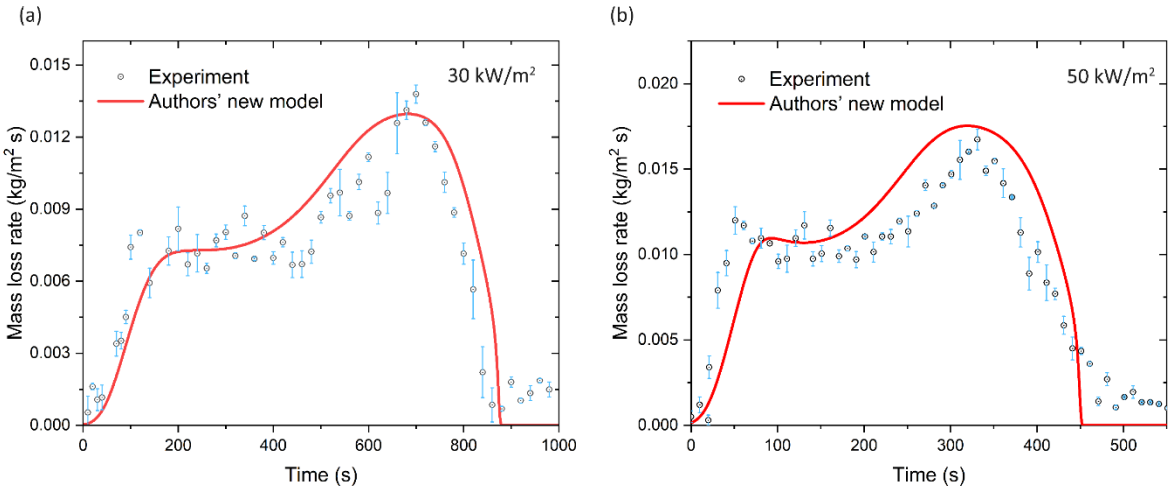

Figure 3.13 Comparisons between the authors' modelling and cone calorimeter experiments for wood at (a) 30 kW/m^2, and (b) 50 kW/m^2 heat flux

Figure 3.13 shows comparisons of mass loss rate (MLR) between modelling using the authors' model and experiment results for wood. Error bars denote the standard deviation of variations between two tests. Two distinctive stages of wood reaction can be observed in both modelling and experiments. The first stage is the preliminary pyrolysis reaction of the virgin wood. This stage starts when the wood starts to pyrolyze, at about 40s. As the burning proceeds and a char layer is formed on the surface of the wood, the MLR value decreases and the surface temperature increase becomes slower. The second stage is pyrolysis of the char beginning at about 200s. As heat goes deeper into the wood and temperature keeps increasing, and more

volatiles are released. When the heat absorbed by the remaining residue and the heat loss reach equilibrium, there is no more pyrolysis reaction.

As shown in Figure 3.13, the modelling results agree well with the experiment results, for all different stages of wood decomposition. To assess accuracy of the authors' model, the error between the authors' model simulation results and test results is calculated using the averaged deviations as follows [115]:

$$Err = \frac{\left[\sum_{N=1}^{N\max}(\phi_{ref,N}-\phi_N)^2\right]^{1/2}}{\phi_{ref,\max}N_{\max}} \times 100\% \quad (3.27)$$

Where N is the number of a data point, $N_{\max}$ is the maximum number of data points, $\phi_{ref,N}$ is the N_{th} reference data, ϕ_N is the N_{th} compared data, and $\phi_{ref,\max}$ is the maximum reference data to scale the data values. Using the experimental data as reference, the error of the first peak in Figure 3.13(a) and Figure 3.13(b) are 3.75% and 4.59%, respectively. Over the entire testing period, the errors are 1.35% and 2.19% for 30 and 50 kW/m^2, respectively.

4.2.2 Noncharring gasification-PMMA

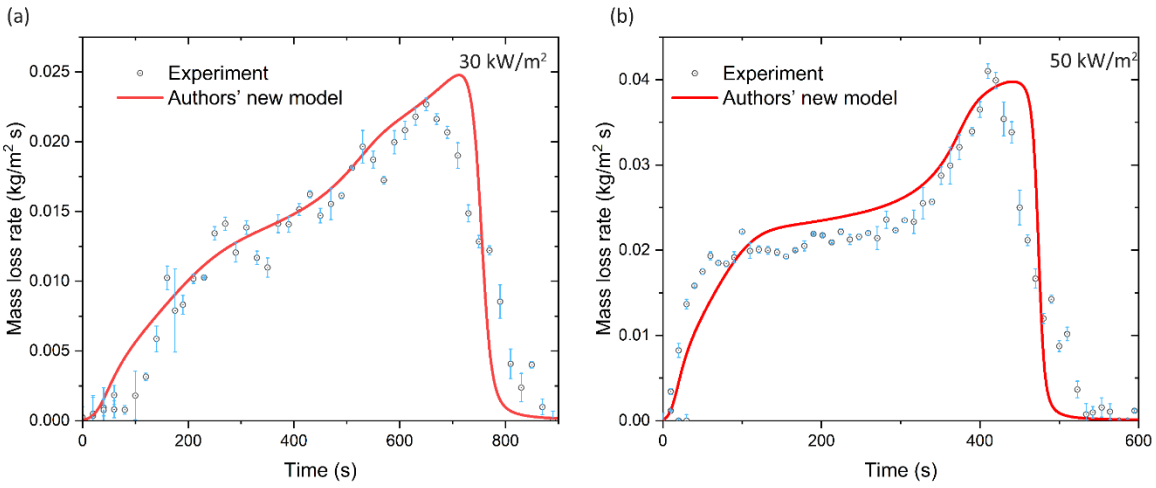

Figure 3.14 Comparisons between modelling and experiments for PMMA at (a) 30 kW/m^2, and (b) 50 kW/m^2 heat flux

Figure 3.14 makes similar comparisons for the 10 mm thick PMMA element, as Figure 3.13 for wood. The immediate impression is that the two sets of results are very close, demonstrating validity of the authors' simplified 1D model. PMMA decomposition exhibits three stages as described by Tewarson[116]: solid , melting and boiling liquidity. After first period of heating

the solid, the firsts stage begins with the PMMA sample igniting and the mass loss rate(MLR) rising very quickly. Then, MLR first increases smoothly. When all of the solid phase turns into liquid, a huge peak MLR emerges. This is due to the thermal feedback that reach the bottom of the solid PMMA. The last step of decomposition involves a reduction in MLR and consumption of the remaining PMMA. For both heat flux levels, the authors' new model captures all these different stages correctly. Although some discrepancies are present when comparing the experiment and simulation result profiles, the errors, as calculated using Eq. 3.27 (1.27% and 1.62% for 30 and 50kw/m^2), are small. The burning behaviours of PMMA can be considered to be accurately predicted.

3.4.3 Prediction of vertical burning and upward flame spread

In previous sections, accuracy of the different submodels of the authors' new model has been demonstrated, including the 1-D combined heat and mass transfer and decomposition submodel, the heat flux submodel through comparison with cone calorimeter test results and additional FDS simulation results for cone calorimeter tests, and the assumption of flame instantaneously reaching steady state.

In this application example, the totality of the authors' new model for predicting vertical flame spread over a vertical combustible element is examined. This is done by comparison against the results of two full-scale experiments and corresponding FDS simulations for a wood wall and a PMMA wall. The PMMA and wood wall tests were carried out by Delichatsios[108] and FMRC [117] respectively.

Table 3.7 Additional input data in the upward flame spread model

Property	Combustion efficiency	Radiation fraction	Heat of combustion (kJ/kg)
Wood	1.0[55]	0.35[55]	17000[55]
PMMA	1.0[55]	0.35[55]	25300[55]

3.4.3.1 Wood wall test (Delichatsios [108])

Figure 3.15(a) shows the setup for the wood wall test of Delichatsios[108]. A wood panel measuring 0.61 m wide by 2.4 m high was mounted in the middle of a wall, surrounded by high insulation panels on both sides. The front and top of the specimen were open to the ambient condition.

The authors' FDS model is constructed the same as the experiment. For the wood panel test, the size of the domain is 0.6 m × 1.2 m × 2.4 m (in x, y and z direction). According to Ma's mesh size calculator method [118], a 2.5 cm grid size was used in the authors' FDS simulation model. The same properties as previously used for Wood, detailed in Tables 3.5,3.6 were used in the application study presented hereafter. To represent the real experiment condition, the back side of wood was assumed to be insulated. The wood fuel was defined by chemical formula $C_1H_{1.7}0_{0.74}N_{0.002}$ with a soot yield $y_s = 0.004$ and a CO yield of $y_{co} = 0.01$ [84]. Table 3.7 presents additional input data for the flame properties. Unless otherwise specified, all input parameters are default values for FDS.

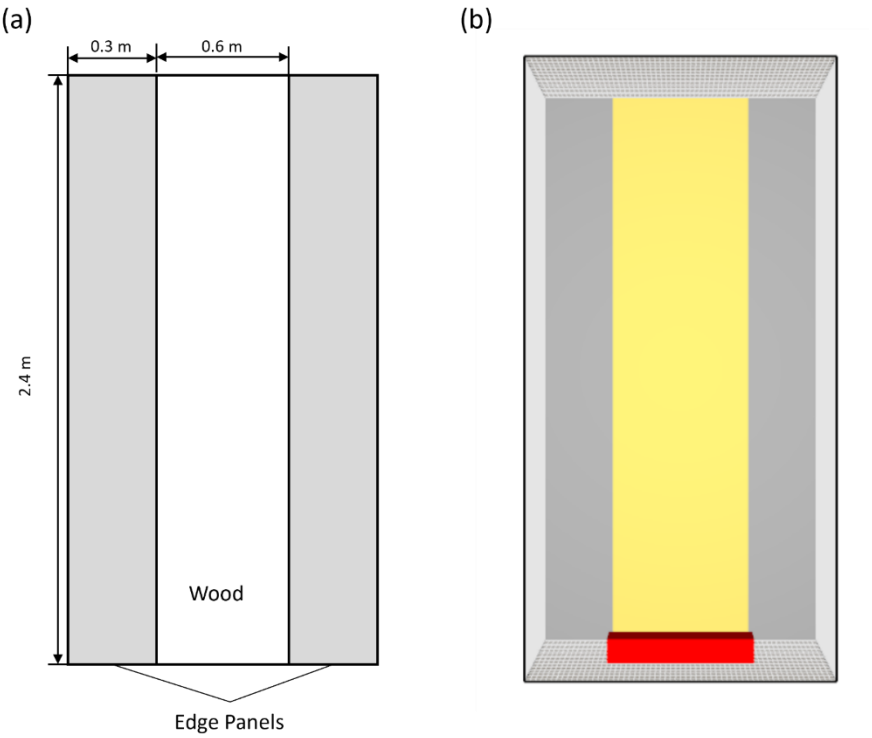

Figure 3.15 (a) Delichatsios' wood panel test[108], and (b) the authors' corresponding FDS model

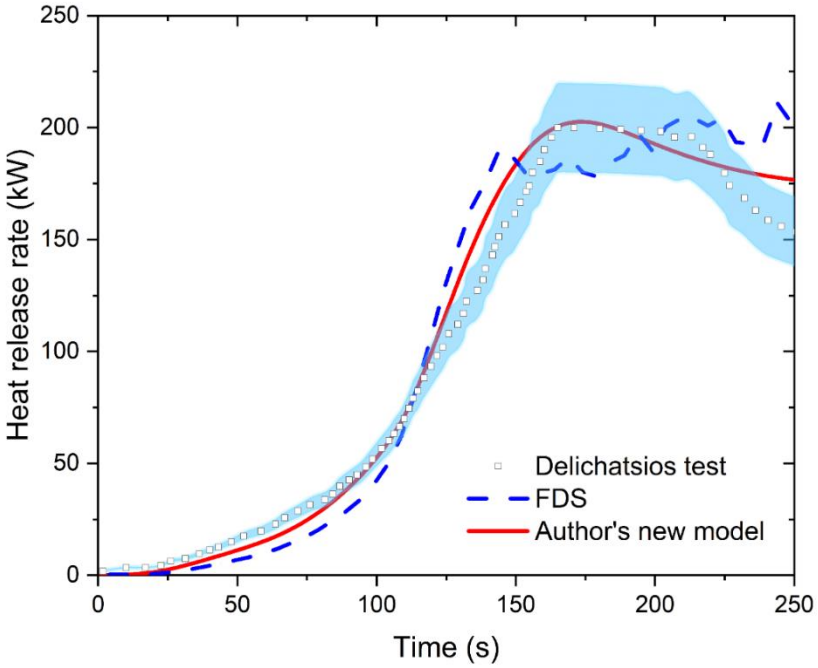

Figure 3.16 Comparison for heat release rate results between the authors' simulations and Delichatsios' experiment[108]

Figure 3.16 compares all three sets of results for the total additional heat release rates (excluding that of the burner). Using Eq. (3.27) and the experimental results between 0-200s as reference data, the error of the authors' FDS model and simplified model is 0.83% and 0.4%, respectively, demonstrating the authors' appropriate use of FDS and validity of the authors' new model.

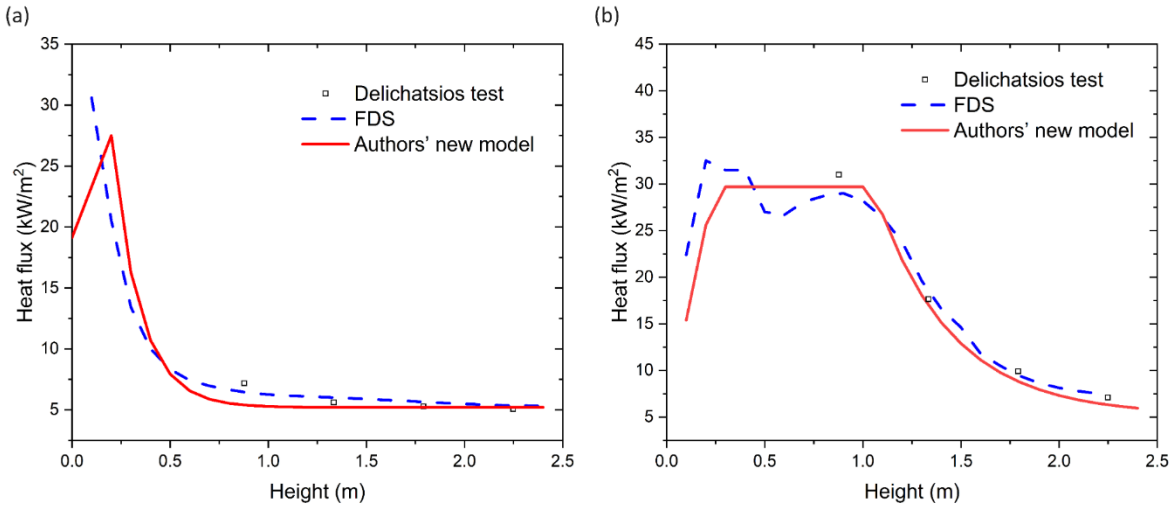

Figure 3.17 Comparison for heat flux results between the authors' simulations and Delichatsios' experiment [108], at (a) 50s and (b)100s

Figure 3.17 compares heat flux distributions at two different time. The heat flux levels are in close agreement with that in experiment and FDS. Again using Eq. 3.27 and the experimental results as reference data, the error values for the authors' FDS model & simplified model at 50s and 100s are 1.69% & 2.50% and 1.93% & 1.79%, respectively. This good agreement confirms that the semi-empirical flame feedback sub-model is suitable.

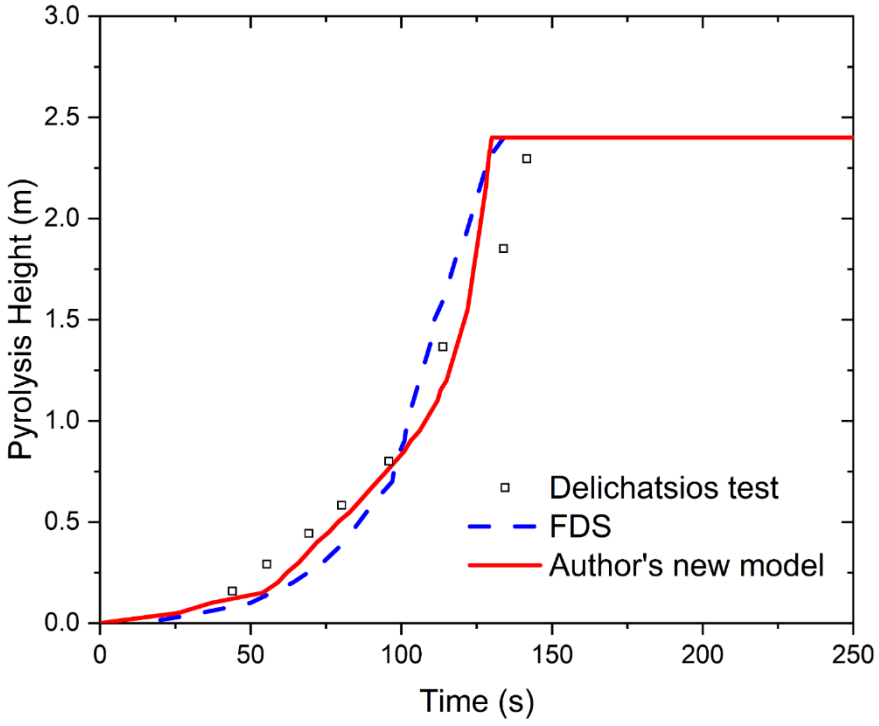

Figure 3.18 Comparison for pyrolysis heights of a 2.4 m x 0.61 m vertical wood element between the authors' FDS and simplified model simulations and Delichatsios's experimental data [108].

Figure 3.18 compares the three sets of results for pyrolysis height growth-time relationship. For wood, the pyrolysis front is defined as when the pyrolysis temperature reaches 650K [119]. Using Eq. 3.27 and the experimental data as reference, the error values for the authors' FDS and simplified model simulation results are 1.26% and 1.04%, respectively. The agreement is again very good, showing that the authors' model is able to accurately calculate upward flame spread.

Figure 3.19 shows a selection of temperature contours and char fraction evolution in time. The qualitative pattern of upward spread of the pyrolysis front is clearly observed. Pyrolysis starts when the surface temperature is 650k which is reached at about 50s (Figure 3.19(a)) at the

bottom. As pyrolysis begins, the heating and pyrolysis accelerate and the flame rapidly covers a large area of the material (Figure 3.19(b) at 100s). At t=150s, all of the sections along the height are in a state of 'pyrolysis'. This demonstrates that the authors' model correctly captures all expected features of upward flame spread for charring material.

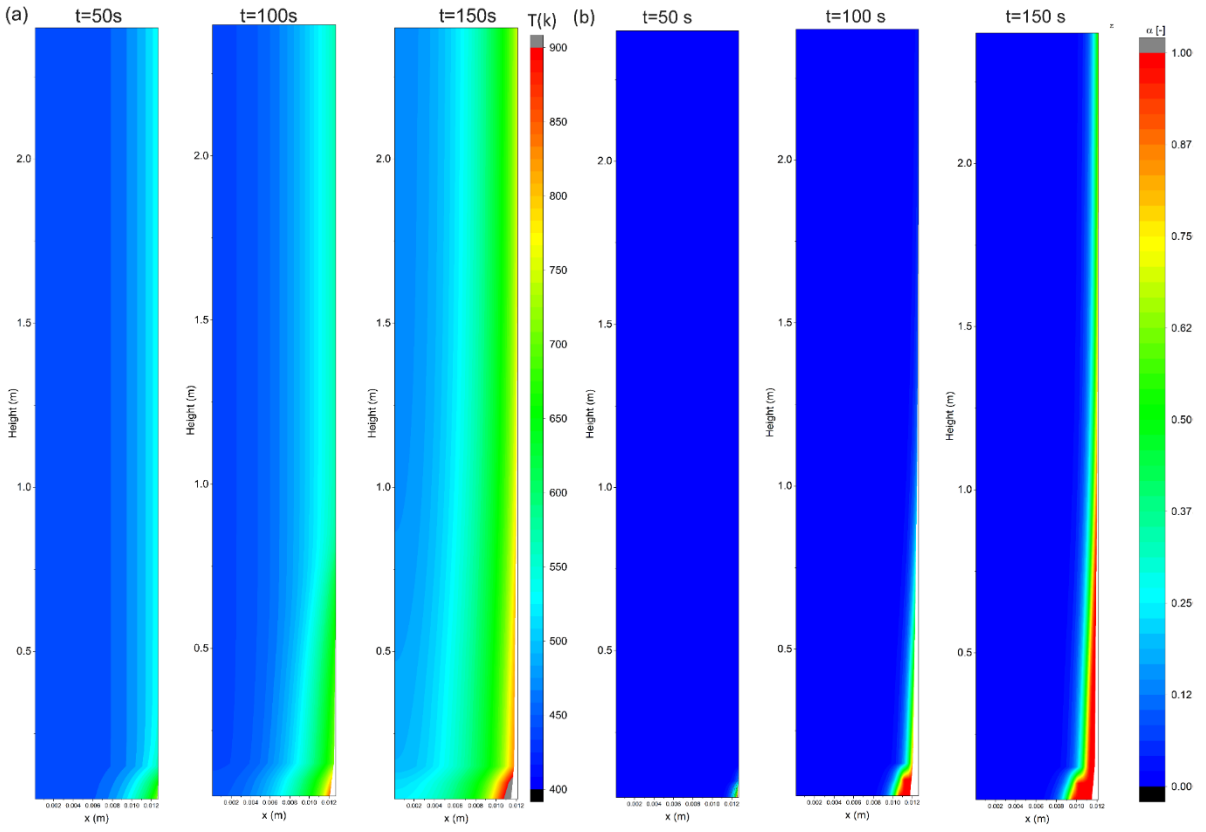

Figure 3.19 (a) Temperature contour, (b) char fraction after 50s, 100s, and 150s for a wood element with initial thickness of 12.7 mm.

3.4.3.2 PMMA test (FMRC[117])

Figure 3.20 shows the setup for the FMRC PMMA test [117]. In the middle of the wall, there is a PMMA panel measuring 0.025 m × 0.6 m × 5 m (thickness, width and height). The side and top the PMMA panel are covered with non-combustible insulation. The authors' FDS model is constructed as close to the experiment as possible. The size of computation domain is 0.6 m × 1.2 m × 8 m (in x, y and z direction). Based on Ma's mesh size calculator [118], a 5 cm grid size was used in the authors' FDS simulation model. The same properties previously used for PMMA, as detailed in Tables 3.2-4, were used in the application study presented hereafter. To mimic the experiment condition, the back side of PMMA was assumed to be insulated. The chemical formula of PMMA was $C_5H_80_2$ and its combustion reaction has a soot

yield $y_s = 0.022$ and a CO yield of $y_{co} = 0.01$. Table 3.7 presents additional input data for the flame properties. Unless otherwise specified, all input parameters are default values for FDS.

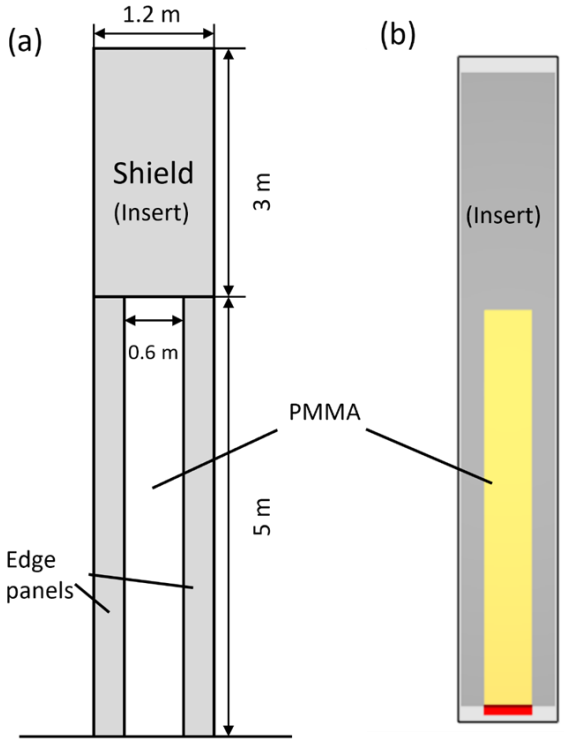

Figure 3.20 (a) FMRC PMMA wall test[117], and (b) the authors' FDS simulation model

As can be seen from Figure 3.21, the computed heat release rate results compare reasonably well with the experimental data. The results in Figure 3.21 suggest some differences between the calculation results using the authors' simplified model and experimental results or FDS simulation results. The error between the authors' simplified model and test results of heat release rate before 400s, as calculated by Eq. (3.27), is 9.4%. The noticeably large difference in the initial period may be attributed to inaccurate modelling of ignition. However, once sustained burning occurs (after 400s), the simplified model results follow the test results closely with the maximum difference being 1.15%, while that for FDS is 1.8%. After about 1180s, all results remain almost steady stage due to stoppage of the pyrolysis front and a constant amount of gasified volatiles entering the flame. The magnitude of the maximum predicted RHR using the authors' simplified model is very close to those of the FMRC experiment and the authors' FDS simulation.

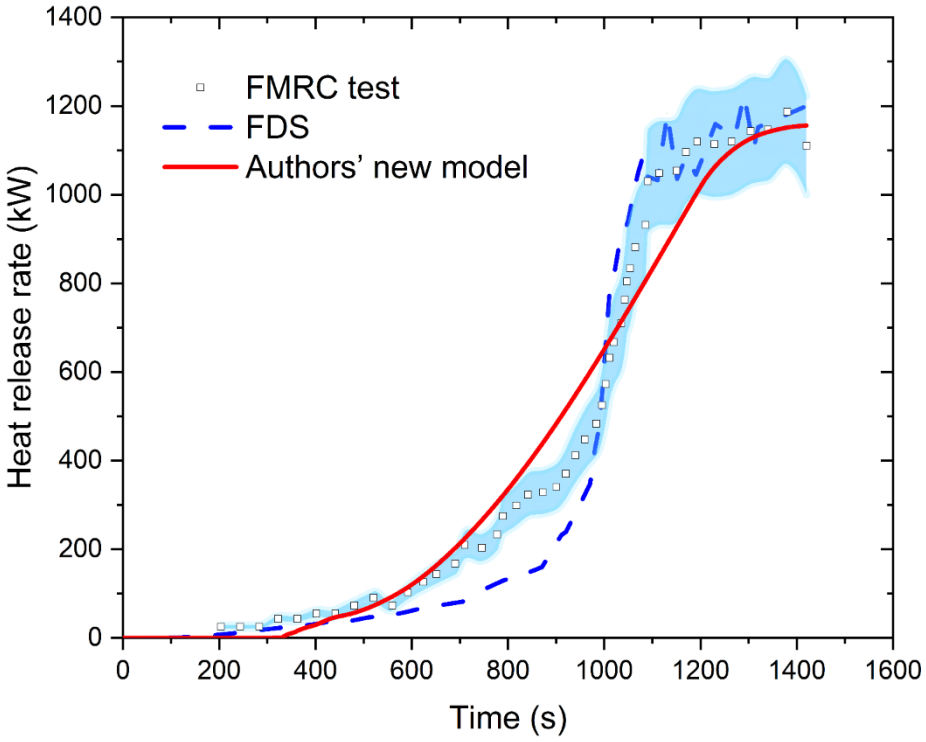

Figure 3.21 Comparison for heat release rate results for a 5.0 m x 0.58 m vertical PMMA element, between the authors' FDS and simplified model simulations and FMRC experiment [117]

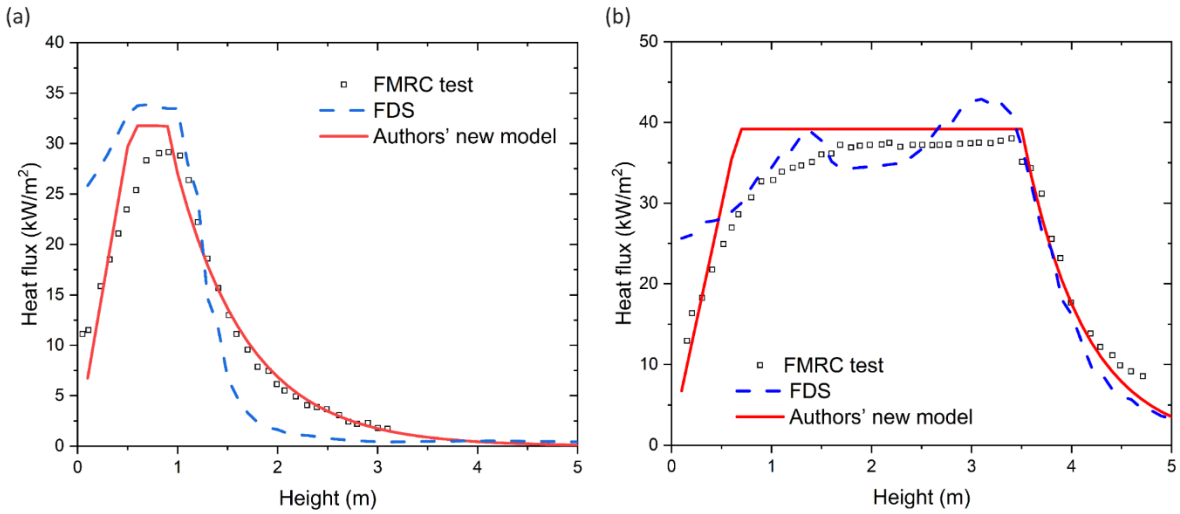

Figure 3.22 Comparison for transient shapes of heat flux between the authors' FDS and simplified model simulations and FMRC experiment [117], at (a) 600s, and (b) 1000s

Figure 3.22 presents heat flux distribution comparisons between the FMRC experiment and the authors' FDS and simplified model simulations. The net heat flux calculated in both the authors' simplified model and FDS simulation are consistent with the experimentally measured heat

flux by FMRC[117]. Using Eq. 3.27 and the experimental results as reference data, the error values for the authors' FDS & simplified model at 50s and 100s are 2.1% & 1.33% and 1.70% & 1.97%, respectively.

This comparison also confirms that it is suitable to describe heat flux distribution above the pyrolysis front by the exponential decay function of Eq. (3.8) as suggested by the authors.

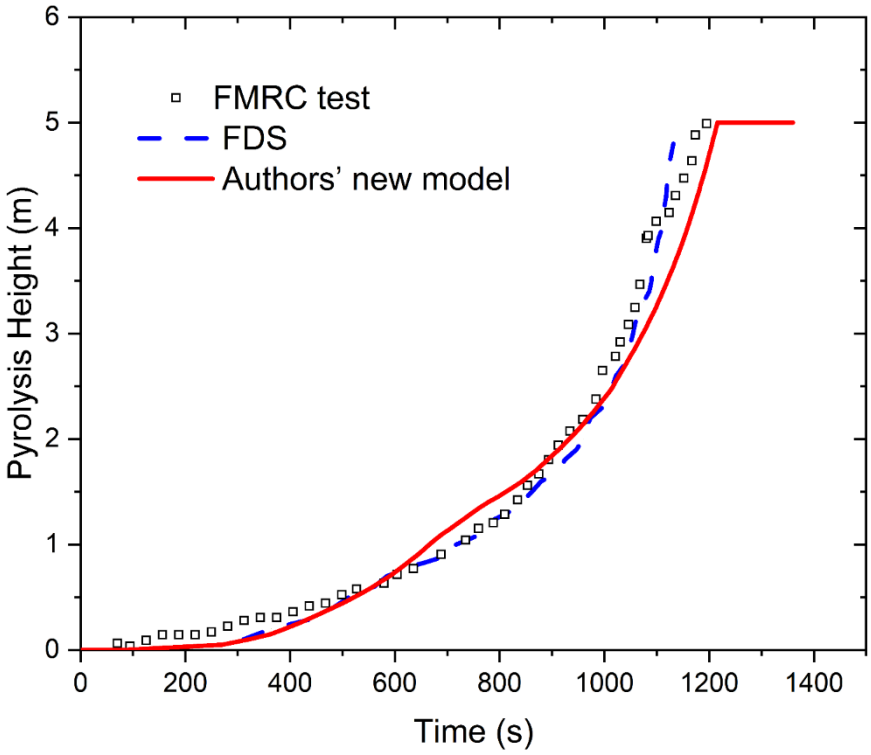

Figure 3.23 Comparison of pyrolysis heights for a 5.0 m x 0.58 m vertical PMMA between simulations and FMRC experiment[117]

Figure 3.23 compares pyrolysis front predictions with experimental data and the authors' FDS simulation. The pyrolysis front for PMMA is defined as when the surface temperature reaches 580k [120]. For pyrolysis height, the error value calculated using Eq. 3.27 and the experimental results as reference data for the authors' FDS model and simplified model over the entire period of test is 0.85% and 0.69%, respectively.

The results in Figure 3.23 for pyrolysis height show slightly better agreement than the results for RHR in Figure 3.21. This is because in both the experiment and the authors' FDS simulation, the surface temperature at the mid-point of the surface was used to determine pyrolysis height. This disregards the small width effect that would be present in RHR results.

There is also evidence to indicate good qualitative prediction of pyrolysis front propagation using the authors' simplified model. Figure 3.24 shows temperature contour evolutions in time for a PMMA panel of 25mm in thickness. After reaching the pyrolysis temperature of 580K (at 500s), the PMMA thickness decreases due to mass loss process and volumetric shrinkage. The maximum surface temperature after pyrolysis is almost constant (680K, at 1000s and 1200s). This phenomenon is consistent with test measurements of Wasan [121].

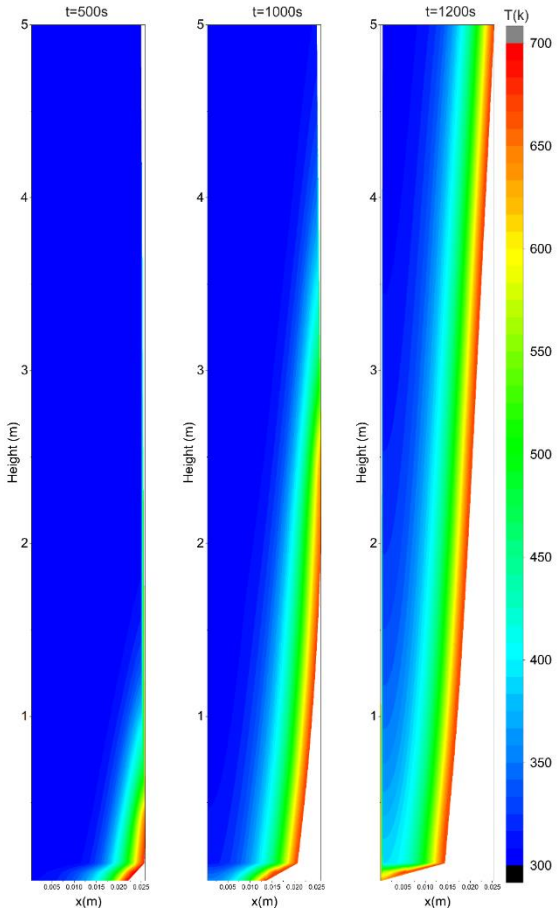

Figure 3.24 A selection of temperature fields for a PMMA element with 25mm initial thickness.

3.4.3.3 CPU time

The times for using the authors' simplified model for calculations of upward flame spread of wood and PMMA elements are 153s and 470s respectively. These are compared to FDS simulation times of 6h and 53h respectively. The FDS simulation time is 2 orders of magnitude longer than the authors' new model.

3.5. Conclusions

This chapter presents the development and validation of a simplified, efficient and accurate model for predicting transient upward flame spread on combustible vertical surface. Such an efficient model is possible because the gas phase can be represented by a theoretical model of flame height-heat release rate relationship. This model includes further simplifications on heat flux to the surface, heat and mass transfer and decomposition. This chapter has presented details of these sub-models and their separate validations. Validation of the model is completed by using the model to predict two full-scale upward fire spread tests on wood and PMMA wall panels, and comparison of the model's calculation results against the authors' FDS simulation results. The main conclusions of this chapter are:

1) It is acceptable to adapt the steady state flame height equation to transient flame height exposed to transient heating. The Tu and Quintiere's [17] steady state correlation for flame height can be used. This has been checked by comparison against the authors' FDS simulation results under variable heat release rates, simulating medium, fast and ultra-fast T-squared fires.
2) Heat flux of the flame and plume to the vertical surface is calculated by using the Spalding mass transfer corrections for convective heat in the pyrolysis region and a semi-empirical correlation for radiative heat flux. Validation of the heat flux is by comparison against the experimental results of Hasemi [67] for line fire tests with various heat release rates.
3) The assumption of 1-Dimensional combined heat and mass transfer and decomposition is checked against the results of the authors' cone calorimeter tests and the authors' additional ANSYS &FDS simulation results.
4) Validity and accuracy of the authors' new simplified model for efficient modelling of upward flame spread over vertical combustible element is demonstrated by comparison of total heat release rate, distribution of decomposition rate and temperature profile over the height of the element, and time histories of decomposition and temperature at different locations, for two full-scale upward flame spread fire tests, conducted by Delichatsios[108] for a wood wall panel and by FRMC[117]for a PMMA wall panel.
5) The FDS simulation time is two orders of magnitude longer than the authors' new simplified model.

Chapter 4 Modelling of flame spread on ventilated façade

4.1. Introduction

Ventilated Façade (VF) system, an example of which is shown in Figure 4.1, is a key innovative construction technique that is commonly used to meet stringent requirements of reducing energy consumption and the cost of buildings. It has a double-walled structure with an inner insulation and a cladding panel on the exterior, separated by a cavity.

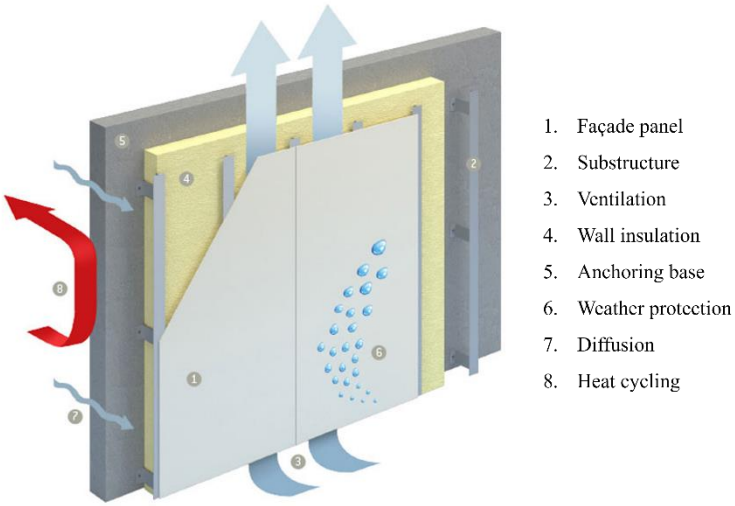

Figure 4.1 An example of ventilated façade under normal working condition[7]

However, in a fire event, if the cavity is not effectively sealed at floor levels, the same chimney effect in the cavity poses a fire threat[122], since the flame and hot mixed gases may spread through the ventilated cavity from the floor in fire to floors above. Fires spreading through ventilated cavities may spread more quickly than through the exterior surface of façades, based on recent incidents worldwide [123, 124]. The Grenfell tower fire in London in 2017 is probably the most tragic illustration of the hazard of internal flame spread through cavity.

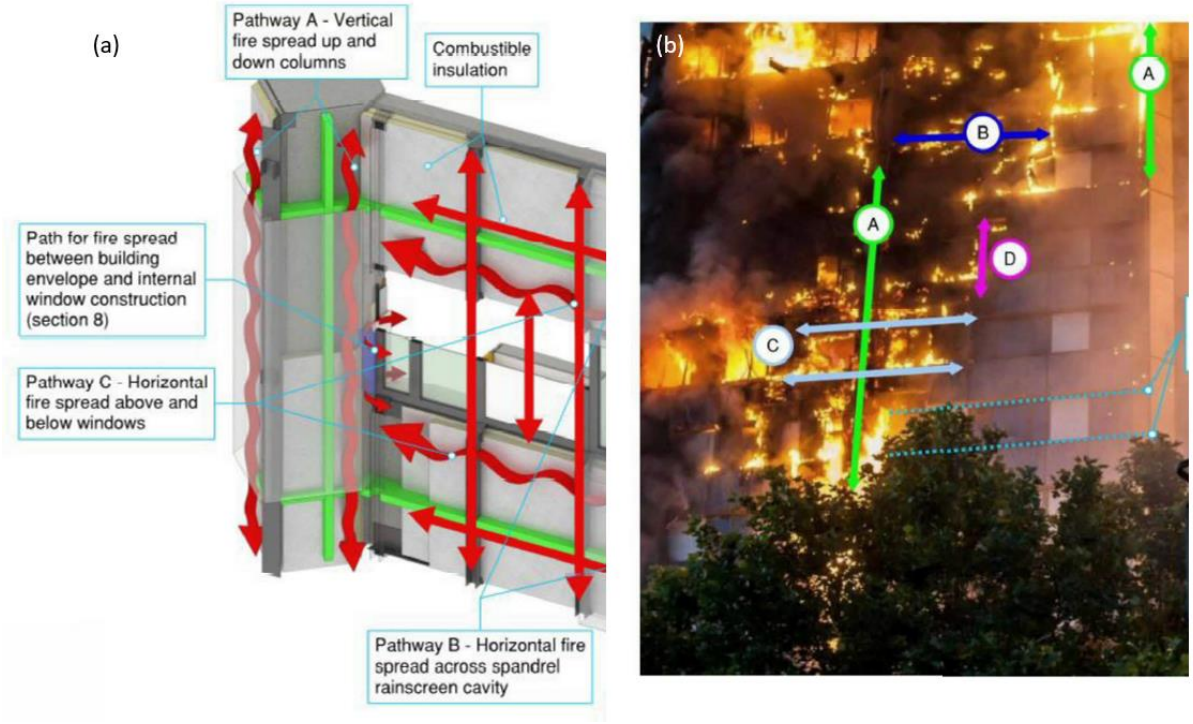

Figure 4.2 An illustration of interior flame spread within the column cavity of Grenfell Tower to support combustion[123]

Despite several authors having highlighted the importance of flame spread with cavity of ventilated façade, there has been no systematic investigation on how this effect can be conveniently assessed quantitatively in engineering practice. This is likely the result of the assumption that the cavity is blocked at floor levels, as mandated in building regulations for fire safety. For example, the Approved Document B for fire safety in England and Wales[24] states that cavity barriers must expand and seal the cavity when exposed to fire and provide 15 minutes of fire resistance. However, for a variety of reasons (e.g. in appropriate use of cavity blocking materials, lack of access to the cavity for maintenance), there is a potentially high risk of uninterrupted cavity, as fact evidenced in the recent Grenfell Tower fire[6].

The aim of this chapter is to establish an efficient method for quantitatively assess the fire performance of VF systems. Chapter 3 of this thesis has developed a method for rapid and accurate modelling of flame spread over cladding elements without cavity. This Chapter extends the modelling methodology of Chapter 3 to complete ventilated façade systems with uninterrupted cavity.

Figure 4.3 shows a schematic of a building façade with uninterrupted cavity with a fire inside the cavity. The general mechanism of flame spread in cavity is as follows:

(1) An initial flame is driven from the outside to ignite any combustible insulation material around the cavity.

(2) Flame spreads upwards to heat further materials along the height of the cavity.

(3) Combustible materials around the cavity are decomposed and ignited to cause further combustion and increased rate of heat release.

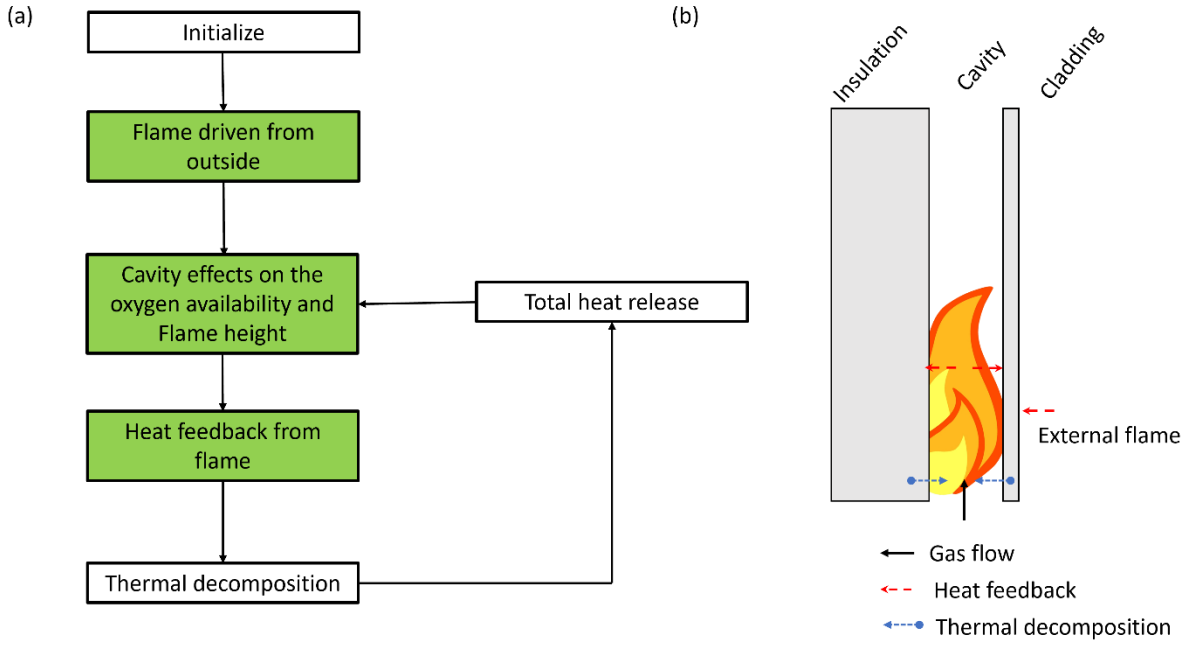

Figure 4.3 (a) Mechanism of flame spread inside cavity, (b) Illustration of cavity flame spread

Chapter 3 has already described and validated the model for decomposition of combustible materials. Therefore, the additional challenges for modelling flame spread in the cavity of ventilated façade are:

- The initial flame size driven into the cavity through opening from the fire on the outside to ignite the insulation within the cavity (Section 4.2).
- Flame height correlation inside the cavity (section 4.3).
- Heat flux distribution inside the cavity (section 4.4).

It is assumed that the insulation material is attached to a non-combustible backing, therefore, any decomposition of the combustible insulation is released into the cavity to cause burning. The cladding is heated from both inside the cavity and outside fire. For simplicity, referring to Figure 4.3(b), the left half of the decomposed cladding material moves to the cavity and the right half of the decomposed cladding material moves to the outside.

4.2 Initial flame size within the cavity

In this research, it is assumed that the initial flame size within the cavity is driven by a fire through an opening in the insulation, as illustrated in Figure 4.5, as driven result of the stack effect caused by temperature difference within the cavity. The model for solar chimney based on the same theory can be adopted for cavity fire. Solar chimneys usually include a heated wall, a bottom opening, and a top opening (see Figure 4.4). The main difference is the source of heat, in cavity fires, the air is heated by the combustion of gas fuels.

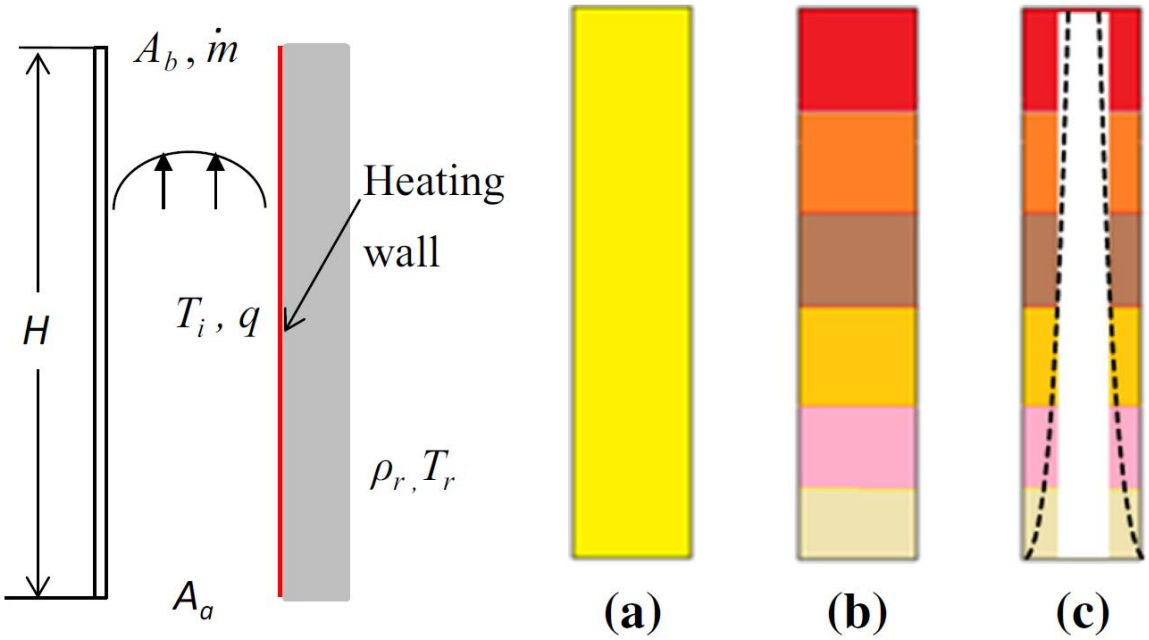

Figure 4.4 Model representations of solar chimneys: (a) single zone model; (b) stratified model; (c) plume model[125, 126]

Therefore, analytical models for ventilated cavity in facade should be included to calculate the air flow at the opening. In terms of analytical models for ventilated cavity, the following three are representative: namely the single -zone model[127], stratified model[128], and plume model[126]. The single zone model for ventilated cavity is developed earlier and is now extensively employed. The cavity's temperature and density are both assumed to be uniform within the cavity. The air temperature in the cavity has a significant impact on the mass flow rate. The stratified model takes into account changes in temperature and density as a function of vertical height. The plume model is proposed by He[126], which considers a thermal boundary layer at each heated wall. These three models were evaluated by Shiyi[129] to check

the airflow rate. All these models can give the same results as the experiment. Therefore, the simplest one is modified for the cavity fire.

A sketch of the wall cavity is presented in Figure 4.5. Assumptions based on the modified single zone model:

(1) Steady-state flow inside the cavity.
(2) The mixed gas is assumed to be driven through the cavity bottom opening due to the temperature difference between the inside and outside of the cavity.
(3) The cavity is heated by the combustion of mixed gas flowing from the outside.
(4) Flame fully occupies the cavity volume up to flame height but not beyond.

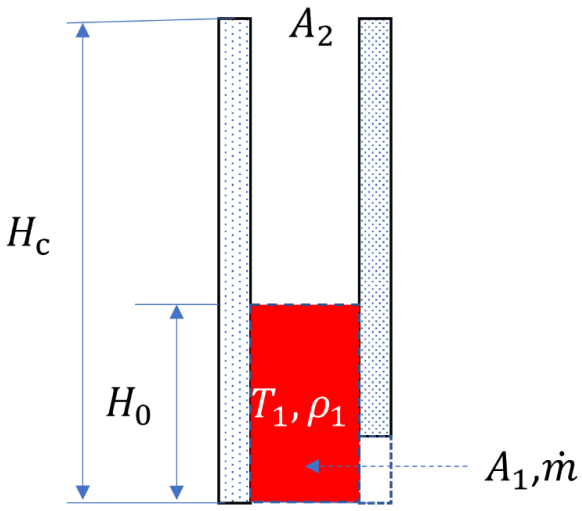

Figure 4.5 Schematic of the cavity fire model

A force balance can be made where the gravity force is set equal to the resistance force created at the entrance of the cavity and the force due to change in momentum of the heated gas inside the rack.

$$P_{r,a} = P_{r,b} + \sum \left(\frac{k}{2}\rho u^2\right)_i + P_f + \int_0^H \rho_i g \, dh \tag{4.1}$$

Where $P_{r,a}$ and $P_{r,b}$ are the pressure at the two openings of the cavity; The total local pressure losses are shown by the second term on the right. The channel's friction loss is the third term. As a result of $P_{r,b} = P_{r,a} - \rho_r g H$, the following can be obtained

$$\rho_r g H - \int_0^H \rho_i g \, dh = \sum \left(\frac{k}{2}\rho u^2\right)_i + P_f \tag{4.2}$$

Friction loss for pipe flow is used , and the following equation can be obtained:

$$P_f = \int_0^H \frac{C_f}{2}\frac{1}{d_h}\rho_i u^2 dh \tag{4.3}$$

The following equation may be derived by substituting mass flow rate for flow velocity in Eqs. (4.2) and (4.3).

$$\rho_{r,a} gH - \int_0^H \rho_i g\, dh = \frac{k_a}{2A_a^2}\frac{\dot{m}^2}{\rho_{i,a}} + \frac{k_b}{2A_b^2}\frac{\dot{m}^2}{\rho_{i,b}} + \frac{f}{2A_h^2}\frac{H}{d_h}\frac{\dot{m}^2}{\overline{\rho_i}} \tag{4.4}$$

Where m is the mass flow rate ($m = \rho_r u_r A$) inside the cavity, A is bottom opening area of the cavity, and $\rho_{r,a}$ is the density at the inlet.

When the ventilated cavity is modelled as a single zone, the temperature and density, the density ρ_i inside the cavity assumed is constant. Thus

$$\rho_{r,a} gH - \rho_i gh = \frac{k_a}{2A_a^2}\frac{\dot{m}^2}{\rho_i} + \frac{k_b}{2A_b^2}\frac{\dot{m}^2}{\rho_i} + \frac{f}{2A_h^2}\frac{H}{d_h}\frac{\dot{m}^2}{\overline{\rho_i}} \tag{4.5}$$

The ideal gas law is given by Ref.[130] .

$$\rho_i T_i = \rho_0 T_0 \tag{4.6}$$

Where T_i and T_0 is the cavity's and ambient temperature, respectively.

The mass flow rate of the gas from outside through the cavity opening can be calculated by Eq. (4.4)

$$\dot{m} = C_d \rho_i A_a \sqrt{\frac{2gH(T_i - T_r)}{T_r}} \tag{4.7}$$

$$C_d = \left(k_a + k_b \frac{A_a^2}{A_b^2} + \frac{fH}{d_h}\frac{A_a^2}{A_h^2}\right)^{-\frac{1}{2}} \tag{4.8}$$

Where $C_d = \left(k_a + k_b \frac{A_a^2}{A_b^2} + \frac{fH}{d_h}\frac{A_a^2}{A_h^2}\right)^{-\frac{1}{2}}$ is the discharge coefficient. A discharge coefficient about $C_d = 0.5\sim0.6$ works well for most chimney predictions[126, 129].

It is assumed that all the gas entering the base of the cavity is mixed gas and that combustion occurs over a shallow height just inside the cavity, raising the gas temperature from the reference temperature, T_r, to the bulk value, T_f.

The total heat release rate in the cavity is obtained as:

$$Q_c = \dot{m}\, C_p\, (T_i - T_0) \tag{4.9}$$

Where Q_c correspond to the released heat flux within the cavity.

The flame height was found [131] to be proportional to the heat release rate. In the following section, we will examine their relationship (Eq. (4.10)). After combining Eq. (4.7), (4.9) and (4.10), the mass flow rate at the inlet of the cavity can be calculated.

The general data used in the cavity fire modelling are listed in Table 4.1. In the literature[132, 133], the temperature of flame one would expect the temperature at the average flame height as defined by[132] to be 600ºC.

Table 4.1 A summary of input data for modelling

Meaning	Symbol	Value	Unit	Ref.
Coefficient of discharge	C_d	0.5	-	[126, 129]
Specific heat capacity of air	C_p	1005	J/kg k	[130]
Ambient air density	ρ_r	1.205	Kg/m^3	[130]
Ambient temperature	T_0	288.15	K	[130]
Mean flame temperature	T_f	600	ºC	[132]

4.3 Flame height correlation inside the cavity

Most of the research studies that are relevant to flame spread in cavity are related to fire behaviour in confined spaces in rack storage arrangements. Karlsson [70], Ingason [134], and Ingason and Ris [72] have conducted experiments on 2D and 3D rack storage fire. Their investigations have attempted to quantify relationships of flame height as a function of heat release rate inside cavity, fuel type and wall separation distance (W in figure 4.6).

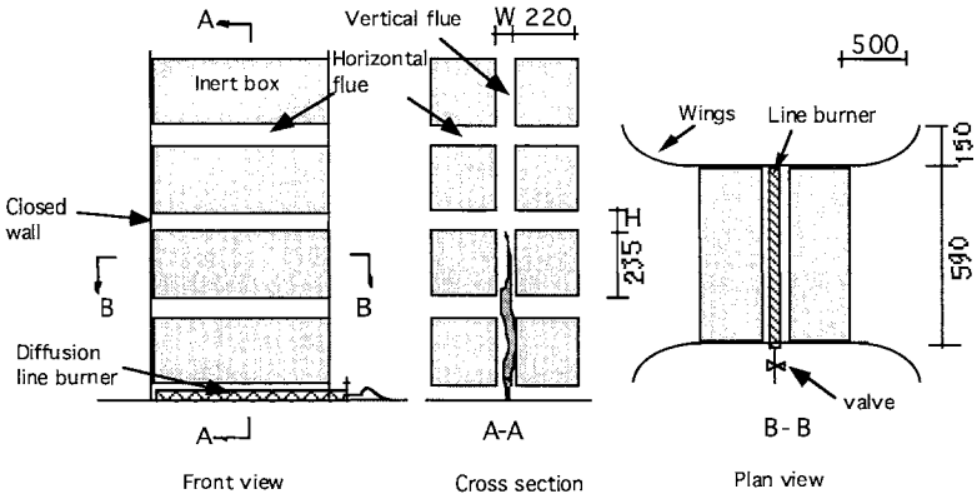

Figure 4.6 A 2-D rack storage with non-combustible material[71].

Different flame height correlations for storage rack fires have been proposed by Karlsson[70] and Ingason[71]. In Karlsson's study, both horizontal (W) and vertical separation (h) distances between storage boxes is used, and the height correlation equation is as follows:

$$\frac{z_f}{Q'^{2/3}} = 0.00242 \left[\frac{W}{Q'^{2/3}}\right]^{-0.496} \left[\frac{h}{Q'^{2/3}}\right]^{-0.070} \tag{4.9}$$

where z_f is flame height, W is cavity width, and h is the vertical gap between boxes.

As with Karlsson, the same storage racks are used by Ingason, however, Ingason closed the vertical gaps in their experimental setup to prevent any air inflow from sides, which can be considered more closely resemble the cavity fire spread problem of this research. A linear relationship between z_f and Q'/W was proposed by Ingason:

$$z_f = 0.307 + 9.15^{-4} \cdot \left(\frac{Q'}{W}\right) \tag{4.10}$$

Figure 4.7 compares Ingason's equation for flame height with Karlis' [73] experimental results for cavity fires with different heat release rates. Ingason's proposed linear correlation fits well with the experimatal flame height results of Karlis[73]. Ingason's correlation will be used in this research.

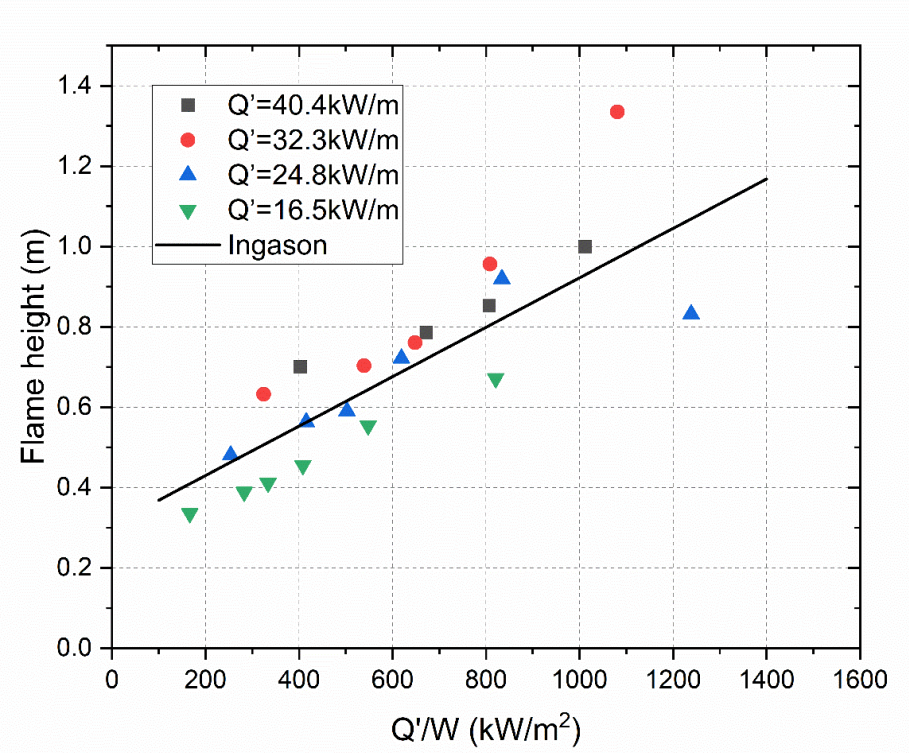

Figure 4.7 Comparison between Ingason's linear correlation model for flame height[71] with the experimental results of Karlis' [73]

4.3 Heat flux distribution inside the cavity

The wall around the cavity is heated by a heat flux boundary of the flame. The general description is:

$$\dot{q}''_w = \dot{q}''_f - \dot{q}''_{rerad} \tag{4.11}$$

where $\dot{q}''_f$ is the heat flux from flame, $\dot{q}''_{rerad}$ is the heat loss due to radiation.

In previous research studies by others [60, 75], a constant value of heat flux, typically equal to 25-30 kW/m^2, is used for $\dot{q}''_w$. Analytical refined derivation of $\dot{q}''_w$ need some physical and chemical properties of flame. However, these properties are often not available. An empirical profile is used in this research, and this is based on the following best fit function determined by Brehob [55]:

$$\dot{q}''_w(z,t) = \begin{cases} \dot{q}''_{wo} \cdot \exp\left[-1.37\left(\frac{z-z_p}{z_f-z_p}\right)\right] & z > z_p \\ \dot{q}''_{wo} & z \le z_p \end{cases} \tag{4.12}$$

where $\dot{q}''_w(z,t)$ is the incident heat flux at position z along the height at time t, z is the height above the bottom opening from which burning starts, z_f is the flame height, z_p is the pyrolysis front, and q''_{wo} is given by $q''_{wo} = kz_f$, where k=47734 W/m^3[94]. z_p represents the height at which decomposition begins.

In order to validate the author's model for simulating flame spread in cavity of ventilated building façade system, it is necessary to check accuracy of the sub-models that have been described above, as well as the entire model.

4.4 Validation case 1: Initial flame driven into cavity

In section 4.2, a theoretical model was developed to predict mass flow rate inside cavity. In order to verify this theoretical model, this section compares theoretical results with simulation results using FDS.

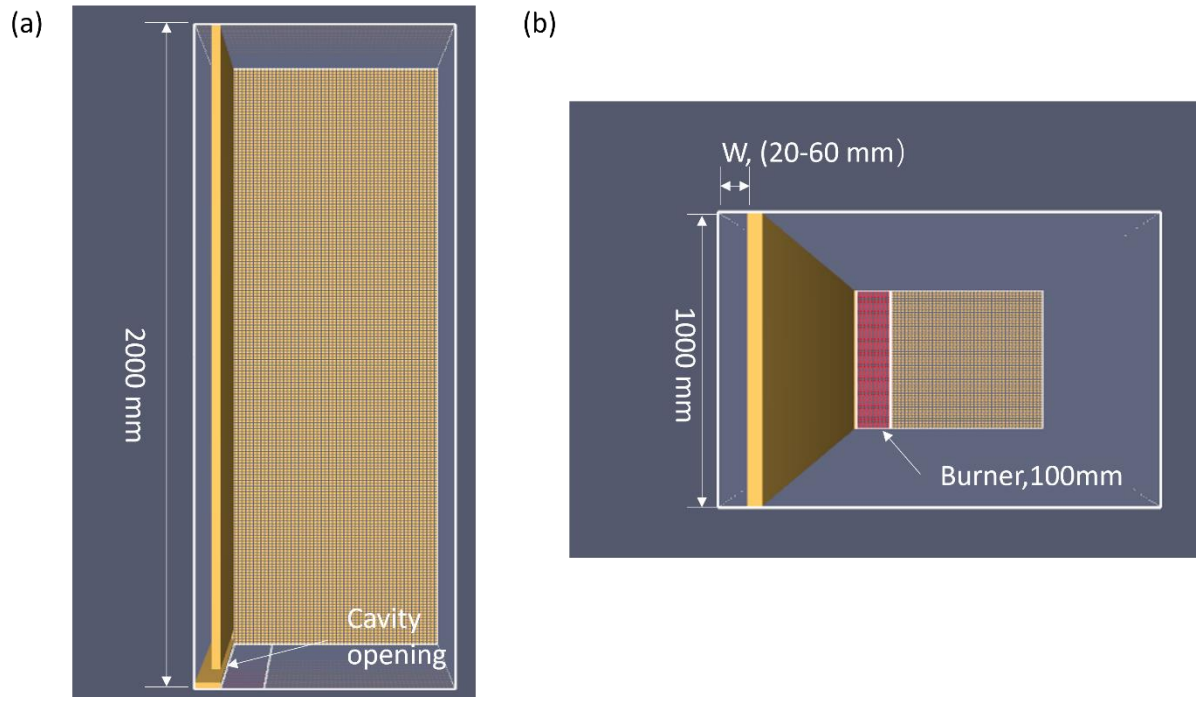

Figure 4.8 Calculation domain for validation case 1

Figure 4.8 shows the validation case. The FDS numerical simulation domain is 600mm*1000mm*2000mm (in the x, y and z directions respectively). The cavity ranges from 20 to 60 mm. A horizontal opening exists at the bottom of the wall from which flame is driven

into the cavity. The opening is the same size as the cavity. A propane gas burner is placed next to the opening. Open boundary is assumed for all the no-obstructed boundaries.

The FDS's simple chemistry combustion model is used in the simulation and theoretical calculations. The output of the gas is defined as heat release rate per unit area. The burner size is 4000 kW/m².The mesh size is taken at 5*5*5 mm, equating to 4 cells in the narrowest dimension.

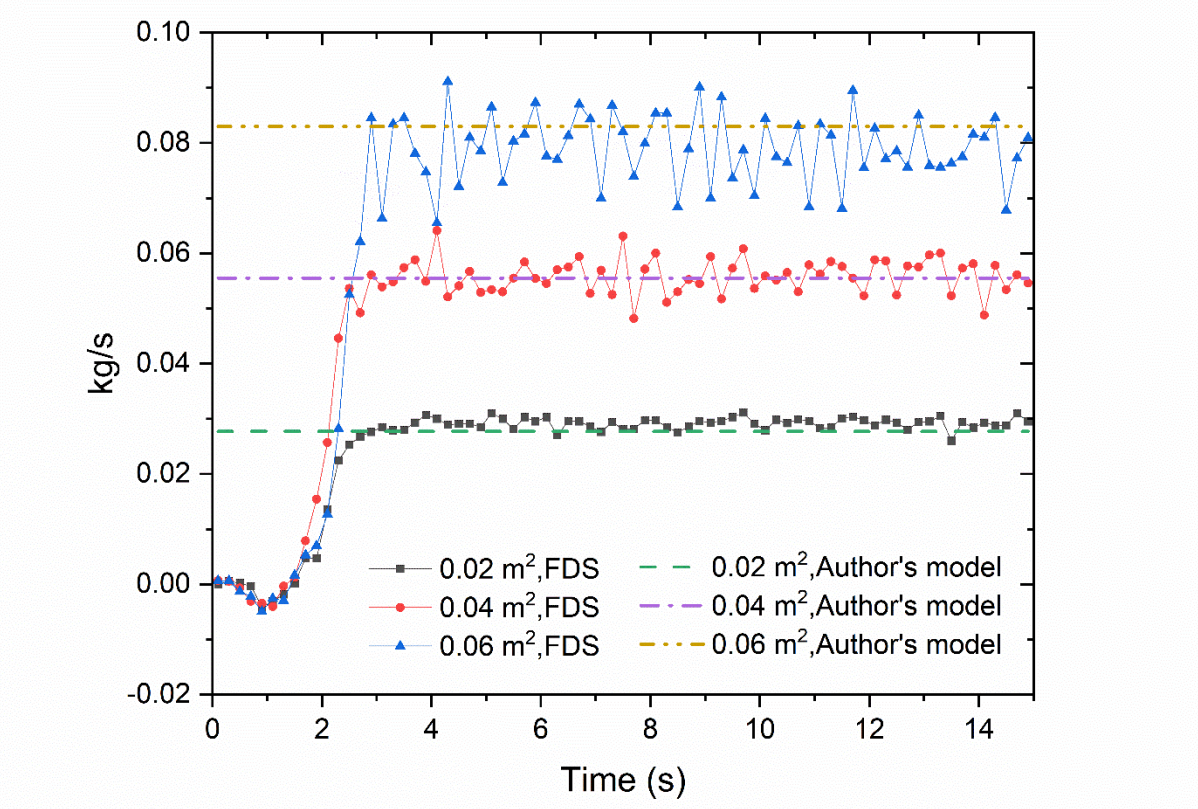

Figure 4.9 Comparison for mass flow rate calculated by using the author's single zone model in section 4.2 and FDS simulation results

Figure 4.9 compares plots of mass flow rate predicted by the author's single zone model (section 4.2) and FDS simulation results for varying cavity width (A_1 in Figure 4.5). The author's theoretical model assumes steady state flow. FDS simulation results indicate steady state is reached very quickly, around 4s after ignition. The author's single zone model slightly under predicts the flow into cavity at lower flow rates (opening size), but over predicts the flow at higher flow rates. These differences are mainly caused by using the flame temperature to represent the average temperature inside the cavity. However, the differences are small. For opening areas of 0.02, 0.04, and 0.06 m^2, the average differences between the author's single

zone model and FDS simulation results are 5.0%, 3.2%, and 5.6%, respectively. In general, the author's single zone model can be considered to be acceptable.

4.5 Validation case 2: Heat flux distribution in cavity

This validation case checks the sub-models on correlation of heat flux distribution along the height of cavity with cavity width and maximum heat flux at the bottom. It is based on the tests of Karlis[73].

Figure 4.10 illustrates the experimental setup of Karlis [73]. Two parallel-facing non-combustible calcium silicate boards were used in the experiment. A propane burner, which had an outlet area of 8 x 391 mm, was placed in the cavity, but adjacent to one of the two walls. In the bottom, the burner's length was the same as the wall's. Both the top and bottom of the cavity were open to allow air flow in.

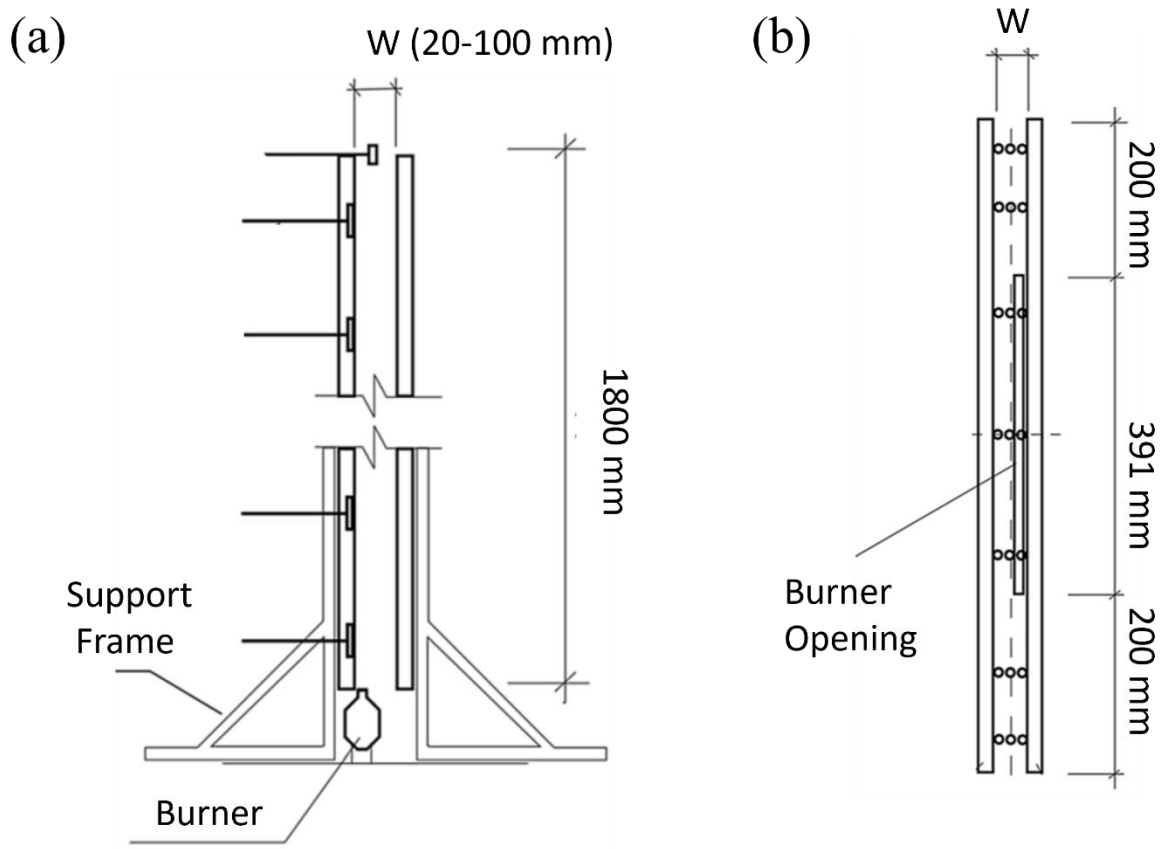

Figure 4.10 Experimental setup of Karlis[73] (a) side view (b) top view.

The full experimental program investigated the effects of changing the burner size and cavity

width, as summarized in Table 4.2. The distance between the two walls (cavity width) varied betweem 2cm and 10cm, and the heat release rate (RHR) of the gas burner gives a per metre value of 16.5kW/m, and 32.3 kW/m along the horizontal length of the cavity.

Table 4.2 Main parameters of the Experimental Program of Karlis[73]

Series	Q'(kW/m)	Cavity width, W(m)
I	16.5	0.02,0.04,0.06, 0.1
II	24.8	0.02,0.04,0.06, 0.1
III	32.3	0.02,0.04,0.06, 0.1

In the experimental program of Karlis [2], measurements were made for flame height, heat flux distribution along height of the wall. These results can be used to validate both the assumption of using the flame height correlation of Ingasson [6] (presented in Figure 4.7) and heat flux distribution along the wall height developed by the author as explained in detail in 4. 3.

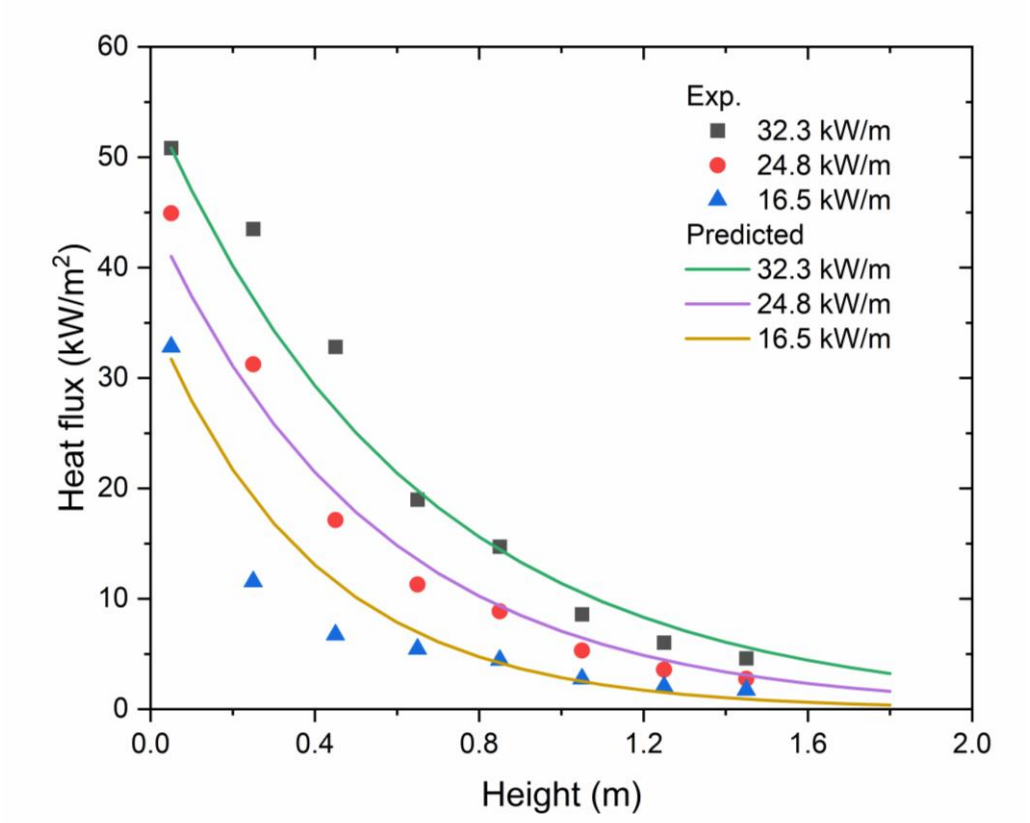

Figure 4.11 Comparison bwteen the author's sub-model on heat flux distribution along cavity height and the experimental results of Karlis [73] for a cavity width of 0.04 m with different burner sizes

Figures 4.11-4.12 compare the author's model calculation results, based on implementing the

theory described in section 4.3, with the experimental results of Karlis' [73], for different burner sizes at the same cavity width and different cavity widths at one particular cavity width. As shown in Figures 4.11-4.12, the heat flux inside a cavity increases as its width is reduced. The author's calculation equations in section 4.3 correlate reasonably well with the test results of Karlis [23].

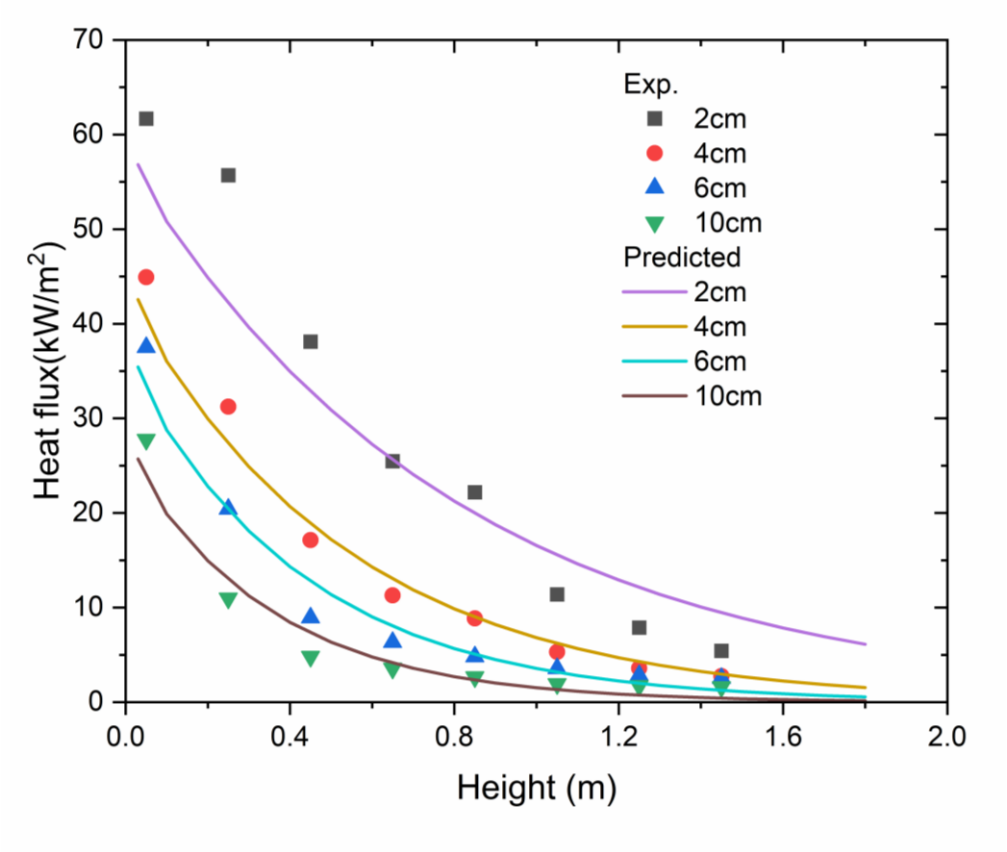

Figure 4.12 Comparison between the author's calculation results and experimental heat flux results of Karlis [23] for the case of (Q'=24.8 kW/m) with different cavity widths

4.6 Validation case 3: Flame spread in cavity with combustible materials

When combustible cladding materials are involved in ventilated façade, the heat release rate inside the cavity is not steady state, but varies with time. The additional heat released in the cavity is due to decomposition of combustible materials in the cladding materials surrounding the cavity.

For this validation, the author's modelling results are compared to the experimental results of

Sun[135] who performed fire tests on U-shaped exterior combustible surfaces, as Illustrated in Figure 4.13. The walls were constructed of gypsum boards covered by rigid PU form. The sample was mounted on an insulating gypsum board which was held by an aluminium frame.

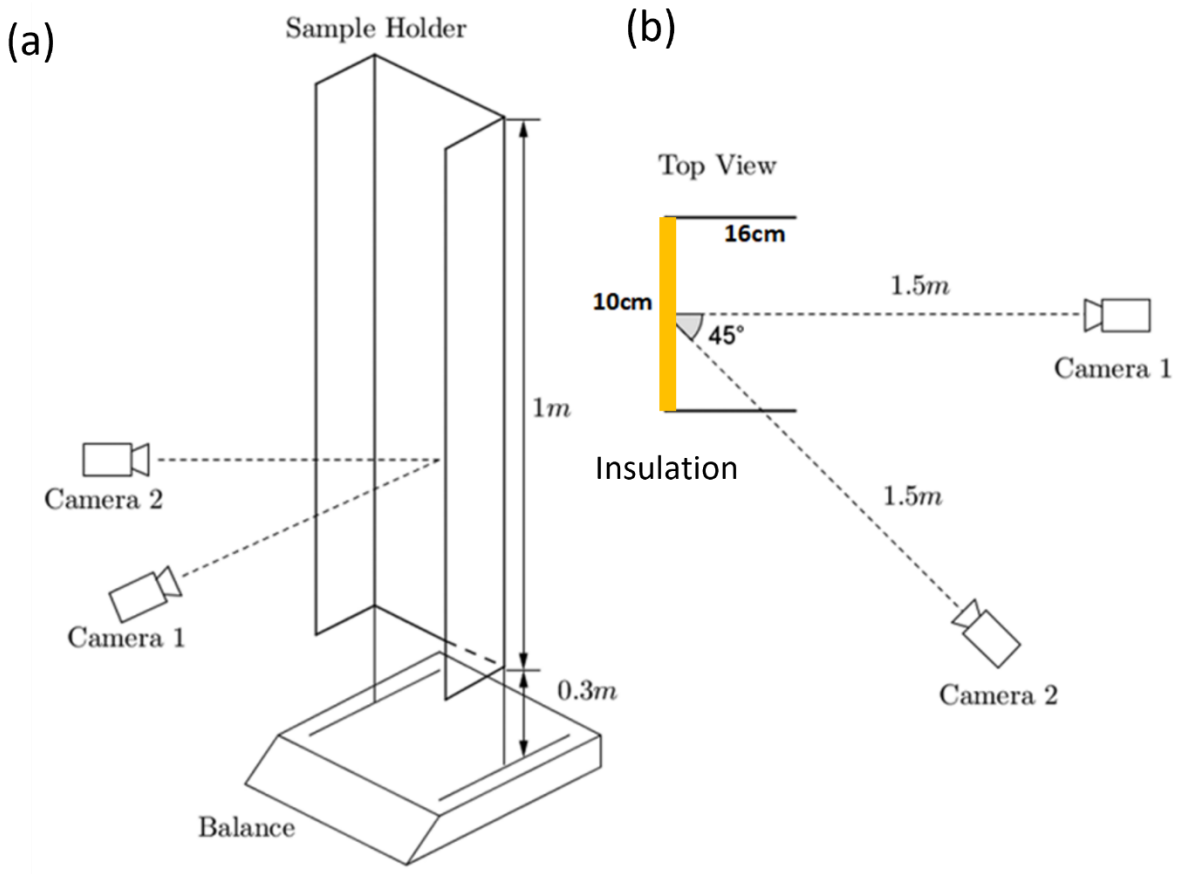

Figure 4.13 Experimental setup of Sun [12]: (a) Schematic, (b) cross-section showing materials

Tables 4.3 and 4.4 list the various material properties of PU foam used in the author's simulations and their sources. For PU, a two-step reaction mechanism, as depicted in equations 4.12 and 4.13, is assumed with the associated kinetic values in Table 4.4.

$$PU \rightarrow 0.84Polyol + 0.16Pyrolysis\ gase \tag{4.12}$$

$$Polyol \rightarrow 0.05Char + 0.95Pyrolysis\ gases \tag{4.13}$$

Table 4.3 Condensed phase parameters of PU[136]

Name	Density (kg/m³)	Cond. (W/(m·K))	Spec. Heat (kJ/(kg·K))	Emissivity
PU	60	0.02	1.3	0.9
Polyol	1012	0.15	2.0	0.9
Char	1012	0.15	2.0	0.9

Table 4.4 Reaction parameters of PU[136]

From	To	Pre-Exp. Factor (1/s)	Act. Energy (kJ/mol)	Heat of Reaction (kJ/kg)	Heat of combustion (kJ/kg)
PU	Polyol	1.68×10^{8}	135	1960	9600
Polyol	Char	8.74×10^{9}	175	1960	17500

To check that the combustion was not steady state and that additional combustion occurred due to decomposition of the combustible materials, Figure 4.14 compares the author's model calculated results of flame height with the test results of Sun[135]. The average flame height is well predicted by in the author's model.

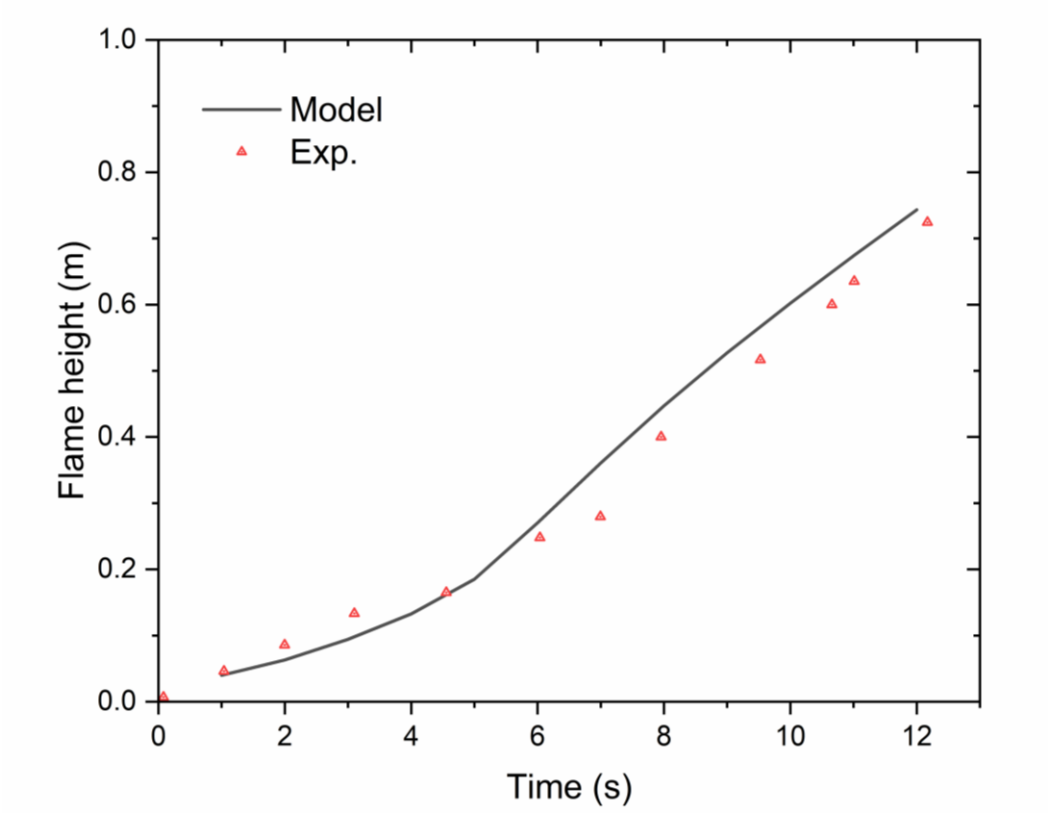

Figure 4.14 Comparison between the author's modelling results and the experimental results of Sun [135] for flame height

4.7 Validation case 4: BS8414 full scale fire test on ventilated facade

The previous sections have validated the sub-models of the author's new model for modelling flame spread in ventilated façade. This section presents validation of the author's model for simulating fire and flame spread in full-scale ventilated façade systems.

Following the tragic fire accident of the Grenfell Tower in London, an independent Expert Advisory Panel was established by government to advise on immediate actions that could be put into place to make tall buildings safer. As part of this initiative, a series of full-scale tests according to the British Standard BS8414 for fire performance of façade systems.

A total of 7 fire tests were carried out, and 3 of which involved façade with ventilated cavity. The test types are polyethylene, fire retardant polyethylene and mineral wool. The thermal/chemical properties of the fire-retardant polyethylene used in that test are not available. Mineral wool is non-combustible. As a result, only the ventilated cavity test with polyethylene was simulated using the author's model.

Figure 4.15 shows the general arrangement of the test. According to the study of Anderson and Jansson's [137], the initial flame height from the burner chamber is 2.71m. Therefore , equivalent heat release rate per unit width of the burner used in the model should be 265 kW/m .

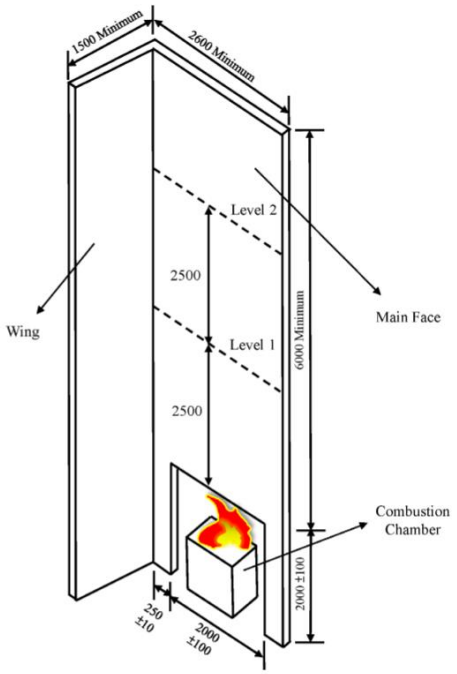

Figure 4.15 Schematic of full scale ventilated facade fire test according to BS8414-1

For this comparison study, the experimental results were taken from the BRE-DCLG-1 report [138]. Figure 4.15 shows details of the construction. The tested cladding system buildup (from the masonry substrate to the external finish) is as follows:

- 100 mm thick rigid PIR foam insulation boards,
- 50mm ventilated cavity,
- 4m thickness Aluminium composite material panels (ACM).

The ACM panels were comprised of 3 mm thick polyethylene (PE) filler and two sheets of 0.5 mm thickness aluminium on the front face. The aluminium layers did not burn but melt when exposed to high temperatures. Therefore, as simplification, the external finish layer is assumed to be polyethylene (PE) only, as shown in Figure 4.16.

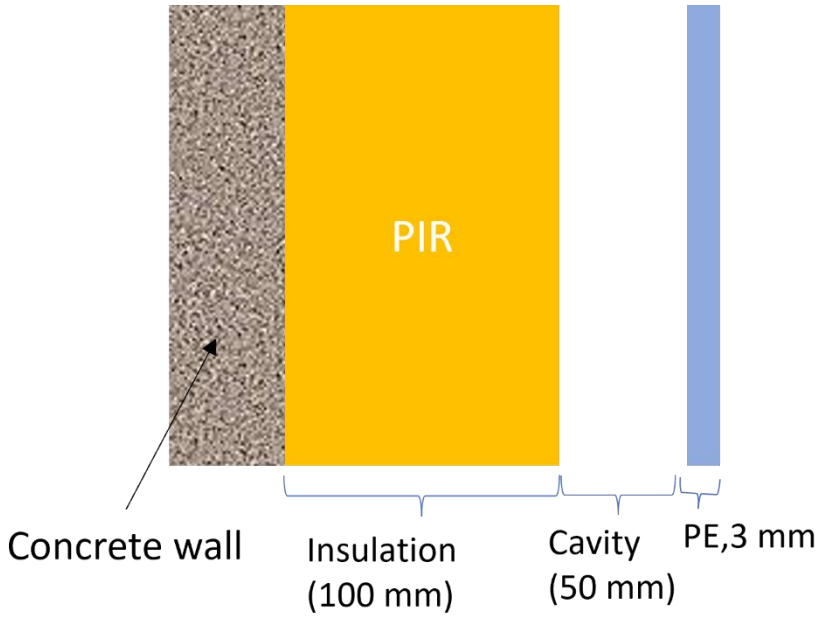

Figure 4.16 Model of the cross section view of the external wall used in BRE tests as part of Grenfell fire investigation [138]

Table 4.5 lists all other material properties for PE and PIR that were used in the author's simulation. A three step pyrolysis reaction [137, 139] was employed for PIR in Table 4.6. Figure 4.17 shows that the simulated weight loss using 3-step reaction input values agrees well with the measured data of Chaudhari[139].

Table 4.5 Condensed phase parameters of PU[136]

Name	Unit	PE	PIR
Density	kg/m³	1360[137, 140, 141]	35[137, 142]
Cond.	W/(m·K)	0.021[137, 140, 141]	0.045[137, 143]
Spec. Heat	kJ/(kg·K)	3.5[137, 140, 141]	1.5[137, 143]
Emissivity	-	0.92[137, 140, 141]	0.95[137, 143]
Absorption coef.	m^{-1}	1300[137, 140, 141]	3200[137, 143]
Gas permeability	m^2	$5.8*10^{-6}$	$5.8*10^{-6}$
Pre-Exp. Factor	1/s	$4.88*10^{22}$[99]	-
Act. Energy	kJ/mol	349[99]	-
Heat of Reac.	kJ/kg	920[84, 99, 144]	1750[137, 139]
Heat of combustion	MJ/kg	46.3[84, 144]	26.3

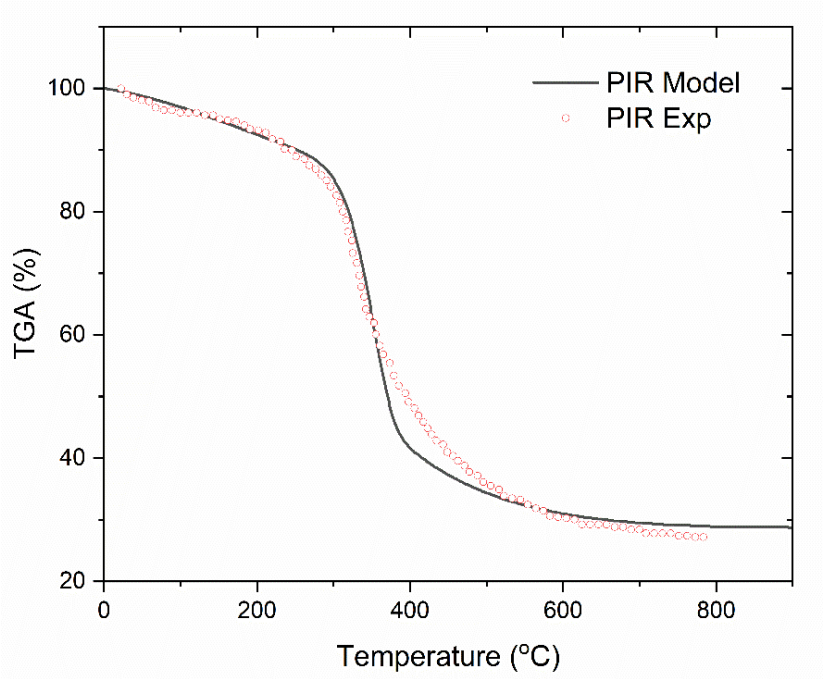

Figure 4.17 Comparison between TGA tests and three step reaction model for PIR (20k/min)[139]

Table 4.6 Parameters for three thermal decomposition process of polyisocyanurate (PIR) foam[137, 139]

Reac. #	Reaction Equation	A (s^{-1})	E (J/mol)	ΔH_r (kJ/kg)
1	PIR→0.75 PIR_Int1+0.25 Gas	5.68×10^{8}	8.96×10^{4}	160
2	PIR_Int1→0.45 PIR_Int2+0.55 Gas	2.84×10^{7}	1.24×10^{5}	93.7
3	PIR_Int2→0.82 Char+0.18 Gas	6.85×10^{3}	8.85×10^{4}	206

According to BS8414-1, the pass criterion is that the Level 2 external thermocouple temperature should not exceed 600°C and there should not be any continuous flaming beyond the top of the rig (6m). These conditions were reached in the BRE-DCLG Test 1 at 525 seconds. Therefore, the test was terminated at this time, rather than running for the full duration of 1800 seconds.

Figure 4.18 and 4.19 compare temperature data between the author's simulation results and the test results for both Level 1 and Level 2 thermocouples in the centre line above the combustion chamber. As seen in Figure 4.18, the agreement is good, considering complexity of the system and simplisity of the author's model. The author's model slightly underestimates temperatures at the beginning stage. Two factors contribute to this phenomenon. The first is underestimation of the initial fire source of the wood crib, and the second is random fluctuations of the flame.However, the intial error does not influence the final result for assessing façade performance.

Similar conclusions can be drawn for Level 2 temperature at L2. In the test, the measured temperature increased slowly after 150s and remained at about 200°C before increasing sharply when a continueous flame reached this point. The model results indicate that temperature at this level did change much until 150s, but increases after the flame tip is 1m below Level 2.

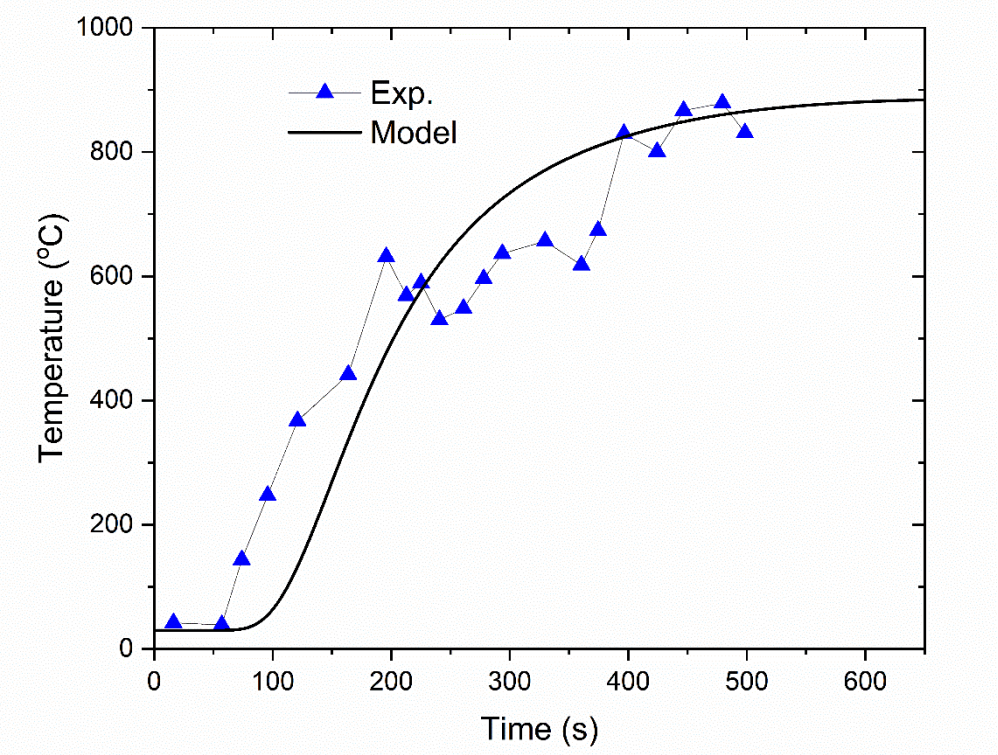

Figure 4.18 Comparison between the author's simulation results and measured Level 1 temperature from BRE-DCLG-1 test data.

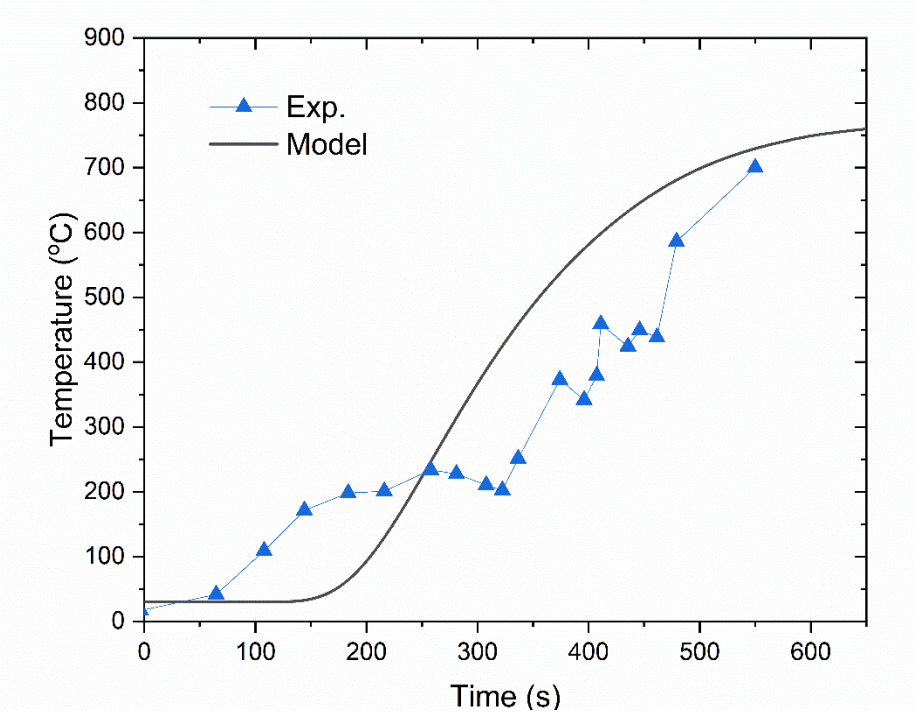

Figure 4.19 Comparison between the author's simulation results and measured Level 2 temperature from BRE-DCLG-1 test data.

In addtion to the above mentioned temperature results in the original testset [138], observations

were also made. An overview of these observations is shown in Table 4.7. Based on table 4.7, the test results of falme height vs time were deduced. Figure 4.20 shows a compariosn of flame height vs time between the test and the author's modelling. As can be seen in Figure 4.20, there is a good agreement between the predicted and measured flame height. The maximum discrepancy is 22.4% and the lowest discrpancy is 7.%. The length of time it takes for the flame to ascend to the test's peak rig in the test was 475 seconds, which compares reasonably well with the simulation result of 425 seconds. Both simulation and test results indicate that this façade system could not pass the full-scale test.

Table 4.7 Visual observations from the BRE-DCLG fire test of polyethene cladding[138]

Time (s)	Description
120	Flame tips to mid-height of panels 1C&1D
165	Flame tips to Level 1
225	Flame tips to mid-height of panels 2C&2D
405	Flame tips at top of panels 2C&2D
475	Frequent flaming at the top of the rig

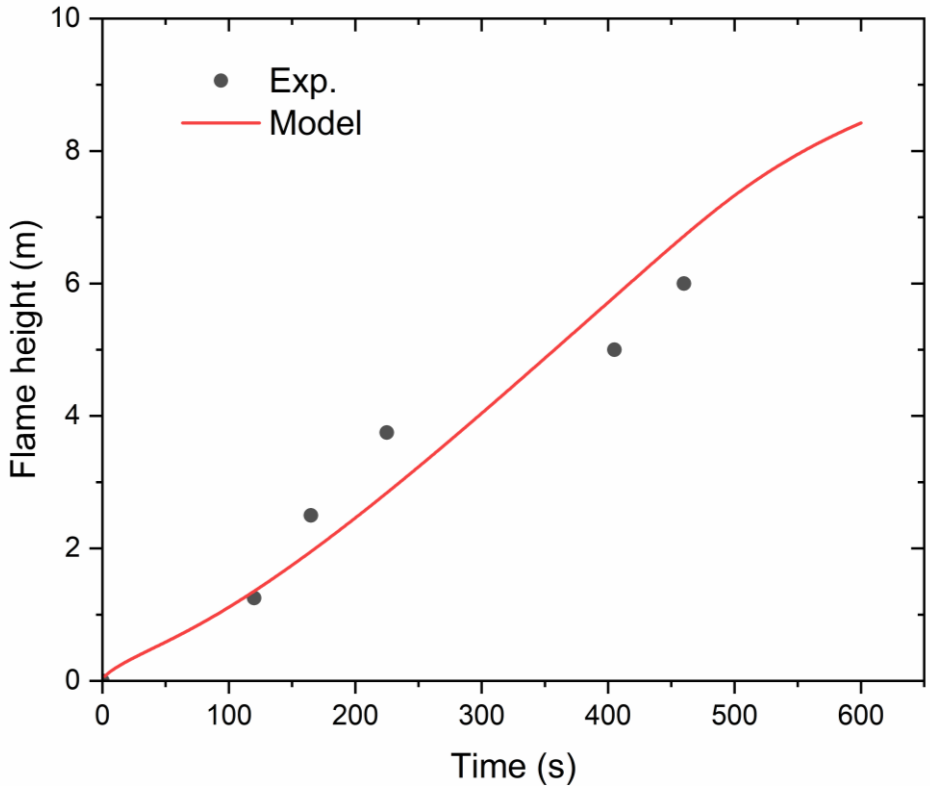

Figure 4.20 Comparison between the author's simulation results and observation based test results for flame height of test BRE-DCLG-1

4.8 Conclusions

1. This chapter has presented he development and validation of a simulation model for effiient assessment of fire and flame spread within the cavity of ventilated façade. The simulation model is validated against FDS simulation results and a full scale ventilated façade fire test. The main conclusions of this research are:The Ingason model for cavity flame height – heat release rate correlation can be used.
2. The author's simple model for heat distribution along the height of cavity can be used, based on analysis of the test data of Karlis [23].
3. The author's proposed model for heat driven into cavity through a cavity opening next to a fire source predicts close results with FDS simulation results.
4. The author's simulation model is able to predict the full scale ventilated façade test involving combustible insulation and external facing materials, based on comparison of temperature data recorded at two different levels, and flame height.

Chapter 5 Assessment of using the Single Burning Item classification for specification of materials on the external surface of buildings

5.1 Introduction

The Grenfell Tower fire in London, which occurred over a 24-floor building in June 2017, has tragically claimed 72 lives. TV images and subsequent fire investigations have identified fire spread on the external surface of the building as a main cause of the tragedy. This has directly led to the immediate change in fire safety regulations in England and Wales to specify that non-combustible materials should be used on the external surface of residential buildings above 18 m. Before this change, the external surface of buildings can use European Class B materials (materials of limited combustibility) based on the Single Burning Item (SBI) test result. Regardless of the recent change in England and Wales building regulations, the basis of specification is SBI test. And this SBI material classification based specification is widely adopted in Europe and similarly elsewhere[2]. However, since each SBI classification can represent a wide range of materials, it is questionable whether a material reaction to fire specification can truly represent fire spread performance over the external surface of buildings. This chapter aims to use the simplified simulation method, described in detail in Chapter 3, to investigate whether using the SBI based material classification system is suitable to specify materials on the external surface of buildings.

For the above purpose, the British Standard test method BS 8414[4] is assumed to represent the true behaviour of the external surface of buildings in fire, and the criteria in BR 135[7] are suitable to determine whether the external surface performance is acceptable.

Since before the immediate change Grenfell fire, the acceptable material classification is B, this chapter sets out to answer the following two specific questions:

(1) If a material is Class B according to the SBI test, would it pass the external surface fire performance criteria in BS135? If not, what are the conditions under which Class B materials cannot be used?
(2) If a material is Class C according to the SBI test, would it pass the external surface fire performance criteria in BS 135? If yes, what are the conditions under which Class C materials can be used?

This chapter assumes that buildings are clad with only one single material with the back side insulated. In reality, the façade of a building consists of a combination of different materials with or without ventilated cavity. This will be dealt with in Chapter 6.

The input data in the author's simulation model are fundamental properties of materials, related to chemical reaction kinetics of materials and thermal properties of materials. In contrast, the SBI classification is a composite value based on a specific fire test arrangement. Therefore, it is necessary to relate the fundamental properties of materials necessary for running the author's simulation model to a specific SBI specification. This is achieved through performing an inverse analysis, as presented in Section 5.2.

5.2 An inverse method for determination of fundamental combustion and thermal properties of materials

5.2.1 SBI test

The Single Burning Item (SBI) test is shown in Figure 5.1. In this test, an L-shaped specimen made of the same material with dimensions shown in Figure 5.1a is exposed a specific fire source supplied by a triangular gas burner placed at the corner of the test specimen producing an output of 30 kW resulting in a maximum heat exposure of 40 kW/m^2 on the test specimen.

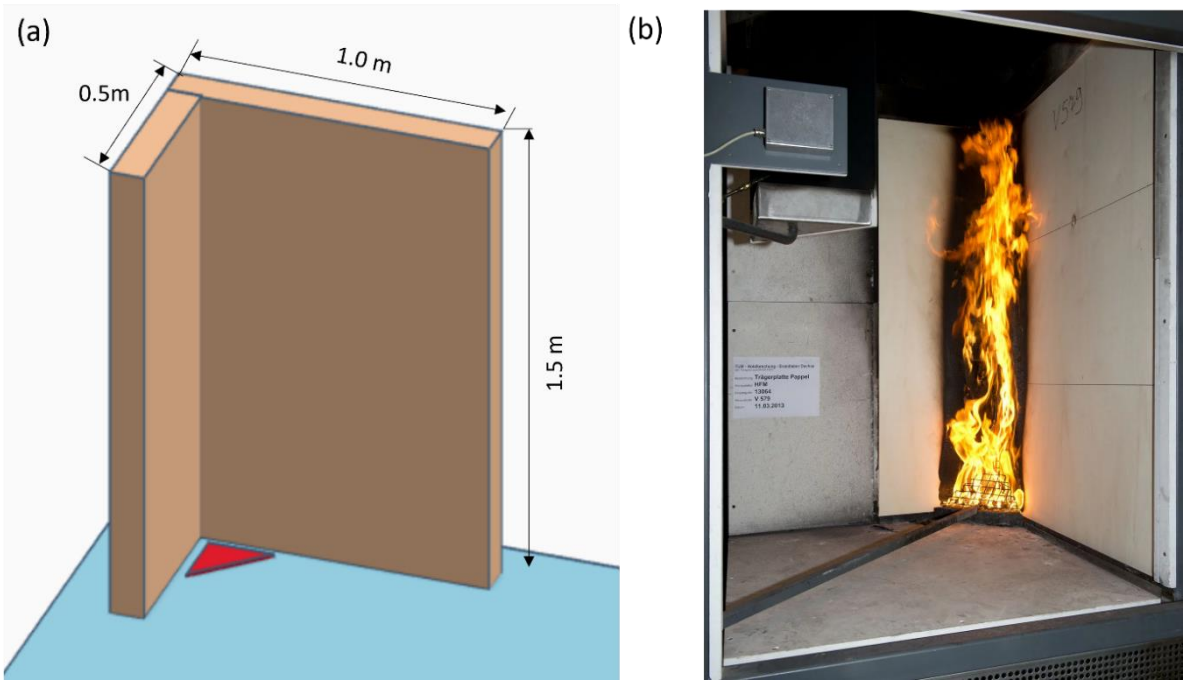

Figure 5.1 SBI test: (a) specimen dimensions, (b) a test in progress [2]

During an SBI test, the heat release rate (RHR) is continuously recorded. For determination of the material's SBI classification, the following two values are calculated: FIGRA is the changing secant slope of the RHR-time curve, and THR_{600s} is the total heat released during the first 600 s of the test.

$$FIGRA = 1000 \cdot max.\left(\frac{RHR(t)}{t-0}\right) \tag{5.1}$$

$$THR_{600s} = \sum_{0s}^{600s} RHR(t) \cdot \Delta t \tag{5.2}$$

where RHR is the rate of heat release (in kW), and t is time (in seconds) elapsed from the start of the test.

The SBI classifications for materials are summarized in Table 5.1.

Table 5.1 European material reaction to fire Classes based on SBI test[2]

Class	**Criteria**
A2/B	FIGRA ≤120 W/s; and THR_{600s} ≤7.5 MJ
C	FIGRA ≤250 W/s; and THR_{600s} ≤15 MJ
D	FIGRA ≤ 750 W/s
E	other

5.2.2 An inverse method to link fundamental combustion and thermal properties of materials with SBI classifications

The values of fundamental combustion and thermal properties of a material are those that achieve a particular SBI classification. There are two problems when implementing this principle.

Firstly, each SBI Class represents a range of SBI test results. Since the purpose of this study is to check whether any Class B material can pass the full-scale BS8414 fire test, the upper bound limits in Table 5.1 for Class B materials of FIGRA=120W/s and THR_{600s} =7.5MJ are used. Similarly, for Class C materials, since the aim of this study is to check whether the worst performing Class C material can pass the BS 8414 fire test, the upper bound limits in Table 5.1 of FIGRA=250W/s and THR_{600s} =15MJ are used.

The second problem concerns a lack of a unique link between any specific set of combustion and thermal properties of a material with its SBI Class. To resolve this problem, as will be described in detail in Section 5.3, construction materials that would be used on the external surface of buildings are divided into a number of groups, with fixed properties for some of the combustion and thermal properties of the materials that only have minor or moderate effects on their SBI classification. The remaining properties of the material are then changed to obtain a particular SBI class (B or C).

Therefore, although the input data for the simulations of this research are based on real materials, in terms of the ranges of their combustion and thermal properties, they are artificial materials as a result of the above outlined inverse analysis. Clearly, the inverse method of determining material properties cannot be carried out experimentally. Neither would there be any resources for such an exercise. Therefore, the author's model described in Chapter 3 was adapted to simulate the SBI test. This is explained in detail in section 5.2.3.

The results of material properties based on this inverse analysis are then used to simulate their performance under the BS 8414 fire test condition using the simplified method in Chapter 3 in conjunction with the acceptance criteria in BS 135.

5.2.3 Simulation of SBI test

To apply the one-dimensional flame spread model developed in Chapter 3 to simulate the SBI test, two assumptions are necessary to adapt the model to the features of the SBI test arrangement.

First, the fire source in the SBI test is located in the corner. This reduces free air entrainment to the flame thereby lengthening the flame height. Secondly, in an SBI test, the flame may spread horizontally. However, in the flame spread model in Chapter 3, it is assumed that the flame only spreads vertically. Therefore, the effect of the lateral spread of flame should be compensated. Details for these two adaptations are as follows.

Flame height

A well-known equation for corner wall fire is provided by Hasemi et al [145, 146]:

$$Z_f = 0.075\dot{Q}'^{3/5} \tag{5.3}$$

where $\dot{Q}^*$ is the characteristic heat release rate in kW/m and Z_f is the corner fire flame height.

Heskestad[147] gave the following slightly different correlation equation:

$$Z_f = -0.061 + 0.4\dot{Q}'^{3/5} \tag{5.4}$$

Heskestad's correlation was developed by assuming that the mass flow is roughly one quarter of the flow from an unbounded fire with four times the energy release rate[147, 148]. This method tends to over-predict the flame height. Therefore, Hasemi's flame height correlation will be used in the author's simulation of SBI test.

Pyrolysis width

In the early stages of an SBI test, the pyrolysis width is the width of the burner. Later, due to lateral heat transfer, the burning area widens. For simplicity, a constant equivalent burning width of 0.15m on each wing of the specimen can be assumed, as suggested by Hakkarainen [149] based on trial and error.

5.2.4 Validation of the author's simulation of SBI test

As validation of the assumptions made in the previous section for the author's simulation of the SBI test, the author's modelling results are compared with two SBI test results, one on 35 mm thick Isoflax insulation material[150], and one on 12 mm thick medium-density fiber (MDF) board[151]. The back of these test materials was non-combustible and can be assumed to be

insulated. Tables 5.2 and 5.3 list the combustible and thermal properties of Isoflax and MDF, from Hjohlman[150] and Hietaniemi[151] respectively. Isoflax is a non-charring material.

Table 5.2 Material parameters of MDF[151]

Parameter	Unit	Value
Density	Kg/m^3	700
Conductivity	W/ (m K)	0.15
Heat capacity	kJ/ (kg k)	1.5
A	1/s	2.38E+6
E	kJ/kmol	1.05E+05
Heat of reaction	kJ/kg	400
Heat of combustion	MJ/kg	13.3
Density-char	Kg/m3	80
Conductivity-char	W/ (m K)	0.2
Heat capacity-char	kJ/ (kg k)	2.5
Nu-fuel	kg/kg	0.78
Nu-residue	kg/kg	0.22
Thickness	m	0.012

Table 5.3 Material parameters of Isoflax[150]

Parameter	Unit	Value
Density	Kg/m^3	24.3
Conductivity	W/ (m K)	0.058
Heat capacity	kJ/ (kg k)	2.03
A	1/s	1.03E+22
E	kJ/kmol	1.25E+05
Heat of reaction	kJ/kg	3000
Heat of combustion	MJ/kg	15.5
Thickness	m	0.035

Figure 5.2 and Figure 5.3 compare the author's simulation results and the test results for MDF and Isoflax specimens respectively. The agreement is good, especially the early stage of combustion that determines the critical FIGRA index used in SBI classification. The more noticeable difference between the author's simulation results and SBI test results can be

attributed to the inaccuracy in modelling lateral flame spread. In the author's model, the drop is much more rapid than observed in the tests because the later stage continual flame spread could not be simulated. However, this difference has no influence on the materials SBI classification.

Table 5.4 compares the two key values of FIGRA and THR_{600s} for the two materials between the author's simulations and test results. The results are reasonably close, with the maximum difference in FIGRA being 10.09% and in THR_{600s} being 27.4%. In both cases, the author's simulation results give exactly the same SBI Class as the test.

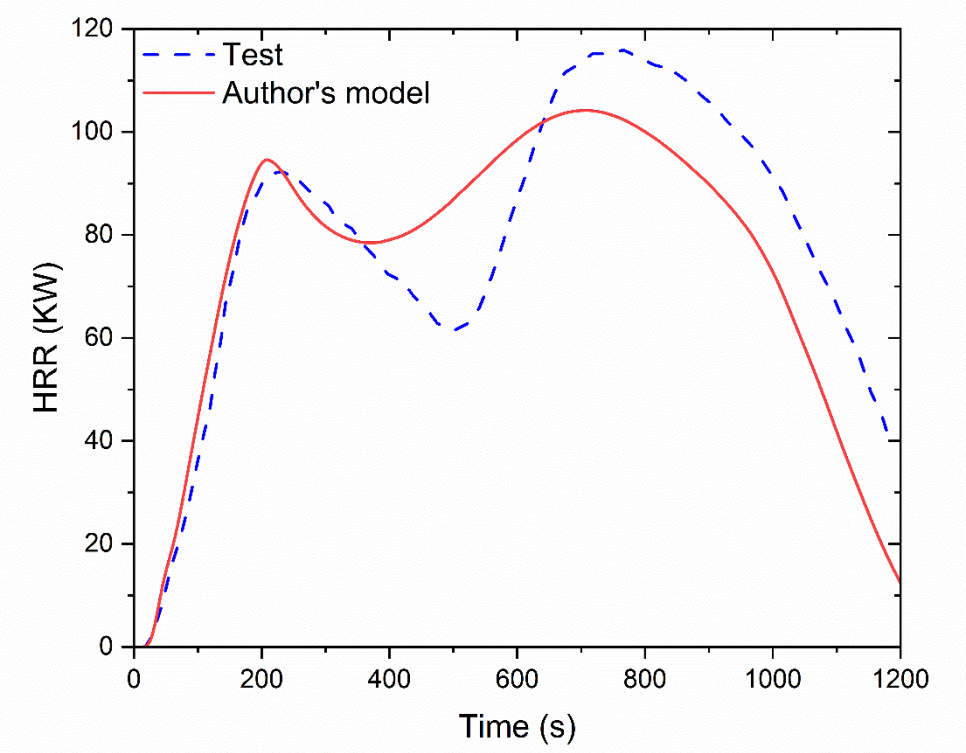

Figure 5.2 Comparison for heat release rate – time curve between the author's simulation and test results of Hietaniemi[151] for MDF

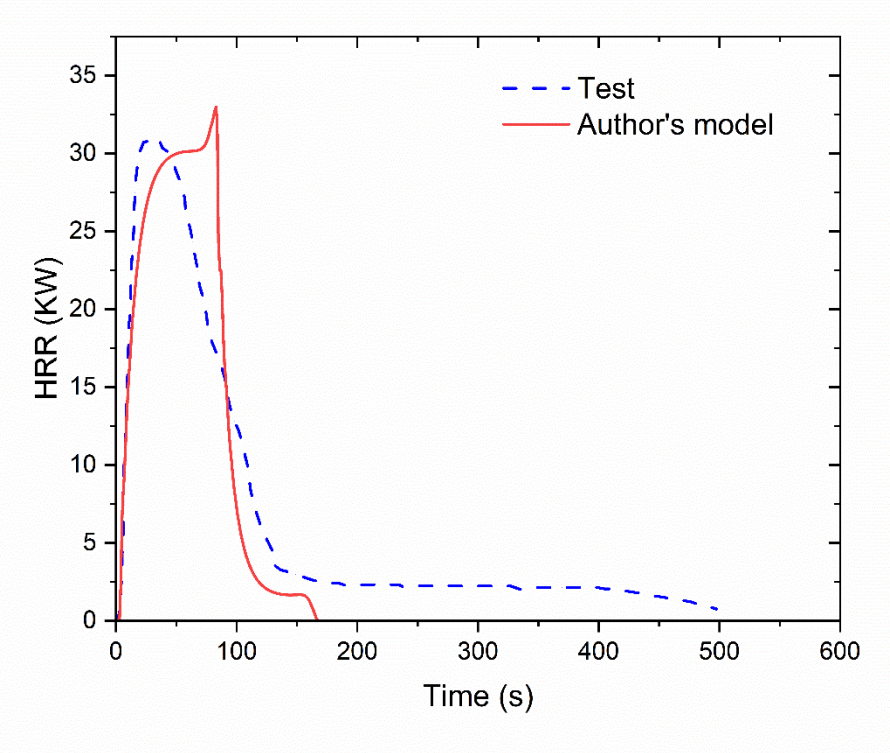

Figure 5.3 Comparison for heat release rate – time curve between the author's simulation and test results of Hjohlman[150] for Isoflax

Table 5.4 Summary of comparison between the authors' modelling and test results

Material	Test or simulation	FIGRA, in W/s (% difference)	THR_{600s} in MJ (% difference)	SBI classification
MDF	Test [9]	421 (10.09)	36.7 (4.6)	D
	Simulation	467	38.4	D
Isoflax	Test [8]	1544 (4.6)	3.93 (27.4%)	E
	Simulation	1472	2.85	E

5.3 Determination of material property combinations in inverse analysis

As mentioned in 5.2.2, there is no unique link between any fundamental combustion and thermal property of materials with SBI Class. However, because there are a large number of such fundamental properties, it is not possible to cover all possible combinations of these different properties to identify specific combinations that would give a particular SBI Class (B or C in this research). Therefore, a sensitivity study of SBI classification is carried out to

identify the material properties that are highly influential on SBI classification, and with those that are not deemed influential having fixed values.

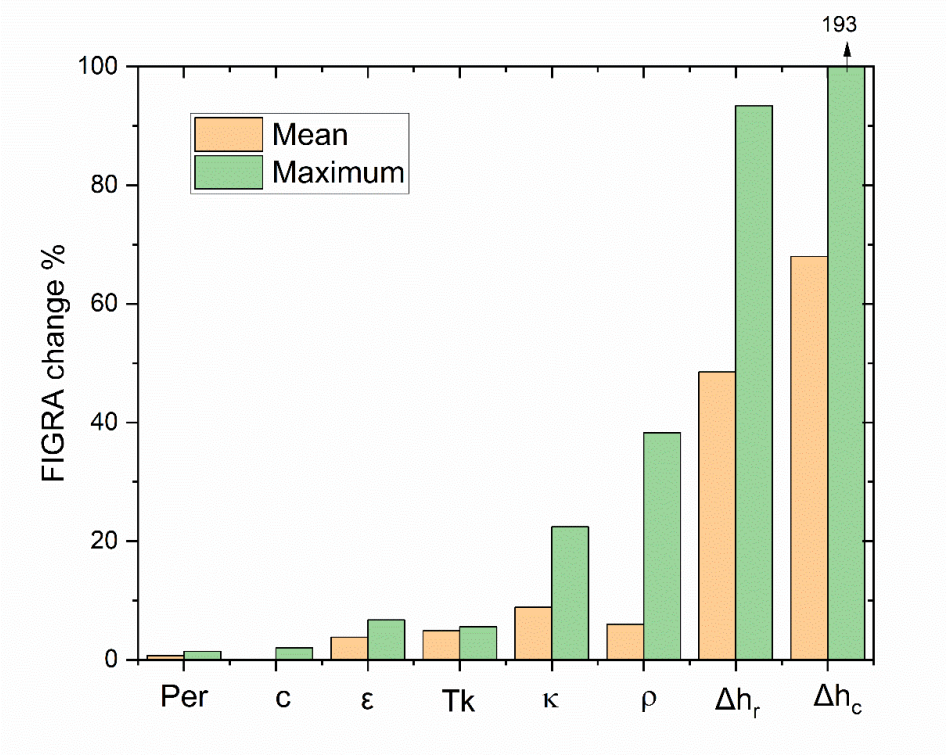

Figure 5.4 Sensitivity of various input material parameters on FIGRA

The sensitivity analysis is based on MDF, by changing a particular input value of the MDF material property by ±25% to examine the mean and maximum changes in FIGRA of the material. The results are shown in Figure 5.4. The FIGRA result is very sensitive to variations in chemical reaction properties. This is expected because these properties directly determine the rate of mass loss or pyrolysis of the material to become fuel input. Among physical and thermal properties of the material, gas permeability (Per), specific heat (c), emissivity (ε) and thickness (Tk) have minor effects and can be assumed to be fixed in inverse analysis. In contrast, thermal conductivity (k), density (ρ), heat of reaction (Δh_r) and heat of combustion (Δh_c) have strong influences on FIGRA. Therefore, their values will be varied in further inverse analysis to identify how they would be combined with chemical kinetics parameters that are used in Arrhenius equations.

These properties are usually unknown. However, for typical insulations, they tend to fluctuate within narrow ranges. To determine the boundary value of each property, various insulation-

related literature sources were reviewed. Table 5.5 summarizes the ranges of values of insulation materials' thermal properties.

Table 5.5 Thermal properties of common insulation materials

	Density (kg/m^3)	Conductivity (W/(m k))	Specific heat (kJ/(kg k))	References
Stone wool	40-200	0.033-0.040	0.8-1.0	[152, 153]
Glass wool	15-75	0.031-0.037	0.9-1.0	[154, 155]
Polyisocyanurate	30-45	0.018-0.028	1.4-1.5	[156-158]
Recycled PET	30-60	0.034-0.039	1.2	[159]
Phenolic foam	35-200	0.018-0.028	1.3-1.4	[160-162]
Mineralized wood fibres	320-600	0.06-0.107	1.8-2.1	[163, 164]
Cellulose	30-80	0.034-0.039	1.3-1.6	[165, 166]
Aerogel(panels)	10-70	0.013-0.015	1	[167, 168]
Polystyrene	15-40	0.031-0.038	1.25-1.7	[169, 170]
Polyurethane	15-45	0.022-0.27	1.3-1.4	[170]
Wood fibers	50-270	0.038-0.05	1.9-2.1	[171]

Therefore, in this research, materials can be divided into four broad groups (D1, D2, D3, D4) with densities of 30,60,120,240 kg/m^3, as indicated in Table 5.5. The thermal conductivity exhibits a linear increase with increase of density for conventional material and non-linear variation for non-linear for organic materials[172]. There is no good equation to correlate these two properties. Therefore, thermal conductivity is considered as an independent property. Four values of thermal conductivity are used: 0.02, 0.04, 0.08, and 0.16 W/m.K.

Data for heat of reaction in literature are inconsistent. In a recent study by Stoliarov[105], the heat of reaction values of 10 polymers were measured, as shown in Table 5.6. In this research, three heat of reaction values are considered, being lower bound, average, and upper bound values of HR1=700, HR2=1300 and HR3=2500 kJ kg^{-1}, respectively. Heat of reaction is considered an independent material parameter.

Table 5.6 Heat of reaction of polymeric materials [105]

Polymer	Heat of reaction (kJ kg^{-1})

Poly(methylmethacrylate)	870
Poly(oxymethylene)	2540
Polyethylene	920
Polypropylene	1310
Polystyrene	1000
Polyamide 6,6	1390
Poly(ethylene terephthalate)	1800
Bisphenol A polycarbonate	830
Poly(vinylidene fluoride)	2120
Poly(vinyl chloride)	710

Similarly, the heat of combustion of materials varies in a range of 8MJ/kg to 25 MJ/kg [144]. In this research, three values are considered, being the lower bound, average, and upper bound values of HC1=8 MJ/kg, HC2=16 MJ/Kg, and HC3=25 MJ/Kg, respectively. Heat of combustion is also treated as an independent material property.

Therefore, it is assumed that density, thermal conductivity, heat of reaction and heat of combustion are the only independent material property variables

Table 5.7 Variations of thermal properties and chemical properties in simulations

No.	Density ($kg\ m^{-3}$)	N0.	Thermal conductivity (W/ (m K))	No.	Heat of reaction (kJ/kg)	No.	Heat of combustion (MJ/kg)
D1	30	K1	0.02	HR1	700	HC1	8
D2	60	K2	0.04	HR2	1300	HC2	16
D3	120	K3	0.08	HR3	2500	HC3	25
D4	240	K4	0.16				

The chemical reaction kinetics parameters, represented by E and A in Arrhenius equation [144, 173] can have large variations. They can be combined to give a variety range of mass loss (rate of pyrolysis) values. Table 5.7 lists their lower bound, average and upper bound values, based on a number of sources[173, 174].

Table 5.8 Variations of Arrhenius parameters

Value type	E(kJ/mol)	A

Lower boundary	102	1.6×10^{26}
Average	218	1.0×10^{16}
Upper boundary	334	6.5×10^{6}

However, E and A are not treated as independent material properties. The simulation uses the average value of 1.0×10^{16} for A. The value of E is adjusted within the ranges in Table 5.8 to give the exact values of FIGRA or THR_{600s} to reach the minimum threshold for SBI Class B or C for combinations of P1-P4, K1-K4,HR1-HR3 and HC1-HC3.

Therefore, a total of 144 combinations are considered, being 4 density values (P1-P4), 4 thermal conductivities (K1-K4), three heat of reaction values (HR1-HR3), three heat of combustion values (HC1-HC3). Appendix A lists all the combinations used in simulations.

5.5 Results of inverse analysis

Figures 5.5 presents selective results of materials with a density of 30 kg/m^3 and changing heat of reaction, heat of combustion and thermal conductivity. Because the heat of combustion values for HC1, HC2 and HC3 are different, The RHR curves have three distinctive grouping. The SBI class of materials is determined by FIGRA. However, despite achieving the same FIGRA, different materials can have very different RHR-time curves, because the heat of combustion directly relates to the peak value and total heat released when a given amount of material is burned. However, for these materials, the THR_{600s} value does not determine their SBI class.

Figures 5.6 plot results for materials with a constant value of heat of combustion while varying other values. Due to a constant value of heat of combustion, the THR values for these materials are almost identical. However, the peak RHR values are different due to different values of thermal conductivity and heat of reaction. For example, the peak RHR value of a material with lower heat reaction gives a higher peak value of RHR because the reaction happens fast. As SBI classification is based on FIGRA and THR_{600s}, the peak value of RHR has some influence.

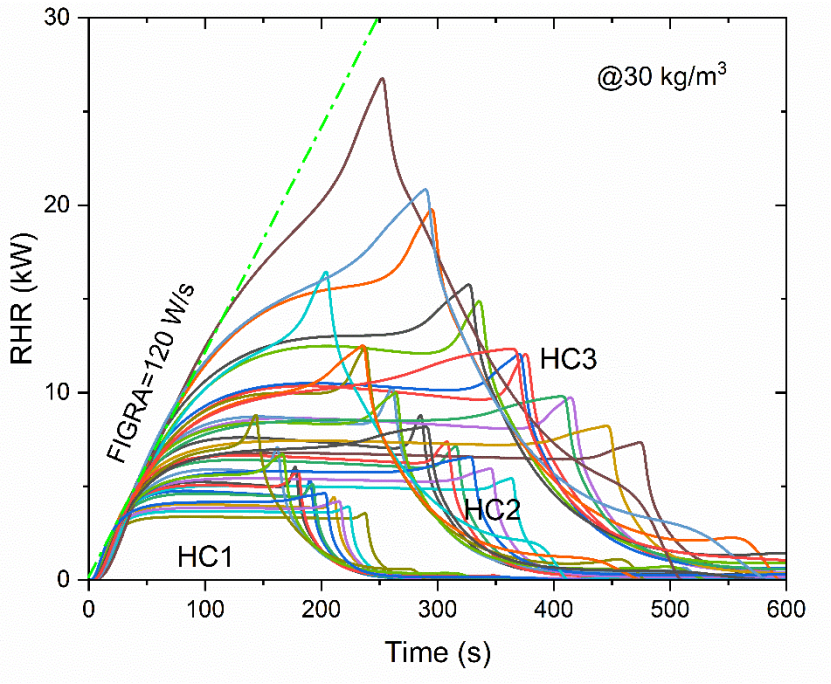

Figure 5.5 RHR curves of Class B materials with different values of heat of combustion, heat of reaction and thermal conductivity

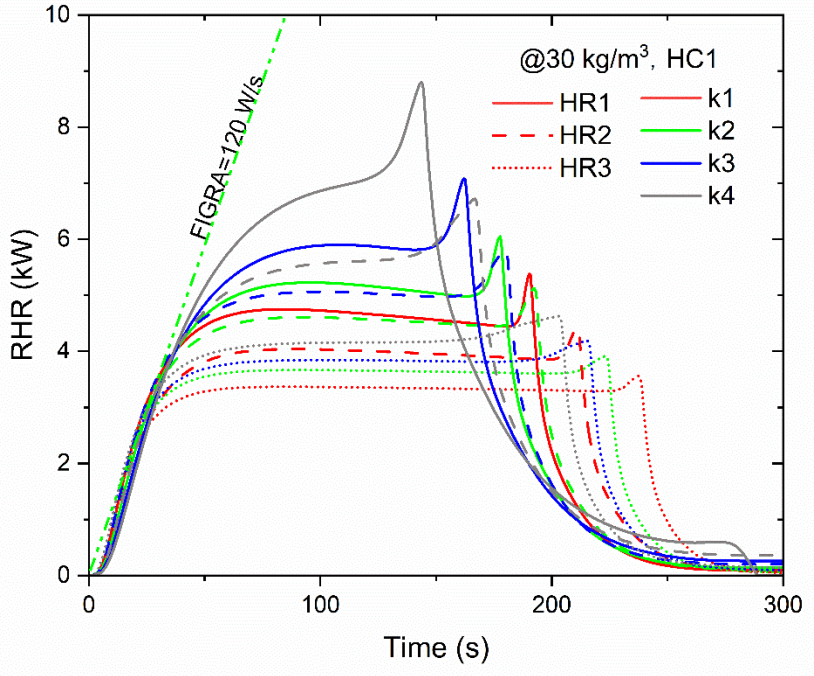

Figure 5.6 RHR curves of Class B materials with a constant value of heat of combustion combined with different values of heat of reaction and thermal conductivity (HC1 in figure 5.6)

Tables 5.10 summarise the combinations of material properties that would just reach Class B thresholds. Appendices B and C present all SBI simulation results for Class B and Class C materials respectively.

Table 5.9 Combinations of material properties

No.	Combinations	No.	Combinations	No.	Combinations	No.	Combinations
1	D1-HC1-HR1-K1	37	D2-HC1-HR1-K1	73	D3-HC1-HR1-K1	109	D4-HC1-HR1-K1
2	D1-HC1-HR1-K2	38	D2-HC1-HR1-K2	74	D3-HC1-HR1-K2	110	D4-HC1-HR1-K2
3	D1-HC1-HR1-K3	39	D2-HC1-HR1-K3	75	D3-HC1-HR1-K3	111	D4-HC1-HR1-K3
4	D1-HC1-HR1-K4	40	D2-HC1-HR1-K4	76	D3-HC1-HR1-K4	112	D4-HC1-HR1-K4
5	D1-HC1-HR2-K1	41	D2-HC1-HR2-K1	77	D3-HC1-HR2-K1	113	D4-HC1-HR2-K1
6	D1-HC1-HR2-K2	42	D2-HC1-HR2-K2	78	D3-HC1-HR2-K2	114	D4-HC1-HR2-K2
7	D1-HC1-HR2-K3	43	D2-HC1-HR2-K3	79	D3-HC1-HR2-K3	115	D4-HC1-HR2-K3
8	D1-HC1-HR2-K4	44	D2-HC1-HR2-K4	80	D3-HC1-HR2-K4	116	D4-HC1-HR2-K4
9	D1-HC1-HR3-K1	45	D2-HC1-HR3-K1	81	D3-HC1-HR3-K1	117	D4-HC1-HR3-K1
10	D1-HC1-HR3-K2	46	D2-HC1-HR3-K2	82	D3-HC1-HR3-K2	118	D4-HC1-HR3-K2
11	D1-HC1-HR3-K3	47	D2-HC1-HR3-K3	83	D3-HC1-HR3-K3	119	D4-HC1-HR3-K3
12	D1-HC1-HR3-K4	48	D2-HC1-HR3-K4	84	D3-HC1-HR3-K4	120	D4-HC1-HR3-K4
13	D1-HC2-HR1-K1	49	D2-HC2-HR1-K1	85	D3-HC2-HR1-K1	121	
14	D1-HC2-HR1-K2	50	D2-HC2-HR1-K2	86	D3-HC2-HR1-K2	122	
15	D1-HC2-HR1-K3	51	D2-HC2-HR1-K3	87	D3-HC2-HR1-K3	123	
16	D1-HC2-HR1-K4	52	D2-HC2-HR1-K4	88	D3-HC2-HR1-K4	124	
17	D1-HC2-HR2-K1	53	D2-HC2-HR2-K1	89	D3-HC2-HR2-K1	125	D4-HC2-HR2-K1
18	D1-HC2-HR2-K2	54	D2-HC2-HR2-K2	90	D3-HC2-HR2-K2	126	D4-HC2-HR2-K2
19	D1-HC2-HR2-K3	55	D2-HC2-HR2-K3	91	D3-HC2-HR2-K3	127	
20	D1-HC2-HR2-K4	56	D2-HC2-HR2-K4	92	D3-HC2-HR2-K4	128	
21	D1-HC2-HR3-K1	57	D2-HC2-HR3-K1	93	D3-HC2-HR3-K1	129	
22	D1-HC2-HR3-K2	58	D2-HC2-HR3-K2	94	D3-HC2-HR3-K2	130	
23	D1-HC2-HR3-K3	59	D2-HC2-HR3-K3	95	D3-HC2-HR3-K3	131	D4-HC2-HR3-K3
24	D1-HC2-HR3-K4	60	D2-HC2-HR3-K4	96	D3-HC2-HR3-K4	132	D4-HC2-HR3-K4
25	D1-HC3-HR1-K1	61	D2-HC3-HR1-K1	97	D3-HC3-HR1-K1	133	D4-HC3-HR1-K1
26	D1-HC3-HR1-K2	62		98		134	
27	D1-HC3-HR1-K3	63		99		135	
28	D1-HC3-HR1-K4	64		100		136	
29	D1-HC3-HR2-K1	65	D2-HC3-HR2-K1	101	D3-HC3-HR2-K1	137	
30	D1-HC3-HR2-K2	66	D2-HC3-HR2-K2	102	D3-HC3-HR2-K2	138	
31	D1-HC3-HR2-K3	67		103		139	
32	D1-HC3-HR2-K4	68		104		140	
33	D1-HC3-HR3-K1	69	D2-HC3-HR3-K1	105	D3-HC3-HR3-K1	141	D4-HC3-HR3-K1
34	D1-HC3-HR3-K2	70	D2-HC3-HR3-K2	106	D3-HC3-HR3-K2	142	D4-HC3-HR3-K2
35	D1-HC3-HR3-K3	71	D2-HC3-HR3-K3	107	D3-HC3-HR3-K3	143	
36	D1-HC3-HR3-K4	72	D2-HC3-HR3-K4	108	D3-HC3-HR3-K4	144	

5.5 Assessment of suitability of using SBI classification to specify external materials of buildings

Figure 5.7 shows the setup, and dimensions and burner size of BS8414 full-scale fire test and the author's simulation model. In the author's model, the panel is simplified to represent 1D vertical flame spread along the dashed line of AB in the centre of the panel as illustrated in figure 5.7. According to Anderson and Jansson's study[137], the initial flame height from the burner chamber is 2.71m. That's equivalent to the 265 kW/m for the burner in the model. The heat release growth process of wood crib burner used in the BS 8414 full-scale fire test is shown in Figure 5.8.

The acceptance criteria according to BR 135[7] are: flame not extending beyond the top of the test rig (6m) or the thermocouples at level 2 (5m) not exceed 600^{o}C . The author used Ahmad and Faeth's correlation[32] (Eq. 3.7 in Chapter 3) for flame temperature. The temperature at 5 m is 466.6 ^{o}C when flame height reaches 6m, so only criteria for flame height is used.

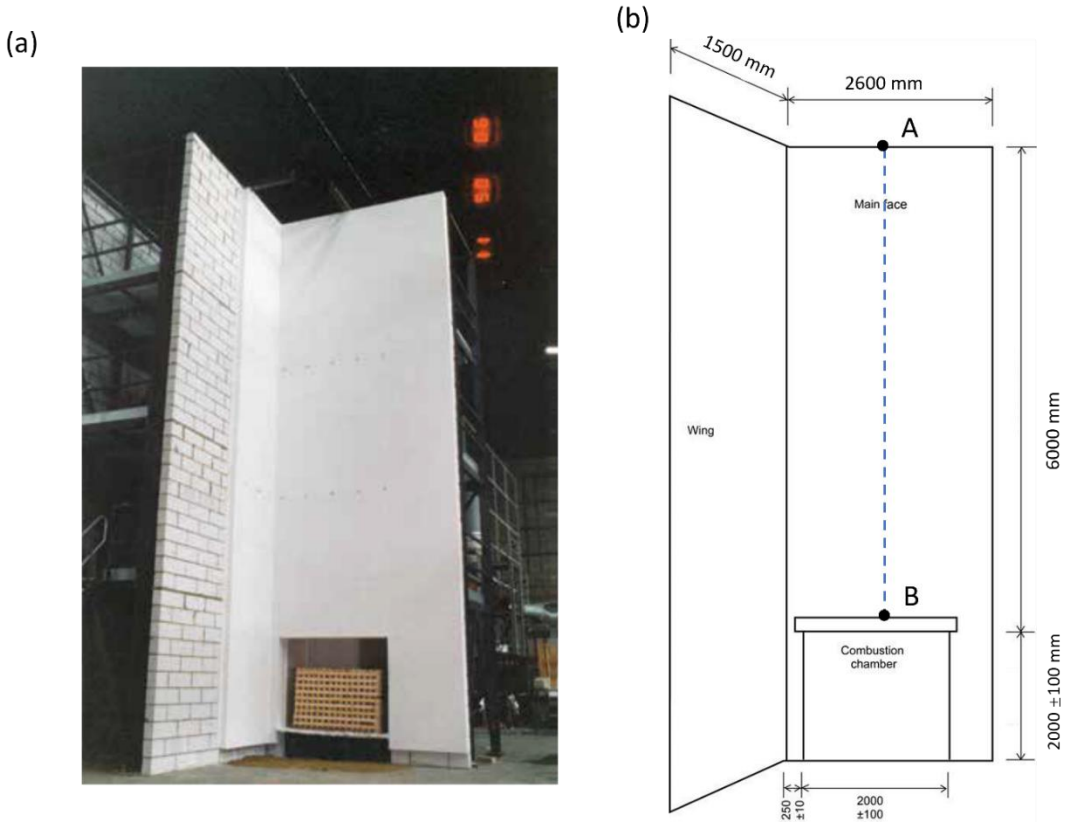

Figure 5.7 BS 8414 fire test and simulation model: (a) A typical test, (b) dimensions and burner size

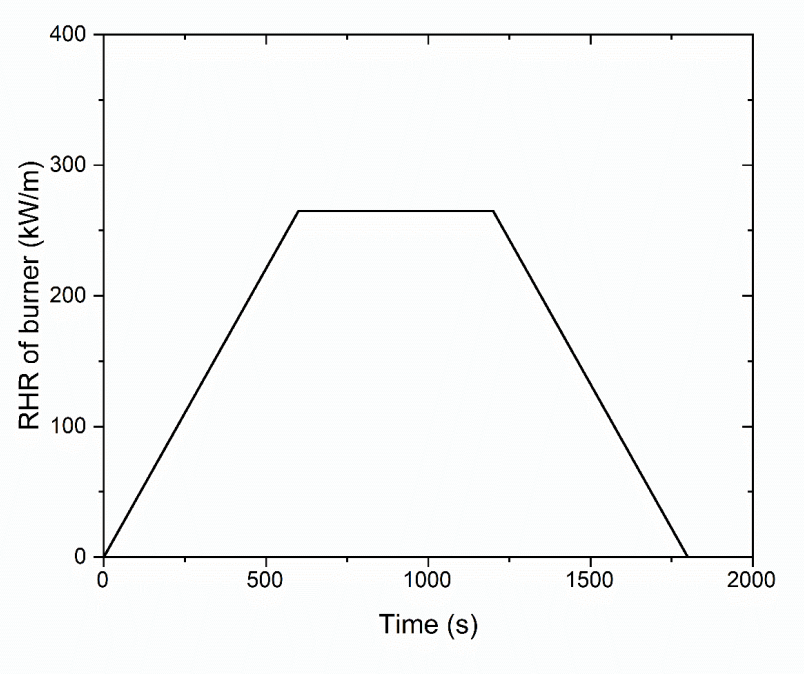

Figure 5.8 Heat release rate used in the model for the BS8414-1 wood chamber[137]

5.6.1 Assessment of SBI Class B materials

Figures 5.9-5.13 present selective results of flame height-time curves for varying density, heat of reaction, heat of combustion, and thermal conductivity. Also plotted in these figures are the BR135 acceptance criteria for flame height of 6m. Appendix D presents all simulation results.

These results indicate that while SBI Class B materials would be able to achieve acceptable performance according to BR135 in the majority of cases, in some cases, Class B material may not pass the BS8414 test.

Among all Class B materials, low density (<30 kg/m^3) materials tend to be able to fulfil the acceptance criterion for BS 8414 test (flame height not above 6m), except for materials with the highest heat of combustion, the lowest heat of reaction and the highest thermal conductivity (HC3-HR1-k4).

Both density and heat of combustion are important factors affecting flame height. In figures 5.9-5.12, flame height increases with increasing density. Within each of these figures, flame height also increasing with heat of combustion. This is expected because a higher value of these two variables means increased total heat as well as accumulating effects. If other parameters are the same (thermal conductivity, heat of reaction), a high value of any of these two variables means sustaining high rate of heat release for longer in the fire test and with previous ignited

materials continuing contributing to the release of heat of newly decomposed material, thus enabling the flame to project to great heights. With increasing density, more combinations of Class B material would not pass the full-scale test acceptance criterion. For example, for materials with densities of 60kg/m^3 and 120kg/m^3, 6 and 10 of the total 36 material combinations would fail the test, respectively. For a density of 240 kg/m^3, only materials with the lowest heat of combustion (HC1) would pass the test.

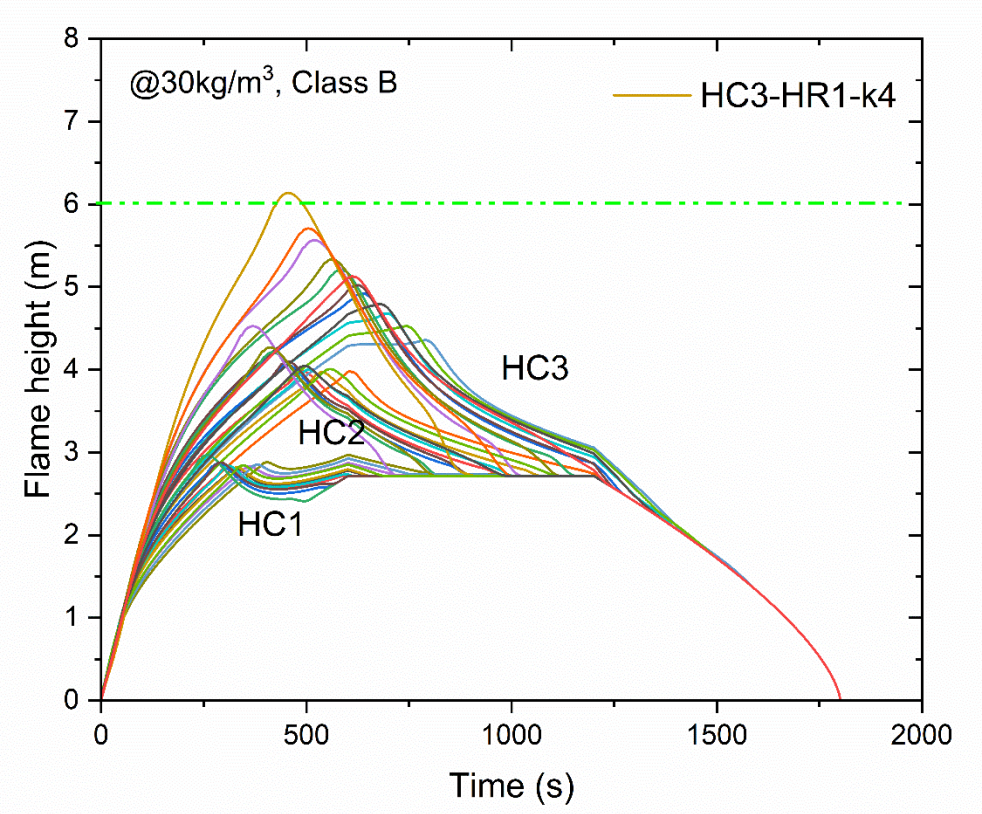

Figure 5.9 Variations in flame height of Class B materials with a density of 30 kg/m^3

In contrast, heat of reaction and thermal conductivity have only moderate influence on flame height, as shown in Figure 5.10. Heat of reaction and thermal conductivity do not have strong influences on flame height results because they only alter the decomposition of solids. In contrast, heat of combustion is directly related to the burning of gaseous species, which changes the total heat release and flame height.

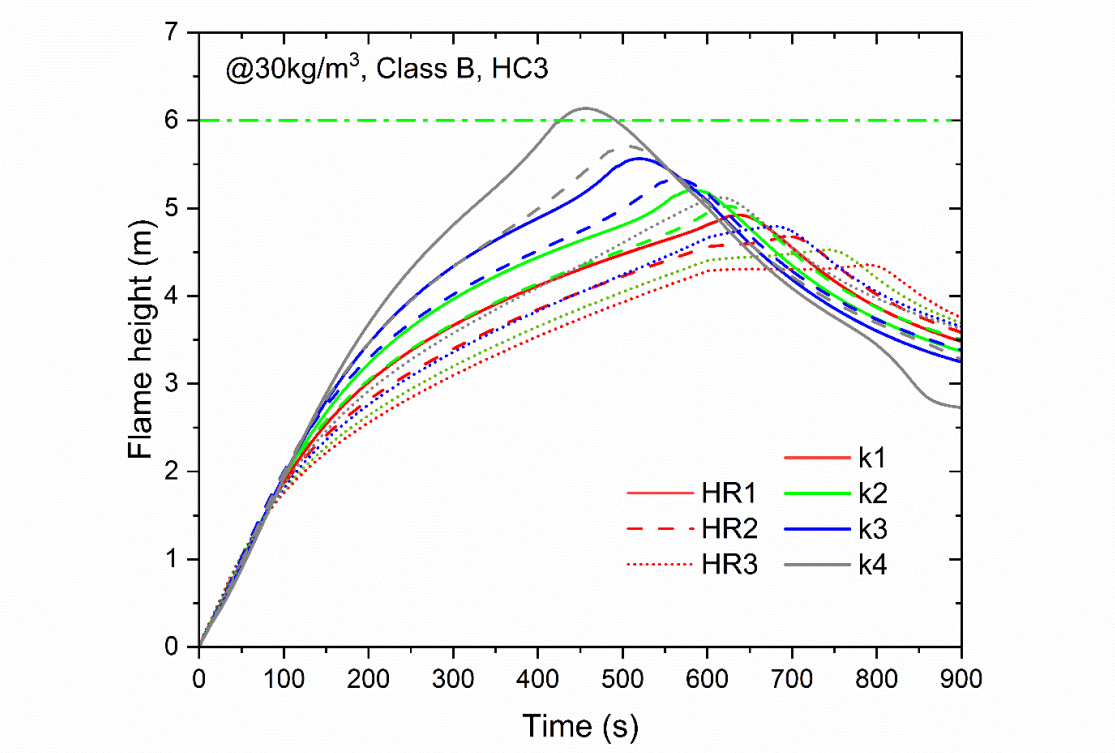

Figure 5.10 Variations in flame height of class B materials with different heat of reaction and thermal conductivity (HC3 in figure 5.10)

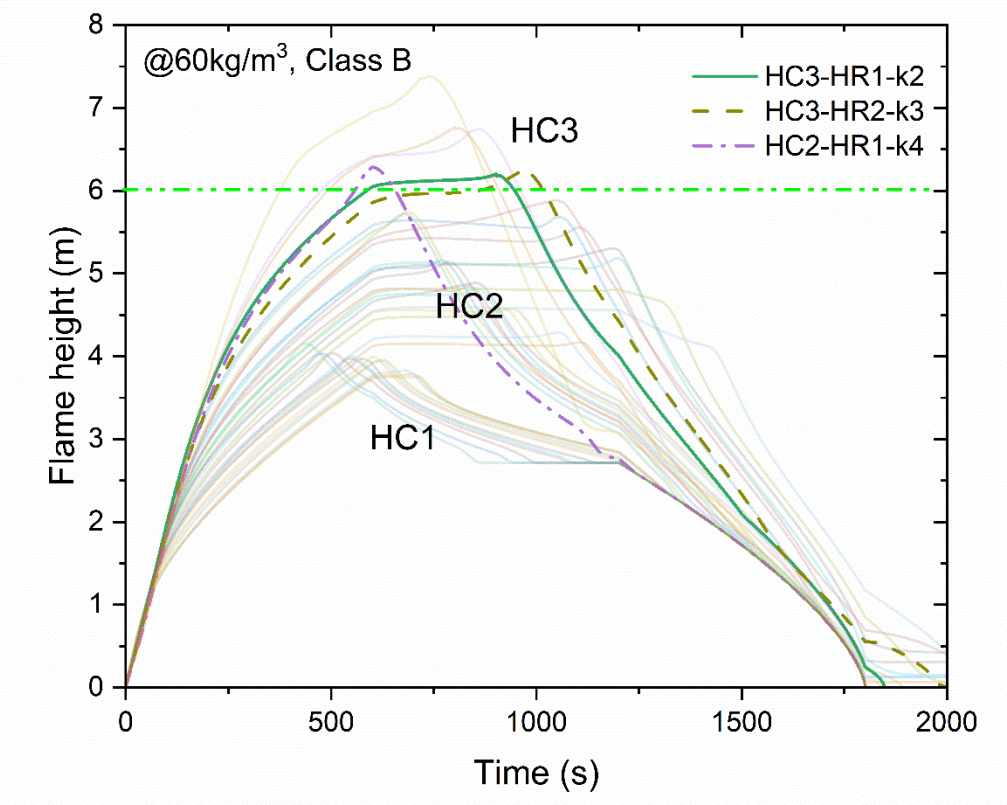

Figure 5.11 Variations in flame height of class B material with a density of 60 kg/m^3

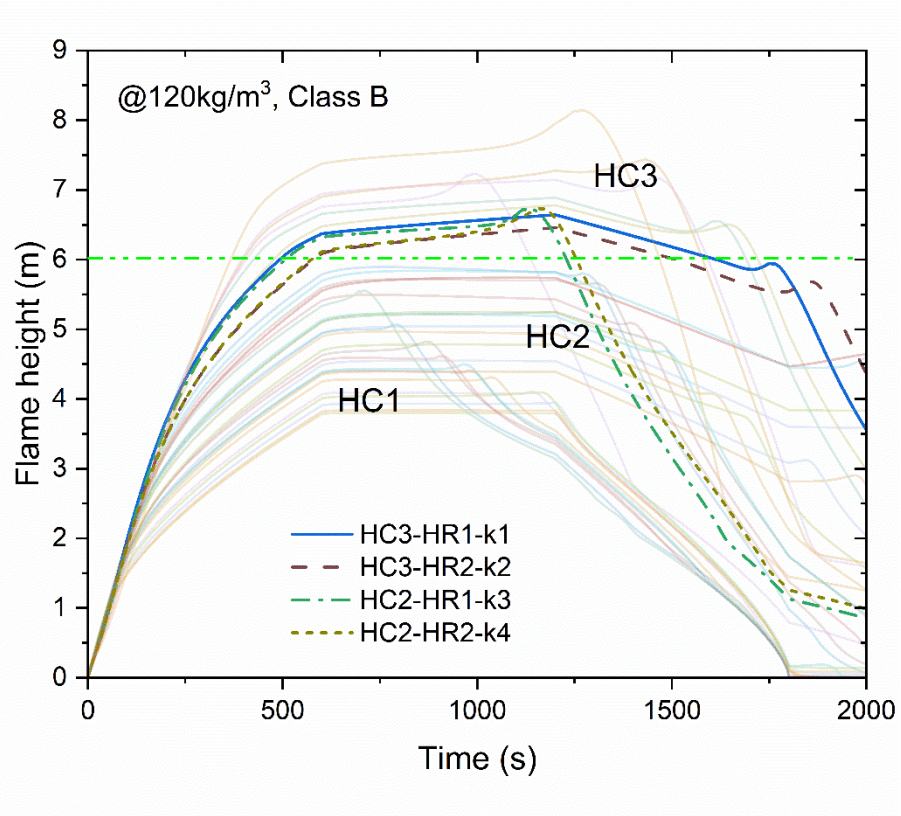

Figure 5.12 Variations in flame height of Class B materials with a density of 120 kg/m^3

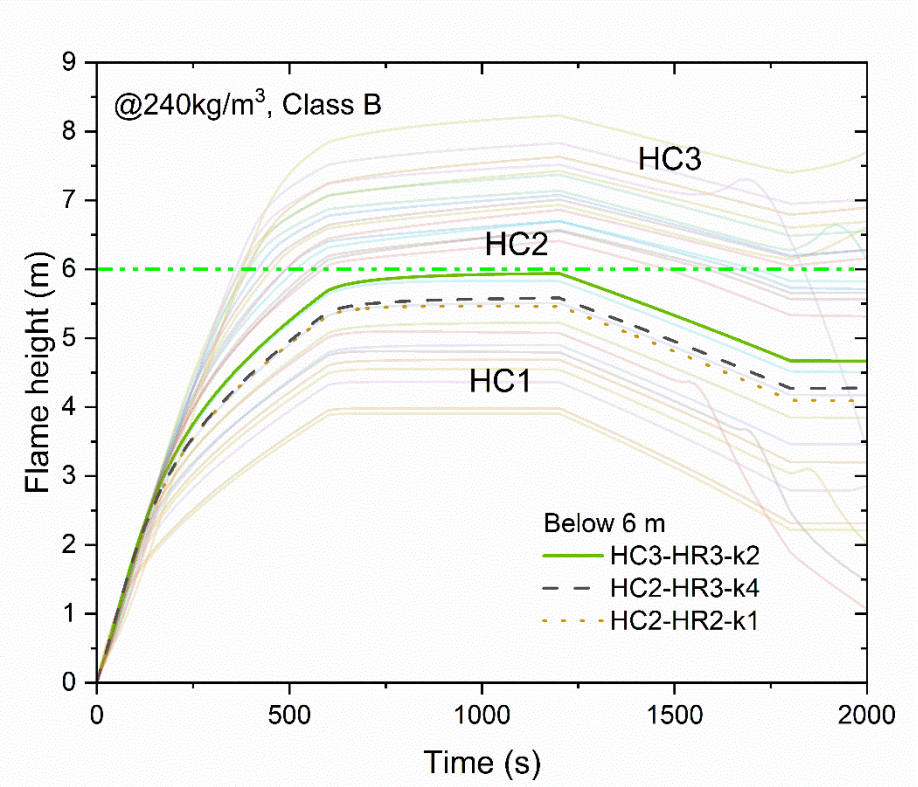

Figure 5.13 Variations in flame height of Class B materials with a density of 240 kg/m^3

As a summary, Table 5.11 lists all the combinations of Class B materials that would not pass the full-scale test. Such information is useful when assessing the suitability of Class B Materials for use in external façade of buildings.

Table 5.10 Cases of Class B materials failing the full-scale test

Density (kg/m^3)	Heat of combustion	Heat of reaction	Thermal conductivity
30	HC3	HR1	K4
60	HC3	HR1	K2-K4
		HR2	K3, K4
	HC2	HR1	K4
120	HC3	HR1	K1-K4
		HR2	K2-K4
	HC2	HR1	K3, K4
		HR2	K4
240	HC3	HR1, HR2	K1-K4
		HR3	K3, K4
	HC2	HR1	K1-K4
		HR2	K2-K4

5.6.2 Assessment of Class C material

Appendix E collates all BS 8414 simulation results for assessing the potential of using Class C materials in external façade.

The same general trends in the previous section for the performance of Class B materials in BS 8414 test also apply to Class C materials, except the values are different. Figure 5.14-5.17 present flame height curves of Class C materials with varying density, within each figure containing results for varying thermal conductivity, heat of reaction and heat of combustion.

The results in these figures indicate that some Class C materials are still capable of passing the full-scale BS 8414 test.

Figure 5.14 indicates that the majority of low-density materials (30kg/m^3) can pass the full-scale test, with the exception of only three cases (HC3-HR1-K4, HC3-HR41-K3, HC3-HR2-K4) which all have the highest value of heat of combustion, the lowest value of heat of reaction, and high values of thermal conductivity. Bearing in mind that low density materials have low thermal conductivity, it is possible that all low-density Class C materials would be able to pass

the full-scale BS 8414 acceptance criterion. Even for densities 60 kg/m^3 and 120 kg/m^3, more than half of the Class C materials could still pass the acceptance criterion.

As summary, Table 5.11 lists all the combinations of Class C materials that could pass the full-scale BS 8414 fire test criterion for flame height.

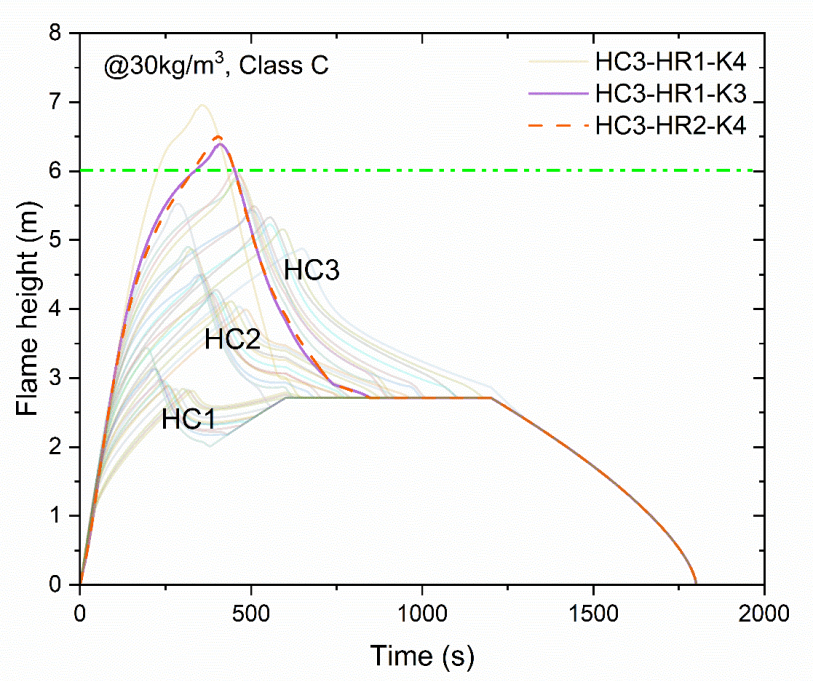

Figure 5.14 Variations in flame height of Class C material with the density of 30 kg/m^3

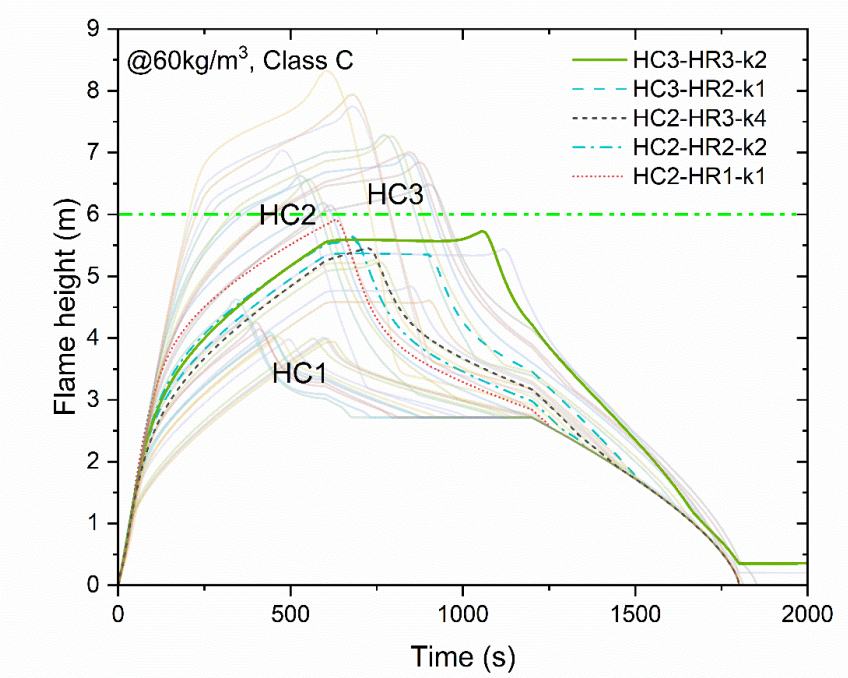

Figure 5.15 Variations in flame height of Class C material with the density of 60 kg/m^3

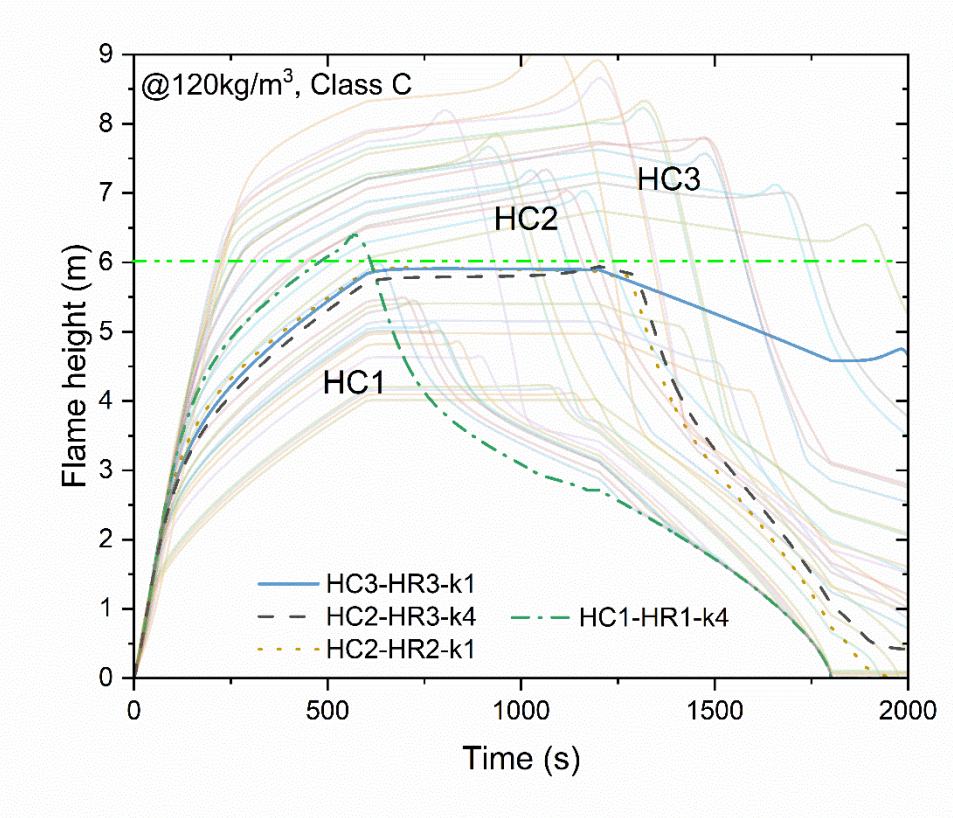

Figure 5.16 Variations in flame height of Class C material with the density of 120kg/m^3

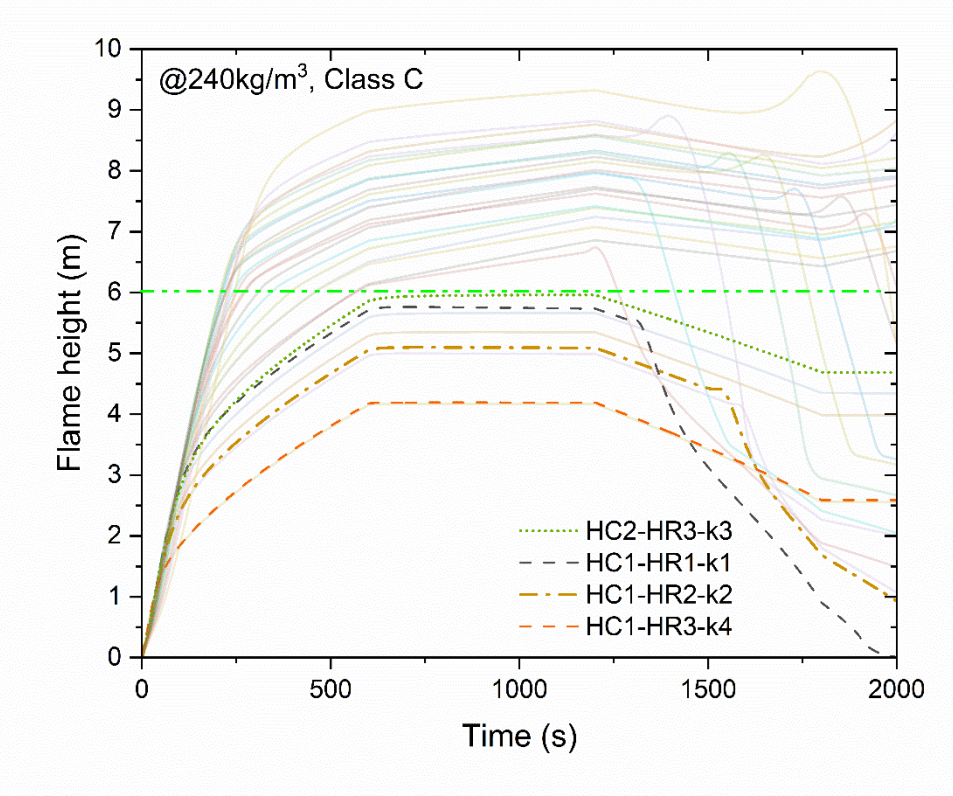

Figure 5.17 The flame height of Class C material with the density of 240 kg/m^3

Table 5.11 Combinations of Class C material able to pass BS 8414 full-scale fire test

Density (kg/m^3)	Heat of combustion	Heat of reaction	Thermal conductivity
30	HC1, HC2	HR1-3	K1-K4
	HC3	HR1	K1, K2
		HR2	K1-K3
		HR3	K1-K4
60	HC1	HR1-3	K1-K4
	HC2	HR3	K1-K4
		HR2	K1, K2
		HR1	K1
	HC3	HR3	K1, K2
		HR2	K1
120	HC1	HR1	K1-K3
		HR2, HR3	K1-K4
	HC2	HR3	K1-K4
		HR2	K1
	HC3	HR3	K1
240	HC1	HR1	K1
		HR2	K1, K2
		HR3	K1-K4
	HC2	HR3	K1-K3

5.7 Case study

The previous two sections are based on artificial materials whose properties were obtained by inverse analysis of SBI test. However, there are many commercially available materials with properties that fall within the combinations of Class B and Class C materials that would not pass the full-scale test and that would pass the full-scale test respectively.

For example, Table 5.12 lists a number of common commercially available insulation materials. Among them, phenolic foam is Class B but its density can be quite high (200kg/m^3), thus potentially causing the material to fail the BS 8414 fire test. In contrast, Aerogel is Class C, but its density is very low and it is possible for this material to pass the BS 8414 fire test.

Table 5.12 Thermal properties of commercially available insulation materials

	Density (kg/m^3)	Cond. (W / (m k))	Spec. heat (kJ/ (kg k))	Fire classification	Reference

Stone wool	40-200	0.033-0.040	0.8-1.0	A1-A2-B	[152, 153]
Glass wool	15-75	0.031-0.037	0.9-1.0	A1-A2	[154, 155]
Polyisocyanurate	30-45	0.018-0.028	1.4-1.5	B	[156-158]
Recycled PET	30-60	0.034-0.039	1.2	B	[159]
Phenolic foam	35-200	0.018-0.028	1.3-1.4	B	[160-162]
Mineralized wood fibers	320-600	0.06-0.107	1.8-2.1	B	[163, 164]
Cellulose	30-80	0.034-0.039	1.3-1.6	B-C-E	[165, 166]
Aerogel(panels)	10-70	0.013-0.015	1	C	[167, 168]
Polystyrene	15-40	0.031-0.038	1.25-1.7	E	[169, 170]
Polyurethane	15-45	0.022-0.04	1.3-1.4	E	[170]
Wood fibers	50-270	0.038-0.05	1.9-2.1	E	[171]

This section simulates the performance of these two materials under SBI test condition and BS 8414 test condition.

Additional material properties related to chemical kinetics for simulating their behaviour in fire usually are not provided by manufacturers. They were obtained from the literature. Table 5.12 lists the values of these additional properties and their sources of information.

Table 5.13 Additional material property parameters used for Phenolic foam and Aerogel

Parameter	Unit	Phenolic	Aerogel
A	1/s	1.03E+13[175]	1.0E+22[176, 177]
E	kJ/kmol	2.05E+05[175]	3.0E+05[176, 177]
Heat of reaction	kJ/kg	1000[144, 178]	1600
Heat of combustion	MJ/kg	15[144, 179]	8.5[167]

Figures 5.18 and 5.19 present SBI and BS 8414 simulation results for Phenolic foam and Figures 20 and 21 for Aerogel. Figure 18 indicates that the Phenolic foam material would achieve SBI classification B with a FIGRA value of 112.4 W/s (120 W/s) and a THR_{600s} value of 7.45 MJ (<7.5MJ). However, this material in BS 8414 test would fail the test acceptance, with the flame height of 6m being exceeded for 111s.

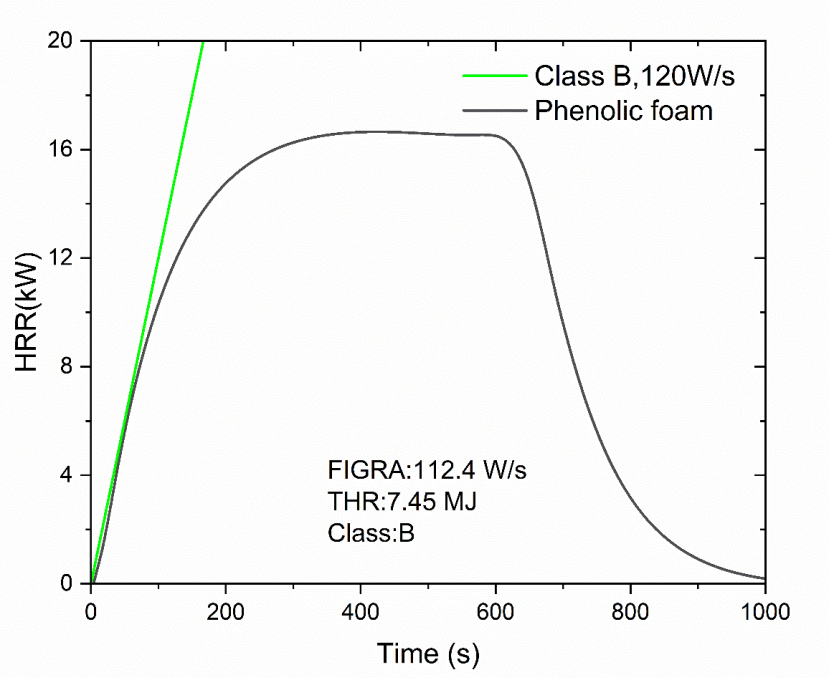

Figure 5.18 Simulation result of RHR of Phenolic foam in SBI test

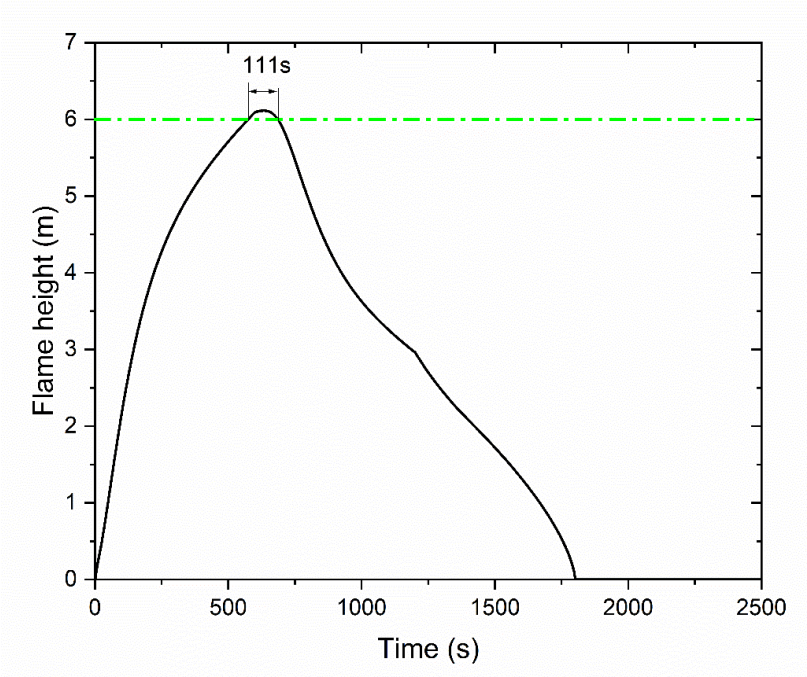

Figure 5.19 Simulation result of flame height versus time for phenolic foam in BS8414 test

In contrast, although Figure 5.20 indicates that Aerogel is Class C material, with a FIGRA value of 167.2 kW/s (>120 kW/s), the BS 8414 simulation results in Figure 5.21 suggests that this material would comfortably pass the BS 8414 fire test acceptance criterion with the maximum flame height being 4.43m which is much lower than the 6m acceptance condition.

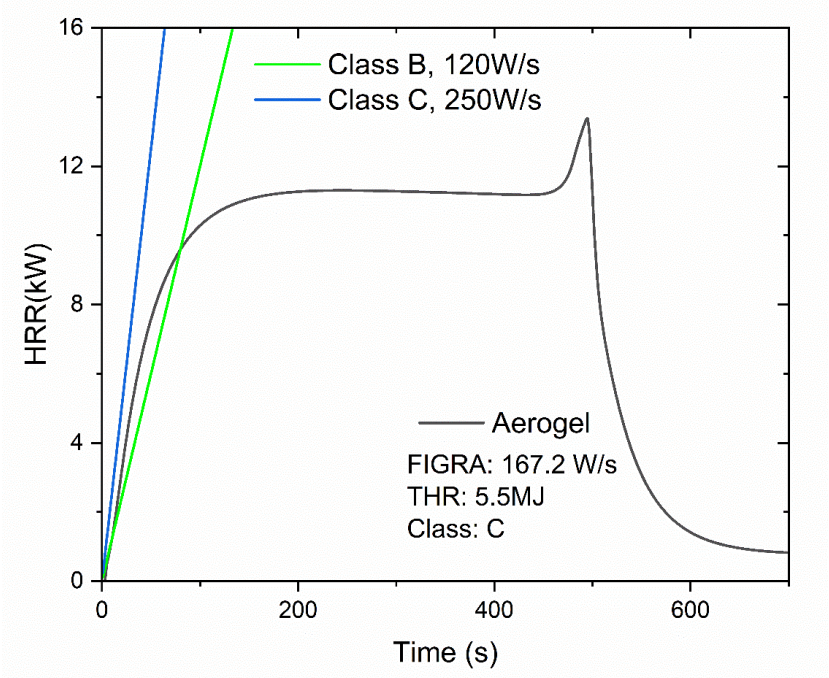

Figure 5.20 Simulation results of RHR of aerogel in SBI test

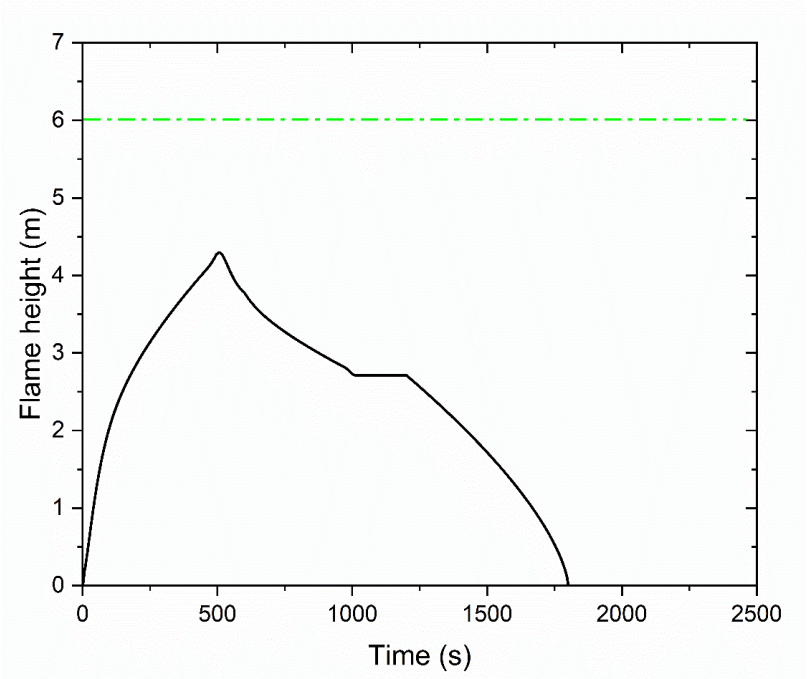

Figure 5.21 Simulation results of flame height versus time for aerogel in BS8414 test

5.8 Conclusions

This chapter has investigated the suitability of using the SBI classification to determine whether a material can be used in the external façade of buildings. This was done by modelling how the material would perform in the full-scale BS 8414 fire test for external façade and whether the material would be able to pass the test acceptance criterion for flame height. The material properties were obtained by inverse analysis so that their combinations would exactly achieve the relevant thresholds for Class B and Class C materials according to SBI test.

The following conclusions can be drawn:

1. The SBI Classification of material is mainly affected by its density, thermal conductivity, heat of reaction and heat of combustion.
2. In contrast to the above, the heat of reaction and thermal conductivity of a material has only moderate effects on flame height when the material is used in BS 8414 full scale fire test.
3. The majority, but not all Class B materials would be able to pass the BS 8414 full scale fire test criterion for flame height. The Class B materials that do not pass the acceptance criterion are combinations of high density (>120kg/m^3) and high heat of combustion (>16 MJ/kg).
4. Many Class C materials could still pass the BS 8414 full scale fire test criterion for flame height. Such materials are characterised by low density (<60kg/m^3) and low heat of combustion (<16 MJ/kg).
5. Simulation results for SBI test and BS 8414 test using a commercially available Class B (Phenolic foam) and a commercially available Class C (Aerogel) insulation material confirm the two findings above.

If SBI material classification only is used to assess whether a material is suitable for application in external façade, in addition to using the SBI classification, the additional information in conclusions 3 and 4 above should be considered.

Chapter 6 Assessment of using the Single Burning Item classification for specification of materials on the external surface of buildings with composite façade or ventilated facade

6.1 Introduction

Chapter 5 has investigated whether using SBI material classification is suitable as the specification of materials on the external surface of buildings, based on the assessment of using Class B and Class C materials in BS 8414 full-scale façade fire test. In Chapter 5, the façade contains only one single material. In realistic buildings, the façade can consist of a number of materials in either plain façade (PF) without any ventilation in the façade or ventilated façade (VF)[122]. PF typically consists of two layers: a layer of insulation and a layer of finish coat, as show in Figure 6.1(a). The VF system is a double skin construction that includes a thermal insulation layer and an exterior cladding panel, separated by an air cavity, as show in Figure 6.1(b). This chapter performs a similar assessment as in Chapter 5, but for composite plain façade and ventilated façade constructions.

In the UK's Approved document B (ADB)[24] for England and Wales, for residential buildings with a height of over 18 m, the façade materials should achieve the following SBI Classification:

- Any insulation product or filler material should be of limited combustibility and meet the requirement of Euroclass A2 or better;
- The external surface should be Class B or better.

In fact, the above requirement may be considered contradicting to the requirement of Class B material in façade consisting of only one single material. Such a façade may be considered a composite plain façade with the external layer and the insulation layer using the same material, which means both the external layer and the insulation are Class B, rather than the insulation

being Class A2. Furthermore, the same questions as in chapter 5, i.e., whether some Class B material may not be suitable or whether some Class C material may be suitable, exist. However, these questions are not examined further.

Instead, because two or more materials are used in a composite façade system, there is potential of trade-off between the different materials. For example, if the insulation material is non-combustible, can the specification on the external layer be relaxed, or vice versa? The latter is particularly important because the requirement of A2 for the insulation material is very restrictive and prevents a lot of highly insulating materials to be used for energy efficiency. Clearly, the thickness of the outermost layer will affect the results. This additional parameter will be considered in this Chapter.

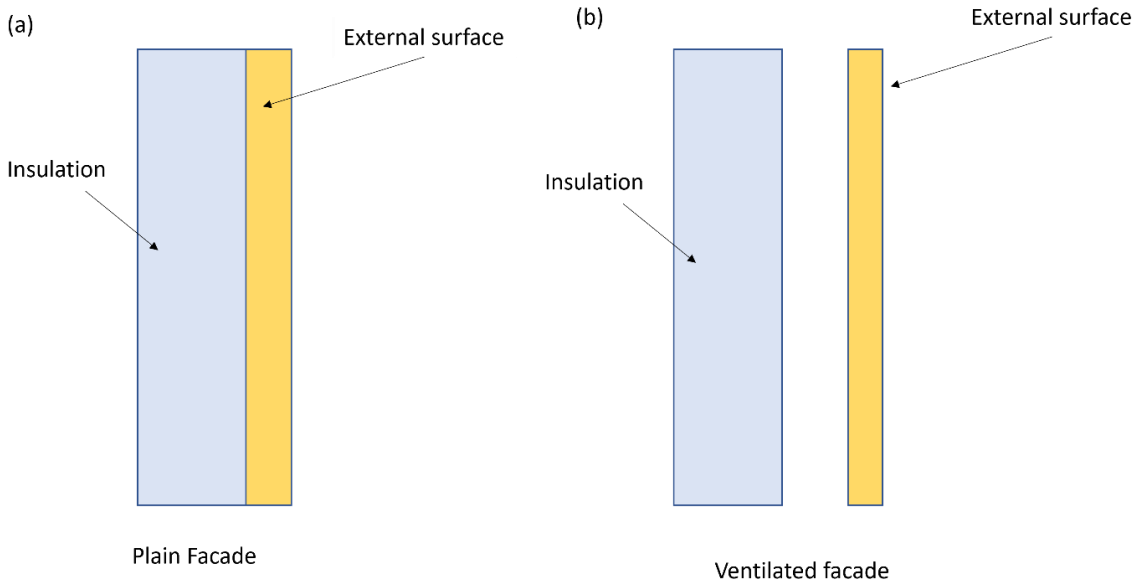

Figure 6.1 Illustration of (a) Plain façade and, (b) Ventilated façade system

Therefore, for PF systems, the specific questions to be investigated in this chapter are:

(1) If the insulation material is non-combustible (e.g. rock mineral wool), what is the appropriate thickness of the external layer that would guarantee that no Class B material would fail the full-scale BS 8414 façade fire test?

(2) If on the other hand, the external layer is non-combustible, what relaxation can be applied to the insulation material, and how this relaxation is affected by thickness of the external layer?

For VF system, fire barriers are required to prevent fire spread from floor to floor. However, as explained in Chapter 4, this requirement may not be fulfilled. The worst-case scenario of unblocked fire movement within the air cavity. The VF system's ventilated cavity may affect material combination compared to PF system, which will be investigated in this chapter.

6.2 Multi-layered PF system

6.2.1 Non-combustible insulation with Class B external surface

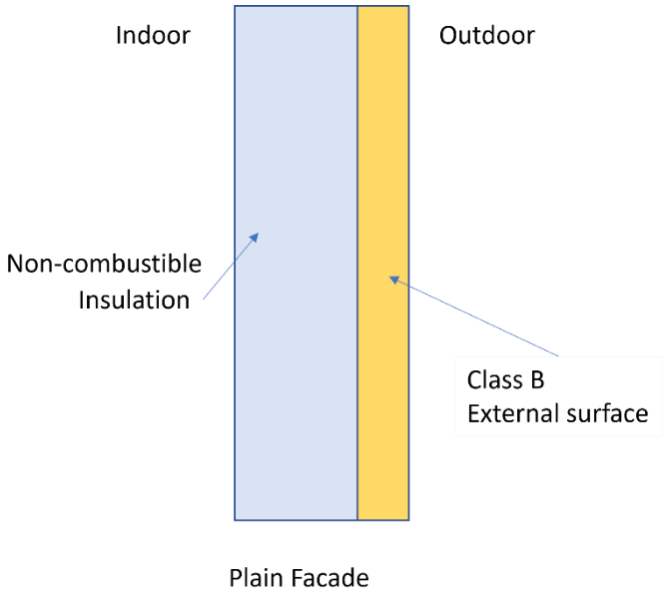

Figure 6.2 PF system with Class B external surface and non-combustible insulation

The results in Chapter 5 indicate that some Class B materials may not be able to pass the BS 8414 full-scale façade fire test. The worst case was HC3-HR1-K4, representing a material with the highest heat of combustion, lowest heat of reaction and the highest thermal conductivity. This material will be used in the assessment here to determine the maximum thickness that this material can be used in the external layer. For this investigation, four densities (60, 120, 240, and 480 kg/m^3) are considered.

Figure 6.3 shows the simulation results of flame height in BS 8414 test setup, the limit of flame height is 6 m. The results in Figure 6.3(a) indicates that for a low density of 60 kg/m^3, there is no limit in thickness of the external layer. With increasing density, flame height increases, and therefore thickness of the external layer has to be limited. Table 6.1 summarises values of the critical thickness beyond which thickness of the external layer should not be used.

Table 6.1 Critical thickness of Class B external layer to pass BS 8414 full-scale façade fire

Density (kg/m^3)	60	120	240	480
Critical thickness (mm)	-	20	7	2.5

(a)

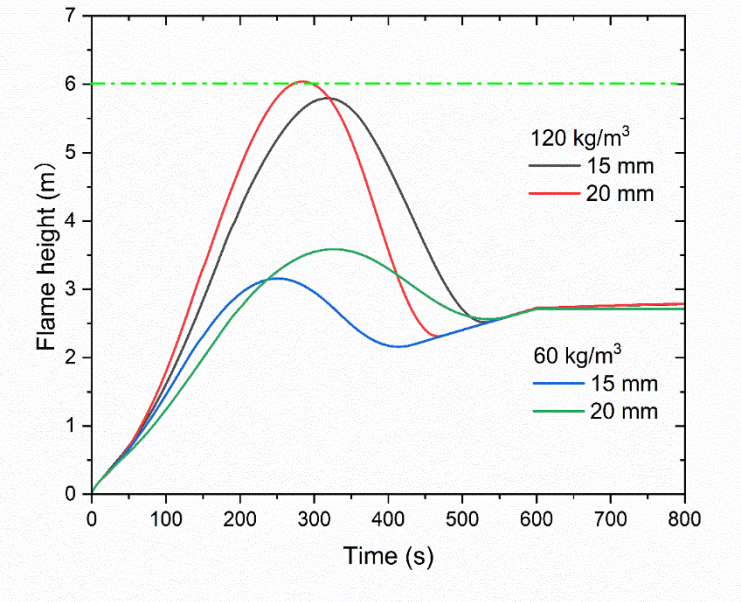

(b)

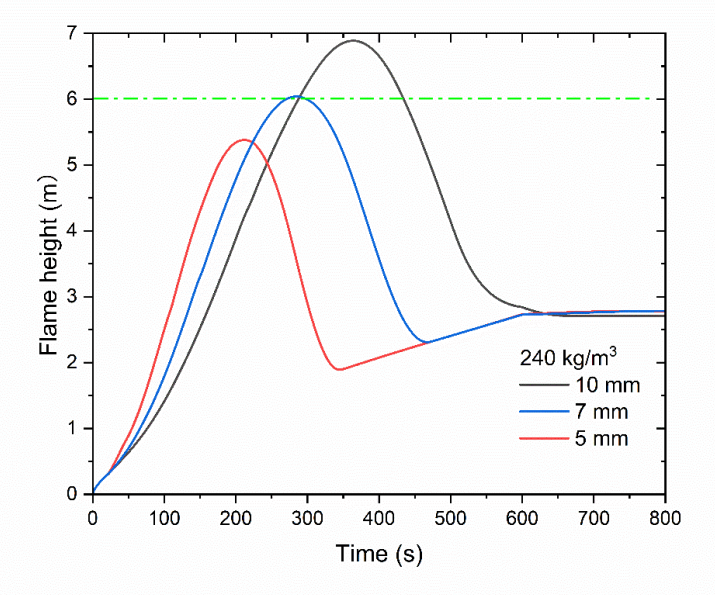

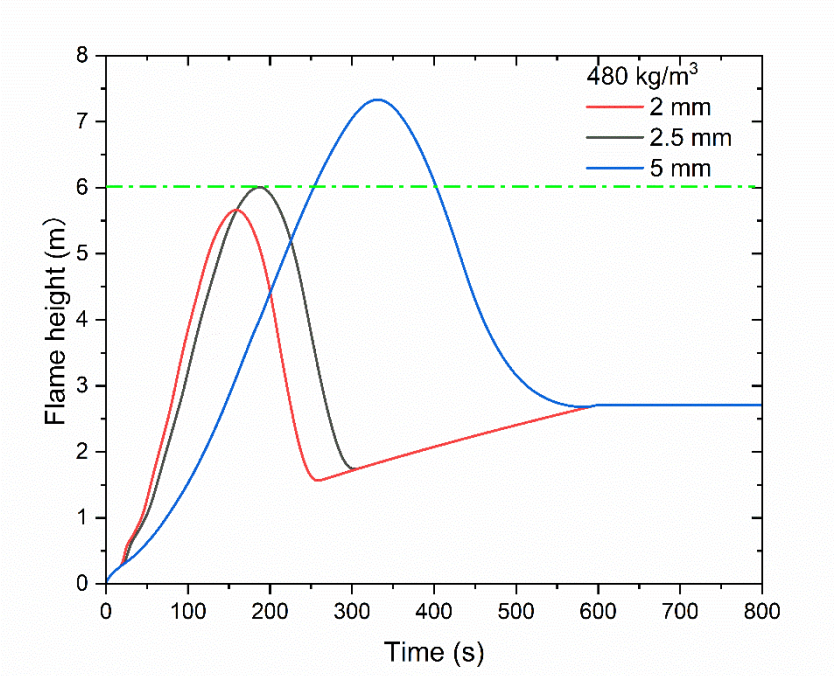

Figure 6.3 Variations of flame height for a PF system with Class B external surface and non-combustible insulation for different densities, (a) 60 and 120 kg/m^3, (b) 240 kg/m^3, (c) 480 kg/m^3

6.2.2 Non-combustible external surface

By encapsulating the insulation material inside a non-combustible external surface, as illustrated in Figure 6.4, it may be possible to relax the requirement of the insulation material.

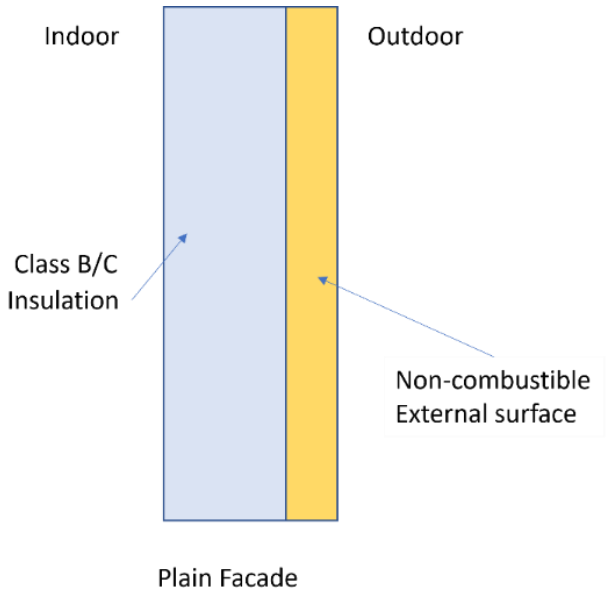

Figure 6.4 Cross section of a PF with a non-combustible external surface

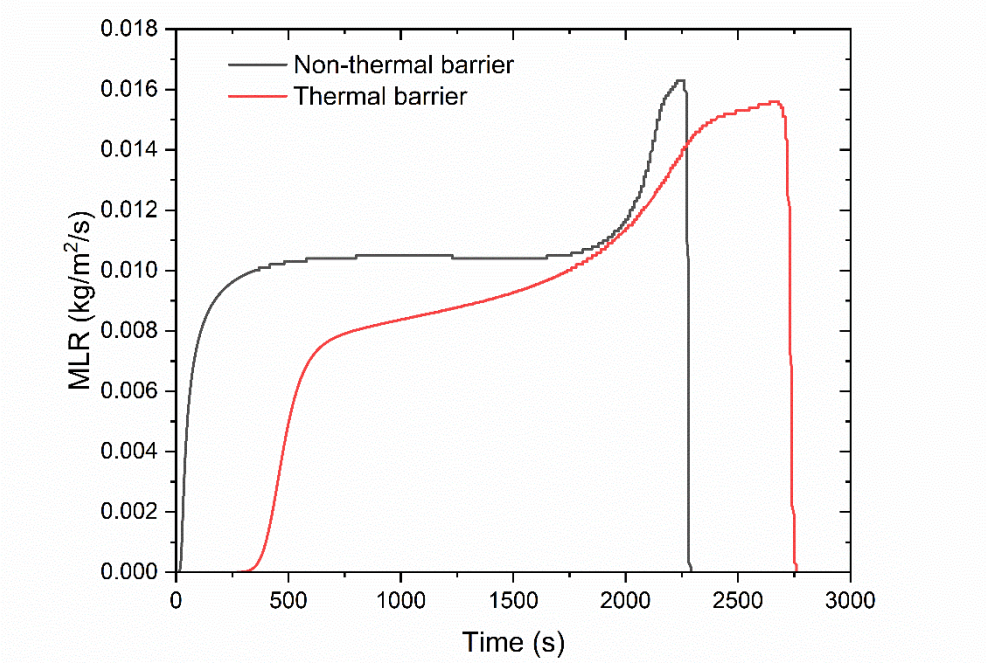

Figure 6.5 Mass loss rate (MLR) obtained with and without thermal barrier

A non-combustible external layer has two benefits to the insulation: delaying decomposition of the insulation material and slowing down movement of the decomposed insulation material to the surface to cause burning. However, in this research, the worst case is assumed such that the effect of slowing down movement of the decomposed insulation material is not considered. This is done by assuming that any decomposed insulation material moves through the non-combustible material instantly to the surface to cause burning.

For example, Figure 6.5 compares mass loss rates of a Class C insulation material (case HC3-HR1-K4, 240kg/m^3 in Chapter 5) with and without being encapsulated by 6.0 mm of steel. With encapsulation, and the pyrolysis time of the insulation material is delayed to 282s. Clearly, the thicker the external non-combustible layer, the longer it will take for the insulation to heat up and then pyrolyze. Therefore, by controlling thickness of the protective layer, it therefore possible to reduce the amount of pyrolysed insulation to become fuel, thereby controlling flame height to pass the full-scale fire test.

This section investigates the critical thickness of using three common materials which can be considered non-combustible (steel, gypsum plasterboard, mineral wool). Table 6.2 lists their thermal properties.

Table 6.2 Thermal properties of three common non-combustible materials [84]

Material	Density (kg/m^3)	Thermal conductivity	Heat capacity
Mineral wool	30	0.04	960
Plasterboard	823	0.24	950
Steel	8000	14	400

Again, the worst material in Chapter 5 for Class B and Class C were used in this investigation so that the results of critical thickness of the external non-combustible layer can be universally applied. The worst Class B and Class C material was combination HC3-HR1-K4.

(a)

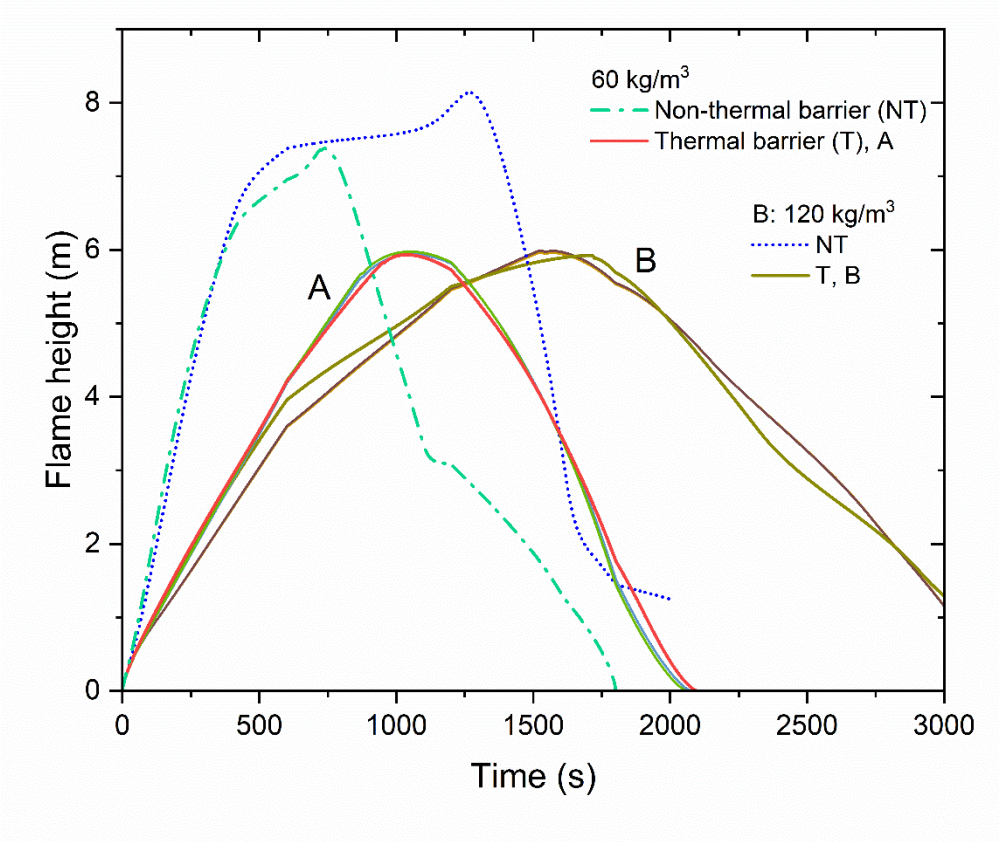

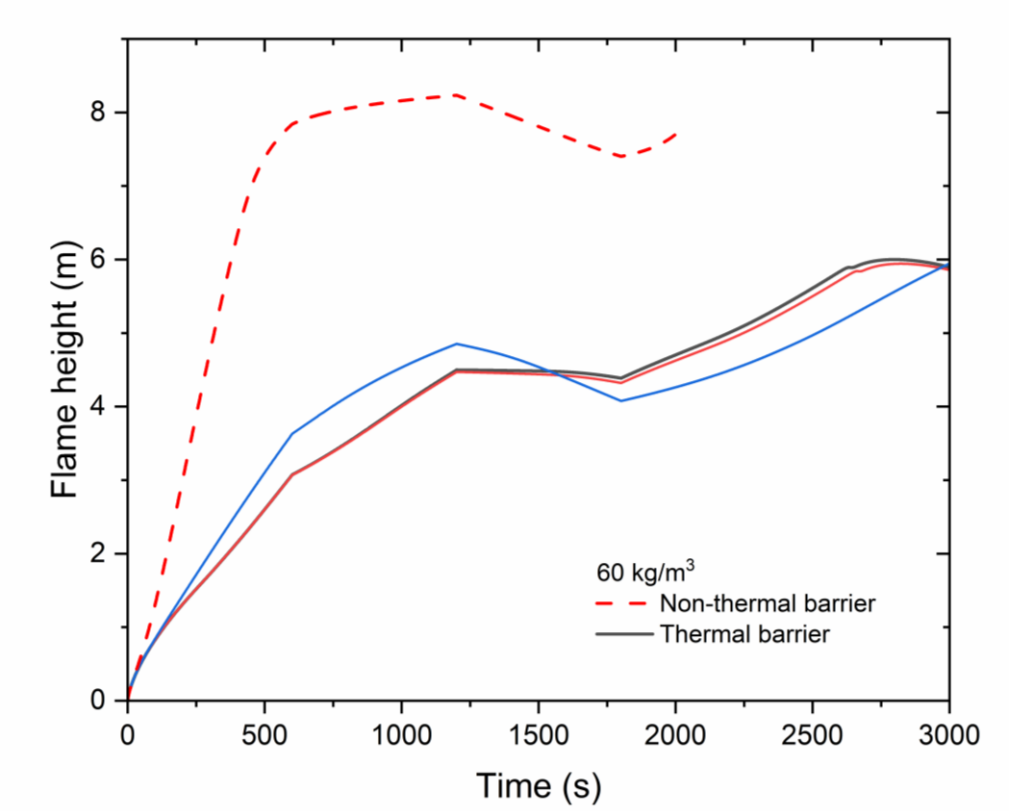

Figure 6.6 Variations of flame height for PF system of Class B insulation with and without thermal barrier layer, for different insulation densities

Figures 6.6 and 6.7 show variations of flame height with and without the non-combustible external layer as thermal barrier.

Tables 6.3 and 6.4 summarise critical thickness values for Class B and Class C insulation materials with different non-combustible external layers. In general, only a very small thickness is sufficient for the non-combustible external layer to encapsulate Class B and Class C materials. If using plasterboard or mineral wool, the very small thickness can be easily achieved. Even if using steel, the thickness of a few mm is not challenging.

Table 6.3 Critical thickness (mm) of the protective layer using different materials for encapsulating Class B material

Insulation Density (kg/m^3)	Mineral wool	Plasterboard	Steel
60	0.5	0.6	0.7
120	0.68	1.0	1.74
240	1.15	1.65	4.1

Table 6.4 Critical thickness (mm) of the protective layer using different materials for encapsulating Class C material

Insulation Density (kg/m^3)	Mineral wool	Plasterboard	Steel
30	0.36	0.36	0.38
60	1.15	1.6	1.65
120	1.16	2.2	3.5
240	1.2	2.4	6.0

(a)

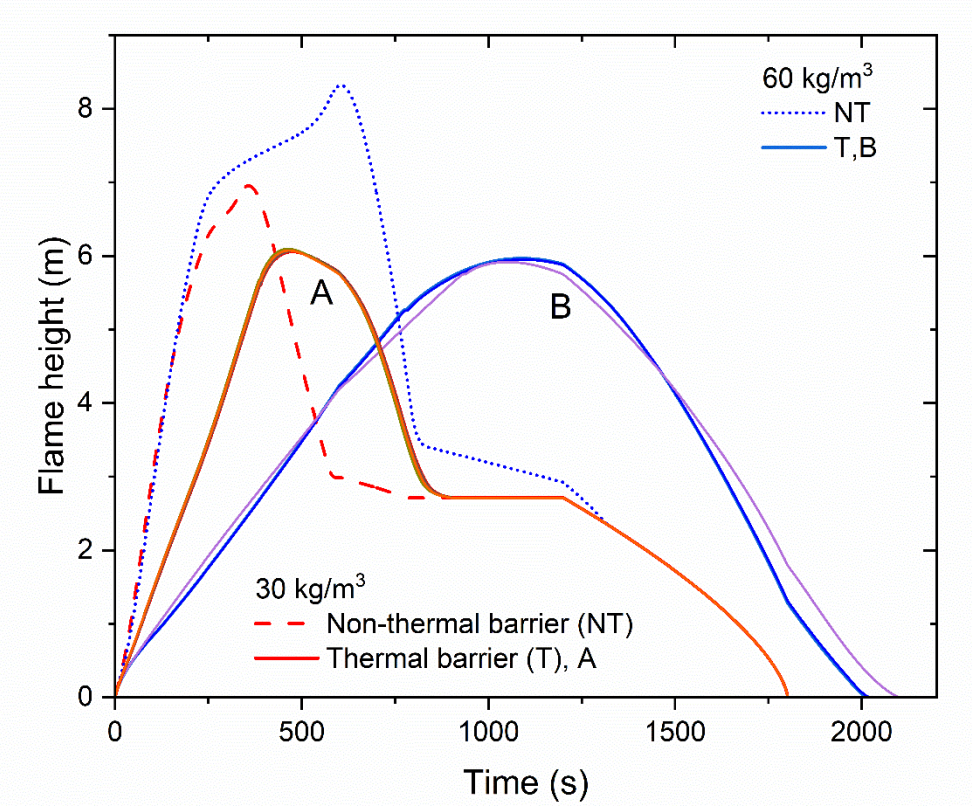

(b)

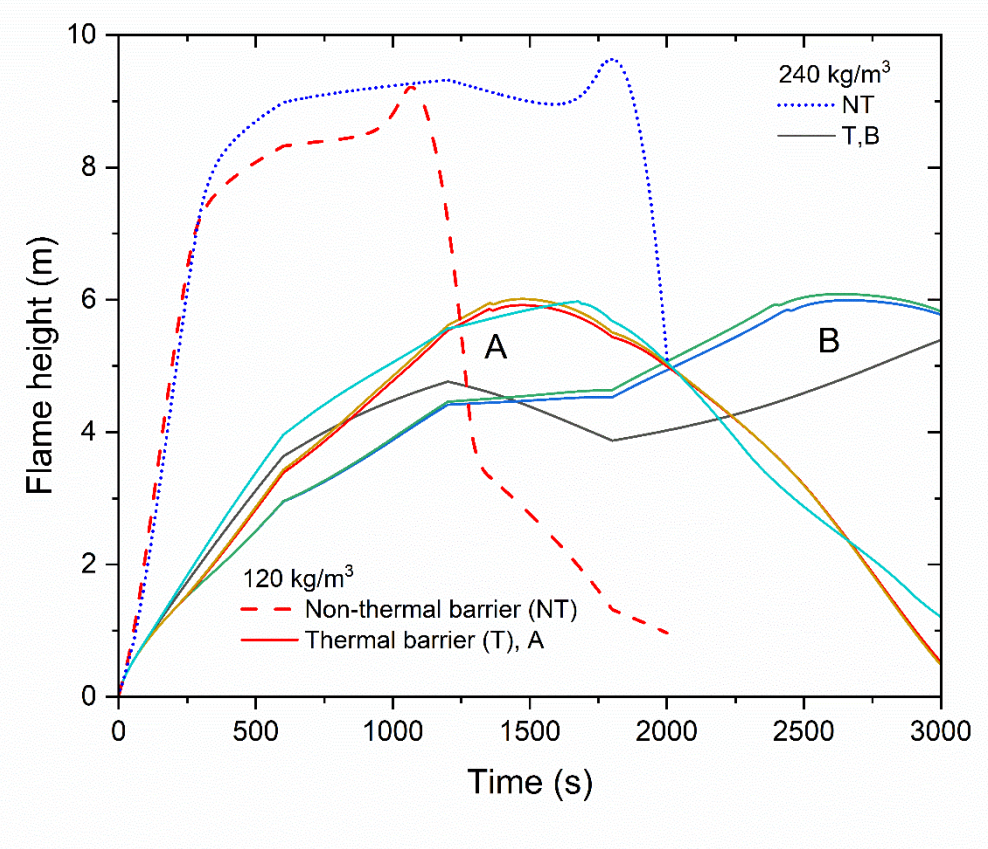

Figure 6.7 Variations of flame height for PF system of Class C insulation with and without thermal barrier layer, for different insulation densities

6.3 Multi-layered VF system

6.3.1 Effect of cavity on fire growth

As a demonstration of increased flame length in VF system compared to equivalent PF system, shown in Figure 6.8, simulations were carried out for the two systems in BS 8414 full-scale test. The insulation material is Class B and has combination of thermal properties of (HC3-HR1-K4, 30 kg/m^3), which was the worst case according to the results in Section 5.5 of Chapter 5. Figure 6.5 shows the general sketch of VF and PF system.

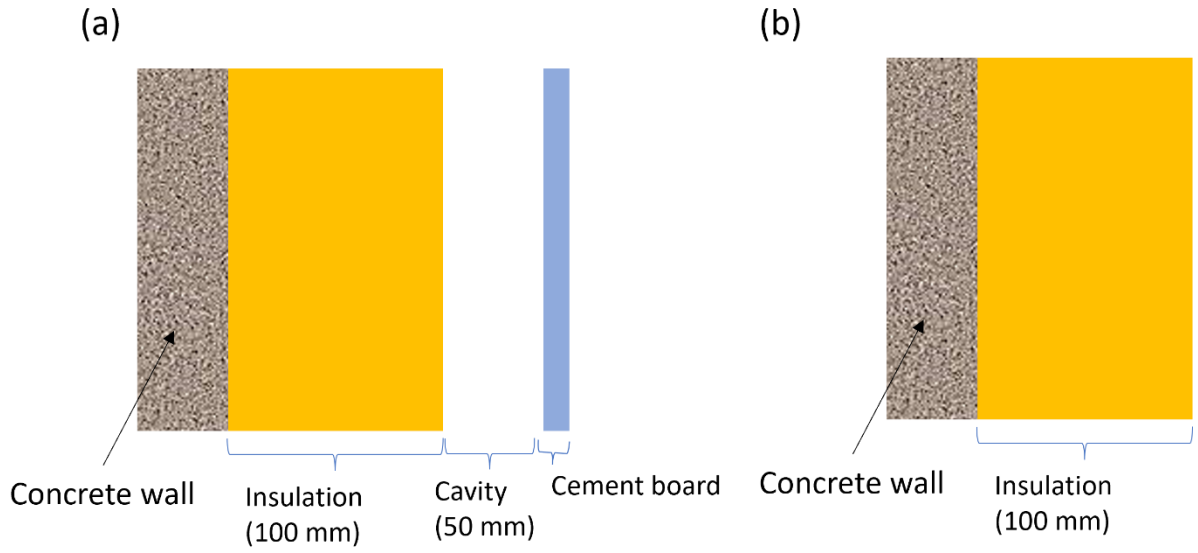

Figure 6.8 Illustration of two exemplar façade systems, (a) with cavity (VF), and (b) without cavity (PF)

Figure 6.9 compares simulation results of flame height for the two systems. Although the same insulation material is used, the ventilated cavity facade burns much more quickly than the non-ventilated system, with a flame spread rate of 0.048 m/s, which is double that of the unventilated system (0.021 m/s). The PF system just passes the BS 8414 fire test but the VF system fails with a maximum flame height of 7.08 m (>6m).

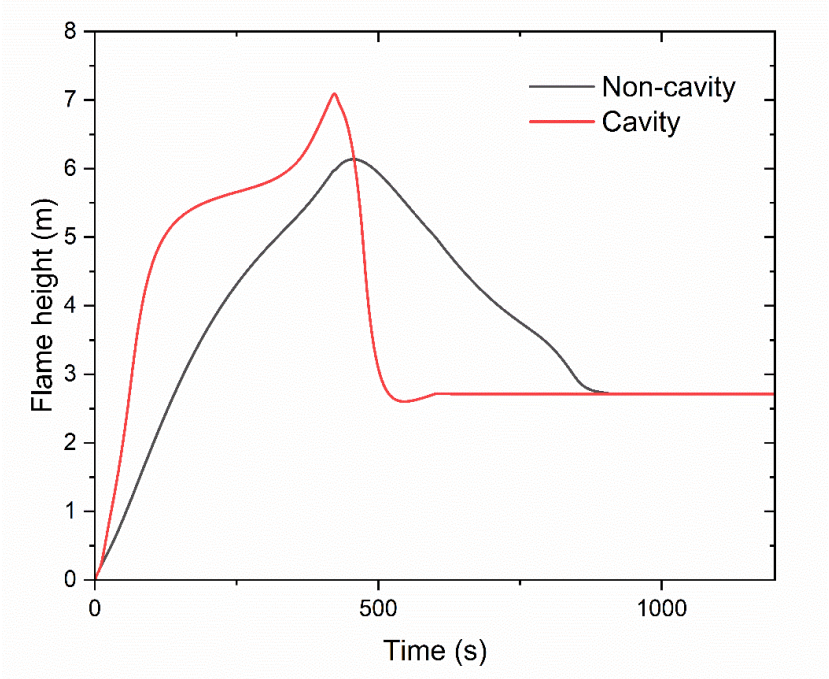

Figure 6.9 Comparison of flame heights of exemplar VF and PF systems

It is therefore necessary to repeat the exercise in Chapter 5 to appraise VF systems, as detailed in the next section.

6.3.2 Fire performance of Class B and Class C materials in VF system

Chapter 5 Table 5.9 has listed all the combinations of Class B material that would not pass the BS 8414 full-scale test when used in PF system. These same materials would not pass the BS 8414 full-scale test if used in VF system. This section further investigates which of the combinations of Class B material would fail to pass the full-scale fire test among those in Chapter 5 that pass the full-scale fire test when used in PF system, due to take the effect of cavity. Table 6.5 lists all the cases to be examined.

Table 6.5 Combinations of Class B material to be evaluated for VF system

Density (kg/m^3)	Heat of combustion	Heat of reaction	Thermal conductivity
30	HC1-2	HR1-HR3	K1-K4
	HC3	HR1	K1-K3
		HR2-HR3	K1-K4
60	HC1	HR1-HR3	K1-K4
	HC2	HR1	K1-K3
		HR2-HR3	K1-K4
	HC3	HR1	K1
		HR2	K1-K2
		HR3	K1-K4
120	HC1	HR1-HR3	K1-K4
	HC2	HR1	K1-K2
		HR2	K1-K3
		HR3	K1-K4
		HR2	K1
		HR3	K1-K4
240	HC1	HR1-HR3	K1-K4
	HC2	HR2	K1
		HR3	K1-K4
	HC3	HR3	K1-K2

Figure 6.10 shows variations of flame height of Class B materials in VF system for different densities. A reassuring feature of these figures is that the majority of Class B combinations that pass the full-scale BS 8414 fire test in PF system would still pass the fire test when used in VF system. Even if the flame height exceeds the limit of 6m, the additional flame height above 6m is very small.

Table 6.6 summarises the few additional combinations of Class B materials that would not pass the full-scale fire test when used in VF system. The number of additional combinations is small.

(a)

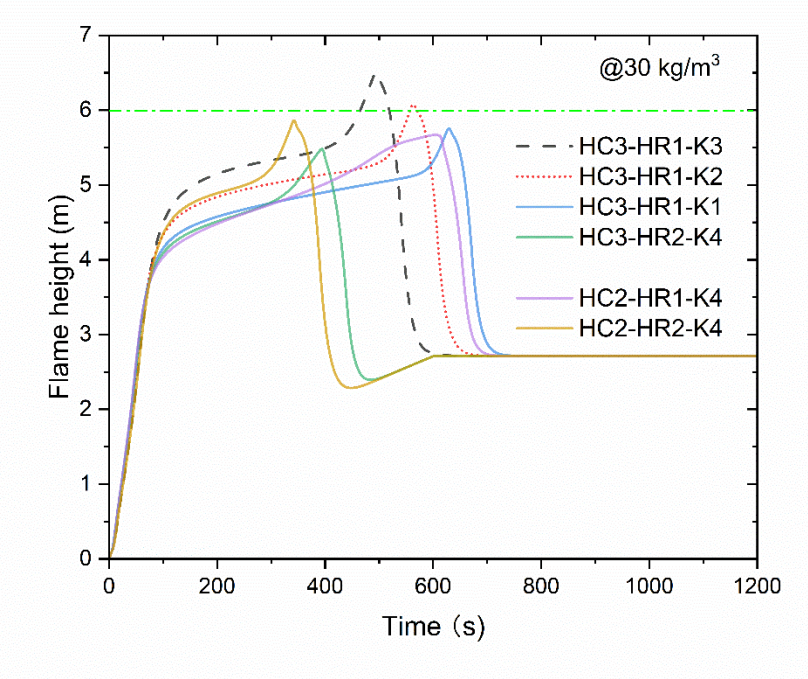

(b)

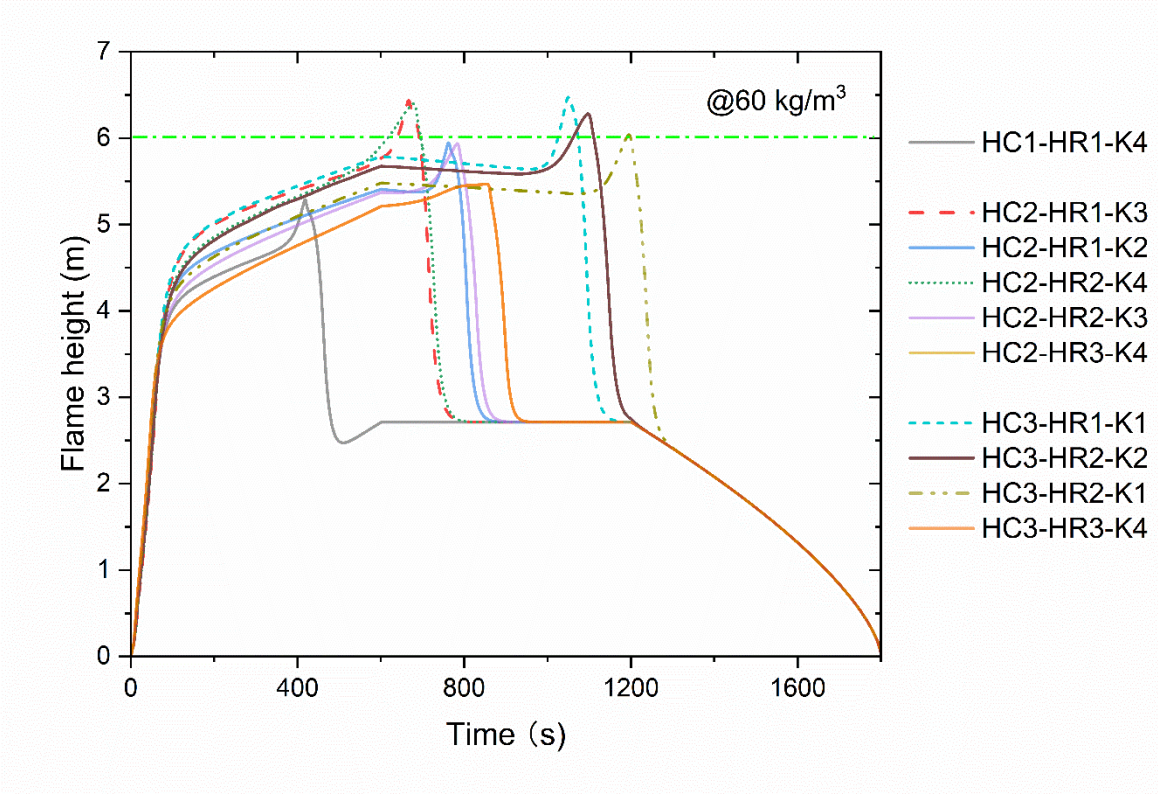

(c)

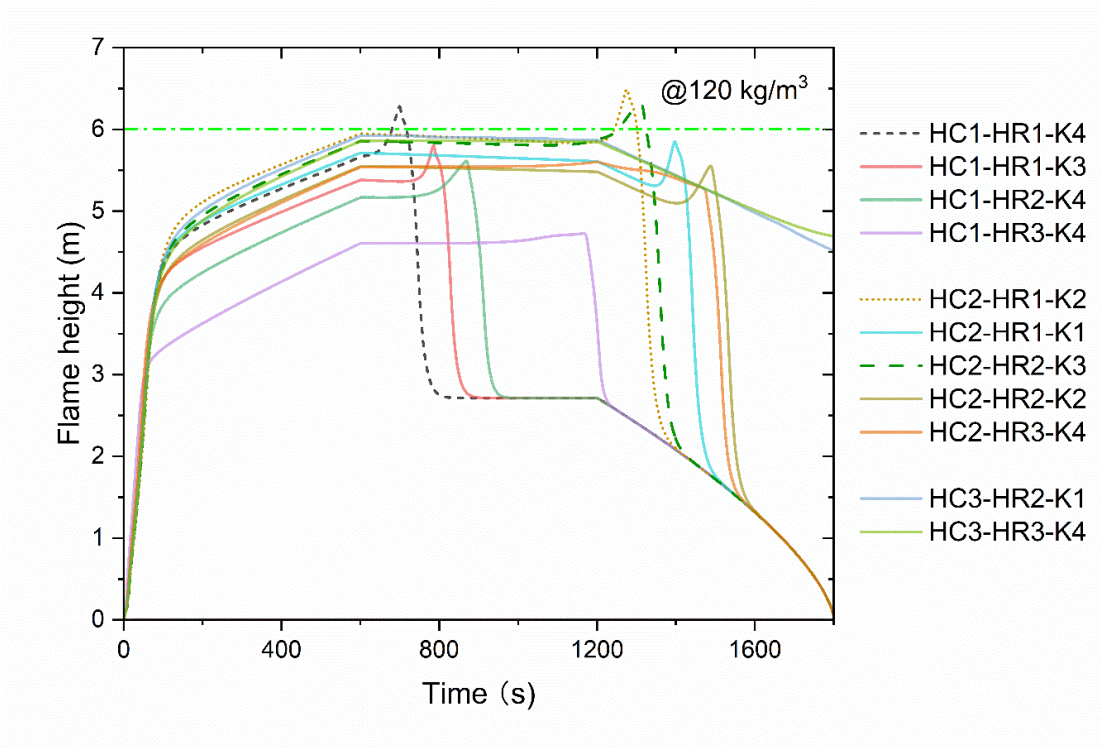

(d)

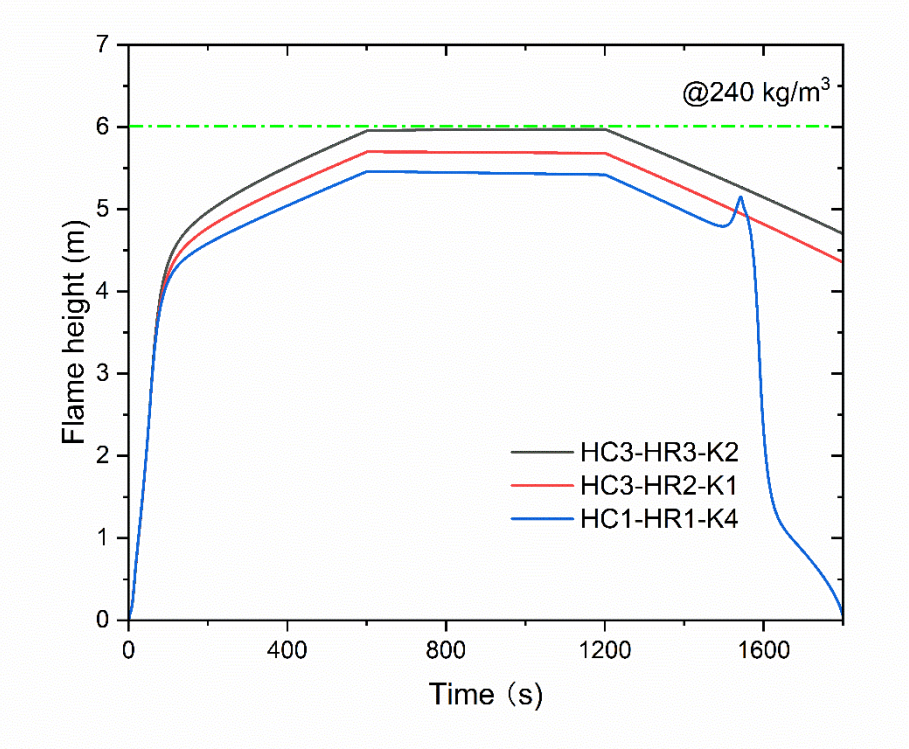

Figure 6.10 Variations of flame height of Class B materials in VF system

Table 6.6 Additional combinations of Class B materials failing the full-scale fire test when used in VF

Density (kg/m^3)	Heat of combustion	Heat of reaction	Thermal conductivity
30	HC3	HR1	K2, K3
60	HC3	HR2	K1,K2
	HC2	HR1	K3
		HR2	K4
120	HC2	HR1	K2
		HR2	K3

The same process is repeated to find the combinations of Class C materials that could pass the full-scale BS 8414 fire test. Figure 6.11 shows flame heights and Table 5.7 summarizes the combinations of Class C materials that would not pass the fire test in VF system among those that would pass the full-scale fire test in PF system. As with Class B materials, even if a combination does not pass the full-scale fire test, the additional flame height above 6 m is small.

(a)

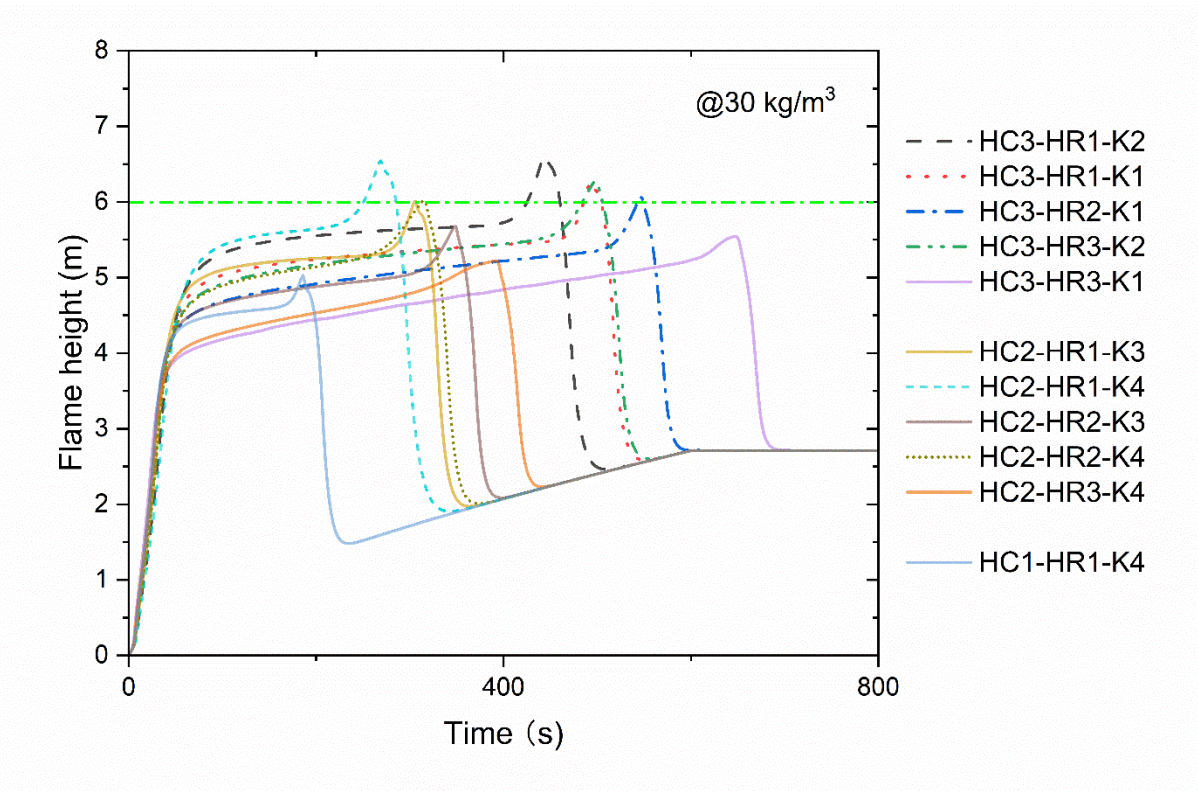

(b)

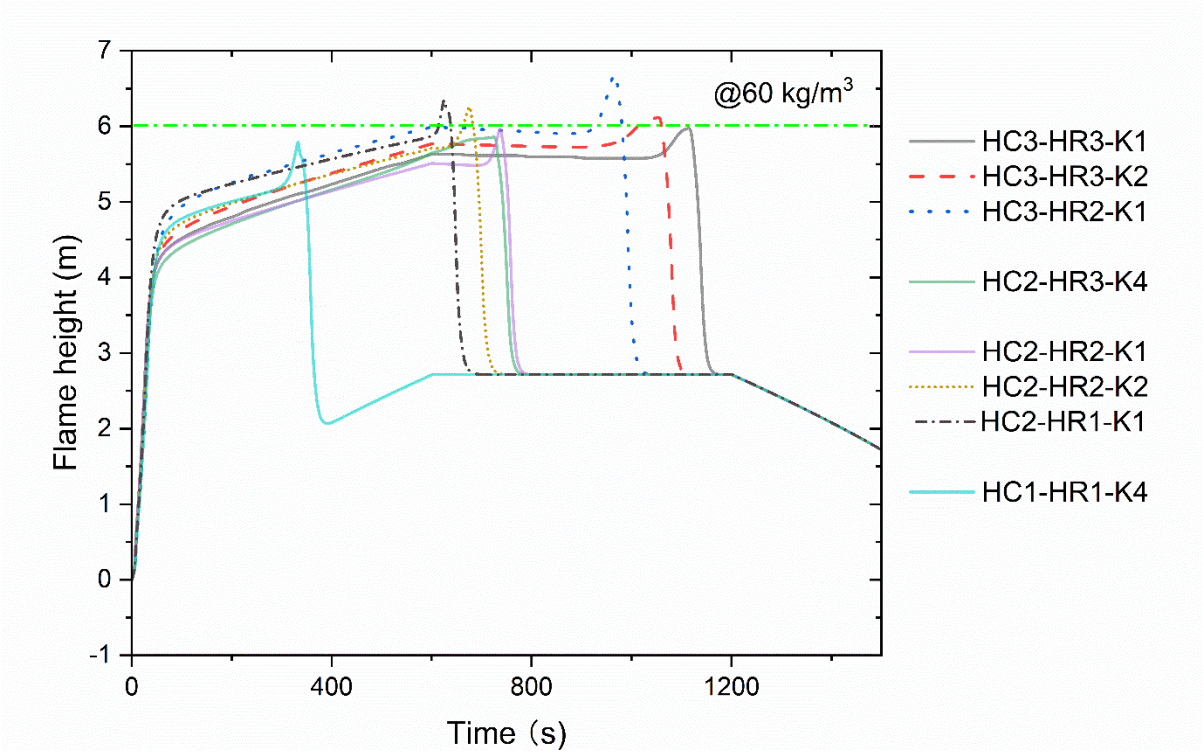
@60 kg/m3
Flame height (m)
Time（s)
HC3-HR3-K1
HC3-HR3-K2
HC3-HR2-K1
HC2-HR3-K4
HC2-HR2-K1
HC2-HR2-K2
HC2-HR1-K1
HC1-HR1-K4

(c)

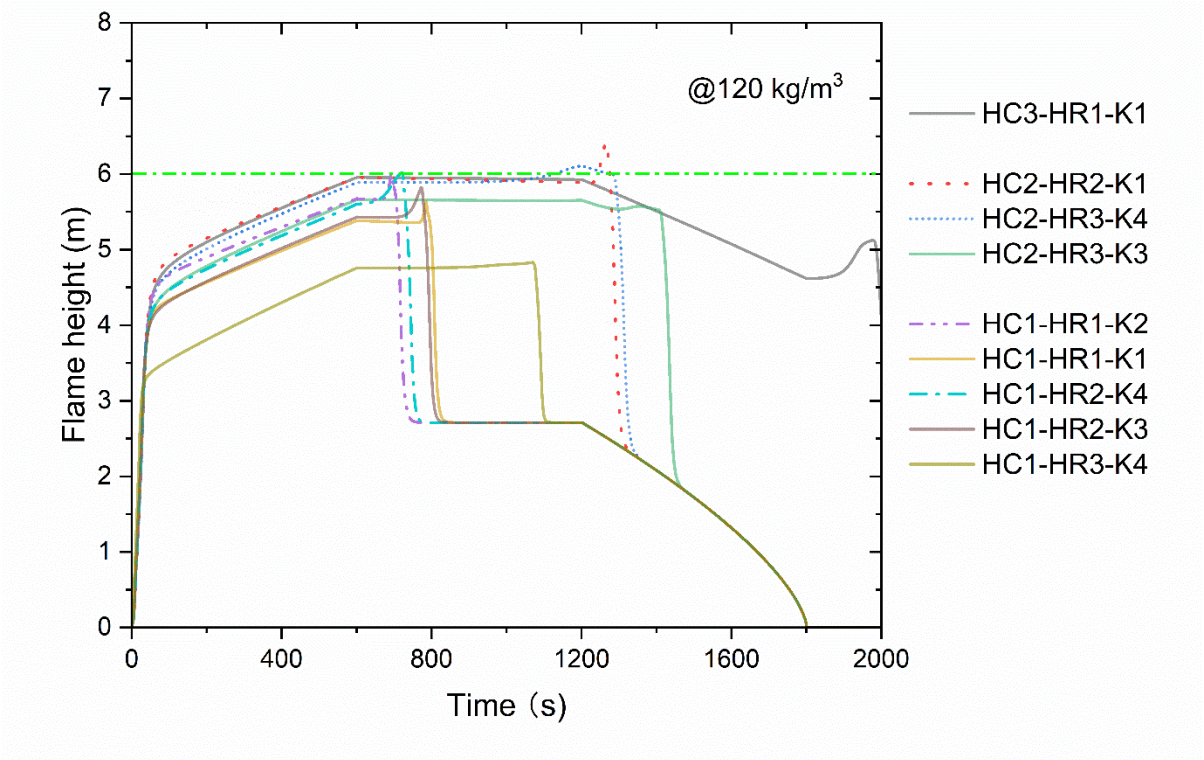
@120 kg/m3
Flame height (m)
Time（s)
HC3-HR1-K1
HC2-HR2-K1
HC2-HR3-K4
HC2-HR3-K3
HC1-HR1-K2
HC1-HR1-K1
HC1-HR2-K4
HC1-HR2-K3
HC1-HR3-K4

(d)

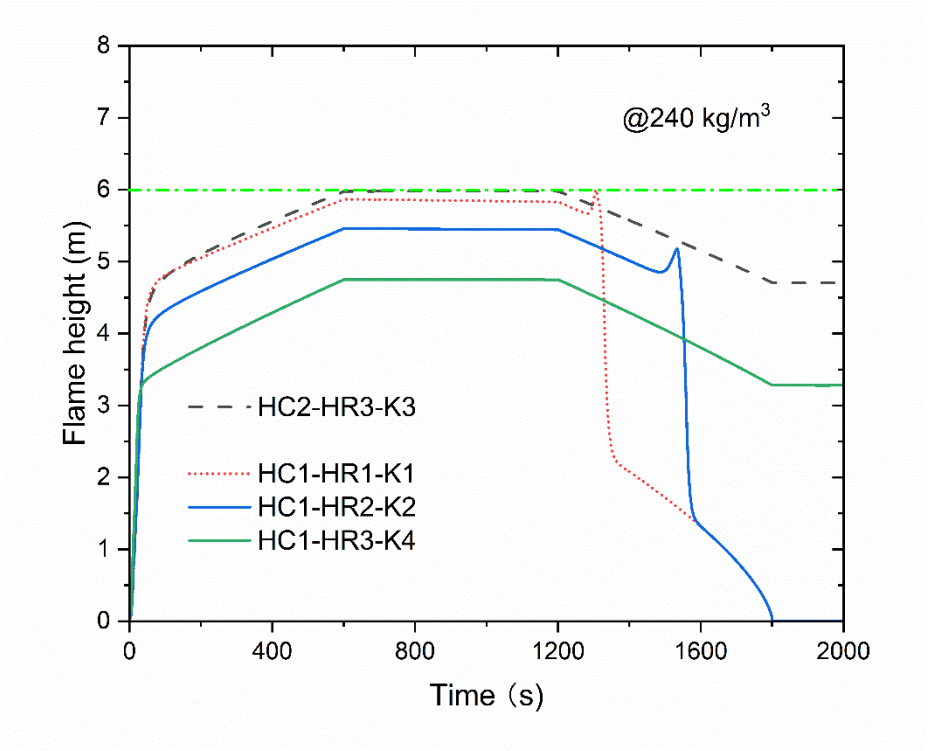

Figure 6.11 Variations of flame height of Class C materials in VF system

Table 6.7 Additional combinations of Class C materials failing to pass the full-scale BS 8414 fire test

Density (kg/m^3)	Heat of combustion	Heat of reaction	Thermal conductivity
30	HC2	HR1	K4
		HR2	K4
	HC3	HR1	K1, K2
		HR2	K1-K3
		HR3	K2-K4
60	HC2	HR1	K1
		HR2	K2
	HC3	HR2	K1
		HR3	K2
120	HC1	HR1	K2-K3
		HR2	K4
	HC2	HR3	K4
		HR2	K1

6.3.3 Effects of a protective layer on insulation

The same investigation in section 6.2.2 where a non-combustible layer encapsulates the insulation material is repeated for VF system as illustrated in Figure 6.12. The external surface is non-combustible. Only gypsum plasterboard is considered as protective layer for comparison. Again, the worst combination HC3-HR1-K4 (highest heat of combustion to generate the most heat, lowest heat of reaction to start decomposition the earliest, and highest thermal conductivity for the quickest heat transfer).

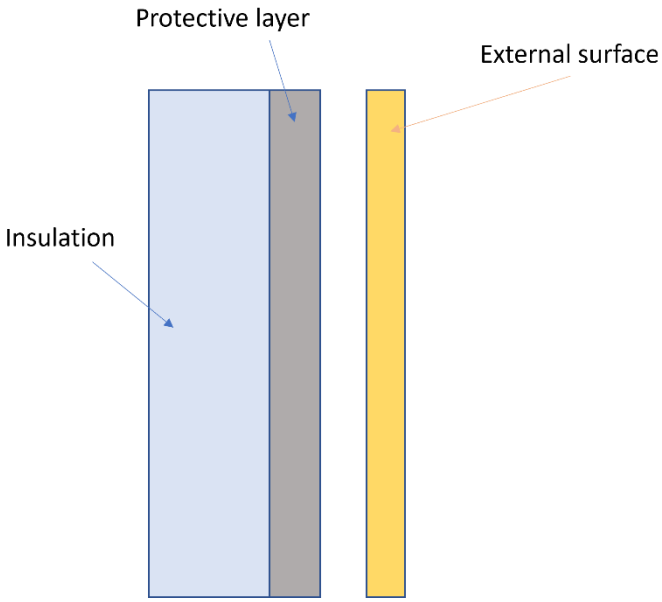

Figure 6.12 VF system with encapsulated insulation.

As for PF system, the required thickness of encapsulation increases with increasing insulation density. However, for the worst case of Class B insulation material, as long as the maximum thickness of the encapsulation non-combustible material is more than 2.2 mm, the VF system would be able to pass the full-scale BS 8414 fire test. If using the worst case of Class C insulation material, the maximum required critical thickness for gypsum plasterboard is 3mm. Figure 6.13 show plots of flame height for these two critical thicknesses of gypsum plasterboard as confirmation. They are also compared with the VF system without the protective layer.

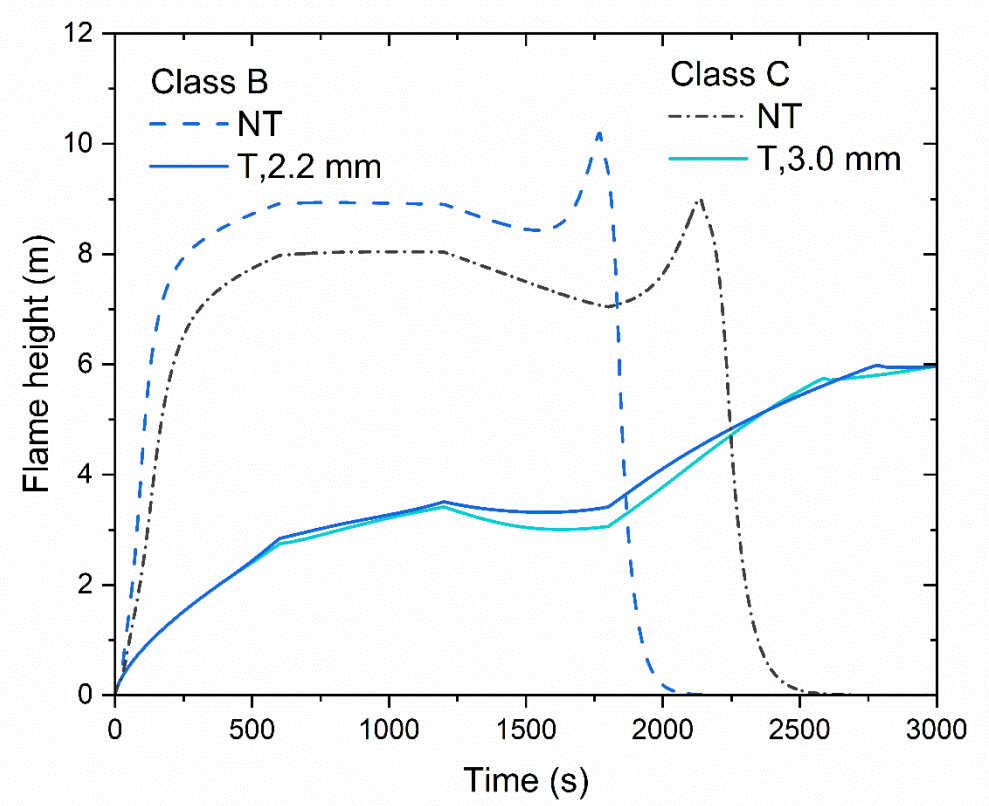

Figure 6.13 Variations of flame height for VF system of Class B and Class C insulation with and without thermal barrier layer

These maximum values of critical thickness are very similar to those in Tables 6.9 and 6.10 for gypsum plasterboard, being 2.2 mm and 3.0 mm respectively. These small thickness values can be easily provided in practice.

6.4 Conclusions

This Chapter extends the work in Chapter 5 on single external insulation material to more realistic situations of multi-layered facade with (ventilated façade, VF) and without (plain façade, PF) cavity. Multi-layered façade allows using flexible combinations the external and insulation materials to achieve the overall objectives of façade fire safety. Based on the results of numerical simulation results of this chapter, the following main conclusions may be drawn:

1. The SBI based material specification for multi-layered façade can be generally applied in the case of the insulation being non-combustible. Under this circumstance, any Class

B material can be used on the external layer provided its thickness does not exceed a critical limit. This critical limit is primarily a function of density of the material, and can be quite low (a few mms) for high density external materials (>240 kg/m^3).

2. The SBI based material specification for multi-layered façade is severely restrictive if the insulation material is encapsulated by non-combustible external surface. Instead of achieving Class A2, even Class C insulation materials can be used provided the thickness of the external layer is not lower than a critical thickness. This critical thickness is no more than a few mms and can be easily achieved in practice.
3. The air cavity in ventilated façade system results in longer flame length in BS 8414 full-scale fire test. However, the numerical simulation results of this chapter suggest that the additional flame length is small. Consequently, the number of additional combinations of Class B materials that do not pass the full-scale BS 8414 fire test is low when compared to those when used in PF system. So is the number of combinations of Class C materials that fail to pass the full-scale BS 8414 fire test when used in VF among those that pass the test when used in PF. Furthermore, if the insulation material in VF system is encapsulated with a protective non-combustible layer, the required minimum thickness for the protective layer can be easily achieved in practice.

Chapter 7 Conclusions and future work

7.1 Introduction

Limiting the risk of fire spread over materials is one of the most important precautions of ensuring fire safety in building. However, despite detailed regulations, fires spread over facade every year, causing devastating consequences often with human casualties. In fact, regulations governing material selection for fire safety can be the source of problem because they are no more than a blunt tool with limited applicability and can be mis-interpreted. The alternative to regulatory control of material selection is through large scale cladding fire test. However, such tests are expensive to conduct and can only cover a very small proportion of different cladding constructions. This research tackles the above problems by developing an efficient and accurate model to simulate upward flame spread in unventilated and ventilated cladding systems. And then uses the validated fire spread model to examine the above issues by carrying out the following investigations: (1) Quantifying the realistic ranges of combustible materials represented by the same SBI classification; (2) Assessing fire spread behaviour of these materials when used as cladding, either on its own, or in combination with another material, both with and without cavity ventilation.

7.2 Detailed conclusions

7.2.1 Numerical flame spread model development and Validation

The model consists of the following main sub-models: a one-dimensional combined heat and mass transfer model perpendicular to the vertical surface to compute gaseous fuel production due to decomposition and combustion of the combustible materials, a simplified model to calculate surface heat flux, and a transient flame growth model based on an existing steady state flame model that takes into account transient heat feedback due to combustion.

Validation of the model is checked by comparison of the predictions of this model against FDS (Fire Dynamic Simulator) simulation results and experimental results wherever available,

including the following: flame growth with variable heat release rates of solid materials under various levels of external irradiation, temperature distribution through thickness of the wall, and propagation of the pyrolysis front. To demonstrate capability of the new model, vertical burning and upward flame spread on 2.4m high panels of wood and 5.0m high panels of PMMA are carried out and compared with FDS simulations. The new model calculation results, including propagation of the pyrolysis front, total heat flux and heat release rate are in good agreement with FDS results. However, the new model requires a fraction (a few minutes of CPU time) of that for carrying out the FDS simulation (CPU time of 2 days).

7.2.2 The extension of the model to take cavity into consideration

A single zone solar chimney model was modified to reproduce the fire driven flow in the cavity. The correlations from the literature for the flame height and heat flux distribution were used. The validation consisted of comparing model results with mass flow rate in FDS, heat flux distribution in Karlis' cavity fire test, and flame spread for combustible material in full-scale test. The reference result can be well reproduced.

7.2.3 Assessment of SBI based classification for specifying material on external facade

The suitability of using the SBI classification to determine whether a material can be used in the external façade of buildings was examined. By inverse analysis, the combinations of properties were determined to achieve the relevant thresholds for Class B and Class C materials, respectively. BS 8414 fire test for external façade was modeled to predict how the material would perform in the fire test and whether it would pass the flame height acceptance criterion. The main conclusions are summarized as follows:

1) The SBI Classification of material is mainly affected by its density, thermal conductivity, heat of reaction and heat of combustion. The value of heat of combustion plays the most important role in fire behaviour of material in BS 8414 full scale fire test. The heat of reaction and thermal conductivity of a material has only moderate effects on flame height
2) The majority, but not all Class B materials would be able to pass the BS 8414 full scale fire test criterion for flame height. The Class B materials that do not pass the acceptance criterion are combinations of high density (>120kg/m^3) and high heat of combustion (>16 MJ/kg).

3) Many Class C materials could still pass the BS 8414 full scale fire test criterion for flame height. Such materials are characterised by low density (<60kg/m^3) and low heat of combustion (<16 MJ/kg).
4) Simulation results for SBI test and BS 8414 test using a commercially available Class B (Phenolic foam) and a commercially available Class C (Aerogel) insulation material confirm the two findings above.

7.2.4 Assessment of external surface with composite façade or ventilated facade

Extend work on single external insulation material to include more realistic situations of multi-layered facade with (ventilated façade, VF) and without (plain façade, PF) cavity. The fire safety criteria can be achieved with multi-layered façade by using flexible combinations of the external and insulation materials.

The following conclusions were drawn:

1) The SBI based material specification for multi-layered façade can be generally applied in the case of the insulation being non-combustible. Under this circumstance, any Class B material can be used on the external layer provided its thickness does not exceed a critical limit. This critical limit is primarily a function of density of the material, and can be quite low (a few mms) for high density external materials (>240 kg/m^3).
2) The SBI based material specification for multi-layered façade is severely restrictive if the insulation material is encapsulated by non-combustible external surface. Instead of achieving Class A2, even Class C insulation materials can be used provided the thickness of the external layer is not lower than a critical thickness. This critical thickness is no more than a few mms and can be easily achieved in practice.
3) The air cavity in ventilated façade system results in longer flame length in BS 8414 full-scale fire test. However, the numerical simulation results of this chapter suggest that the additional flame length is small. Consequently, the number of additional combinations of Class B materials that do not pass the full-scale BS 8414 fire test is low when compared to those when used in PF system. So is the number of combinations of Class C materials that fail to pass the full-scale BS 8414 fire test when used in VF among those that pass the test when used in PF. Furthermore, if the insulation material in VF system is encapsulated with a protective non-combustible layer, the required minimum thickness for the protective layer can be easily achieved in practice.

7.2 Future work

The simplified flame spread model described in this research can provide a good tool and database for the fire engineers to evaluate the fire risk associated with an eternal wall cladding system. The usefulness and capability of the flame spread model could be extended by carrying out the following tasks.

Flame spread model

1) Lateral flame spread: As shown in Figure 4.2, the flame spread in Grenfell tower both vertically and horizontally. Although the rate of lateral flame spread is considerably slower than that of vertical spread, it however aids in the growth of entire fire. Lateral spread can be integrated into the flame model in the future study.
2) Effect of window configuration and position on flame spread: Fire can spread back into a building through window openings. As a result, there is a danger that fire can bypass any compartment floor, resulting in a secondary fire. Flames might break out again if secondary fires are allowed to develop without being extinguished before flashover occurs. Flame spread more intensely due to leap frog effect of external window opening. The behavior of the flame plume is influenced by many factors such fuel loading, window dimensions and shape, ventilation to room and many other factors.
3) Optimization of fire-related properties for multi-layered material: Several CFD models have been developed to predict fire characteristics. Fire-related properties, such as thermal and chemical properties, are needed as input to predict the ignition and flame spread of solid materials. For materials with multilayered structures, it requires sampling each layer and using specific test equipment to measure the properties, which adds a lot of cost and effort. The inadequacies of direct measurement of each fire-related property must be addressed. The optimized fire related properties can be derived using reverse heat transfer method with small scale tests such as cone calorimeter.

Application cases

Historic building fires have recently occurred in countries including Germany, France, and Brazil. The majority of ancient structures are typically timber constructions, which pose a significant fire danger, particularly after years of exposure to the outdoors. It is well known that as time passed, lighting the wood with fire became considerably simpler. Therefore, it is necessary to develop a

fire-related properties' database for assessing the fire risk current wooden building. A possible method of conservation and preservation should be found.

Appendix A Combinations of material properties

Table A.1 Combinations of material properties

No.	Combinations	No.	Combinations	No.	Combinations	No.	Combinations
1	D1-HC1-HR1-K1	37	D2-HC1-HR1-K1	73	D3-HC1-HR1-K1	109	D4-HC1-HR1-K1
2	D1-HC1-HR1-K2	38	D2-HC1-HR1-K2	74	D3-HC1-HR1-K2	110	D4-HC1-HR1-K2
3	D1-HC1-HR1-K3	39	D2-HC1-HR1-K3	75	D3-HC1-HR1-K3	111	D4-HC1-HR1-K3
4	D1-HC1-HR1-K4	40	D2-HC1-HR1-K4	76	D3-HC1-HR1-K4	112	D4-HC1-HR1-K4
5	D1-HC1-HR2-K1	41	D2-HC1-HR2-K1	77	D3-HC1-HR2-K1	113	D4-HC1-HR2-K1
6	D1-HC1-HR2-K2	42	D2-HC1-HR2-K2	78	D3-HC1-HR2-K2	114	D4-HC1-HR2-K2
7	D1-HC1-HR2-K3	43	D2-HC1-HR2-K3	79	D3-HC1-HR2-K3	115	D4-HC1-HR2-K3
8	D1-HC1-HR2-K4	44	D2-HC1-HR2-K4	80	D3-HC1-HR2-K4	116	D4-HC1-HR2-K4
9	D1-HC1-HR3-K1	45	D2-HC1-HR3-K1	81	D3-HC1-HR3-K1	117	D4-HC1-HR3-K1
10	D1-HC1-HR3-K2	46	D2-HC1-HR3-K2	82	D3-HC1-HR3-K2	118	D4-HC1-HR3-K2
11	D1-HC1-HR3-K3	47	D2-HC1-HR3-K3	83	D3-HC1-HR3-K3	119	D4-HC1-HR3-K3
12	D1-HC1-HR3-K4	48	D2-HC1-HR3-K4	84	D3-HC1-HR3-K4	120	D4-HC1-HR3-K4
13	D1-HC2-HR1-K1	49	D2-HC2-HR1-K1	85	D3-HC2-HR1-K1	121	D4-HC2-HR1-K1
14	D1-HC2-HR1-K2	50	D2-HC2-HR1-K2	86	D3-HC2-HR1-K2	122	D4-HC2-HR1-K2
15	D1-HC2-HR1-K3	51	D2-HC2-HR1-K3	87	D3-HC2-HR1-K3	123	D4-HC2-HR1-K3
16	D1-HC2-HR1-K4	52	D2-HC2-HR1-K4	88	D3-HC2-HR1-K4	124	D4-HC2-HR1-K4
17	D1-HC2-HR2-K1	53	D2-HC2-HR2-K1	89	D3-HC2-HR2-K1	125	D4-HC2-HR2-K1
18	D1-HC2-HR2-K2	54	D2-HC2-HR2-K2	90	D3-HC2-HR2-K2	126	D4-HC2-HR2-K2
19	D1-HC2-HR2-K3	55	D2-HC2-HR2-K3	91	D3-HC2-HR2-K3	127	D4-HC2-HR2-K3
20	D1-HC2-HR2-K4	56	D2-HC2-HR2-K4	92	D3-HC2-HR2-K4	128	D4-HC2-HR2-K4
21	D1-HC2-HR3-K1	57	D2-HC2-HR3-K1	93	D3-HC2-HR3-K1	129	D4-HC2-HR3-K1
22	D1-HC2-HR3-K2	58	D2-HC2-HR3-K2	94	D3-HC2-HR3-K2	130	D4-HC2-HR3-K2
23	D1-HC2-HR3-K3	59	D2-HC2-HR3-K3	95	D3-HC2-HR3-K3	131	D4-HC2-HR3-K3
24	D1-HC2-HR3-K4	60	D2-HC2-HR3-K4	96	D3-HC2-HR3-K4	132	D4-HC2-HR3-K4
25	D1-HC3-HR1-K1	61	D2-HC3-HR1-K1	97	D3-HC3-HR1-K1	133	D4-HC3-HR1-K1
26	D1-HC3-HR1-K2	62	D2-HC3-HR1-K2	98	D3-HC3-HR1-K2	134	D4-HC3-HR1-K2
27	D1-HC3-HR1-K3	63	D2-HC3-HR1-K3	99	D3-HC3-HR1-K3	135	D4-HC3-HR1-K3
28	D1-HC3-HR1-K4	64	D2-HC3-HR1-K4	100	D3-HC3-HR1-K4	136	D4-HC3-HR1-K4
29	D1-HC3-HR2-K1	65	D2-HC3-HR2-K1	101	D3-HC3-HR2-K1	137	D4-HC3-HR2-K1
30	D1-HC3-HR2-K2	66	D2-HC3-HR2-K2	102	D3-HC3-HR2-K2	138	D4-HC3-HR2-K2
31	D1-HC3-HR2-K3	67	D2-HC3-HR2-K3	103	D3-HC3-HR2-K3	139	D4-HC3-HR2-K3
32	D1-HC3-HR2-K4	68	D2-HC3-HR2-K4	104	D3-HC3-HR2-K4	140	D4-HC3-HR2-K4
33	D1-HC3-HR3-K1	69	D2-HC3-HR3-K1	105	D3-HC3-HR3-K1	141	D4-HC3-HR3-K1
34	D1-HC3-HR3-K2	70	D2-HC3-HR3-K2	106	D3-HC3-HR3-K2	142	D4-HC3-HR3-K2
35	D1-HC3-HR3-K3	71	D2-HC3-HR3-K3	107	D3-HC3-HR3-K3	143	D4-HC3-HR3-K3
36	D1-HC3-HR3-K4	72	D2-HC3-HR3-K4	108	D3-HC3-HR3-K4	144	D4-HC3-HR3-K4

Table A.2 THR_{600s} results of the different combinations for Class B material

No.		No.		No.		No.	
1	0.87	37	1.88	73	3.53	109	4.53
2	0.90	38	1.95	74	3.99	110	5.21
3	0.95	39	2.21	75	4.79	111	6.34
4	0.95	40	2.21	76	4.79	112	6.97
5	0.82	41	1.77	77	2.76	113	3.38
6	0.86	42	1.81	78	3.22	114	3.81
7	0.90	43	1.95	79	3.55	115	4.48
8	0.95	44	2.11	80	4.22	116	4.46
9	0.78	45	1.63	81	2.10	117	2.34
10	0.80	46	1.65	82	2.18	118	2.50
11	0.82	47	1.67	83	2.39	119	3.25
12	0.85	48	1.75	84	2.64	120	2.90
13	2.13	49	4.57	85	6.40	121	8.38
14	2.29	50	5.01	86	7.54	122	9.83
15	2.52	51	5.80	87	9.47	123	12.47
16	2.88	52	6.86	88	11.87	124	14.26
17	1.97	53	3.95	89	4.92	125	6.14
18	2.00	54	4.39	90	5.58	126	7.08
19	2.31	55	4.79	91	6.96	127	8.82
20	2.56	56	5.70	92	8.56	128	10.69
21	2.56	57	5.70	93	8.56	129	10.69
22	1.85	58	3.11	94	3.81	130	4.63
23	1.91	59	3.69	95	4.36	131	5.42
24	2.12	60	4.34	96	5.54	132	6.31
25	3.81	61	6.93	97	9.83	133	11.84
26	4.26	62	8.41	98	11.34	134	13.46
27	5.06	63	10.02	99	12.70	135	16.03
28	6.10	64	13.06	100	15.17	136	16.03
29	3.48	65	5.43	101	7.29	137	9.51
30	3.87	66	6.17	102	7.29	138	11.23
31	4.46	67	7.78	103	10.18	139	13.84
32	5.35	68	9.92	104	12.59	140	13.83
33	3.10	69	3.96	105	5.06	141	6.18
34	3.25	70	4.54	106	5.52	142	7.31
35	3.51	71	5.27	107	6.83	143	8.68
36	3.94	72	6.49	108	6.83	144	10.04

Appendix B Results from reverse modelling of SBI test (CLASS B)

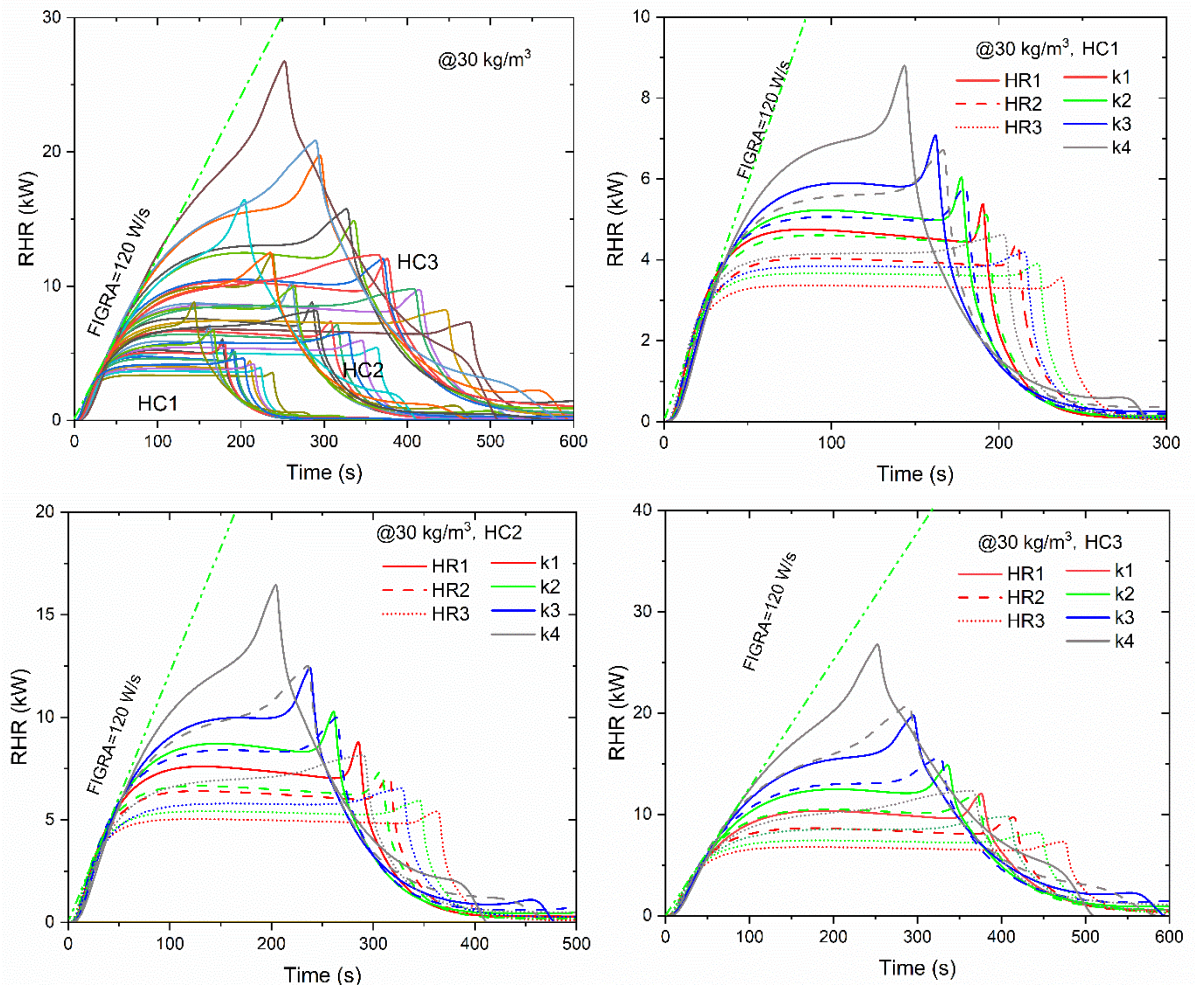

Figure B.1 RHR curves of Class B materials with a density of 30 kg/m^3

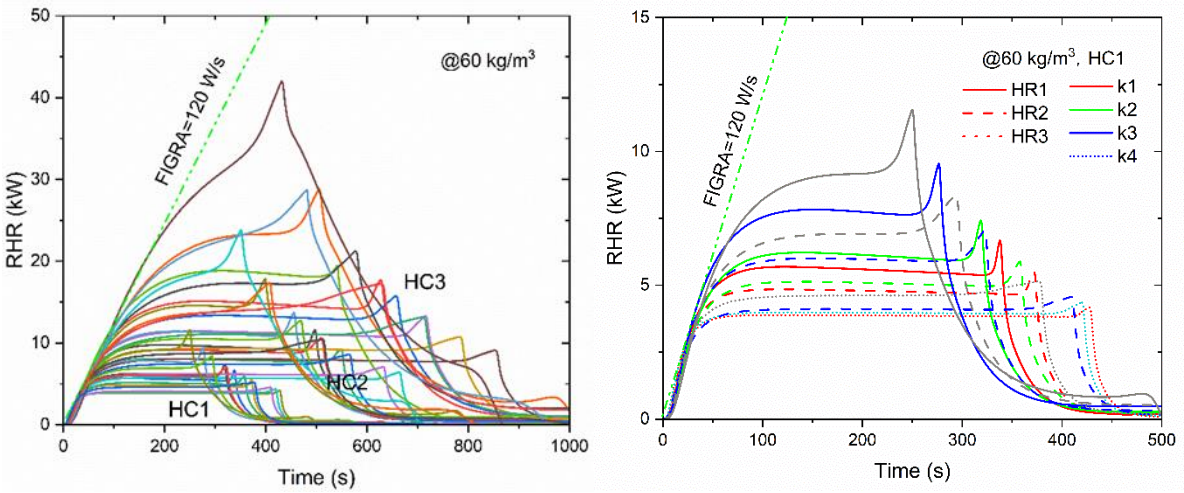

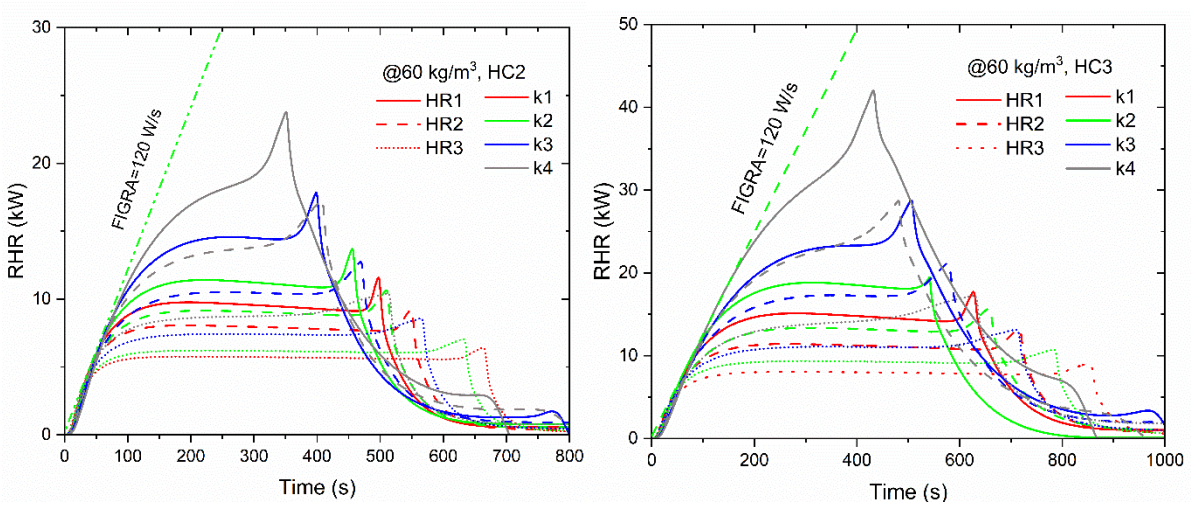

Figure B.2 RHR curves of Class B materials with a density of 60 kg/m^3

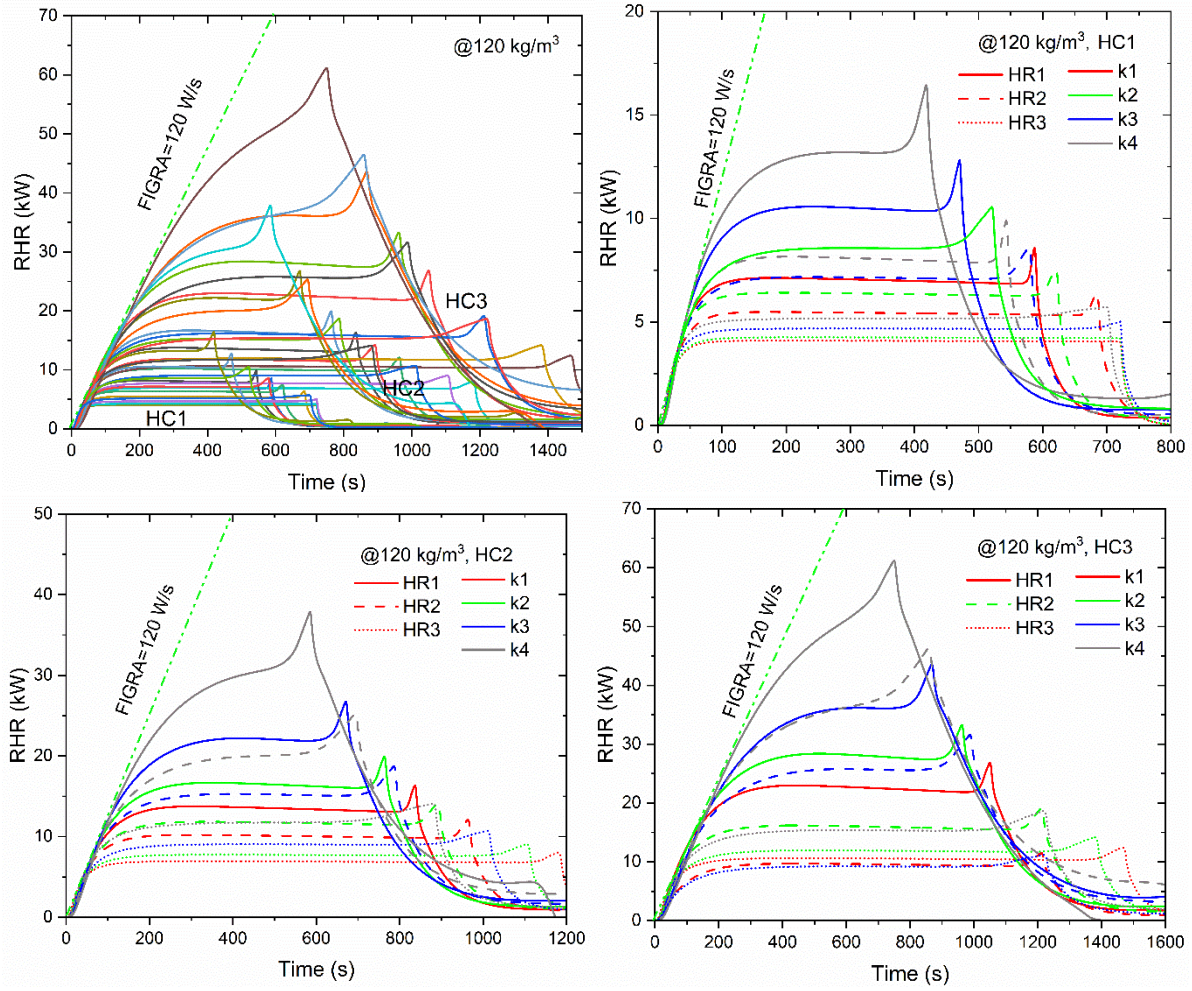

Figure B.3 RHR curves of Class B materials with a density of 120 kg/m^3

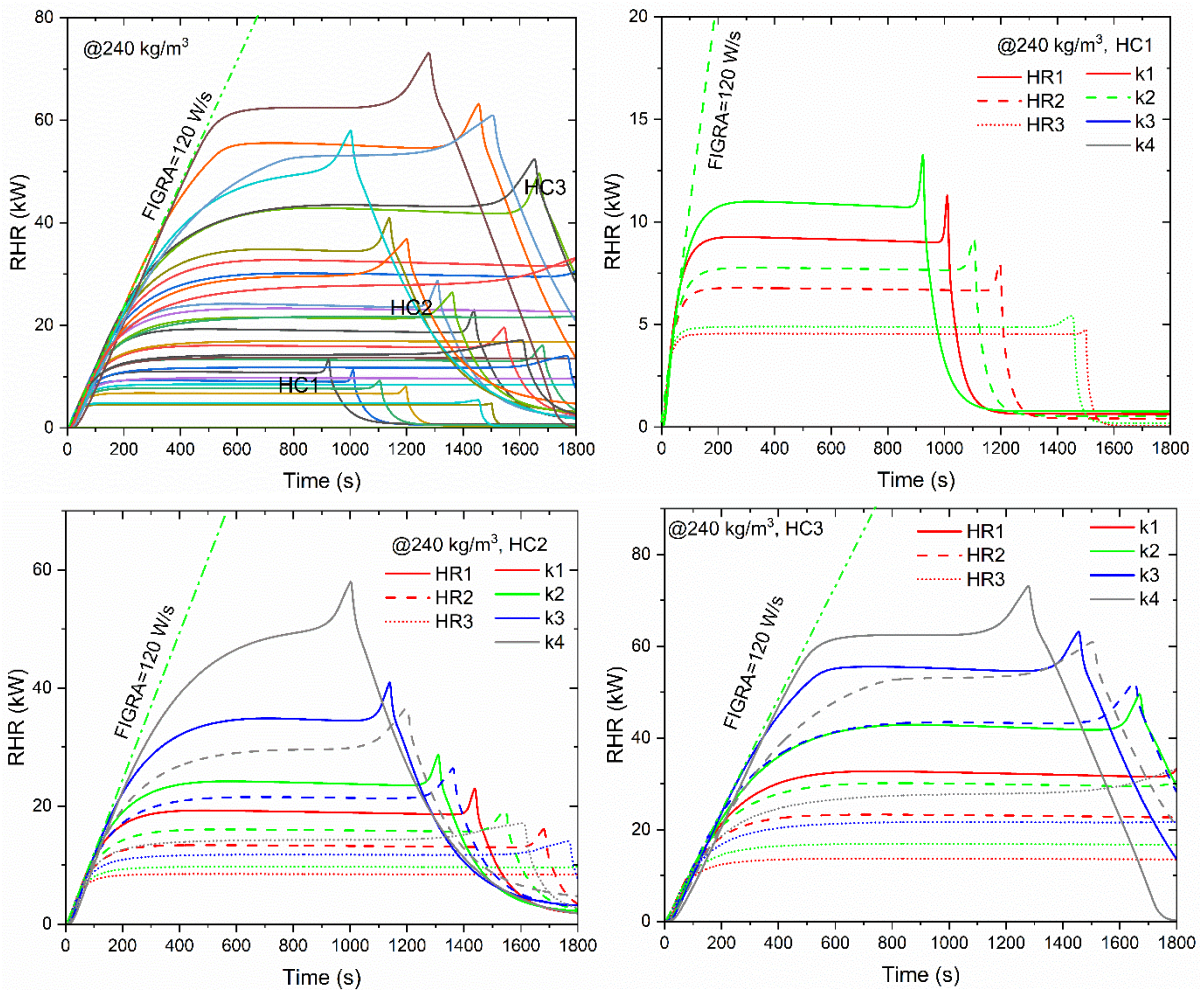

Figure B.4 RHR curves of Class B materials with a density of 240 kg/m^3

Appendix C Results from reverse modelling of SBI test (CLASS C)

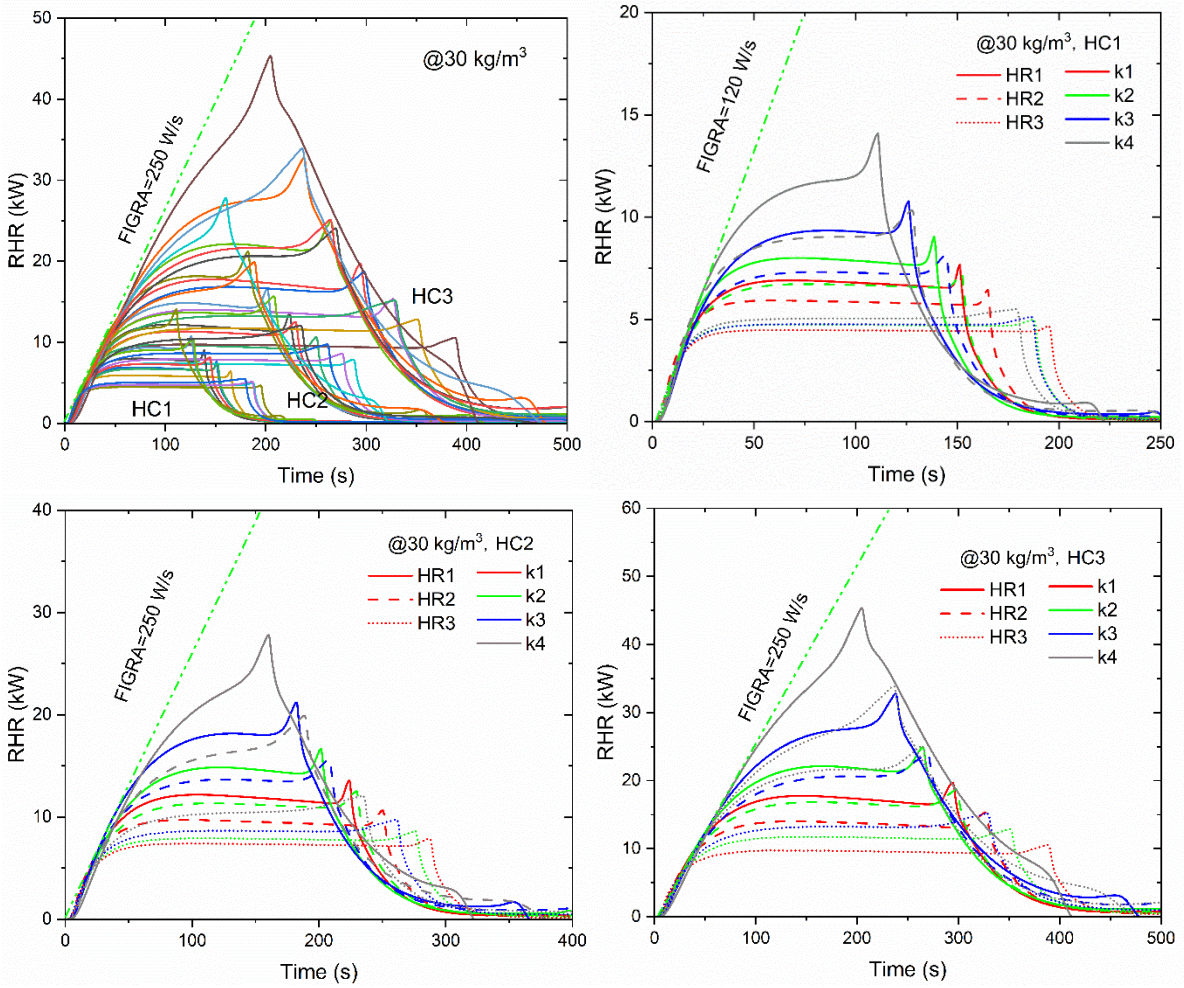

Figure C.1 RHR curves of Class C materials with a density of 30 kg/m^3

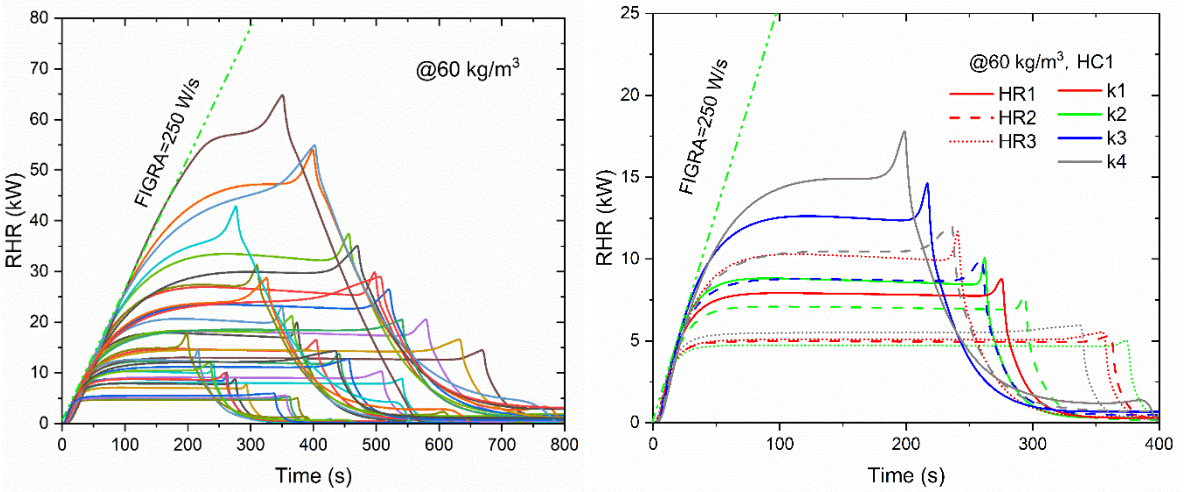

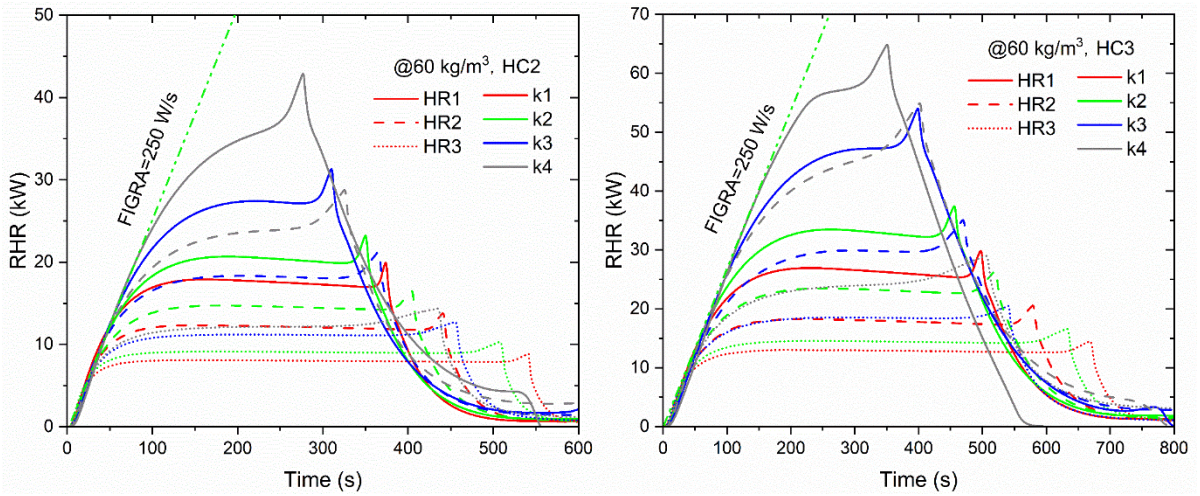

Figure C.2 RHR curves of Class C materials with a density of 60 kg/m^3

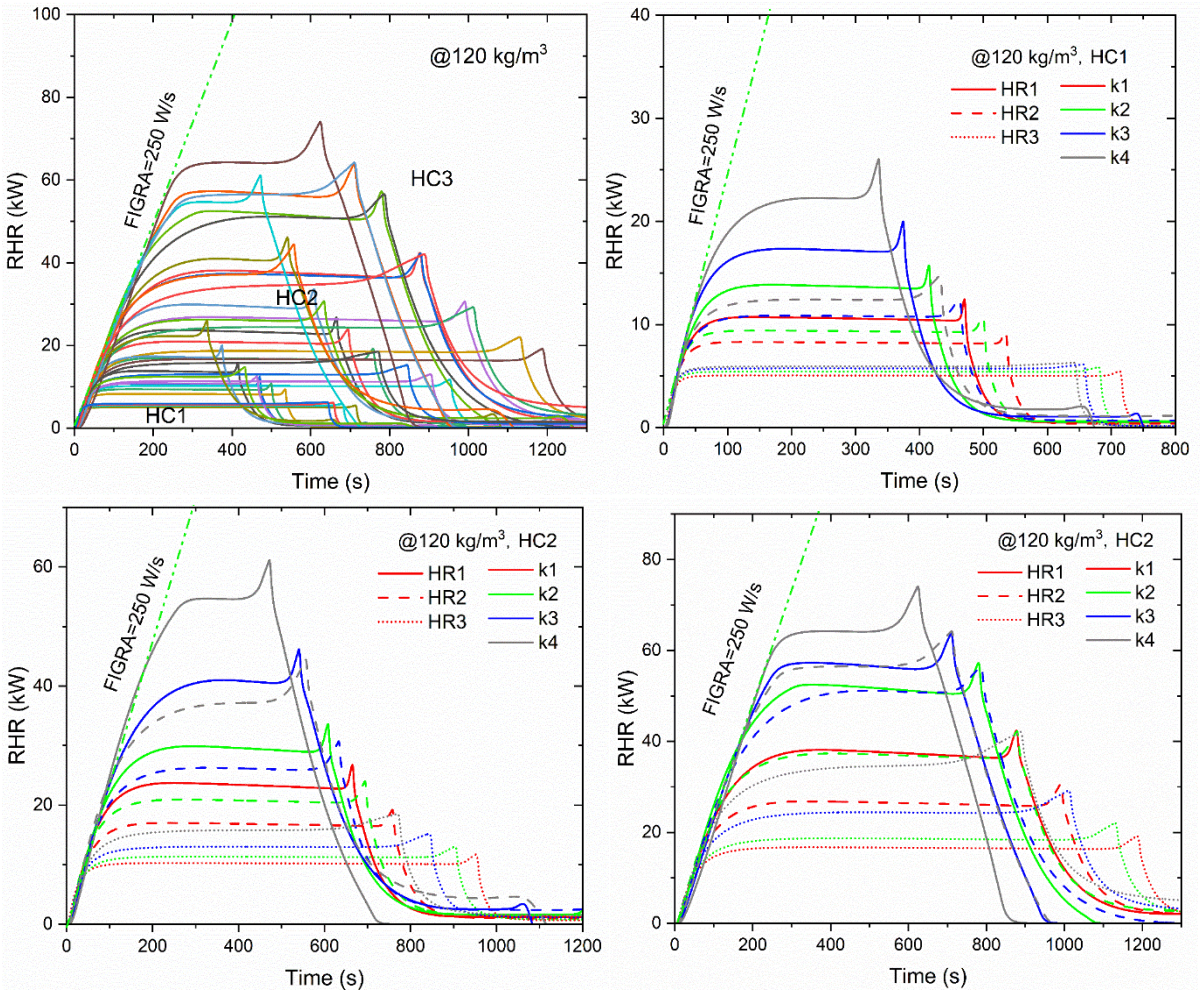

Figure C.3 RHR curves of Class C materials with a density of 120 kg/m^3

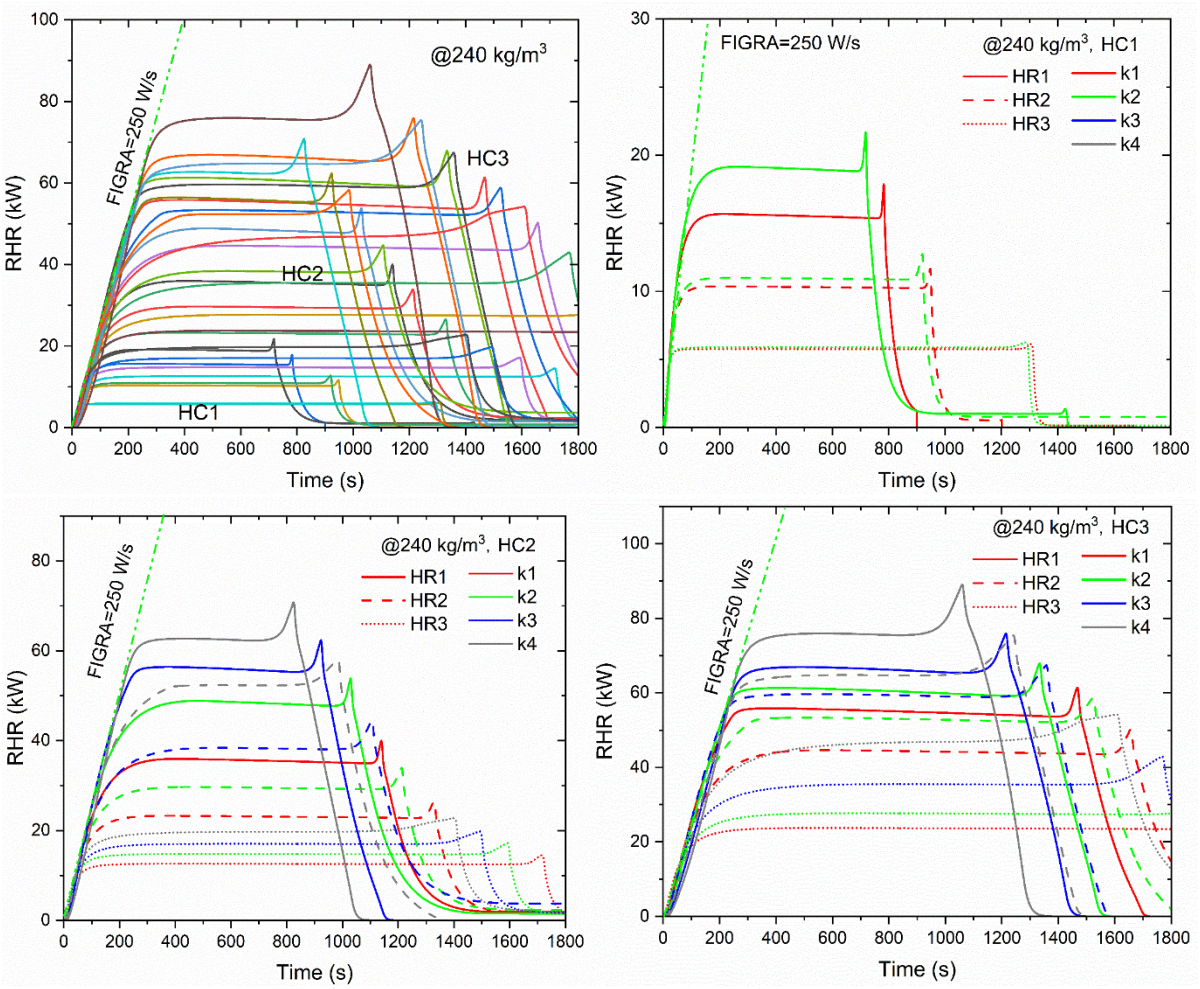

Figure C.4 RHR curves of Class C materials with a density of 240 kg/m^3

Appendix D Results from modelling of Full-scale test (CLASS B)

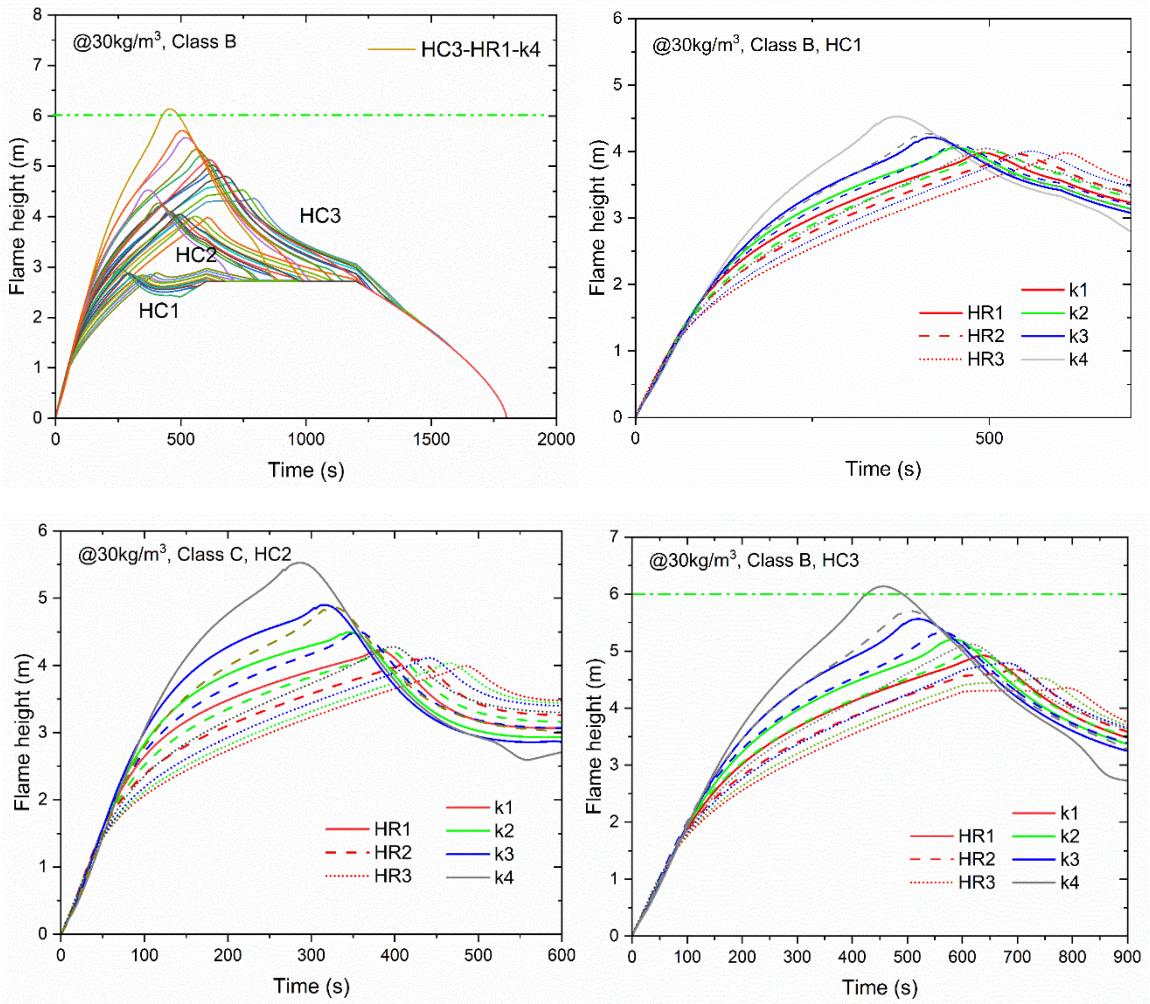

Figure D.1 Variations in flame height of Class B materials with a density of 30 kg/m^3

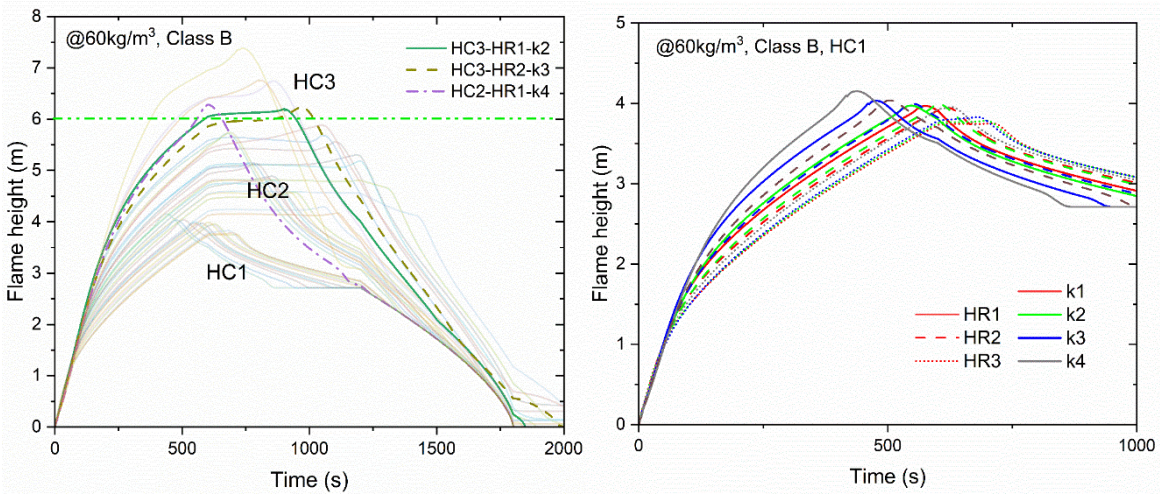

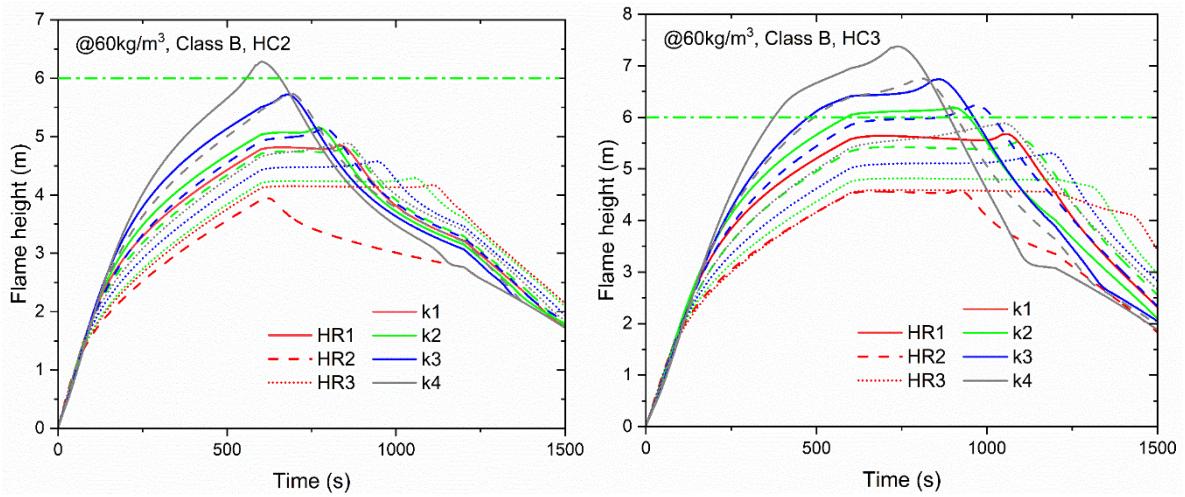

Figure D.2 Variations in flame height of Class B materials with a density of 60 kg/m^3

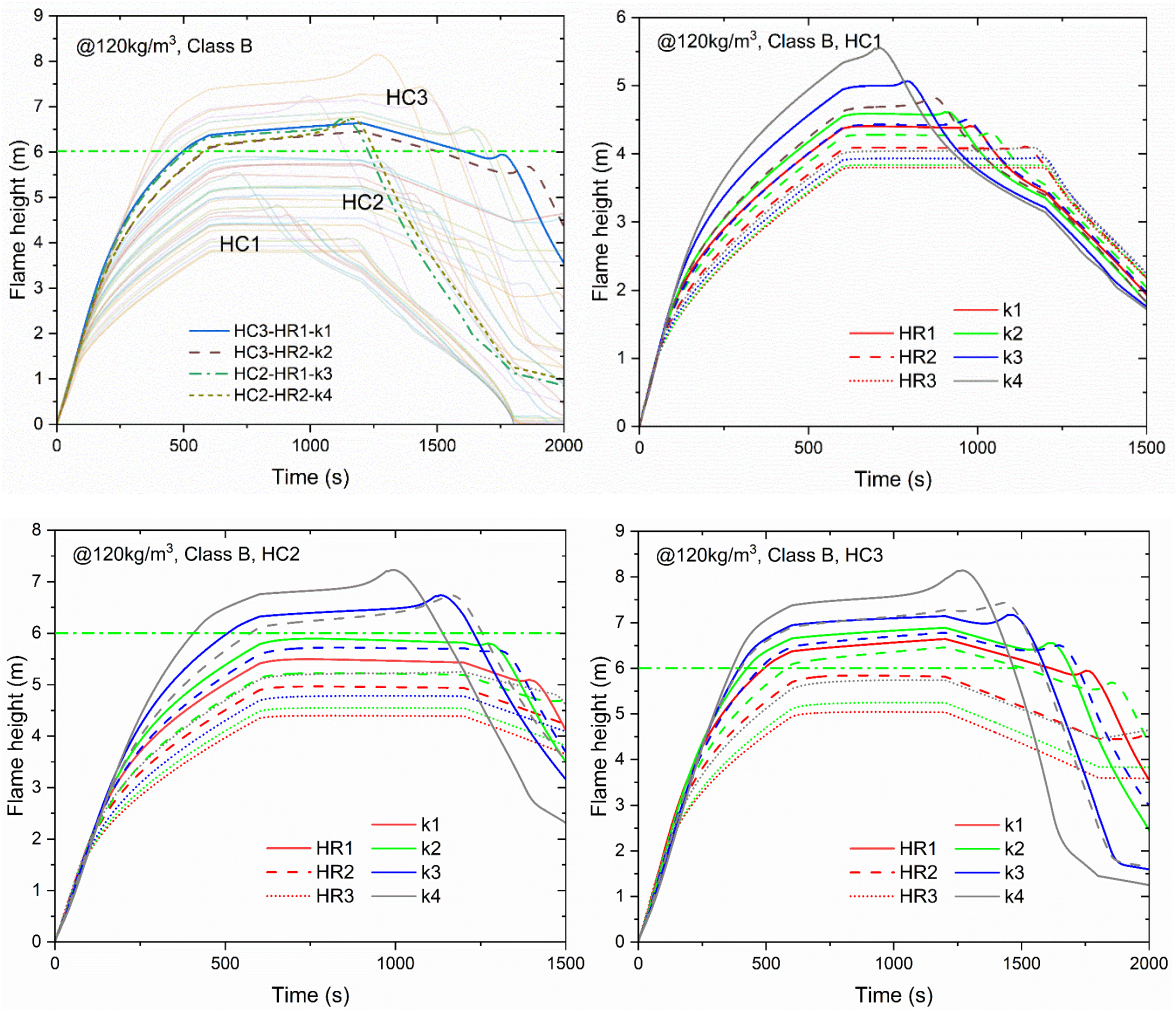

Figure D.3 Variations in flame height of Class B materials with a density of 120 kg/m^3

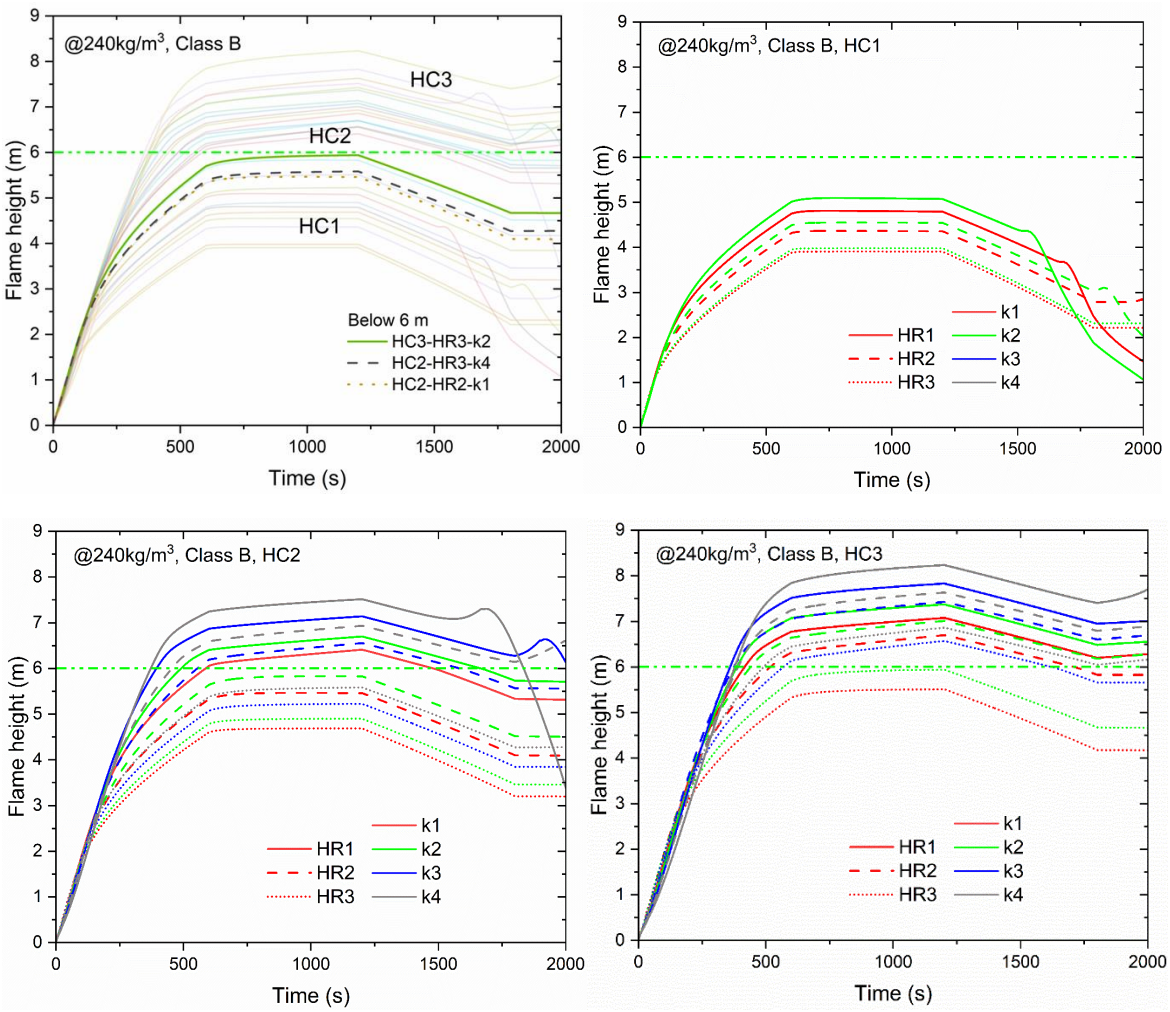

Figure D.4 Variations in flame height of Class B materials with a density of 240 kg/m^3

Appendix E Results from modelling of Full-scale test (CLASS C)

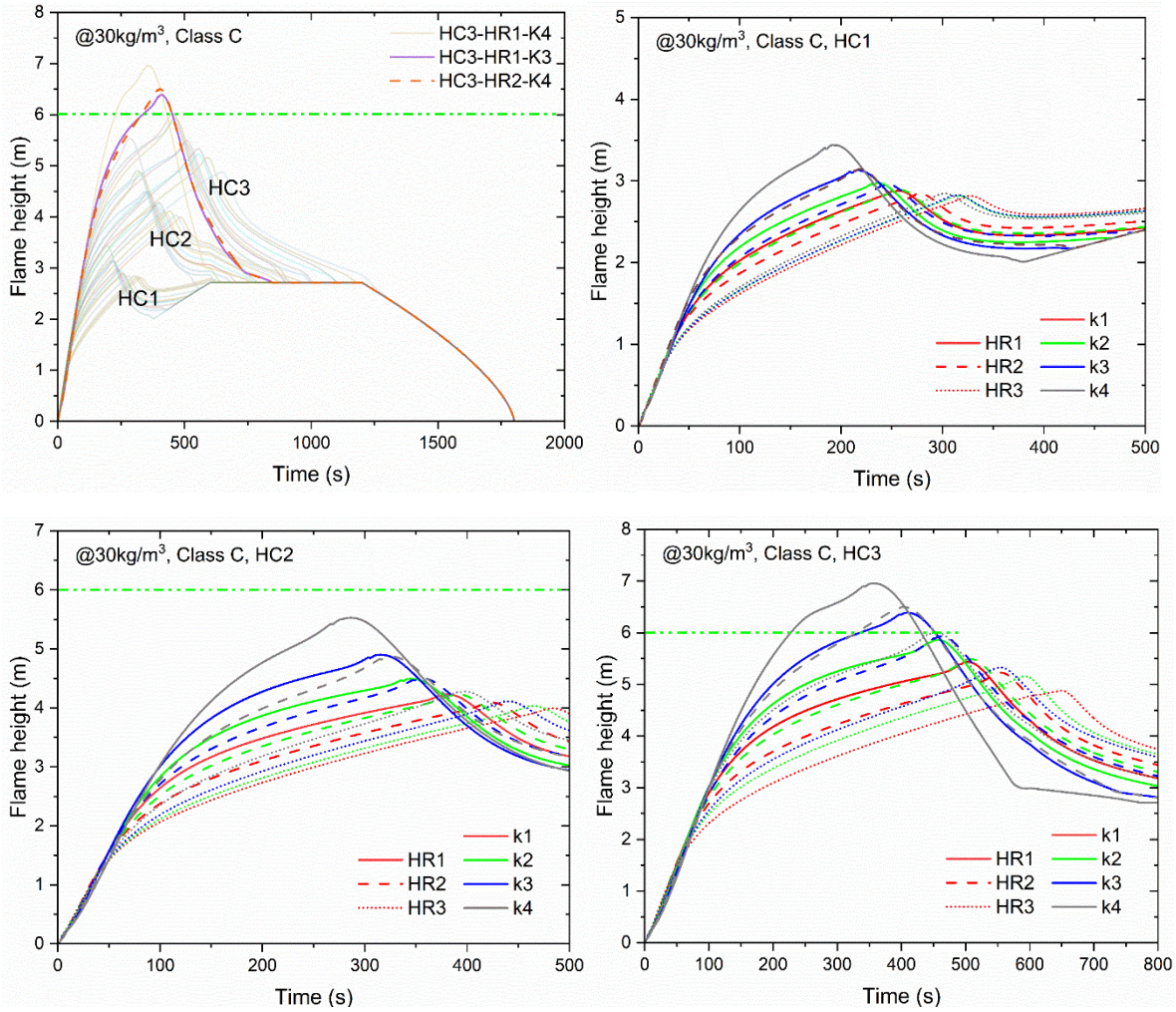

Figure E.1 Variations in flame height of Class C materials with a density of 30 kg/m^3

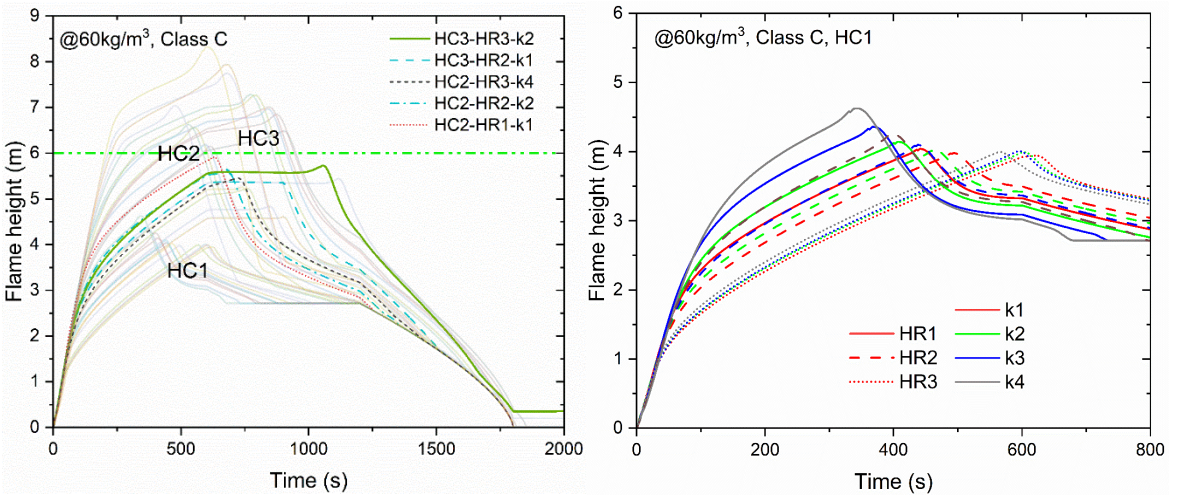

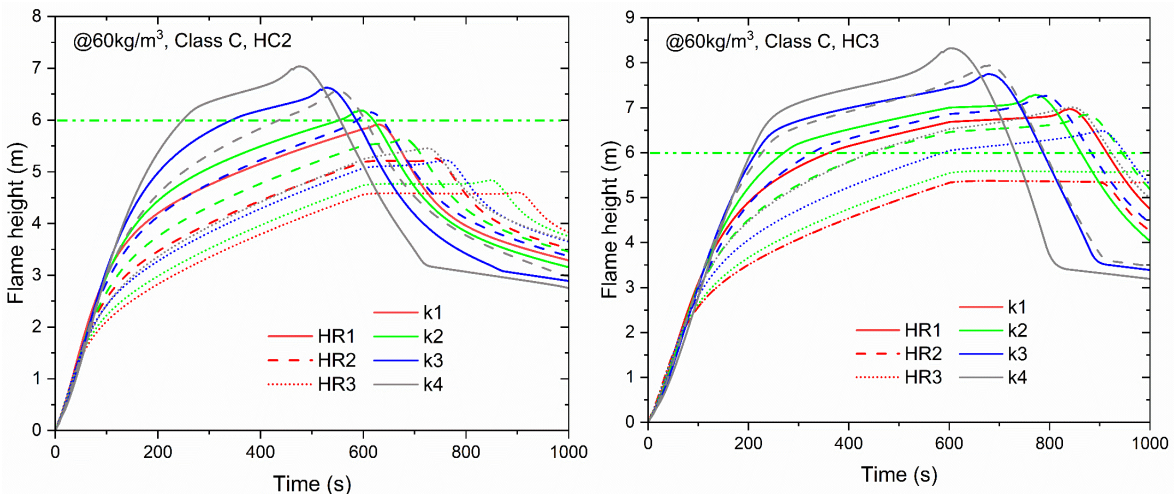

Figure E.2 Variations in flame height of Class C materials with a density of 60 kg/m^3

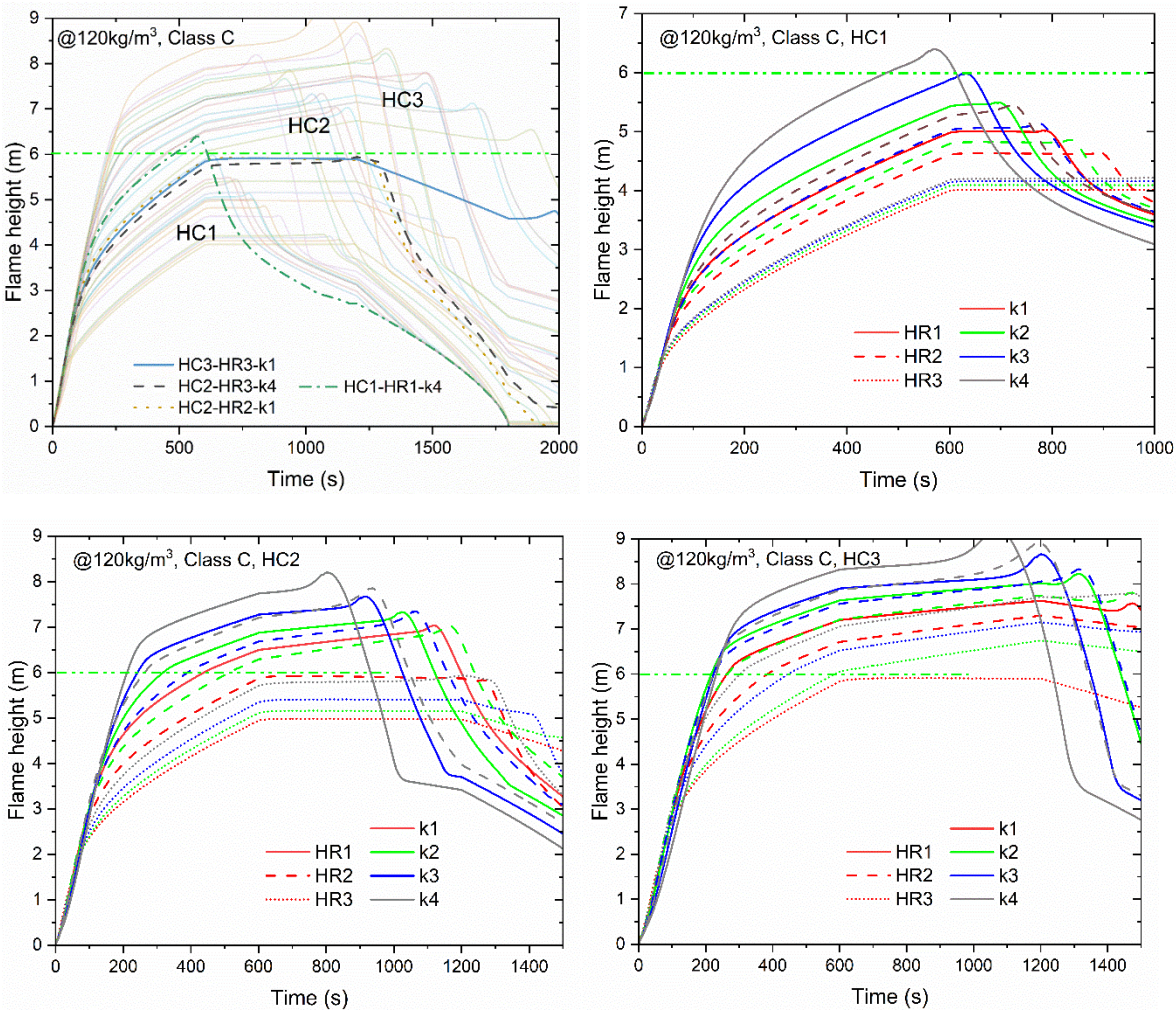

Figure E.3 Variations in flame height of Class C materials with a density of 120 kg/m^3

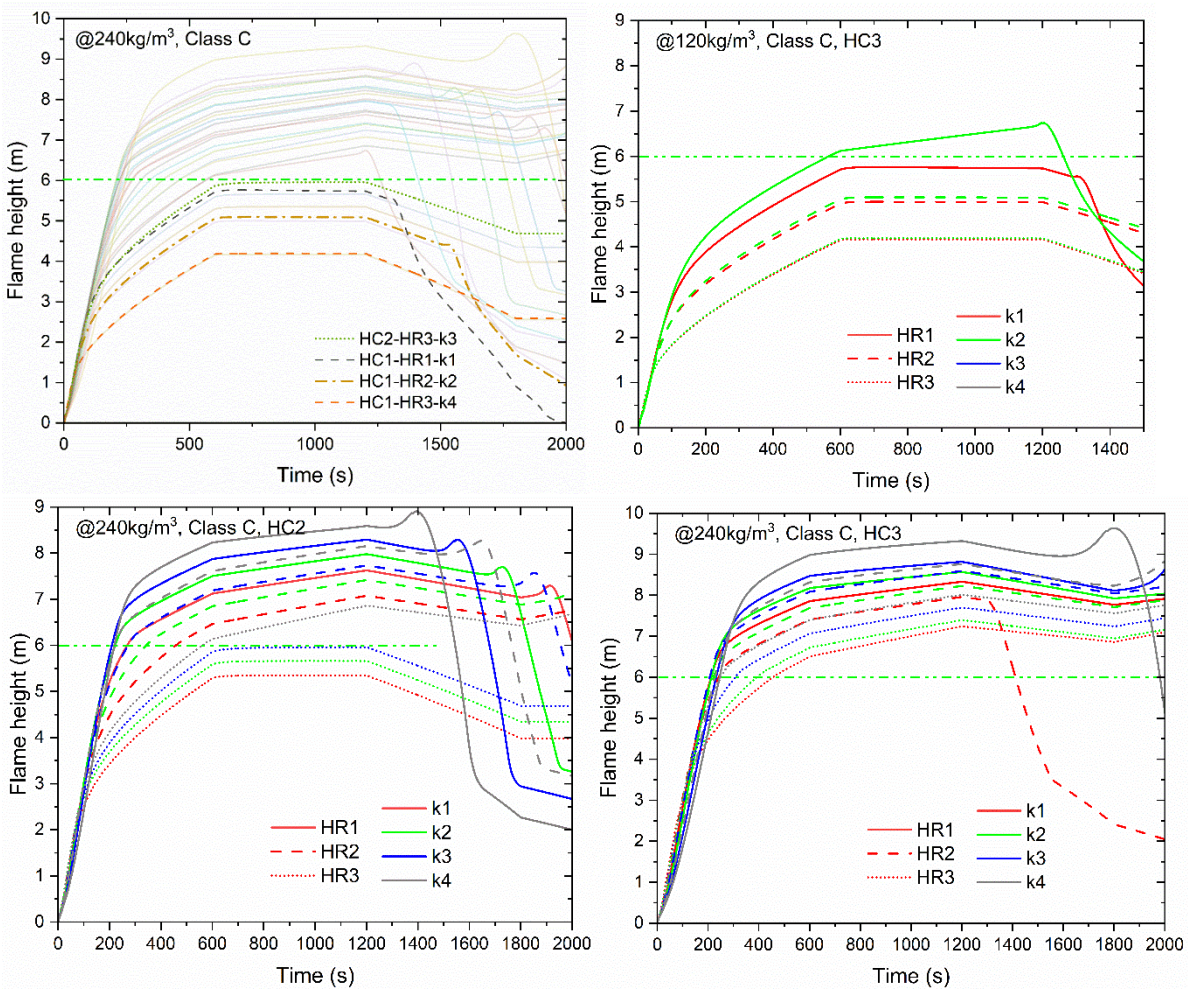

Figure E.4 Variations in flame height of Class C materials with a density of 240 kg/m^3

Reference

[1] Babrauskas V. The cone calorimeter. In. The cone calorimeter. Springer, 2016, pp. 952-80.
[2] British Standard B, EN 13823: 2002, Reaction to fire tests for building products. Building products excluding floorings exposed to the thermal attack by a single burning item, British Standards Institution, London, UK, 2002.
[3] DSTU E, 13501-2: 2016, Fire classification of construction products and building elements. Part;2: 13501-2.
[4] BSI, BS 8414 Fire performance of external cladding systems - Part 1: Test method for non-loadbearing external cladding, British Standards Institute, 2015.
[5] Institution BS. BS 9414:2019 Fire performance of external cladding systems. In. BS 9414:2019 Fire performance of external cladding systems., BSI, 2019.
[6] Moore-Bick MA DND, Mothersole J, Grenfell Tower Inquiry, Open Government, London, 2019: 978-1.
[7] Colwell S, Baker T, BR 135: Fire Performance of external thermal insulation for walls of multistorey buildings, BRE trust, Watford, 2013.
[8] ISO E, 1182: 2010. Reaction to fire tests for products—Non-combustibility test, London, BSI Standards Publication, 2010.
[9] BSI B. 476-4 Fire Tests on Building Materials and Structures—Part 4: Non-Combustibility Test for Materials. In. 476-4 Fire Tests on Building Materials and Structures—Part 4: Non-Combustibility Test for Materials. British: British Standards Institution, 1970.
[10] ASTM E, E136, Standard Test Method for Behavior of Materials in a Vertical Tube Furnace at;750.
[11] Standard A. AS 1530: methods for fire tests on building materials, componentes and structures. In. AS 1530: methods for fire tests on building materials, componentes and structures. Sidney, 2005.
[12] 268 N, Standard Test Method for Determining Ignitability of Exterior Wall Assemblies Using a Radiant Heat Energy source, 2017.
[13] DIN IE, Reaction to fire tests for building products ó Determination of the heat of combustion (ISO 1716: 2002); German version EN ISO 1716: 2002, 2002.

[14] ASTM E, 1354-04a: Standard Test Method for Heat and Visible Smoke Release Rates for Materials and Products Using an Oxygen Consumption Calorimeter, American Society for Testing and Materials, West Conshohocken, 2004.
[15] Standard B, 476: Part 7: 1968, Fire tests on building ma-terials and structures. Surface spread of flame test for materials.
[16] ISO E, 13785-2. Reaction-to-fire tests for façades–Part 2: Large-scale test, Addis Abeba: ESA, 2002.
[17] -1 D. Fire behaviour of building materials and building components–Part 1: building materials; concepts, requirements and tests. In. Fire behaviour of building materials and building components–Part 1: building materials; concepts, requirements and tests. Beuth Verlag Berlin, 1998.
[18] Association NFP, NFPA 285 Standard Fire Test method for evaluation of fire propagation characteristics of exterior non-load-bearing wall assemblies containing combustible components, National Fire Protection Association, Quincy, 2012.
[19] Fire S, 105 External wall assemblies and facade claddings. Reaction to fire, SP Technical Research Institute of Sweden, 1994;16.
[20] CAN/ULC-S134-13, Standard Method of Fire Test of Exterior Wall Assemblies, 2013.
[21] AS5113, Fire propagation testing and classification of external walls of buildings, 2016.
[22] Schulz J, Kent D, Crimi T, Glockling JL, Hull TR, A critical appraisal of the UK's regulatory regime for combustible façades, Fire technology, 2021;57: 261-90.
[23] McKenna ST, Jones N, Peck G, Dickens K, Pawelec W, Oradei S, Harris S, Stec AA, Hull TR, Fire behaviour of modern façade materials–Understanding the Grenfell Tower fire, Journal of hazardous materials, 2019;368: 115-23.
[24] Government H. The building regulations 2010, Approved Document B (fire safety) volume 1: dwellings. In. The building regulations 2010, Approved Document B (fire safety) volume 1: dwellings. HM Government London, 2019.
[25] Trombly B, The international building code (IBC), CMGT 564-Term Paper, 2006.
[26] China MoPSoPsRo. GB 50045-2005 code for fire protection design of tall buildings. In. GB 50045-2005 code for fire protection design of tall buildings. 2005.
[27] Security PsRoCMoP. Civil construction insulation systems and external decorative fire Interim Provisions In. Civil construction insulation systems and external decorative fire Interim Provisions 2009.

[28] Kokkala M, Thermal models of flame spread, Reaction to fire of combustion products Area B: Fire Modelling: 364-86.
[29] Mowrer FW, Williamson RB. Flame spread evaluation for thin interior finish materials. In. Flame spread evaluation for thin interior finish materials. Routledge, 2006, pp. 689-98.
[30] Williams F. Mechanisms of fire spread. In. Mechanisms of fire spread. Elsevier, 1977, pp. 1281-94.
[31] Orloff L, De Ris J, Markstein G. Upward turbulent fire spread and burning of fuel surface. In. Upward turbulent fire spread and burning of fuel surface. Elsevier, 1975, pp. 183-92.
[32] Ahmad T, Faeth G. Turbulent wall fires. In. Turbulent wall fires. Elsevier, 1979, pp. 1149-60.
[33] Karlsson B, A mathematical model for calculating heat release rate in the room corner test, Fire Safety Journal, 1993;20: 93-113.
[34] Grant G, Drysdale D, Numerical modelling of early flame spread in warehouse fires, Fire Safety Journal, 1995;24: 247-78.
[35] Tsai K-C, Using cone calorimeter data for the prediction of upward flame spread rate, Journal of thermal analysis and calorimetry, 2013;112: 1601-06.
[36] Quintiere JG, A semi-quantitative model for the burning rate of solid materials, Fire Safety Science, 1992;1: 3-25.
[37] Chen Y, Delichatsios M, Motvalli V, Material pyrolysis properties, part I: an integral model for one-dimensional transient pyrolysis of charring and non-charring materials, Combustion Science and Technology, 1993;88: 309-28.
[38] Chen Y, Motevalli V, Delichatsios M, Material pyrolysis properties, Part II: methodology for the derivation of pyrolysis properties for charring materials, Combustion Science and Technology, 1995;104: 401-25.
[39] Moghtaderi B, Novozhilov V, Fletcher D, Kent J, An integral model for the transient pyrolysis of solid materials, Fire and Materials, 1997;21: 7-16.
[40] Spearpoint M, Quintiere J, Predicting the burning of wood using an integral model, Combustion and Flame, 2000;123: 308-25.
[41] Weng W, Fan W, A pyrolysis model of charring materials considering the effect of ambient oxygen concentration, Fire and Materials: An International Journal, 2007;31: 463-75.
[42] Bryden KM, Hagge MJ, Modeling the combined impact of moisture and char shrinkage on the pyrolysis of a biomass particle☆, Fuel, 2003;82: 1633-44.

[43] Bryden KM, Ragland KW, Rutland CJ, Modeling thermally thick pyrolysis of wood, Biomass and Bioenergy, 2002;22: 41-53.
[44] Melaaen M, Numerical analysis of heat and mass transfer in drying and pyrolysis of porous media, Numerical Heat Transfer, Part A Applications, 1996;29: 331-55.
[45] Shen D, Fang M, Luo Z, Cen K, Modeling pyrolysis of wet wood under external heat flux, Fire safety journal, 2007;42: 210-17.
[46] Kung H-C, A mathematical model of wood pyrolysis, Combustion and Flame, 1972;18: 185-95.
[47] Kung H-C, Kalelkar AS, On the heat of reaction in wood pyrolysis, Combustion and Flame, 1973;20: 91-103.
[48] Di Blasi C, Modeling and simulation of combustion processes of charring and non-charring solid fuels, Progress in energy and combustion science, 1993;19: 71-104.
[49] Benkoussas B, Consalvi J-L, Porterie B, Sardoy N, Loraud J-C, Modelling thermal degradation of woody fuel particles, International Journal of Thermal Sciences, 2007;46: 319-27.
[50] Boonmee N. Theoretical and experimental study of autoignition of wood. University of Maryland, College Park, 2004.
[51] Lautenberger C, Fernandez-Pello C, Generalized pyrolysis model for combustible solids, Fire Safety Journal, 2009;44: 819-39.
[52] McGrattan K, Hostikka S, McDermott R, Floyd J, Weinschenk C, Overholt K, Fire dynamics simulator user's guide, NIST special publication, 2013;1019.
[53] Ding Y-m, Wang C-j, Lu S-x, Large eddy simulation of fire spread, Procedia engineering, 2014;71: 537-43.
[54] Azhakesan M, Shields T, Silcock G, On the nature, influence and magnitudes of flame heat transfer during surface flame spread, Fire Safety Journal, 2000;35: 189-222.
[55] Delichatsios M, Mathews M, Delichatsios M, An upward fire spread and growth simulation, Fire Safety Science, 1991;3: 207-16.
[56] Lattimer B, Quincy M, Heat fluxes from fires to surfaces in SFPE handbook of fire protection engineering, Society of Fire Protection Engineers, 2002.
[57] Brehob E, Kim C, Kulkarni AK, Numerical model of upward flame spread on practical wall materials, Fire Safety Journal, 2001;36: 225-40.

[58] Kulkarni AK, Brehob E, Manohar S, Nair R, Turbulent upward flame spread on a vertical wall under external radiation, US Department of Commerce, National Institute of Standards and Technology, 1994.
[59] Quintiere J, The application of flame spread theory to predict material performance, Journal of Research of the National Bureau of standards, 1988;93: 61.
[60] Back G, Beyler C, DiNenno P, Tatem P, Wall incident heat flux distributions resulting from an adjacent fire, Fire Safety Science, 1994;4: 241-52.
[61] Quintiere J, The application of flame spread theory to predict material performance, Journal of Research of the National Bureau of Standards, 1988;93: 61-70.
[62] van Hees P. Meestroomvlamuitbreiding bij vloerbekledingen: ontwikkeling en validatie van grootschalige en kleinschalige meettechnieken. Ghent University, 1995.
[63] Sibulkin M, Kim J, The dependence of flame propagation on surface heat transfer II. Upward burning, Combustion Science and Technology, 1977;17: 39-49.
[64] Markstein G, De Ris J. Upward fire spread over textiles. In. Upward fire spread over textiles. Elsevier, 1973, pp. 1085-97.
[65] Heskestad G, Fire plumes, SFPE handbook of fire protection engineering, Nation Fire Protection Association, Quincy, Massachusetts, 1995.
[66] Delichatsios M, Flame heights in turbulent wall fires with significant flame radiation, Combustion Science and Technology, 1984;39: 195-214.
[67] Hasemi Y, Experimental wall flame heat transfer correlations for the analysis of upward wall flame spread, Fire Science and Technology, 1984;4: 75-90.
[68] Tu K-M, Quintiere JG, Wall flame heights with external radiation, Fire technology, 1991;27: 195-203.
[69] Ingason H, Two dimensional rack storage fires, Fire Safety Science, 1994;4: 209-20.
[70] Karlsson B, Thomas PH, Holmstedt G, Flame sizes in a small scale stack: pilot experiments, Citeseer, 1995.
[71] Ingason H, Modelling of a two-dimensional rack storage fire, Fire Safety Journal, 1998;30: 47-69.
[72] Ingason H, De Ris J, Flame heat transfer in storage geometries, Fire Safety Journal, 1998;31: 39-60.
[73] Livkiss K, Svensson S, Husted B, van Hees P, Flame heights and heat transfer in facade system ventilation cavities, Fire technology, 2018;54: 689-713.

[74] ASTM, Standard Test Method for Heat and Visible Smoke Release Rates for Materials and and Products Using an Oxygen Consumption Calorimeter, ASTM International, 2016.
[75] Saito K, Quintiere J, Williams F. Upward turbulent flame spread. In. Upward turbulent flame spread. 1986, pp. 75-86.
[76] Nilsson M, Husted B, Mossberg A, Anderson J, McNamee RJ, A numerical comparison of protective measures against external fire spread, Fire and materials, 2018;42: 493-507.
[77] Anderson J, Boström L, Jansson McNamee R, Milovanović B, Modeling of fire exposure in facade fire testing, Fire and materials, 2018;42: 475-83.
[78] !!! INVALID CITATION !!! [15-17].
[79] An W, Yin X, Cai M, Tang Y, Li Q, Hu X, Influence of U-shaped structure on upward flame spread and heat transfer behaviors of PMMA used in building thermal engineering, Case Studies in Thermal Engineering, 2020;22: 100794.
[80] Gollner MJ, Miller CH, Tang W, Singh AV, The effect of flow and geometry on concurrent flame spread, Fire Safety Journal, 2017;91: 68-78.
[81] Ren F, Hu L, Zhang X, Sun X, Zhang J, Delichatsios M, Experimental study of transitional behavior of fully developed under-ventilated compartment fire and associated facade flame height evolution, Combustion and Flame, 2019;208: 235-45.
[82] Coutin M, Most J, Delichatsios MA, Delichatsios MM, Flame heights in wall fires: effects of width, confinement and pyrolysis length, Fire Safety Science, 2000;6: 729-40.
[83] McDermott RJ, Forney GP, McGrattan K, Mell WE, Fire Dynamics Simulator Version 6: Complex geometry, embedded meshes, and quality assessment, National Institute of Standards and Technology, NIST, 2010.
[84] Hurley MJ, Gottuk DT, Hall Jr JR, Harada K, Kuligowski ED, Puchovsky M, Watts Jr JM, WIECZOREK CJ, SFPE handbook of fire protection engineering, Springer, 2015.
[85] McDermott R, McGrattan K, Hostikka S, Fire dynamics simulator (version 5) technical reference guide, NIST special publication, 2008;1018.
[86] Mitler HE, Algorithm for the mass-loss rate of a burning wall, Fire Safety Science, 1989;2: 179-88.
[87] McGrattan K, Hostikka S, McDermott R, Floyd J, Weinschenk C, Overholt K, Fire dynamics simulator technical reference guide volume 1: mathematical model, NIST special publication, 2013;1018: 175.
[88] Wickström U, Temperature calculation in fire safety engineering, Springer, 2016.
[89] Spalding DB, Combustion of liquid fuels, Nature, 1950;165: 160-60.

[90] Beyler CL. Fire hazard calculations for large, open hydrocarbon fires. In. Fire hazard calculations for large, open hydrocarbon fires. Springer, 2016, pp. 2591-663.
[91] Khan MM, Tewarson A, Chaos M. Combustion characteristics of materials and generation of fire products. In. Combustion characteristics of materials and generation of fire products. Springer, 2016, pp. 1143-232.
[92] Quintiere J, Harkleroad M, Hasemi Y, Wall flames and implications for upward flame spread, Combustion Science and Technology, 1986;48: 191-222.
[93] Orloff L, Modak AT, Alpert R. Burning of large-scale vertical surfaces. In. Burning of large-scale vertical surfaces. Elsevier, 1977, pp. 1345-54.
[94] Mitler HE, Steckler KD, A Model of Flame Spread on Vertical Surface, National Institute of Standards and Technology, NIST, 1995;5619.
[95] Yuen R, Yeoh G, de Vahl Davis G, Leonardi E, Modelling the pyrolysis of wet wood–I. Three-dimensional formulation and analysis, International journal of heat and mass transfer, 2007;50: 4371-86.
[96] Jiang F, de Ris JL, Khan MM, Absorption of thermal energy in PMMA by in-depth radiation, Fire Safety Journal, 2009;44: 106-12.
[97] Linteris G, Zammarano M, Wilthan B, Hanssen L, Absorption and reflection of infrared radiation by polymers in fire-like environments, Fire and materials, 2012;36: 537-53.
[98] Bergman TL, Incropera FP, DeWitt DP, Lavine AS, Fundamentals of heat and mass transfer, John Wiley & Sons, 2011.
[99] Stoliarov SI, Crowley S, Lyon RE, Linteris GT, Prediction of the burning rates of non-charring polymers, Combustion and Flame, 2009;156: 1068-83.
[100] Nakai Y, Yoshimizu H, Tsujita Y, Enhancement of gas permeability in HPC, CTA and PMMA under microwave irradiation, Polymer journal, 2006;38: 376-80.
[101] Grønli MG, Melaaen MC, Mathematical model for wood pyrolysis comparison of experimental measurements with model predictions, Energy & Fuels, 2000;14: 791-800.
[102] Schmal D, Duyzer JH, van Heuven JW, A model for the spontaneous heating of coal, Fuel, 1985;64: 963-72.
[103] Sinha PK, Wang C-Y, Pore-network modeling of liquid water transport in gas diffusion layer of a polymer electrolyte fuel cell, Electrochimica Acta, 2007;52: 7936-45.
[104] Li J, Stoliarov SI, Measurement of kinetics and thermodynamics of the thermal degradation for non-charring polymers, Combustion and Flame, 2013;160: 1287-97.

[105] Stoliarov SI, Walters RN, Determination of the heats of gasification of polymers using differential scanning calorimetry, Polymer Degradation and Stability, 2008;93: 422-27.
[106] Mun S-Y, Cho J-H, Hwang C-H, Effects of External Heat Flux and Exhaust Flow Rate on CO and Soot Yields of Acrylic in a Cone Calorimeter, Applied Sciences, 2021;11: 5942.
[107] Schartel B, Bartholmai M, Knoll U, Some comments on the use of cone calorimeter data, Polymer Degradation and Stability, 2005;88: 540-47.
[108] Delichatsios M, Wu P, Delichatsios M, Lougheed G, Crampton G, Qian C, Lshida H, Saito K, Effect of external radiant heat flux on upward fire spread: measurements on plywood and numerical predictions, Fire Safety Science, 1994;4: 421-32.
[109] Lautenberger C, Fernandez-Pello C, A model for the oxidative pyrolysis of wood, Combustion and Flame, 2009;156: 1503-13.
[110] Tarmian A, Perre P, Air permeability in longitudinal and radial directions of compression wood of Picea abies L. and tension wood of Fagus sylvatica L, 2009.
[111] Ragland K, Aerts D, Baker A, Properties of wood for combustion analysis, Bioresource technology, 1991;37: 161-68.
[112] Hakkarainen T, Post-flashover fires in light and heavy timber construction compartments, Journal of fire sciences, 2002;20: 133-75.
[113] Shi L, Chew MYL, A model to predict carbon monoxide of woods under external heat flux–Part I: Theory, Procedia engineering, 2013;62: 413-21.
[114] Kumar M, Gupta R, Sharma T, Effects of carbonisation conditions on the yield and chemical composition of Acacia and Eucalyptus wood chars, Biomass and Bioenergy, 1992;3: 411-17.
[115] Fukumoto K, Ogami Y, Turbulent diffusion combustion model using chemical equilibrium combined with the eddy dissipation concept for reducing detailed chemical mechanisms: An application of H2-air turbulent diffusion flame, Heat Transfer—Asian Research, 2010;39: 292-313.
[116] Tewarson A, Generation of heat and chemical compounds in fires, SFPE handbook of fire protection engineering, 2002: 82-161.
[117] Wu P, Orloff L, Tewarson A. Assessment of Material Flammability with the FSG Propagation Model and Laboratory Test Methods. In. Assessment of Material Flammability with the FSG Propagation Model and Laboratory Test Methods. NIST Report NISTIR 6030 Gaithersburg, MD, USA, 1996.

[118] Ma T, Quintiere J, Numerical simulation of axi-symmetric fire plumes: accuracy and limitations, Fire Safety Journal, 2003;38: 467-92.
[119] Dietenberger M, Hasburgh L, Wood products thermal degradation and fire, Reference module in materials science and materials engineering, 2016: 1-8.
[120] Huang X, Gollner MJ, Correlations for evaluation of flame spread over an inclined fuel surface, Fire Safety Science, 2014;11: 222-33.
[121] Wasan S, Van Hees P, Merci B, Study of pyrolysis and upward flame spread on charring materials—Part I: Experimental study, Fire and materials, 2011;35: 209-29.
[122] Boström L, Skarin C, Duny M, McNamee R. Fire test of ventilated and unventilated wooden façades. In. Fire test of ventilated and unventilated wooden façades. 2016.
[123] Lane B, Grenfell Tower–fire safety investigation, London, UK: Ove Arup & Partners Limited, 2018.
[124] Nguyen KT, Weerasinghe P, Mendis P, Ngo T, Performance of modern building façades in fire: a comprehensive review, Electronic Journal of Structural Engineering, 2016;16: 69-87.
[125] Wang Z, Zhu Y, Wang F, Wang P, Shen C, Liu J, Proceedings of the 11th International Symposium on Heating, Ventilation and Air Conditioning (ISHVAC 2019): Volume I: Indoor and Outdoor Environment, Springer Nature, 2020.
[126] He G, Zhang J, Hong S, A new analytical model for airflow in solar chimneys based on thermal boundary layers, Solar Energy, 2016;136: 614-21.
[127] Awbi H, Design considerations for naturally ventilated buildings, Renewable Energy, 1994;5: 1081-90.
[128] Sandberg M, Moshfegh B, Ventilated-solar roof air flow and heat transfer investigation, Renewable Energy, 1998;15: 287-92.
[129] Hong S, Wu Q, Ge W, Lv D, Li Z, He G. Evaluation of Three Analytical Solar Chimney Models with Field Data. In. Evaluation of Three Analytical Solar Chimney Models with Field Data. Springer, 2019, pp. 1047-54.
[130] Shi L, Theoretical models for wall solar chimney under cooling and heating modes considering room configuration, Energy, 2018;165: 925-38.
[131] Leung C. A brief review on eight flame spread models. In. A brief review on eight flame spread models. 2004, pp. 237-58.
[132] Quintiere J, Cleary TG, Heat flux from flames to vertical surfaces, Fire technology, 1994;30: 209-31.
[133] McCaffrey BJ, Flames PBD, Some Experimental Results, Nbsir, 1979.

[134] Ingason H, Two dimensional rack storage fires, Fire Safety Science, 1994;4: 1209-20.
[135] Yan W, Shen Y, An W, Jiang L, Sun J, Experimental study on fire risk of buildings' U-shaped exterior wall on flame propagation of insulation material on plain and plateau, Journal of fire sciences, 2015;33: 358-73.
[136] Prasad K, Kramer R, Marsh N, Nyden M, Ohlemiller T, Zammarano M. Numerical simulation of fire spread on polyurethane foam slabs. In. Numerical simulation of fire spread on polyurethane foam slabs. Citeseer, 2009.
[137] Dréan V, Girardin B, Guillaume E, Fateh T, Numerical simulation of the fire behaviour of facade equipped with aluminium composite material-based claddings-Model validation at large scale, Fire and materials, 2019;43: 981-1002.
[138] BRE. Fire test report, DCLG BS 8414 test no.1. In. Fire test report, DCLG BS 8414 test no.1. 2017.
[139] Chaudhari DM, Stoliarov SI, Beach MW, Suryadevara KA, Polyisocyanurate Foam Pyrolysis and Flame Spread Modeling, Applied Sciences, 2021;11: 3463.
[140] Trouvé A, Thermal Properties Database, 2012.
[141] Hietaniemi J, Mikkola E, Design fires for fire safety engineering, Technical Research Centre, Helsinki, Finland, 2010.
[142] Celotex RS5000 data sheet. In. Celotex RS5000 data sheet.
[143] Bytskov G. Numerical simulation of fire performance and test conditions for facade insulation materials. 2015.
[144] Harper CA, Handbook of building materials for fire protection, McGraw-Hill New York, 2004.
[145] Hasemi Y, Tokunaga T, Some experimental aspects of turbulent diffusion flames and buoyant plumes from fire sources against a wall and in a corner of walls, Combustion Science and Technology, 1984;40: 1-18.
[146] Hasemi Y, Tokunaga T. Modeling of turbulent diffusion flames and fire plumes for the analysis of fire growth. In. Modeling of turbulent diffusion flames and fire plumes for the analysis of fire growth. Currently Guest Worker at Center for Fire Research from Building Research …, 1983.
[147] Heskestad G. Fire plumes, flame height, and air entrainment. In. Fire plumes, flame height, and air entrainment. Springer, 2016, pp. 396-428.
[148] Karlsson B, Quintiere J, Enclosure fire dynamics, CRC press, 1999.

[149] Hakkarainen T, Kokkala MA, Application of a one-dimensional thermal flame spread model on predicting the rate of heat release in the SBI test, Fire and materials, 2001;25: 61-70.
[150] Hjohlman M, Andersson P, Van Hees P, Flame spread modelling of complex textile materials, Fire technology, 2011;47: 85-106.
[151] Hietaniemi J, Hostikka S, Vaari J, FDS simulation of fire spread œ comparison of model results with experimental data, VTT building and Transfor. Available: http://www2. vtt. fi/inf/pdf/workingpapers/2004 W, 2004;4.
[152] Technical datasheet available at https://www.rockwool.com/. In. Technical datasheet available at https://www.rockwool.com/.
[153] Technical datasheet available at https://www.kingspan.com/. In. Technical datasheet available at https://www.kingspan.com/.
[154] Technical datasheet available at https://www.knaufinsulation.co.uk/. In. Technical datasheet available at https://www.knaufinsulation.co.uk/.
[155] Technical datasheet available at https://insulation-uk.com/. In. Technical datasheet available at https://insulation-uk.com/.
[156] Vo CV, Bunge F, Duffy J, Hood L, Advances in thermal insulation of extruded polystyrene foams, Cellular Polymers, 2011;30: 137-56.
[157] Axelsson J, Van Hees P, New data for sandwich panels on the correlation between the SBI test method and the room corner reference scenario, Fire and Materials: An International Journal, 2005;29: 53-59.
[158] Technical datasheet available at https://www.ecotherm.co.uk/. In. Technical datasheet available at https://www.ecotherm.co.uk/.
[159] Intini F, Kühtz S, Recycling in buildings: an LCA case study of a thermal insulation panel made of polyester fiber, recycled from post-consumer PET bottles, The international journal of life cycle assessment, 2011;16: 306-15.
[160] Mougel C, Garnier T, Cassagnau P, Sintes-Zydowicz N, Phenolic foams: A review of mechanical properties, fire resistance and new trends in phenol substitution, Polymer, 2019;164: 86-117.
[161] Del Saz-Orozco B, Alonso MV, Oliet M, Domínguez JC, Rodriguez F, Mechanical, thermal and morphological characterization of cellulose fiber-reinforced phenolic foams, Composites Part B: Engineering, 2015;75: 367-72.

[162] Auad ML, Zhao L, Shen H, Nutt SR, Sorathia U, Flammability properties and mechanical performance of epoxy modified phenolic foams, Journal of Applied Polymer Science, 2007;104: 1399-407.
[163] Sahin HT, Simsek Y, Mineral-Bonded Wood Composites: An Alternative Building Materials, Engineered Wood Products for Construction, 2021: 317-34.
[164] Technical datasheet available at https://www.savolit.co.uk/. In. Technical datasheet available at https://www.savolit.co.uk/.
[165] Kymäläinen H-R, Sjöberg A-M, Flax and hemp fibres as raw materials for thermal insulations, Building and environment, 2008;43: 1261-69.
[166] Technical datasheet available at https://www.thermofloc.com/. In. Technical datasheet available at https://www.thermofloc.com/.
[167] Lakatos Á, Csík A, Csarnovics I, Experimental verification of thermal properties of the aerogel blanket, Case Studies in Thermal Engineering, 2021;25: 100966.
[168] Li C, Cheng X, Li Z, Pan Y, Huang Y, Gong L, Mechanical, thermal and flammability properties of glass fiber film/silica aerogel composites, Journal of Non-Crystalline Solids, 2017;457: 52-59.
[169] Al-Homoud MS, Performance characteristics and practical applications of common building thermal insulation materials, Building and environment, 2005;40: 353-66.
[170] Papadopoulos AM, State of the art in thermal insulation materials and aims for future developments, Energy and buildings, 2005;37: 77-86.
[171] Technical datasheet available at https://www.ecomerchant.co.uk/. In. Technical datasheet available at https://www.ecomerchant.co.uk/.
[172] Pásztory Z, An overview of factors influencing thermal conductivity of building insulation materials, Journal of Building Engineering, 2021;44: 102604.
[173] Stoliarov SI, Safronava N, Lyon RE, The effect of variation in polymer properties on the rate of burning, Fire and Materials: An International Journal, 2009;33: 257-71.
[174] Mark JE, Physical properties of polymers handbook, Springer, 2007.
[175] Carlos Domínguez J, Saz-Orozco BD, Oliet M, Virginia Alonso M, Rodriguez F, Thermal degradation kinetics of a lignin particle-reinforced phenolic foam, Journal of Cellular Plastics, 2021;57: 176-92.
[176] Li Z, Zhang Y, Huang S, Wu X, Shi L, Liu Q, Thermal stability and pyrolysis characteristics of MTMS aerogels prepared in pure water, Journal of Nanoparticle Research, 2020;22: 1-14.

[177] Zhang W, Li Z, Shi L, Li Z, Luo Y, Liu Q, Huang R, Methyltrichlorosilane modified hydrophobic silica aerogels and their kinetic and thermodynamic behaviors, Journal of Sol-Gel Science and Technology, 2019;89: 448-57.
[178] Hidalgo JP, McLaggan MS, Osorio AF, Heitzmann M, Maluk C, Lange D, Carrascal J, Torero JL, Protocols for the material library of cladding materials–part I: framework, 2019.
[179] Hidalgo JP, Torero JL, Welch S, Fire performance of charring closed-cell polymeric insulation materials: Polyisocyanurate and phenolic foam, Fire and materials, 2018;42: 358-73.